Functional Polymer Fibre Spinning by Infusion Gyration

A thesis submitted in partial fulfilment of the requirements for transfer to the degree of

Doctor of Philosophy

March 2018

By

Siqi Zhang

Department of Mechanical Engineering

University College London

Torrington Place, London WC1E 7JE, UK

Declaration

I, Siqi Zhang, confirm that the work presented in this thesis is my own. Where information has been derived from other sources, I confirm that this has been indicated in the thesis.

Signature:

Date

Abstract

Fibres show promising applications such as textiles, filtration, sensing and tissue engineering. In this study, an infusion gyration system to produce polymer micro and nano fibres with functions was introduced. By using this method, functional fibres can be formed from polymer solutions mixed with other functional materials.

PEO or PVA water solution was used for making the spinning solutions. The fluorescence protein bound with gold nanoparticles was carried by the PEO water solution, from which the fibres assembled with protein were successfully generated through infusion gyration. A mixed molecular weight PVA combined water solution mixed with processed magnetic nanoparticles achieved fabrication of magnetically controllable fibres have the potential for drug release and its demonstration test showed a positive result.

This spinning system provides control of the polymer solution flow rate during spinning which affects the fibre morphology such as average diameter and size distribution. The relationship between the spinning parameters and the product properties was studied for better understanding of the method. The analysis of infusion gyration and its fibre forming process was carried out.

The fibres were characterised using several methods, such as optical microscopy, SEM, FTIR and UV-Vis, to establish the potential of infusion gyration and to confirm the functions of final fibre product.

The infusion gyration system provides a simple micro and nano scale assembly approach to integrate different protein functionalities into nanofibres with potential applications. Magnetic PVA nanofibres are promising for drug delivery.

Impact Statement

The work presented in this thesis introduces a novel commercially attractive fibre spinning method, uncovers a new fibre generating process and describes several functional fibre products made from using it.

The infusion gyration fibre spinning system developed here could dramatically increase the value and flexibility of the fibre production industry and broaden the variety materials used to create products the fibre industry can offer. By combining the gyration spinning process and the solution inflow (infusion) system, both fibre productivity and structural dimensions can be managed. This system provides an effective way of fibre manufacturing at a relatively large scale. By changing the infusion rate of the polymer solution, it has been demonstrated that the average fibre size can be controlled within hundreds of nanometres and tuned for different applications. This means that designing a specific type of product is possible.

The fluorescent protein integrated within polymer fibres made by infusion gyration show a strong signal of fluorescence which brings a promise of new biomaterials for the future imaging and sensing industry. This simple nanoscale assembly approach to incorporate protein(s) into polymer fibres proves that the protein(s) can be embedded on surface and sub-surface of the fibres. As the integration of protein(s) into polymer fibres keeps the material functioning well biologically, it can offer a fundamental platform in the design and fabrication of novel biomaterials which may be useful in medical treatments.

The magnetic fibres respond quickly to a moving external magnetic field which is tested and shown to be effective in immobilization and triggered release of drugs. This material is biocompatible and remotely controlled. In the future, it can deliver particular drugs to the target which will be released with contactless actuation in clinical use.

To conclude, the infusion gyration system with its making of new products not only opens a gateway of fibre processing research for the laboratory and industry, but also provides a method for biomedical fibre design and generation in an acceptable time frame with a sufficient volume of material used in the future in clinics. More parameters can be added, recorded and changed to the system for designing complicated materials.

Acknowledgements

I would like to offer my warmest thanks to Professor Mohan Edirisinghe and Dr. Suntharavathanan Mahalingam as my supervisors for the guidance and support throughout my whole PhD life for this project.

I gratefully appreciate Professor Candan Tamerler, Banu Taktak Karaca, Sarah Kay VanOosten and Esra Yuca from the University of Kansas for their great help with my work. Also, I would like to express my gratitude to Dr. Ayomi Perera, Professor Shervanthi Homer-Vanniasinkam and Professor Marc-Olivier Coppens for their help with this research.

Sincerely, I thank my friends, research colleagues and all the people who have helped me throughout my study.

Last but not least, I am very grateful for my family who always give me love and support.

Dedication

To

My love

And my parents

Publications & Presentations

Journal papers

Siqi Zhang, Banu Taktak Karaca, Sarah Kay VanOosten, Esra Yuca, Suntharavathanan Mahalingam, Mohan Edirisinghe, Candan Tamerler. (2015). Coupling Infusion and Gyration for the Nanoscale Assembly of Functional Polymer Nanofibres Integrated with Genetically Engineered Proteins. *Macromolecular Rapid Communications, 36*, 1322–1328.

Ayomi Perera*, Siqi Zhang*, Shervanthi Homer-Vanniasinkam, Marc-Olivier Coppens, Mohan Edirisinghe. (2017). Polymer-Magnetic Composite Fibres for Remote-Controlled Drug Release. *Complete submission*. *These authors made equal contributions

Conference Presentations

Siqi Zhang. Smart Nanofibre Spinning by Pressurised Gyration. Oral presentation and poster. PhD Student Conference, Department of Mechanical Engineering, UCL, London, UK. 18th July 2014.

Siqi Zhang. Functional Polymer Nanofibre Spinning by Infusion Gyration. Oral presentation and poster. Chairing one of the sessions. PhD Student Conference, Department of Mechanical Engineering, UCL, London, UK. 25th June 2015.

Siqi Zhang. Functional Polymer Nanofibre Spinning by Infusion Gyration. Poster presentation. EPRSC EHDA Network: International PharmTech Conference 2016, Leicester, UK. 4th November 2016.

Table of Contents

List of Figures

List of Tables

Glossary of Abbreviations

BP	Binding peptide
DC	Direct current
DMF	*N,N*-Dimethylformamide
EDX	Energy-dispersive X-ray spectroscopy
FTIR	Fourier transform infrared spectroscopy
GFP	Green fluorescent protein
LSPR	Localized surface plasmon resonance spectroscopy
MBP	Maltose binding protein
MNP	Magnetic nanoparticle
MRI	Magnetic resonance imaging
NP	Nanoparticle
PAN	Polyacrylonitrile
PBS	Phosphate buffered saline
PBT	Poly(butylene terephthalate)
PCL	Polycaprolactone
PEO	Polyethylene oxide
PET	Poly(ethylene terephthalate)
PLLA	Poly(L-lactide)
PMMA	Poly(methyl methacrylate)
PP	Polypropylene
PS	Polystyrene
PVA	Poly(vinyl alcohol)
SEM	Scanning electron microscopy

Chapter 1.

Introduction

1.1 Background

Polymer nanofibre is an excellent engineering material in various applications such as biomedical textile and tissue engineering because of its high surface-to-volume ratio[1]. The key factor is the diameter of polymer fibre which has to be in the sub-microns or nanometres (e.g. 10×10^{-3}-100×10^{-3} μm) rather than micrometres (e.g. 10-100 μm)[2]. This factor gains flexibility in surface functionalities and superior mechanical performance as well in comparison with any other known material form. Over the last decade or so, a wide variety of techniques have been used to process nanofibres and nanofibrous structures such as drawing, template synthesis, phase separation, self-assembly and electrospinning.

In the fibre industry, drawing is a similar process to dry spinning for making very long single nanofibres one by one. However, drawing can only be used for a viscoelastic material due to its strong cohesion during pulling. The template synthesis uses a nanoporous membrane as a template to process solid or hollow shape nanofibres. Various raw materials such as electronically conducting polymers, metals, semiconductors, and carbons can be fabricated by this method but not for one-by-one continuous nanofibres. The phase separation process takes a relatively long time because it needs to transfer the solid polymer through dissolution, gelation and extraction (solvent, freezing, and drying) into nanoscale porous foam. The self-assembly process also takes a long time to generate continuous polymer nanofibres by organizing individual, pre-existing components into desired functions and patterns. Thus, some researchers regarded electrospinning as a promising method of

generating continuous nanofibres from various polymers for mass production if it is fully developed. However, the yield of the electrospun fibres is relatively low and its long processing time cannot be ignored.

In fact, the most common method in recent years of generating micro or nano fibre from polymer solution is electrospinning which requires high voltage during the process and this system has been studied for decades[3]. Moreover, the yield from the electrospinning process is low from several studies[1]. Centrifugal spinning is an alternative method for producing fibres rapidly with a high yield[4]. The spinning fluid from the rotating part comes out through nozzle tip(s) and forms solidified fibres from the fluid jet.

Another method is a pressurised gyration system using high pressure gas and centrifugal force which has been proven to generate well-aligned fibres on a larger scale[5]. It has a relatively high yield of fibre production compared with solution blowing, etc. The solution is put into the vessel before spinning which requires both high rotating speed and high pressure gas. Despite the versatility of the process, pressurised-gyration consistently produces a range of natural and synthetic polymers with controllable morphologies and functionalities in the submicron diameter range that is otherwise difficult to achieve by standard spinning methods. In a typical parametric plot of rotating speed and working pressure for a polymer solution to be spun, conditions can be obtained that determine the final product shape as either fibres or microbubbles[6]. Moreover, apart from solution physical properties, i.e. viscosity and surface tension, there needs to be a critical minimum concentration of polymer solution to initiate and produce continuous fibres, otherwise an architecture of beads results. A typical pressurised-gyration process consists of simultaneous centrifugal spinning and solution blowing where the combination of centrifugal force and the forces arising

due to dynamic fluid flow act against the surface tension force to generate fine fibres. Even though pressurised-gyration is a simple and robust process, it does not allow control of fluid flow through the fibre generating orifices where generally the infusion rate of the polymer solution influence fibre size, size distribution and morphologies of fibres spun.

In the laboratory practice, it happens that the solution is sprayed out on the inner walls of the protection container not as fibres but as drops because the solution is kept in the rotating vessel during the acceleration stage. It means the solution comes out from orifices before the vessel reaches the fibre forming rotating speed. This becomes the main loss of making use of the polymer solution for spinning fibres.

Therefore, the infusion gyration system was introduced in this study (Figure 1-1).

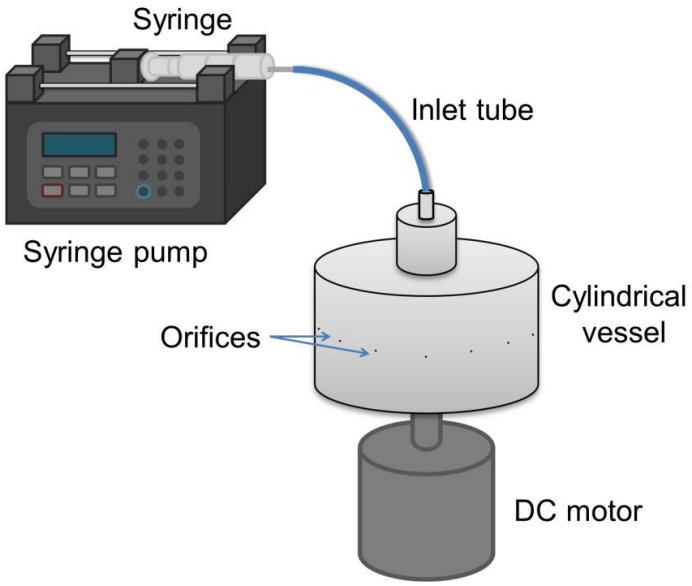

Figure 1-1 Schematic diagram of the infusion gyration spinning process.

It removes the gas pressure but connects to a syringe with a syringe pump (PHD 4400 Programmable, Harvard Apparatus) instead. This system can control the polymer solution flow rate into the cylindrical vessel to prevent solution loss during the process.

Moreover, in some following test experiments, the flow rate factor was researched. It holds the ability to tune the average size of fibre.

Functionalized hybrid fibre has potential applications such as bioengineering and biomedical technology[7]. For tissue engineering, especially scaffolds, biopolymers (aloe vera, silk fibroin and curcumin) have been incorporated into polycaprolactone (PCL) as suitable substrates to make fibres mimicking the functions of extracellular matrix. The protein, such as enzyme, has been tested to improve the activity retention and the dry storage stability using polymer nanofibres as carriers[8]. Functional fibres for releasing a protein drug (bioactive lysozyme) in a sustained manner over a one week period have been achieved by directly dissolving protein molecules in an electrospinning solvent medium and making biodegradable fibrous meshes using electrospinning[9].

In consideration of the advantages of assembling biomaterials into polymer nanofibres and to make full use of nanoscale material properties combined with bio-functions, the fluorescent protein has been selected in use to achieve functional polymer fibres by infusion gyration. The fluorescent protein holds great promise for biotechnology and cell biology[10]. The DsRed fluorescent protein is cloned from Discosoma coral which shows red fluorescence as well as the green fluorescent protein (GFP) from Aequorea jellyfish[11]. Due to the inner structure of the fluorescence protein, it has different excitation and emission wavelengths[12]. This special property of fluorescence protein was used in the mixture of the solution to generate functional fibres, i.e. fluorescent fibres by the infusion gyration system. The fluorescence protein used in this study is designed to bind to gold. Therefore, the gold nanoparticles were required to strengthen the fluorescence capacity for the final fibres. To demonstrate the potential of polymer fibres as a drug delivery platform, remote controllable composite fibres were made

through infusion gyration using PVA solution mixed with magnetic nanoparticles. The drug delivery test has been done to prove its potential of controlled release.

1.2 Aims and Objectives

The aim of this work is to investigate the whole process of making functional polymer micro and nano fibres using infusion gyration. PEO and PVA water solution was utilised and tested as the polymer solution. The fluorescence of the fibres was achieved by gold binding fluorescence protein and gold nanoparticles. Magnetically actuated PVA fibres mixed with magnetic nanoparticles will be made and tested for controlled drug delivery. The infusion gyration system will be tested to control the fibre size as outcome. The relationship between tuneable infusion flow rate and the final fibre size is going to be researched. Variable flow rate was tested and monitored for the fibre size comparison. SEM analysis is used to examine the fibre for the shape and even the fibre size distribution. EDX is used for element analysis in fibre. The characterisation is made by FTIR showing the existence of the protein or enzyme which also indicates the chemical bonding within the fibres. The function of the fluorescence protein bound with gold nanoparticles along polymer fibres needs to be tested in a working status. The fluorescence microscope is used to detect this function for the various fibre batches. The infusion gyration system is going to be researched more to gain the flexibility of adapting different polymer solutions as more polymers will be tested.

1.3 Structure of the Thesis

This dissertation is ordered in chapters focusing on the infusion gyration process to generate functional polymer fibres along with different research work (Table 1-1).

Chapter 1 introduces a brief background to polymer functional micro and nano fibres with the aims and objectives of this project.

Chapter 2 reviews other researchers' work including fibres materials, production methods and applications.

Chapter 3 shows the whole technical details of the experiment for the study. Materials and methods are provided.

Chapter 4 demonstrates the capacity of infusion gyration, for the first time, fabricating fibres. The infusion gyration method can generate micro and nano fibres that are integrated with inorganic binding peptides, namely, the well characterized gold binding dodecapeptide, Au-BP2, was used during the fibre formation process. It is demonstrated that the engineered peptide fibres have the capacity for controlling and directing the nanostructure assemblies. Fibre morphology is studied to detect the relationship between processing parameters and fibre size. Three different combinations of spinning solution are tested and the protein incorporation with final fibres is confirmed through several characterization methods. The bio-hybrid fibres could be further exploited to advance the peptide based materials for bio-fabrication of various protein arrays, plasmon-active nanoassemblies, bio-sensing and nanophotonic devices with controlled organization and architecture.

Chapter 5 reports an efficient method for fabrication of composite microfibres that can be magnetically actuated and are biocompatible, targeting controlled drug release.

Aqueous solutions of polyvinyl alcohol (PVA), incorporated with citric acid coated Fe_3O_4 magnetic nanoparticles (MNPs), are subject to infusion gyration, to generate 100-300 nm diameter composite fibres, with controllable MNP loading. The fibres are stable in polar solvents, such as ethanol, and do not show any leaching of MNPs for over 4 weeks. This material is effective in the immobilization of drugs demonstrated using acetaminophen as an example and achieves triggered release by a moving external magnetic field. Coupled with biocompatibility and lightweight property, this remote actuation ability of the fibres renders enormous potential for them to be used as a functional drug-release agent.

Chapter 6 gives theoretical analysis of infusion gyration and shows its potential for other products.

Chapter 7 brings a conclusion to the study and drafts a possible plan for future work.

Chapter 1	Introduction with polymer fibre background as well as its generation methods. The aims and objectives.
Chapter 2	Literature review of works from different researchers on micro and nano fibre generation.
Chapter 3	Specification of experiments is illustrated in this chapter including materials used and methods.
Chapter 4	Fabrication of PEO fibres with fluorescent protein using infusion gyration.
Chapter 5	Fabrication of PVA fibres with magnetic nanoparticles for drug release.
Chapter 6	Infusion gyration analysis.
Chapter 7	This chapter covers conclusions and future work.

Table 1-1 Structure of the thesis.

Chapter 2.

Literature review

2.1 Introduction

2.1.1 Polymer-based nanofibres

Polymer-based nanofibres have been investigated for a myriad of biomedical applications, including scaffolds for tissue engineering, materials for wound dressing and vehicles for drug delivery[13]. Polymer is a large molecule, or macromolecule, composed of many repeated subunits. They have complicated properties such as melting point, glass transition temperature and mixing behaviour. Even the same polymer has different average molecular weight. However, they have excellent performance in several areas better than metal or ceramics. For example, it has been reported that biomimetic aramid nanofibres with poly(vinyl alcohol) (PVA) composites can be used as load bearing soft tissues with ~9.1 MPa tensile moduli, ~325% ultimate tensile strains and ~26 MPa compressive strengths, superior to cartilage[14]. (Figure 2-1)

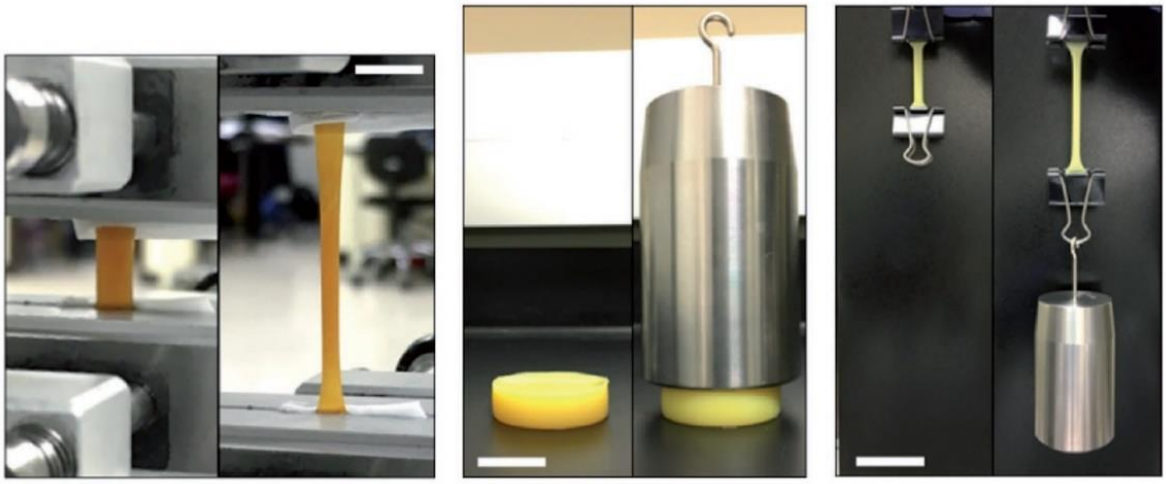

Figure 2-1 A sample of aramid nanofibre with PVA 30 hydrogel with tensile strain (Scale bar: 10 mm), compressive load of 10 N (Scale bar: 30 mm) and tensile load of 10 N (Scale bar: 50 mm)[14].

The amazing properties of polymer help people design special materials with functions such as self-healing reported[15] (Figure 2-2). A 2-mm-thick rectangular sheet (10 mm x 20 mm) was prepared by heating $TUEG_3$ (a polymer synthesised from 1,2-bis(2-aminoethoxy) ethane and 1,1'-thiocarbonyldiimidazole) to 140 °C followed by a natural cooling process.

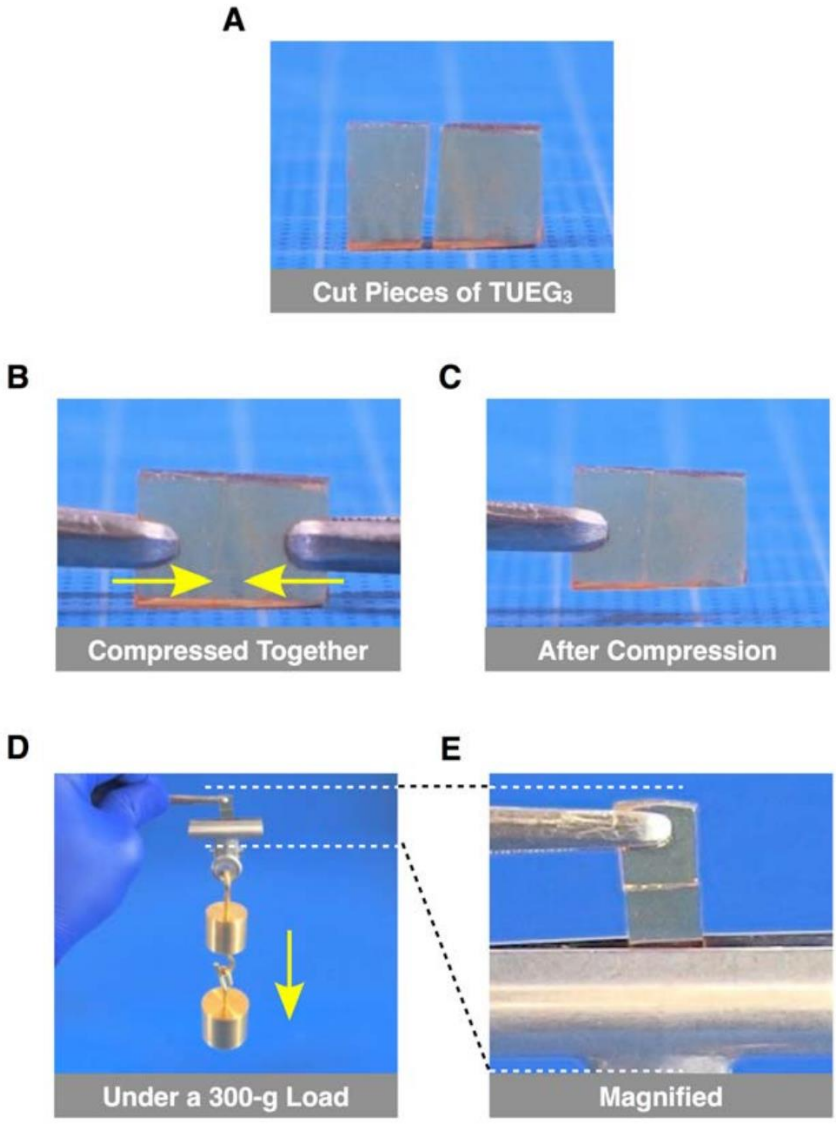

Figure 2-2 Self-healing of polymer material.[15]

Then, to ensure smooth cutting, it was cut using scissors into two pieces under gentle heating by a dryer. These two pieces were tightly pressed together after 10 min cooling for 30 sec. Approximately 0.2 MPa stress was applied to ensure that their freshly cut

surfaces were brought into contact. The merged sheet can bear a tensile load of 300 g indicating successful self-healing of $TUEG_3$.

Micro and nano scale fibres are of particular interest in biomedicine, as their morphology resembles biological tissue. They are also of high surface area and surface energy, and can be organized into porous hierarchical structures, which are highly desirable properties for cell and tissue adhesion, as well as the adsorption of drug molecules. The physical structure of the fibres can be readily customized to adapt to different applications. Furthermore, materials used for fibre formation have been developed to facilitate the incorporation of fibres with biodegradable[16,17] antibiotic properties[18] and even those that include living tissue[19–21]. Extensive progress has also been made in the scale-up of such materials targeting industrial applications[22].

2.1.2 Peptides

Peptides, a material to be used in the study, are the molecular building blocks of the biological world and contribute to the astonishing range of physical, chemical and biological properties displayed by proteins[23,24]. Moreover, peptides play a key role in molecular recognition and self-assembly by offering compartmentalization within organic frameworks where different function(s) may be coupled[24,25]. Functional polymeric fibres are promising candidates to mimic these biological building blocks in designing flexible materials with hierarchical architecture.

However, fabrication of bio-hybrid fibres that mimic even the most fundamental level of hierarchical organization integrated with biological property has been challenging due to the lack of control between dissimilar phases, i.e. organic and inorganic phases. Engineered peptides with inorganic material recognition may be the unique building blocks to exert control over dissimilar nanophases and contribute to hybrid nanofibre formation with added functional properties inherent to the peptide.

Inorganic binding peptides have attracted tremendous interest in the last decade, ranging from assembly of nanoparticles[25,26] to oriented immobilization of proteins[27–29] as well as synthesis of inorganics[30,31] to bio-functionalization of surfaces[32–36]. Previously, selection by combinatorial display methods was described for peptide with the ability to bind to inorganic materials[37–40]. Solid binding peptides have been shown to control the biological-material interface in different application. However, they have not been investigated in their capacity to design functional fibres where the peptide based self-assembly process may be regulated at the molecular level to nucleate architecture and establish an ordered nanostructure. Combinatorial-selected and bio-informatically optimized peptides for their adsorption properties and role in surface binding were studied[41–43].

2.1.3 Magnetic nanoparticles (MNPs)

Magnetic material is widely used to approach movement or action control of products. One of its applications contributing in medical treatment is reported that magnetic oculomotor prosthesis has been used as an implantation for a patient to recover[44]. This treatment simply makes use of the magnetic action force and requires surgery.

Another idea is to remotely control the movement of the magnetic target therefore to active functions without contact, such as hyperthermia therapy or bone regeneration scaffolds[45].

Magnetically triggered release of active pharmaceutical ingredients is a rapidly growing area of research with applications targeted towards efficient, minimally invasive pathways of drug delivery[46–49]. Such studies usually involve the use of superparamagnetic nanoparticles, which are either functionalized as drug-carriers[50,51] or incorporated with polymers to produce composites in the form of membranes[52], liposomes[53–55], protein microspheres[48], gels[52], etc. These materials have become highly significant in the advancement of diagnosis and treatment of cancer, and cardio-vascular diseases, in addition to leading towards breakthroughs in regenerative medicine[56–60].

Polymer composites embedded with magnetic particles were made to achieve remotely actuatable materials which can be applied into soft robotic systems[61] (Figure 2-3).

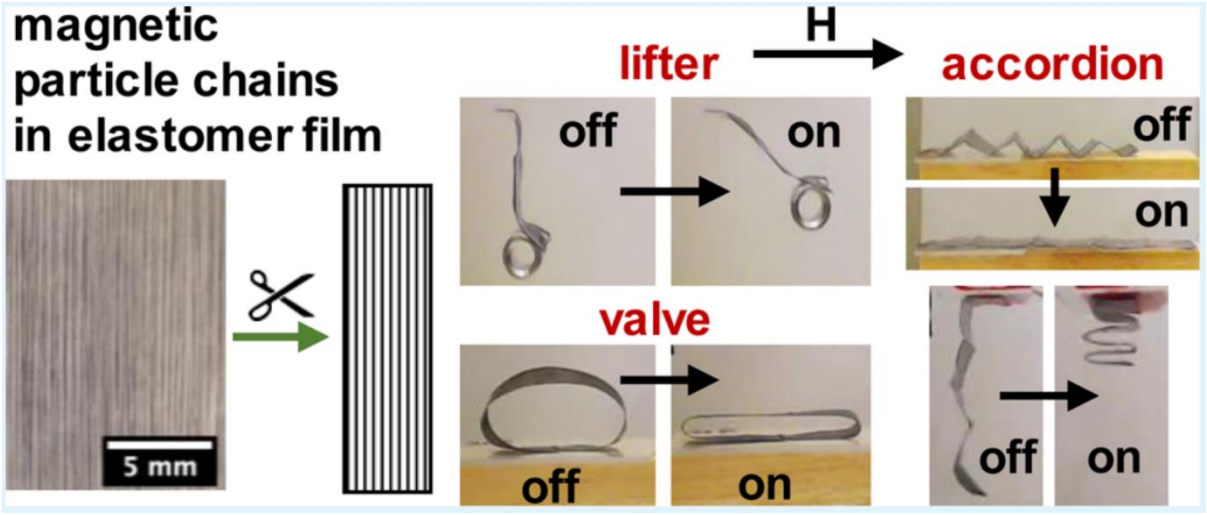

Figure 2-3 Soft robotic system[61]

The magnetic particles used are self-assembled in chains and directed by the magnetic field giving directional response. The folded accordion structures they made caused extension and compression when the magnetic field is applied. This engineered material provides noncontact control and shows great potential for soft devices.

The magnetic component is typically activated *via* hyperthermia or for chemical signals to trigger the release of the drug[62,63]. Actuation of the drug-carrying platform by an external magnetic field (i.e., magnetic actuation), however, remains scarcely explored, but has enormous potential in biomedicine[64,65]. Such systems can potentially lead to remote-controlled, precise and safer pathways of drug delivery, and also pave the way to advances in the rapidly evolving field of micro-robotics, for applications in medicine[65–67].

Recent reports indicate that *in vitro* drug release, in particular, can be improved using conventional carrier such as mesoporous silica, in combination with magnetic nanoparticles (MNPs) for triggered cargo release[68–70]. Such carrier systems have great potential for treatment of cancer and other related diseases[71]. Many carrier systems need physical (e.g., thermal or light) or chemical (e.g., pH or red-ox changes) stimuli or enzymatic catalysis to initiate the release action, which require either invasive procedures or are limited in efficiency and controllability. However, the systems containing MNPs give rapid responses, with non-invasiveness, and can be easily controlled by external magnetic fields. MNPs also have the advantage of being easily integrated with organic components such as polymers to create composite materials with novel and improved capabilities[56]. Moreover, MNPs have been developed as imaging probes for magnetic resonance imaging (MRI) to visualize and

target disease when diagnosing[56]. Several parameters have been seriously considered such as physicochemical properties and nanoparticle surface modifications for improving the MNP performance *in-vivo* which has the potential for drug loading and release for clinical use. Magnetic polymer nanofibres draw attention for similar applications. Tube-shaped nanofibres with nanoparticles in the core were fabricated via coaxial electrospinning. They have magnetic behaviour after spinning either use PCL with FePt[72] (Figure 2-4) or PET with Fe_3O_4[73], but no further concepts for application were reported or tested such as drug load. Also, it is difficult to obtain homogeneous dispersed Fe_3O_4 nanoparticles within polymer nanofibres via electrospinning[74].

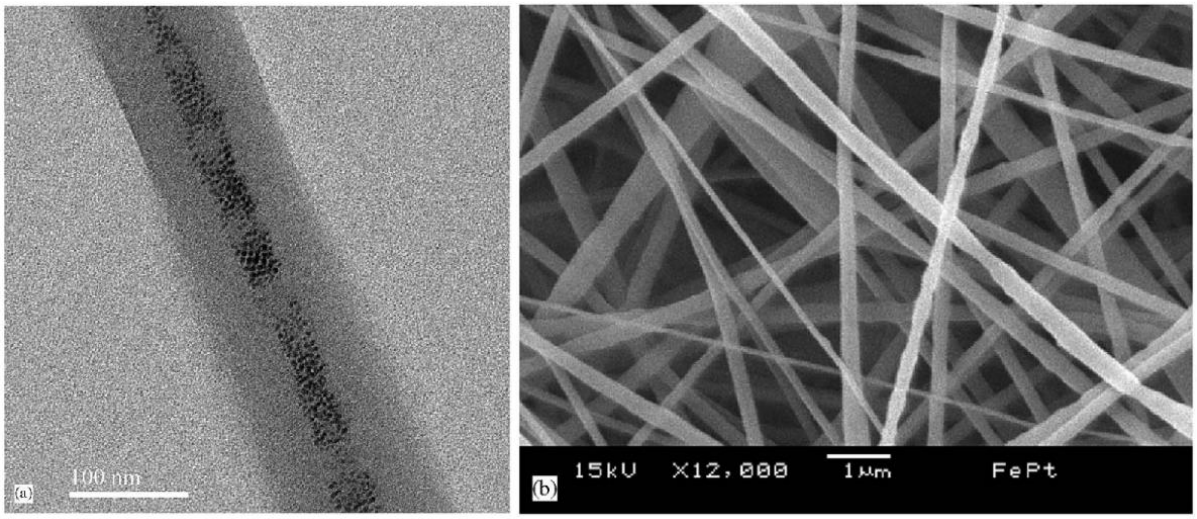

Figure 2-4 The coaxial composite nanofibres (FePt in PCL) using electrospinning. (a) Transmission electron microscopy. (b) Scanning electron microscopy.[72]

2.2 Methods for Fibre Production

Micro and nano fibre producing have been researched in different areas and applications over decades. Many methods for fibre production, both in laboratory scale and industry, have been invented and improved. This section gives a brief review of different methods recently in use by researchers.

2.2.1 Electrospinning

Electrospinning is popular for researchers to generate nanofibres in different fields such as chemical engineering and biomedical application[75]. As a conventional nanofibre generation system, a lot of work has been done to understand and optimize the process[76]. Figure 2-5 shows a typical experiment set-up schematic of electrospinning. The flow which is charged electrically comes from the nozzle and is accelerated by a high electric field[77].

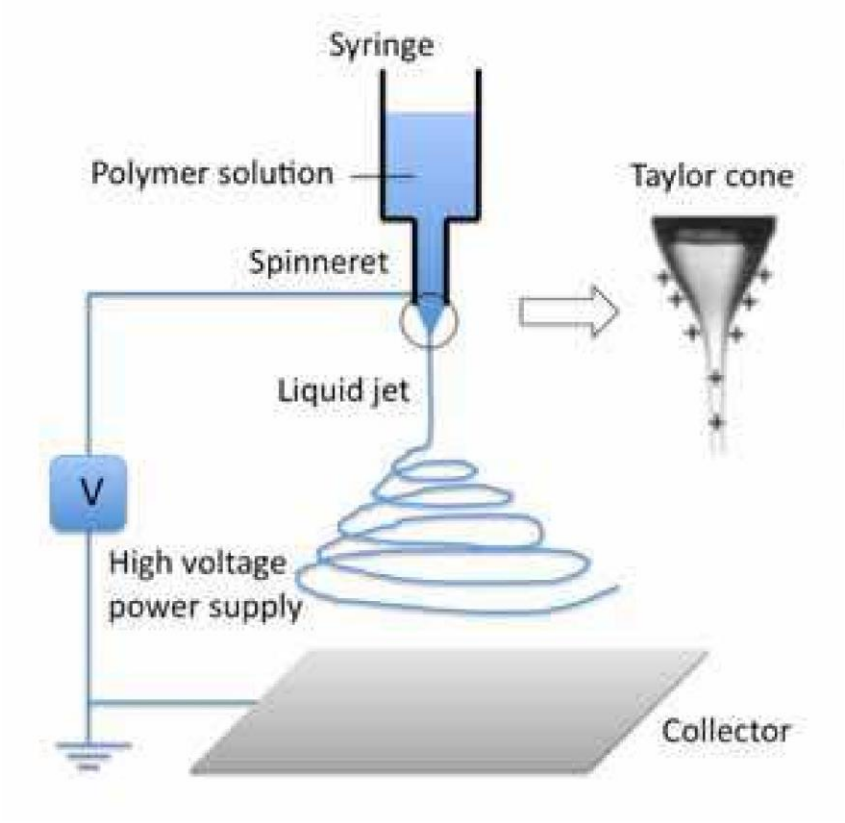

Figure 2-5 Schematic diagram of a typical electrospinning setup[77].

Electrospinning is simple to use to generate micro or nano fibres for small-scale (laboratory scale) production. An external electric field is applied on the pipette tip (spinneret) and a polymer solution is charged to feed through it[78]. On the tip, the droplet is formed as a suspended cone (Taylor cone) because its surface tension is in equilibrium with the electric field[76].

When the surface tension is overcome by the strong electric field, the droplet ejects a tiny jet from its surface to the collecting plate. In the jet stream, the solvent evaporates gradually during the spread of the tiny jet toward the collecting plate. A typical SEM image of PVA fibres spun by electrospinning is shown in Figure 2-6[79].

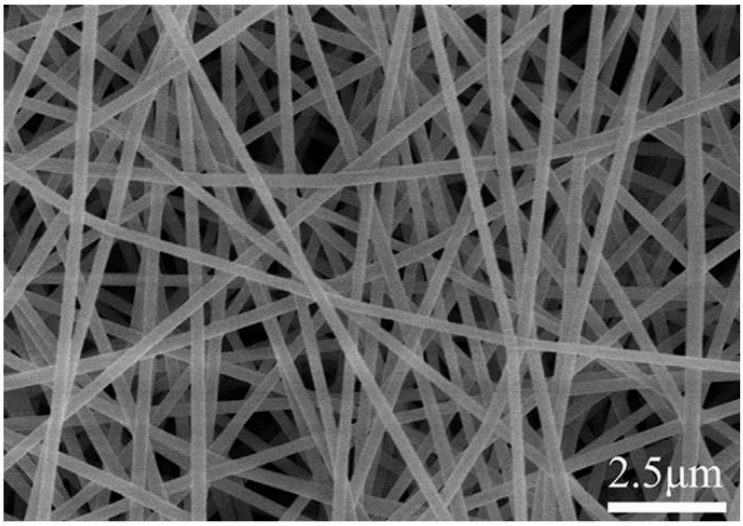

Figure 2-6 SEM image of 7% (w/v) PVA nanofibres by electrospinning[79].

The nanofibre morphology and mechanical properties can be affected by electric field strength, solution properties (viscosity, elasticity, conductivity and surface tension), humidity and temperature. From the experience of electrospinning process control, the flow rate of the polymer solution has an impact on fibre size as well as the applied voltage which is the main parameter greatly affecting fibre formation and its final shape including size, surface structure and number of beads[80] (Figure 2-7).

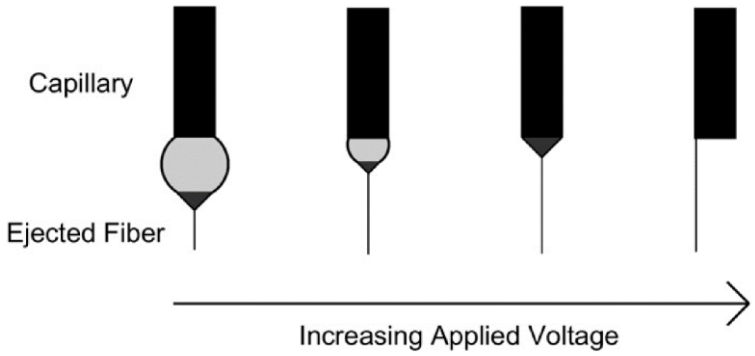

Figure 2-7 Effect of the applied voltage (increasing from left to right) on the pendant drop (depicted in light grey) and the Taylor cone (depicted in dark grey) formation[80].

At the tip of the needle or capillary, a pendant drop is formed with the Taylor cone coming along at lower applied voltages. However, the volume of the pendant drop decreases as the voltage is increased until this Taylor cone forms at the needle tip. The solution stream will be ejected from within the needle if the applied voltage is kept increasing further which results an increase in number of beads.

The reduction of the solution viscosity would also result in fibres with beads along their length[85]. These formed beads may provide the anchorage for load transfer in some applications while using the fibres. However, the beads formation relies on a threshold value of viscosity.

Parameter	Effect on fibre morphology
Applied voltage increasing	Fibre diameter decreasing initially, then increasing (not monotonic)
Flow rate increasing	Fibre diameter increasing (beaded morphologies occur if the flow rate is too high)
Distance between capillary and collector increasing	Fibre diameter decreasing (beaded morphologies occur if the distance between the capillary and collector is too short)
Polymer concentration (viscosity) increasing	Fibre diameter increasing (within optimal range)
Solution conductivity increasing	Fibre diameter decreasing (broad diameter distribution)
Solvent volatility increasing	Fibres exhibit micro-texture (pores on their surfaces, which increase surface area)

Table 2-1 Effects of parameters on fibre morphology for electrospinning[80]

Table 2-1 shows a simple summary of relationships between the processing parameters and the fibre morphology of electrospinning which the study also indicates that the exact relationship differs for each polymer or solvent system[80]. Thus, the quantitative relationships which suit a wide range of polymer or solvent systems can be hard to determine. This, again, confirms that the whole system is very complicated. It also means the flow rate factor is very important during processing and the Taylor cone needs to be considered before the experiment which may apply to other methods sharing the same principle.

Some factors contributing to the mechanical properties of the composite fibres apart from the material properties are surface texture, shape and orientation of fibre reinforcements[85]. To strengthen the matrix material, nanoparticles are also used in some studies as reinforcement. Polymeric based fibres are formed without further treatment which is, however, required for the ceramic and metallic based ones according to the fabrication experience. If the solution for electrospinning is made using volatile solvent, pitted and porous fibres may form. The main mechanism for forming pores and dimples on the fibre surface is phase separation which is induced by using liquid nitrogen between the residual solvent and polymer and by this way using volatile solvent can be avoided. Electrospinning fibres can deliver different drugs like antibiotics and protein because they are flexible in the selection of materials[80].

For the electrospinning process, the yield per spinneret with very small fibre diameters is extremely low[81]. This technique has been explored extensively to achieve hollow, core-shell and microparticle-encapsulated fibres[82]. Without limiting the raw materials, the electrospinning can be used to process particular materials, of which the range is relatively wide as studied[83]. However, one of the electrospinning's limitations is that it

requires the use of high-voltage equipment which also leads to the restriction on the dielectric constant of the spinning solvent by its working principle[84].

Another technique developed for two phase solution spinning is coaxial electrospinning[72,73] (Figure 2-8). The inner needle and outer needle provide different fluid to spin forming core structure fibres.

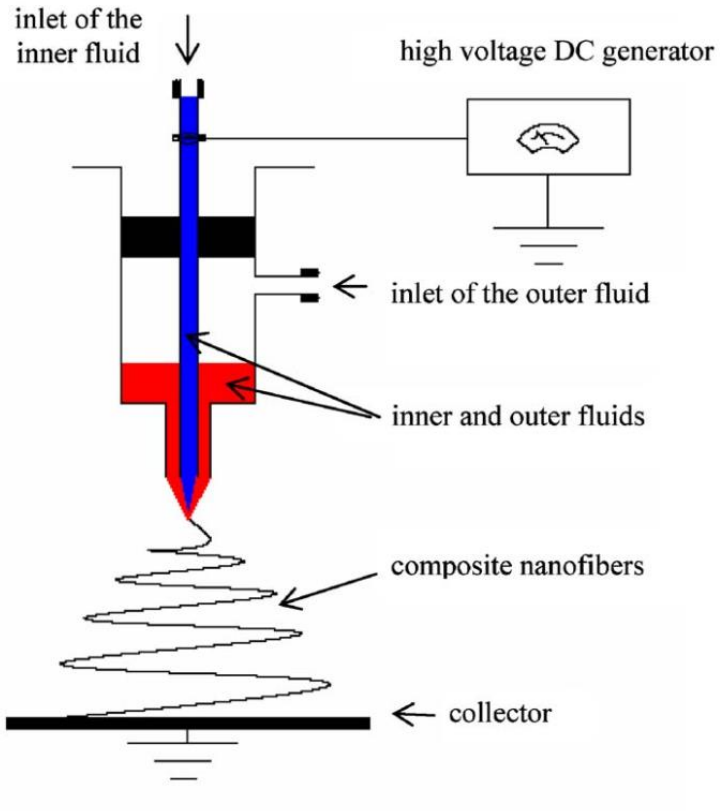

Figure 2-8 Schematic diagram of a typical coaxial electrospinning set-up[72].

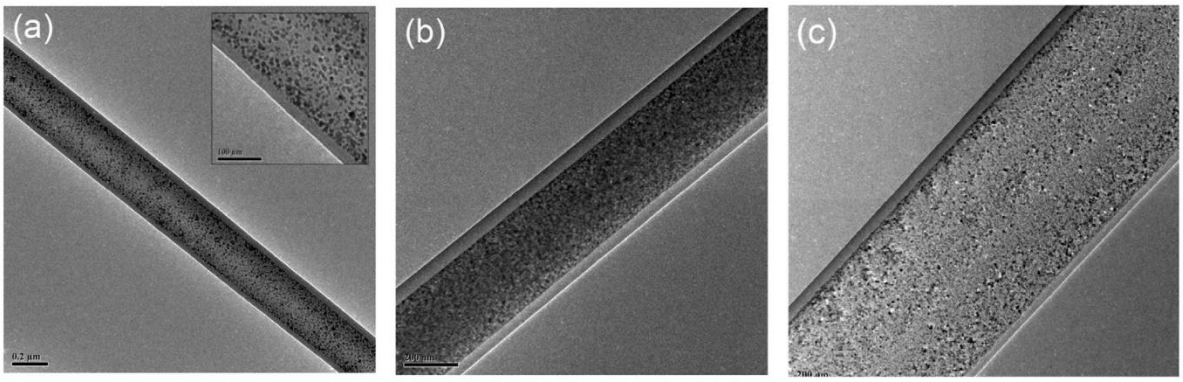

Figure 2-9 Transmission electron microscopy images of core structure nanofibres fabricated by coaxial electrospinning at core flow rates of (a) 5 µl/min, (b) 7 µl/min, and (c) 10 µl/min[73].

The magnetic nanofibres were fabricated by PET as a polymer sheath encapsulating the magneto-rheological fluid as a core using this technique. To achieve this core structure and ensure the magnetic nanoparticles are uniformly dispersed in the core, the values of the core and sheath flow rate are crucial. At different core flow rates of the magneto-rheological fluid, the sheath flow rate was fixed at 5 μl/min and the mass ratio of solution was 1.5:1(Figure 2-9).

2.2.2 Multi-jet electrospinning

Multi-jet electrospinning system was designed to increase the productivity of nanofibre and its fibre cover area on the collector[86]. It shares the same mechanism with electrospinning but has more jets per spinning (Figure 2-10).

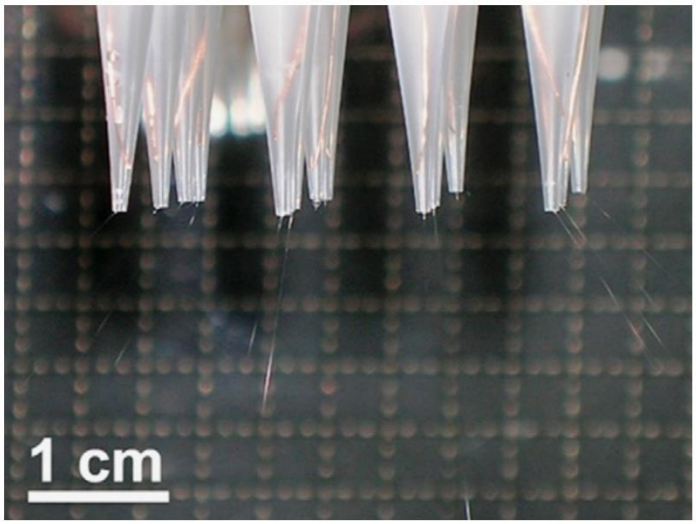

Figure 2-10 Multi-jet electrospinning[86].

The set-ups of multi-jet electrospinning (Figure 2-11) show that the solution and grounded collector can be electrically charged in a different way serving different applications (Figure 2-11 A and B). A secondary electrode, for control purpose, can also be with an electrically charged solution and grounded collector[86]. A different number of jets were tested (2-16) by using PEO solution on this system[86].

In another design of multi-jet electrospinning, several syringes are used as electrodes in parallel alignment to fabricate tissues with different fibre materials gaining more control on each flow of the spinning solution[87] (Figure 2-12). For different material in each syringe, different flow rate can be set to control each fibre size or quantity fulfilling the blend design.

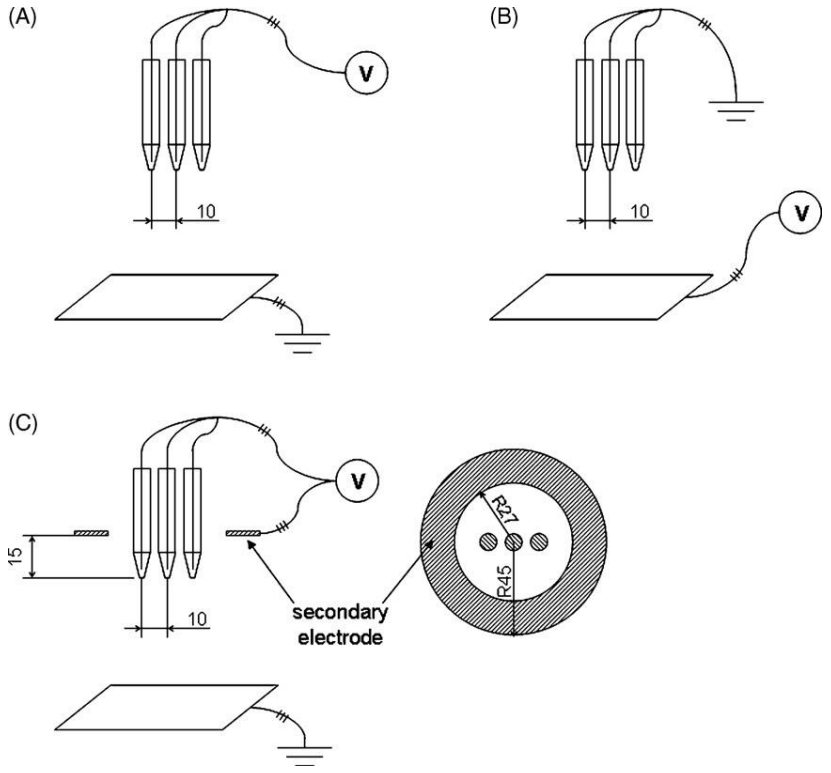

Figure 2-11 Schemes of multi-jet electrospinning set-ups[86].

However, multi-jet electrospinning is more complicated than the single-jet process. One reason is the existence of repulsion among similarly charged solution jets. This should be considered for complex tissue architectures and high efficiencies[87].

For electrospinning, the fibre size is also influenced by the distance between the capillary tip and the collector which was introduced in the last section. Although this distance plays a smaller role rather than applied voltage or flow rate for electrospinning[80]. Normally, the fibre diameter decreases with this distance increasing.

Also, this distance affects the drying process of the polymer fibre which relates to the formation of beads along fibres.

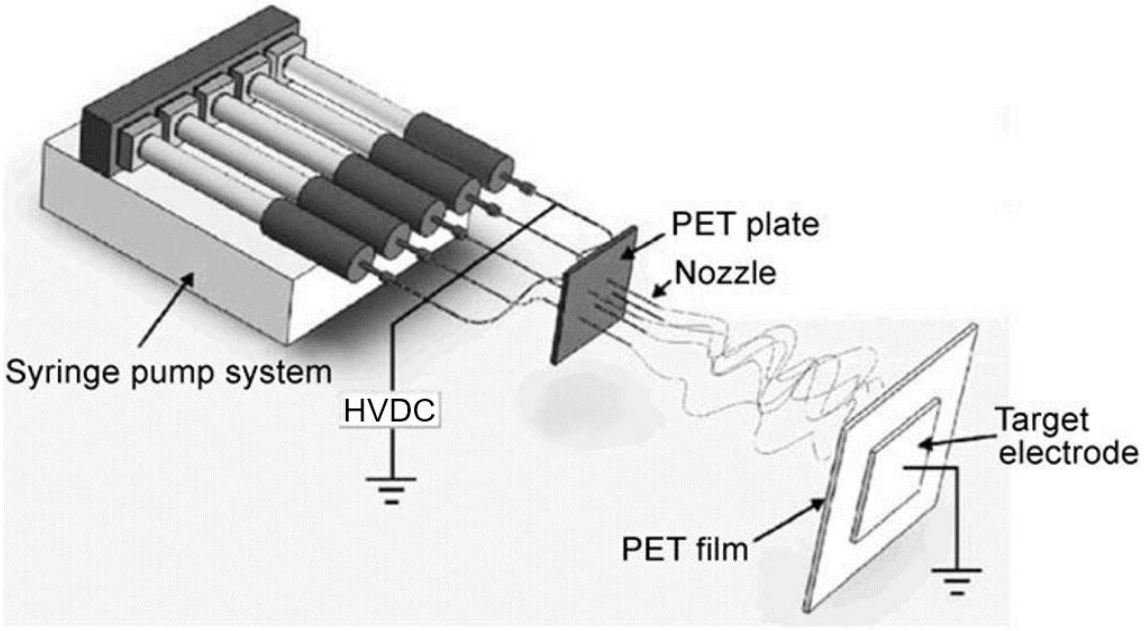

Figure 2-12 An experimental set-up for multi-jet electrospinning. HVDC, high-voltage direct-current power supply[87].

Moreover, collection is the last step of the whole spinning process (even for other spinning methods) before characterization which is important because the samples must be original and their transfer should cause minimum effect. A clean metal plate with or without film protection is needed as a stationary collector for electrospinning. However, different types of designed collector were also developed, such as a rotational collector (a rotating drum/disk)[88], to fulfil a wide range of applications[89].

2.2.3 Rotary jet/Centrifugal spinning

Rotary jet spinning, i.e. centrifugal spinning, is an efficient and rapid method to generate fibres on micro or nano scale at low cost[4]. The apparatus consists of a spinneret (perforated reservoir) which is connected to a motor (variable speed from 4000rpm to 37000rpm) (Figure 2-13). The reservoir, which contains polymer solutions starts rotating and the jet of solution is ejected from a small orifice[90].

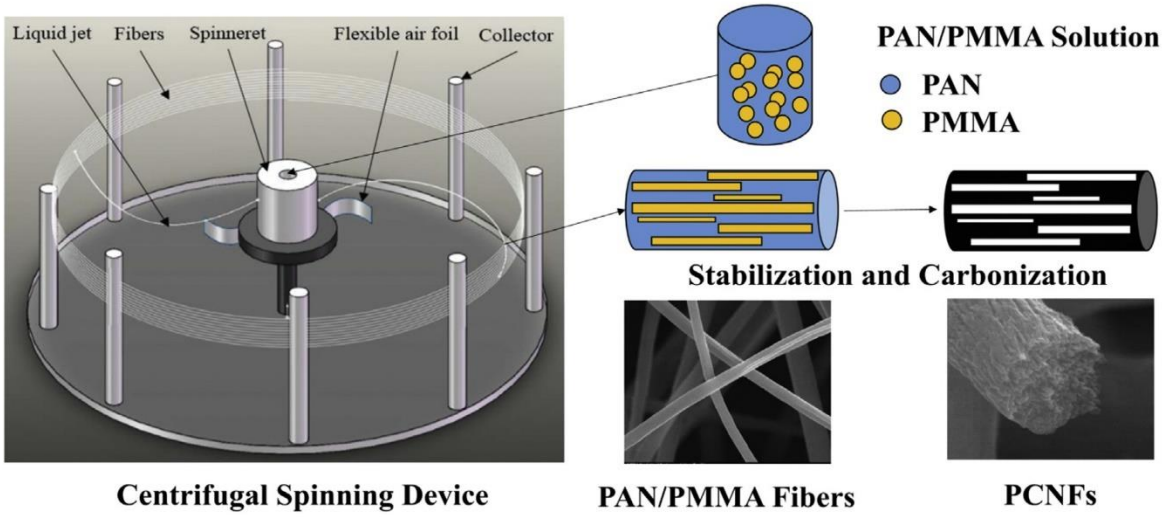

Figure 2-13 Schematic of the centrifugal spinning device preparing polymer fibres[91].

A study shows a simple model for fibre formation by this approach (Figure 2-14): The set-up is shown in (a); The diagram in (b) is seen from the top view where a fibre is ejecting from the spinneret to the collector; Initiation of the jet is in (c) to (f); Images are captured in (d) to (f) demonstrating the jet from the spinneret where the green arrows indicate the end of the jet and the yellow arrows show orifice position; Elongation of the jet is in (g) to (j); In (d) to (f) and (h) to (j), S_0 is 0.85 cm and scale bars are 0.42 cm; Solvent evaporation happens in (k); Fibre colour is an indication of the presence of solvent in the collected fibres, as solvent evaporates, fibre colour changes from red to blue as (l) shows. Colour evolution is consistent with the measured mass change of the spun fibres[90].

The jet is stretched by centrifugal force then the solvent evaporates. The fibres solidify from the jet travelling until it reaches the collector. The process controlling fibre diameter is dominated by the jet extension because most solvent evaporates after fibres have reached the collector plates. PLA solution with different weight concentrations were tested generating fibres using different experimental conditions[92]. Experiments of others using a spinning head (30mm in diameter) were carried out[4].

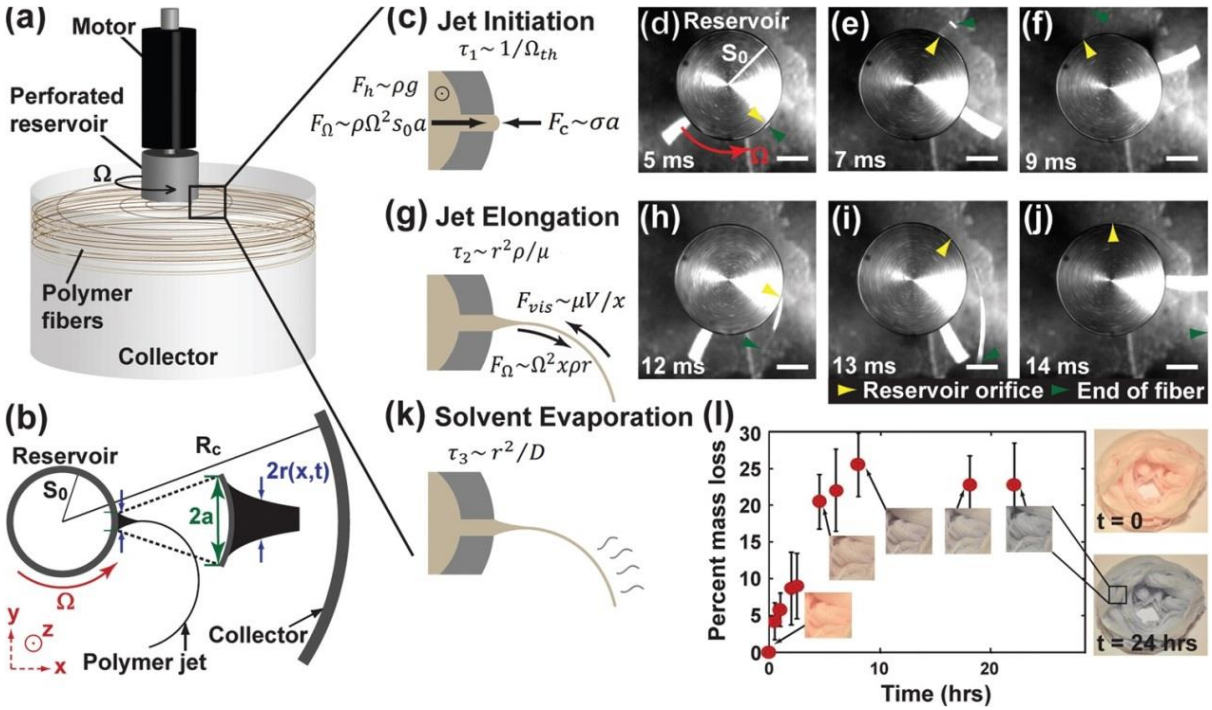

Figure 2-14 Schematic of rotary jet spinning apparatus[90].

The final results of fibre diameters produced by rotary jet spinning can be affected by several factors such as solution concentration, rotational speed, nozzle diameter and nozzle-collector distance (Table 2-2) [4].

	Solution Concentration (wt. %)	Berry Number	Rotational Speed (rpm)	Nozzle Diameter (mm)	Nozzle-Collector Distance (cm)	Fiber Diameter (nm)
	8	7.2	4,000	0.4	10	N/A*
	10	9.0	4,000	0.4	10	406 ± 108
Effect of	12	10.8	4,000	0.4	10	458 ± 135
Concentration	13	11.7	4,000	0.4	10	440 ± 118
	14	12.6	4,000	0.4	10	665 ± 114
	15	13.5	4,000	0.4	10	1077 ± 302
Effect of	13	11.7	2,000	0.4	10	663 ± 232
Rotating	13	11.7	3,000	0.4	10	541 ± 153
Speed	13	11.7	4,000	0.4	10	440 ± 118
Effect of	14	12.6	4,000	0.4	10	665 ± 114
Nozzle	14	12.6	4,000	0.8	10	807 ± 190
Diameter	14	12.6	4,000	1	10	895 ± 256
Effect of Nozzle-	14	12.6	4,000	0.4	10	665 ± 114
Collector	14	12.6	4,000	0.4	20	658 ± 149
Distance	14	12.6	4,000	0.4	30	647 ± 146

*The amount of fibers produced at this solution concentration is inadequate for statistics.

Table 2-2 Fibre diameter statistics of PAN fibres by centrifugal spinning[4].

With the increase of solution concentration or nozzle diameter, the fibre diameter decreases. However, the effect of speed shows opposite results. The nozzle-collector distance has a limited effect. The primary principle enabling the fibre formation process (centrifugal force) directly relates to the spinneret (motor) rotation speed (Figure 2-15) [93].

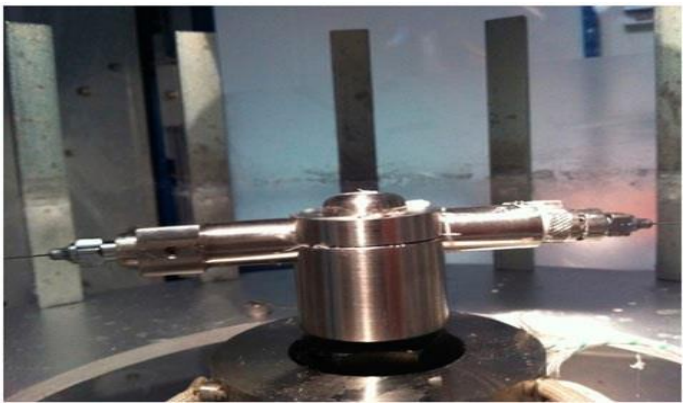

Figure 2-15 Solution spinning spinneret [93].

This method works successfully with PCL/collagen[94]. Moreover, PAN/PMMA fibre was generated which is used for making carbon nanofibres[95] as well as SiO_2/polyacrylonitrile membranes for Li-ion batteries as a separator[96]. As can be seen from Figure 2-15, metal fins were used for better collection of fibres.

2.2.4 Electro-centrifuge spinning

The electro-centrifuge spinning method combines centrifugal and electrical forces. With the control of viscosity of solution, voltage, rotation speed and the flow rate of exiting solution from nozzle, the fibre characterization results show great enhancement compared to electrospinning[97]. The schematic of the set-up is shown in Figure 2-16. A high voltage power is applied to a metallic cylinder (E in the figure, negative electrode) as fibre collector and the nozzle (positive electrode) which is mounted on a circular plate. The system can switch to centrifugal spinning if voltage is not applied.

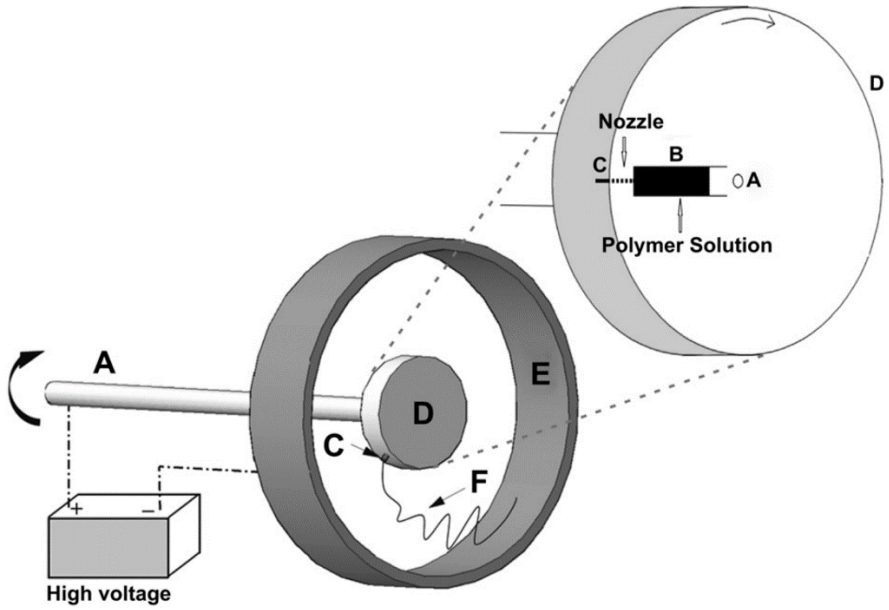

Figure 2-16 Schematic diagram electro-centrifuge spinning of the set-up, (A) axle of rotation, (B) polymer solution container, (C) nozzle tip, (D) encircling cylinder, (E) collector and (F) polymeric jet.[97]

The polymer solution flows through the nozzle and when the circular plate rotates, the solution jet forms. By using centrifugal force and electrical force, the solution becomes a jet at the nozzle exit and the jet is elongated thousands of times to be extremely thin. Long nanofibres can form by the solvent evaporation and be collected on the interior surface of the collector. This system controls voltage and flow rate (by changing the nozzle length) and the effects were studied during fabrication on nanofibre production and diameter[98] (Figure 2-17).

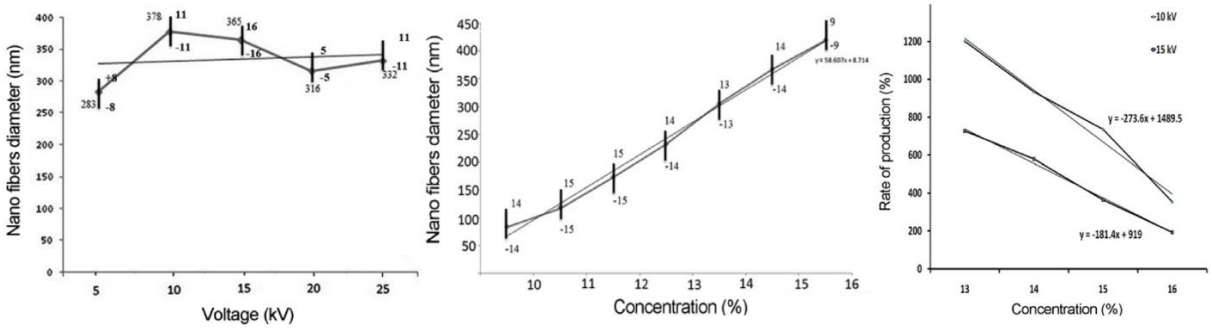

Figure 2-17 The effects of production.[98]

Polymer nanofibre production was tested on this system by using solutions of PAN in DMF and Nylon in formic acid. This approach overcomes the low production rate of

electrospinning. Moreover, it is a powerful method for the spinning solution with extremely low viscosity[97].

2.2.5 Pressurised gyration

The pressurised gyration system uses high pressure gas from a nitrogen cylinder and a high speed rotating vessel to generate micro and nano fibres which can deliver larger scale production[5]. The actual experimental set-up is shown in Figure 2-18. The main working part is a rotary cylindrical vessel (aluminium, 60mm in diameter and 35mm in height) which contains 20 orifices on its circumference. The bottom side of the vessel is attached to a DC motor which provides 10,000rpm, 24,000rpm and 36,000rpm rotating speed. The top cap of the vessel is connected to the pressure lead by a rotary joint. The pressure can be varied up to 0.3 MPa from the gas cylinder (N_2). Aluminium foil is placed around the vessel as a fibre collector which can be replaced by other materials depending on the fibre materials. PEO water solutions were used on this system. Three concentrations were chosen based on the solution viscoelastic nature: 5wt%, 15wt% and 21wt%. Lower concentration promotes bead formation[5].

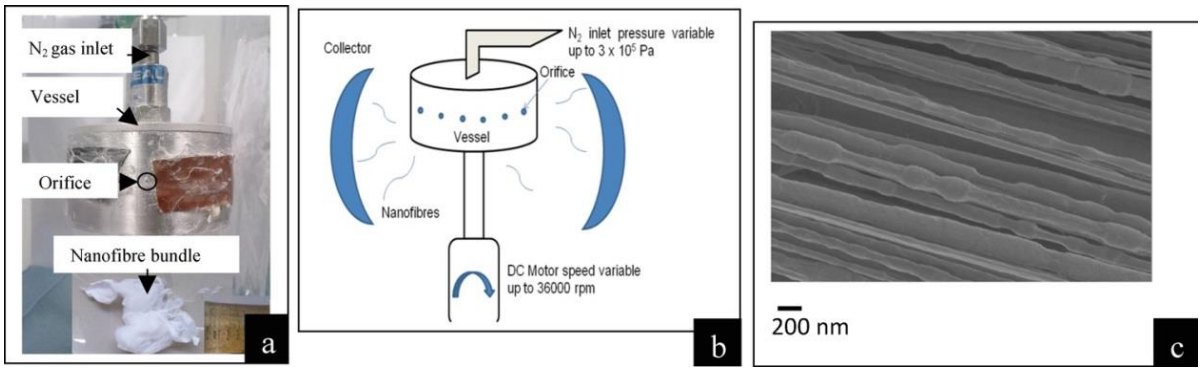

Figure 2-18 (a) Pressurised gyration set-up. (b) Schematic diagram of the set-up. (c) Scanning electron microscopy image of the fibres produced by pressurised gyration[5].

This approach provides fibres with average diameter 60-1000nm. The yield of fibres is much higher than with electrospinning. The relationship between fibre diameter and gas pressure/rotating speed is shown in Figure 2-19 [5].

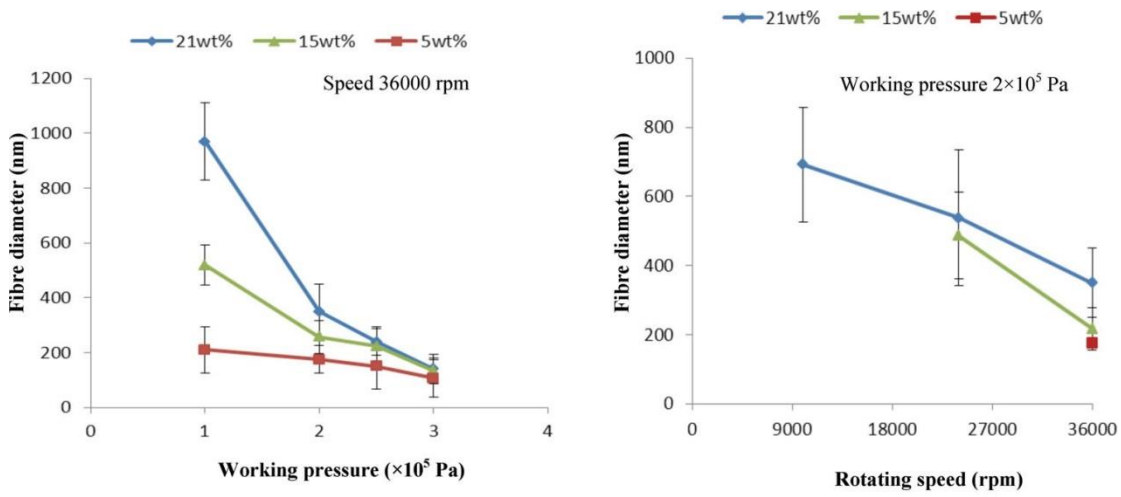

Figure 2-19 The relationship between fibre diameter and working pressure/rotating speed [5].

The Rayleigh–Taylor instability has been introduced as the explanation of forming fibres. The fibre formation in this process is the result of both centrifugal force from high rotating speed and the pushing force from the blowing gas.

The combined force against the surface tension of the polymer solution forms the jet and stretches it out from the vessel orifices into a longer and thinner stream. Then the stream forms a solid dry fibre due to evaporation (Figure 2-18 c).

For pressurised gyration, polymer solution selection mainly relates to its rheological properties, for example, the chain entanglement in the polymer solution[99].

By controlling the pressure delivered and the rotating speed, the fibre diameter could be tuned linearly as well as pore size on fibres. Figure 2-20 shows the SEM images of pore structure on fibres spun by pressurised gyration (with different solvents and gas pressure)[100]. Fibres were made using chloroform (C in the figure), dichloromethane (D) and ethyl acetate (E) at a working pressure of 0, 0.1, 0.2 and 0.3 MPa (0, 1, 2 and 3 along with C, D and E in the figure), respectively.

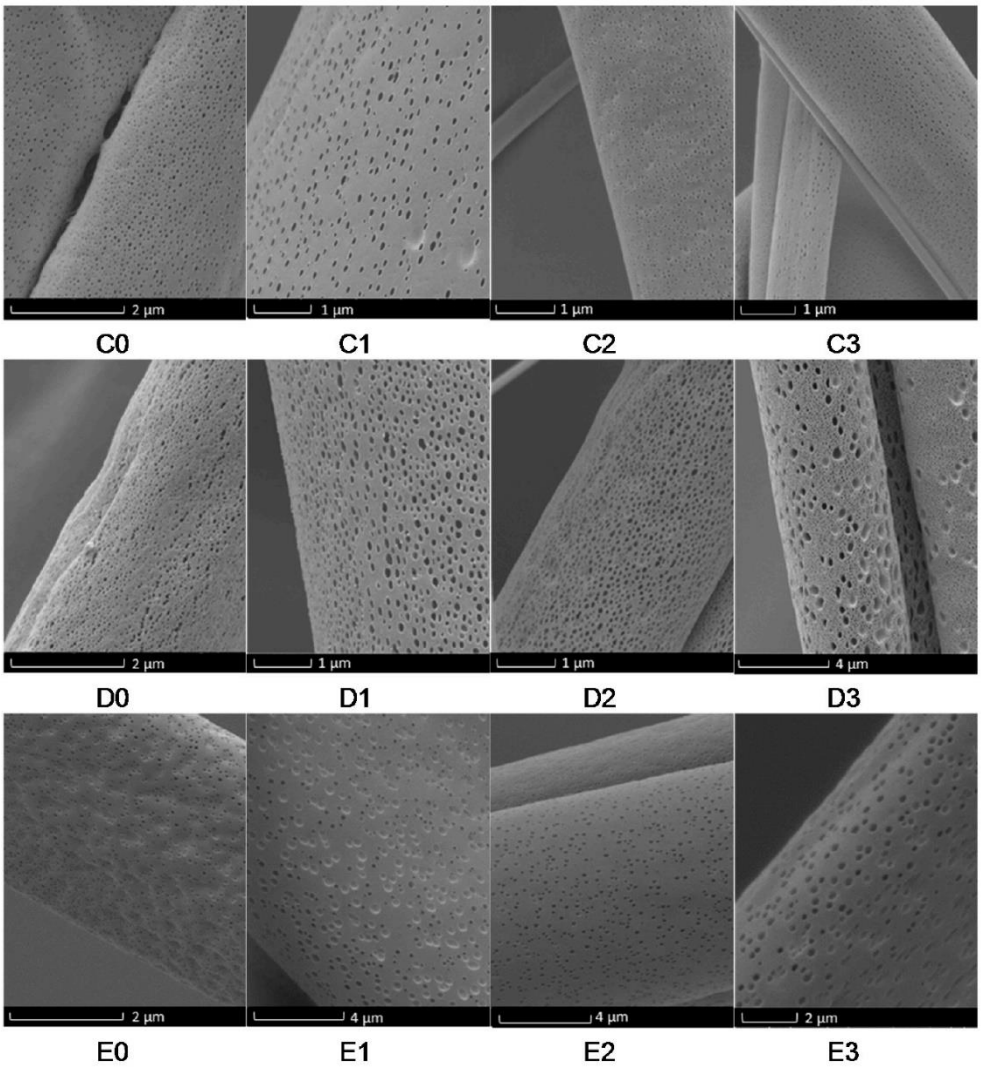

Figure 2-20 Scanning electron microscopy images of PMMA fibres prepared using pressurised gyration[100].

The potential of pressurised gyration can be developed because it is reported generating even micobubbles[6] (Figure 2-21). The effect of different parameters on bubble diameter was studied. Figure 2-21 (a) depicts the bubble diameter change at a gas pressure of 0.02 MPa with a variable rotating speed. Figure 2-21 (c) shows the effect of the gas pressure on bubble diameter at a constant rotating speed of 36,000 rpm. The optical microscopy images of the bubbles generated are shown in Figure 2-21 (b) (10,000 rpm & 0.02 MPa) and Figure 2-21 (d) (36,000 rpm & 0.1 MPa). The change of the bubble diameter at these two parameters is seen to be linear, generally.

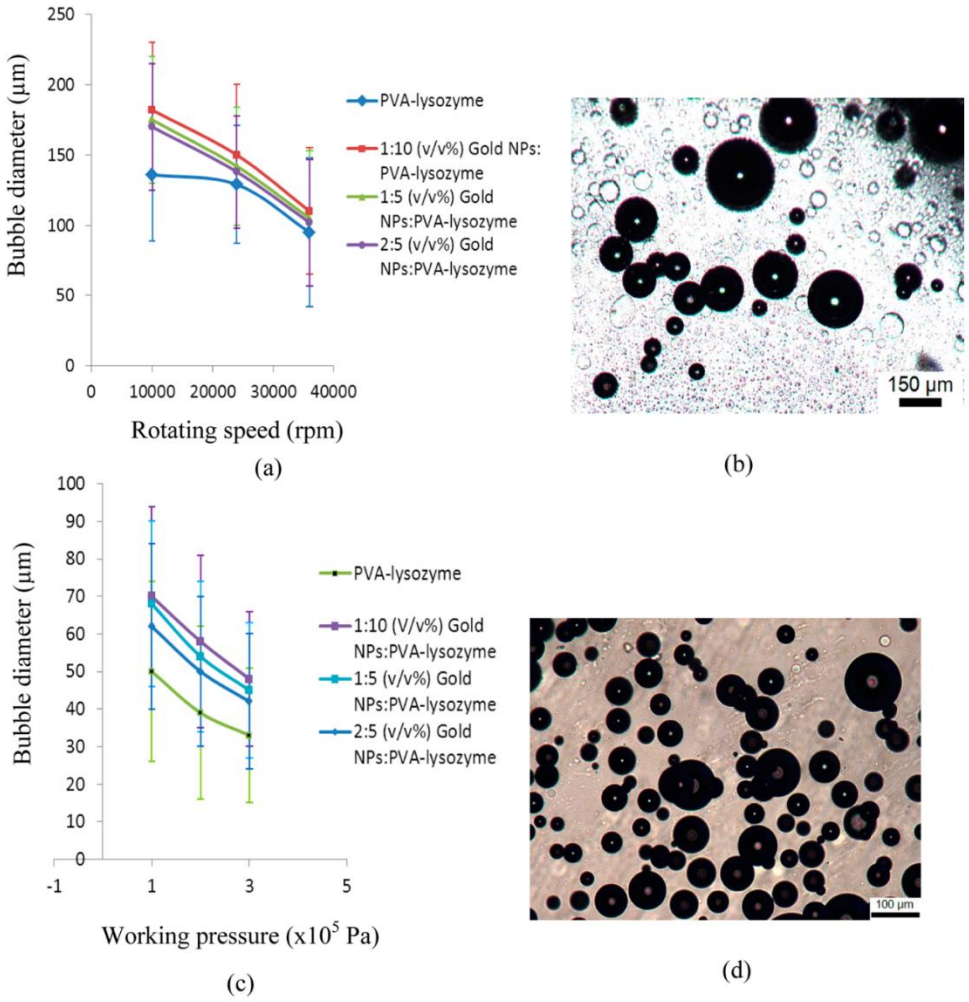

Figure 2-21 Microbubble formation by pressurised gyration (NP is nanoparticle) [6].

Moreover, the relationship between the product form (fibres or bubbles) and spinning parameter (pressure level and motor rotating speed) has been studied (Figure 2-22).

As can be seen in the parametric plot, zone 1 has no bubbles and zone 2 has no fibres. Zone 3 with fibres generated has a boundary to zone 4 with bubbling which relates to the rotating speed.

Furthermore, zone 5 is the fibre formable region for PVA solution only. This confirms that pressurised gyration has the features of processing synthetic polymer fibres, composite fibres and microbubbles.

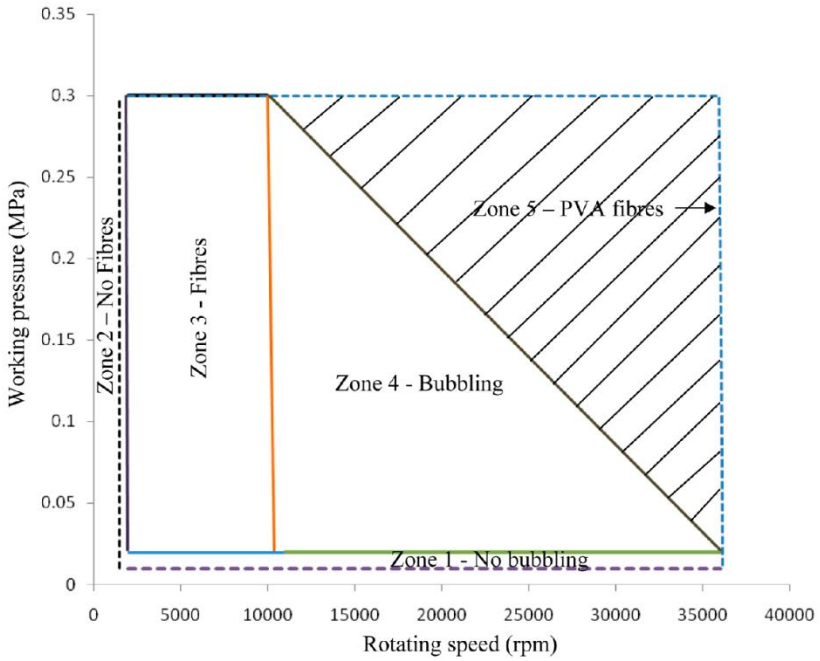

Figure 2-22 The relationship between the product form and the spinning parameter[6].

For fibre collection with pressurised gyration, fins were also used. The fin collector is designed to collect fibres as a mat format[101](Figure 2-23). As some fibres require a specific shape in large scale after spinning for a test or designed application, they need to be in the shape right after the spinning.

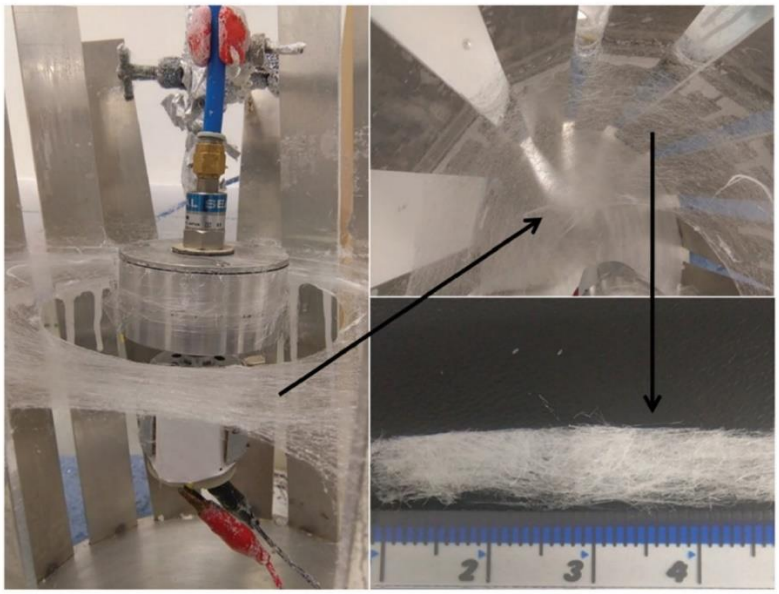

Figure 2-23 The shape memory polymer fibres/mats prepared by pressurised gyration[101].

However, due to the properties of some spinning material, these fibres as final spun product have less flexibility. For example, they can be fragile to form a mat or difficult to bend like a spring. Therefore, fins are used in this collector to keep all the fibres spun in a form. This collector works well with the pressurised gyration producing PLLA/PMMA composite shape memory fibres (Figure 2-23)[101]. The final product achieves a shape memory function proofing the reliability of fin collector.

15 aluminium fins construct the fin collector (Figure 2-24). Several of them need to be removed when using around the motor because they block the path of the crank part.

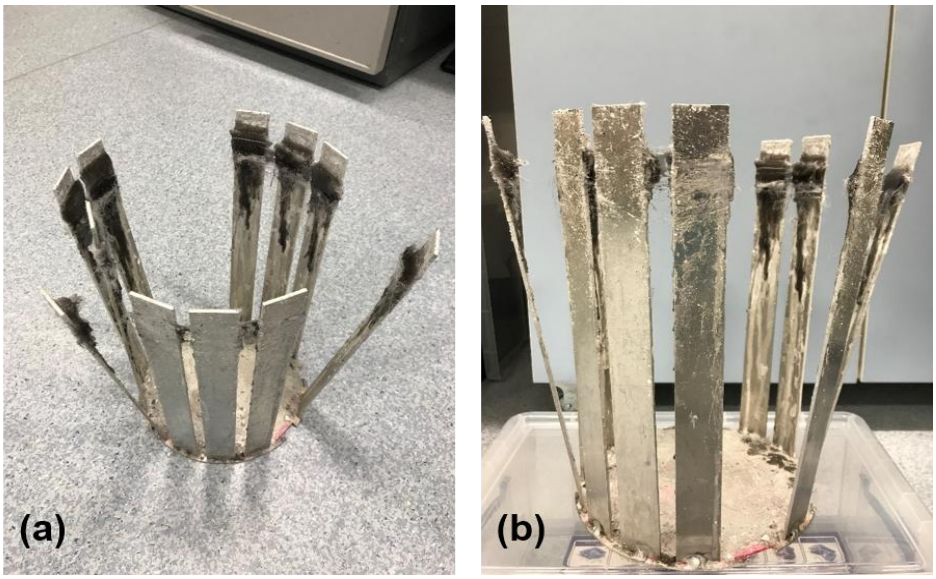

Figure 2-24 Fin collector.

Aluminium is light-weighted for use, and with well mechanical machining property, it is easy for manufacturing and repairing (part replacing). The fin's dimension is 2.5mm×30mm×300mm forming an angle of 80 degree to the horizontal plane with a 10mm gap to each other from the bottom. The round base is 2.5mm thin with a diameter of 200mm.

It is suitable for fibres formed as mat along the metal fins. However, the short distance to the orifices restricts some polymers because they may require more space for the

solvent to evaporate. Moreover, it is very hard to clean as can be seen in Figure 2-24. Therefore, different polymers may mix together on its surface causing impurity of the samples.

2.2.6 Pressure driven spinning

The pressure driven spinning process was devised to overcome the hazards and limitations of the electrospinning system such as the requirement of high voltage which may not be available in some circumstances[102]. The main parts of the device are stainless steel medium bore needles and the autoclavable chamber. The inner bore diameter of the needle varies from a few micrometres to several hundred micrometres. The needle is connected to a pressure chamber constructing a coaxial structure which has six exit orifices around the protruding needle on the surface. The mechanism of spinning microscale or nanoscale fibres on this device is to apply the pressure (0-0.6 MPa) to the chamber and the flow rate to the needle.

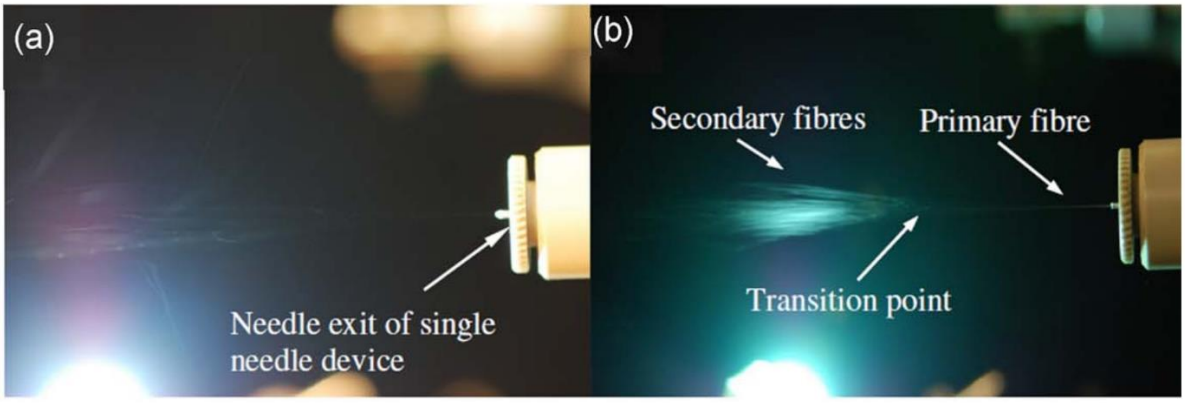

Figure 2-25 The pressure driven spinning process device[102].

Figure 2-25 is shown of the method at the working status of fibre spinning. A syringe pump is used for syringing the prepared solution into the single needle device. The

pressure applied to the chamber provides a pressurised by-pass flow through its exit orifices[102].

Different polymers have been tested fabricating composite fibres by this system such as PEO, PCL, PVA and PLLA. Several have porous texture on their surface. PEO solution was used with different concentrations and with nanosuspensions mixed (SiO_2 nanoparticles and multiwalled bamboo-type nanotubes). The fibre size varies from 35nm to 387nm[102]. The parameters affecting the controlled fibre formation have been investigated. The functional materials generated through this method can be applied to the biomedical area.

2.2.7 Solution blowing

Figure 2-26 shows the schematic diagram of the solution blowing apparatus which utilises high-velocity gas flow as the force to drive polymer solution into fibres[103].

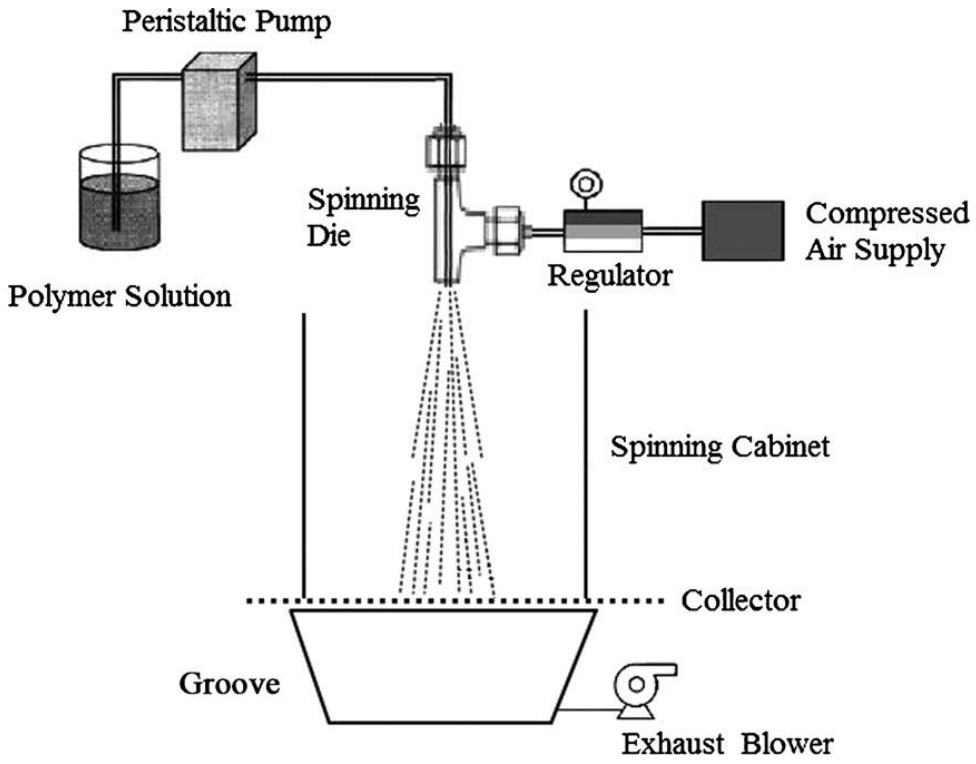

Figure 2-26 Schematic of the solution blowing apparatus[103].

An annular nozzle used as a single nozzle spinning die is coaxially surrounded by a gas cavity (Figure 2-27). The peristaltic pump controls the polymer solution supply. The compressed air goes to the air cavity controlled by the pressure regulator. The stream of gas flow blows the polymer solution stream into fibres when the solution is ejected out of the nozzle tip. A heating unit is equipped to heat the air within the spinning cabinet to accelerate the evaporation of solvent. The exhaust blower under the collector removes air from the evaporated solvent. Cellulose nanofibres (260-1900nm in diameter) were successfully made using this method[103]. Coaxial structure fibres were achieved through blowing cellulose solution (as a core) and PEO solution (as a shell). This set-up uses mesh-like collector[103].

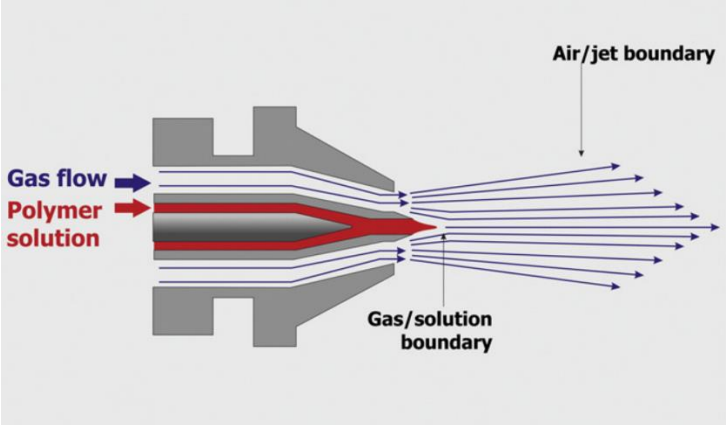

Figure 2-27 Solution blowing process[84].

Furthermore, if the polymer solution or even the polymer material without solvent (like a power) requires high temperature to heat or melt, the solution supply needs to be modified as well as the nozzle for some instance. A melting system, for example, has been introduced into the blowing system to melt and generate fibres which sometimes is also called the melt blowing method. Unlike the solution blowing method described above which normally requires room temperature for the polymer solution, a polymer melt is extruded through an orifice die during melt blowing. The melt with a jet is drawn by the hot air at the same temperature as the molten polymer.

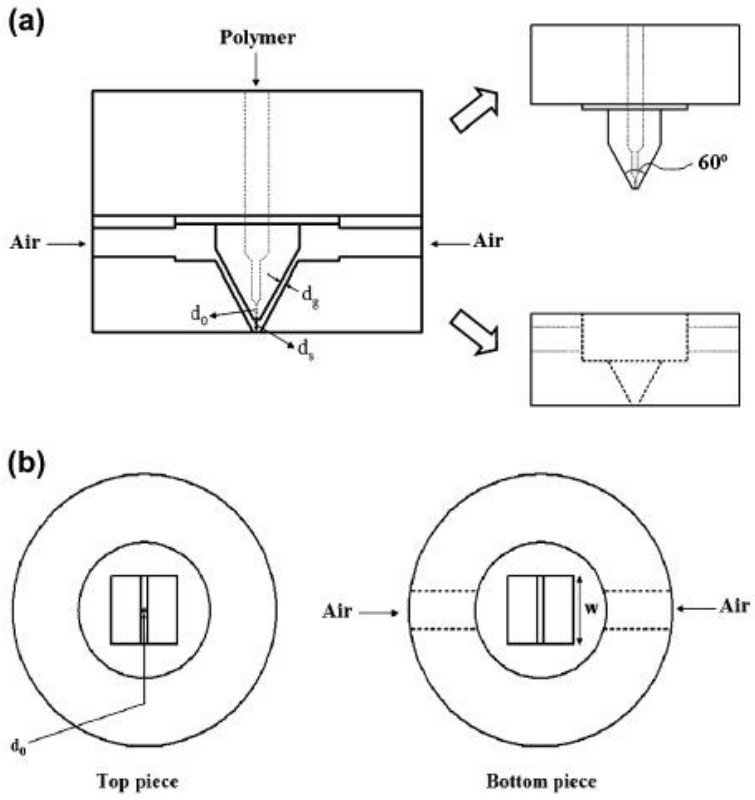

Figure 2-28 Schematic of the die used in the melt blowing method. (a) Sectional views of the die. (b) End-on views of the two parts [104].

The equipment reported has a v-slot form which supplies two air streams (Figure 2-28). Melt blown PS, PP, and PBT micro/nano fibres (average diameters ⩽ 500nm) were made through this method[104].

2.2.8 Pull spinning

Pull spinning apparatus consists of a high-speed rotating bristle which dips into a polymer or protein reservoir and pulls a droplet from the solution into a nanofibre[105](Figure 2-29). The figure shows the schematic of the pull spinning method. From the side view illustration of a fibre, it is seen that the red arrow indicates the location of the bristle/fibre interface as well as the green one points the nozzle location.

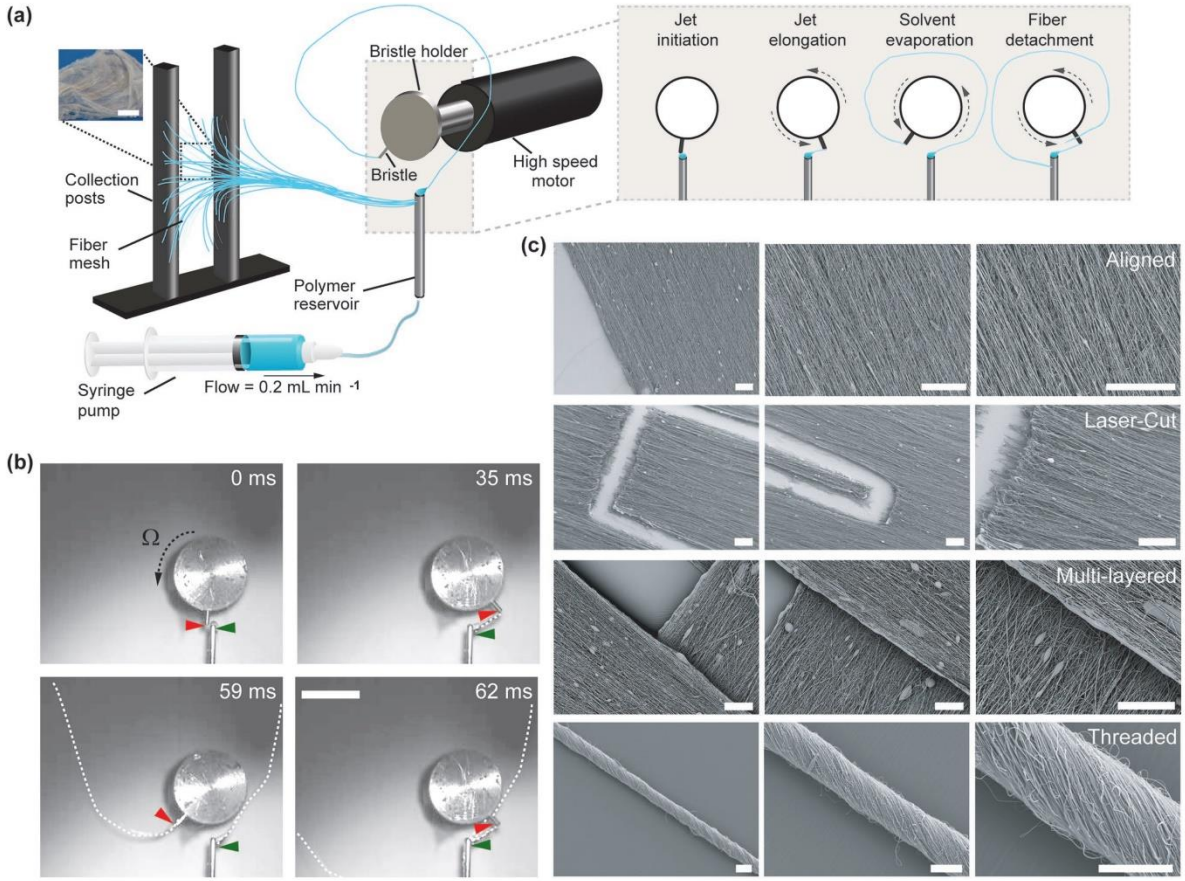

Figure 2-29 Schematic and products of the pull spinning system[105].

Moreover, a fibre formed throughout one revolution is represented by the dashed white line. A nonwoven network would be formed by a multiple layer collection of fibres. Its composition can be adapted to multiple applications as well as the orientation. As a rapid fibre manufacturing platform, textile design is showed. The system uses two posts for fibre collection.

2.2.9 Pressure coupled infusion gyration

After the infusion gyration was invented which will be explained in details in Chapter 3, a T-junction was used to combine the gas pressure and the flow rate into gyration system, i.e. pressure coupled infusion gyration[106] (Figure 2-30).

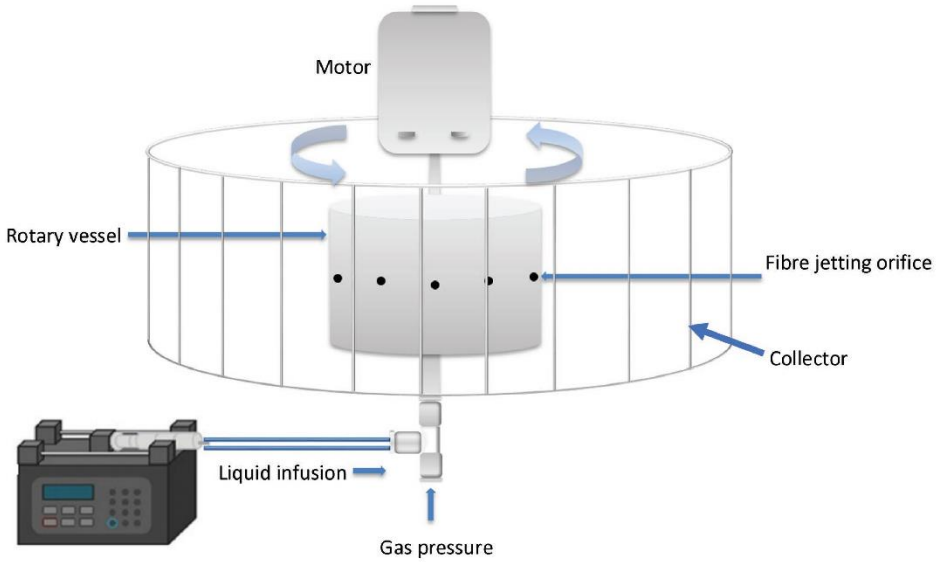

Figure 2-30 Schematic diagram of the pressure coupled infusion gyration equipment[106].

The collection is also studied by this method that the collecting distance affects the fibre shape[106].

A squirrel-cage has been designed and used to help collect the fibres in a round format which is easier to clean because the smaller size fits the cleaning container with water or other solutions (Figure 2-31).

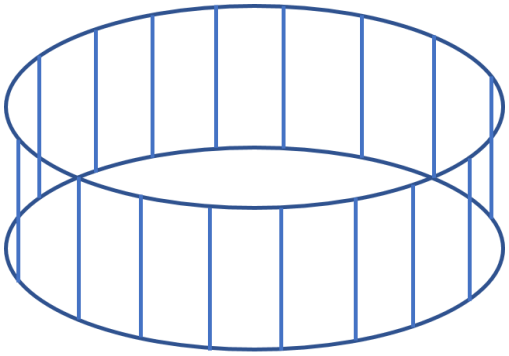

Figure 2-31 Squirrel-cage collector schematic.

A different concentration of PEO-water solution has been tried as well as pressure, rotation speed and flow rate to test the system to map the parameter relationship (Figure 2-32, Figure 2-33).

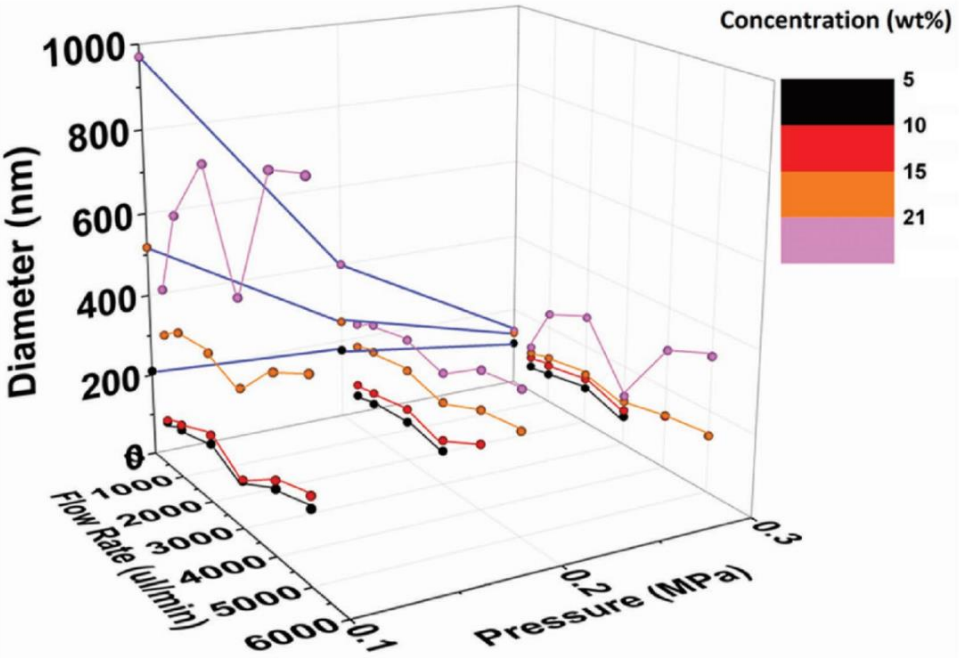

Figure 2-32 Combined effects of the flow rate and the pressure on mean fibre diameter[106].

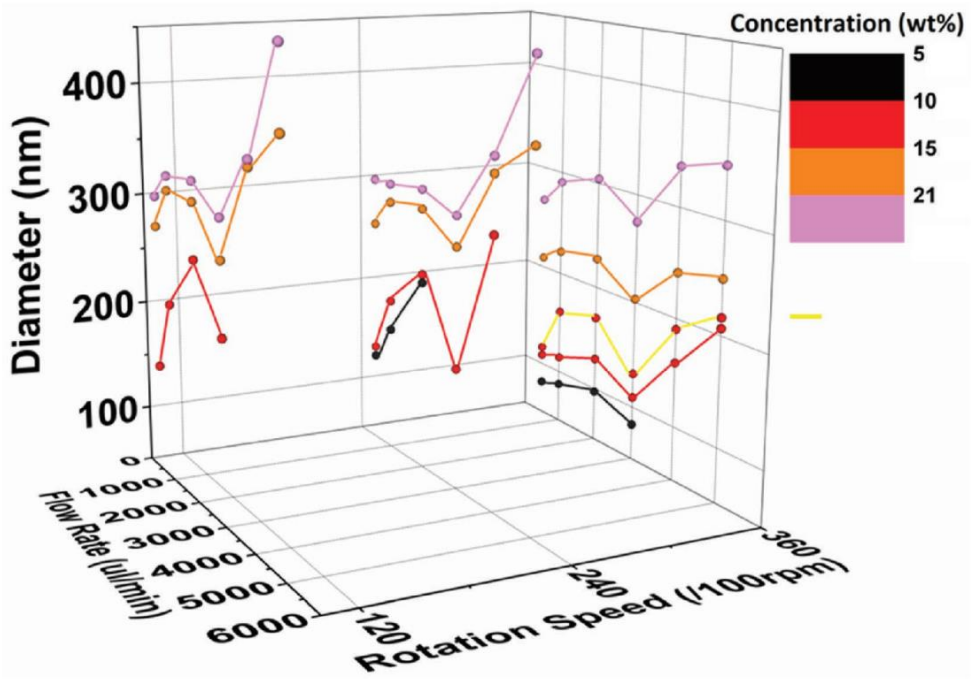

Figure 2-33 Combined effects of the flow rate and rotation speed on mean fibre diameter[106].

It is noticed that there is a drop of mean diameter at the flow rate of 3000 μL/min which happens for different concentrations of PEO-water solution. This was also observed

with infusion gyration showing the complexity of the gyration-serious system which needs will be fully discussed in Chapter 4 and 6.

2.2.10 Summary

From the review of fabrication methods above, the same principle and procedure are shared by many which are pulling of the solution stream into a thinner one to be fibre. This driving force for the electrospinning process which is more widely used is from the strong electric field generated by the high voltage applied, however, the gyration and blowing process apply centrifugal force and gas pressure, respectively. A comparison study of methods has been done by other researchers[107] (Figure 2-34).

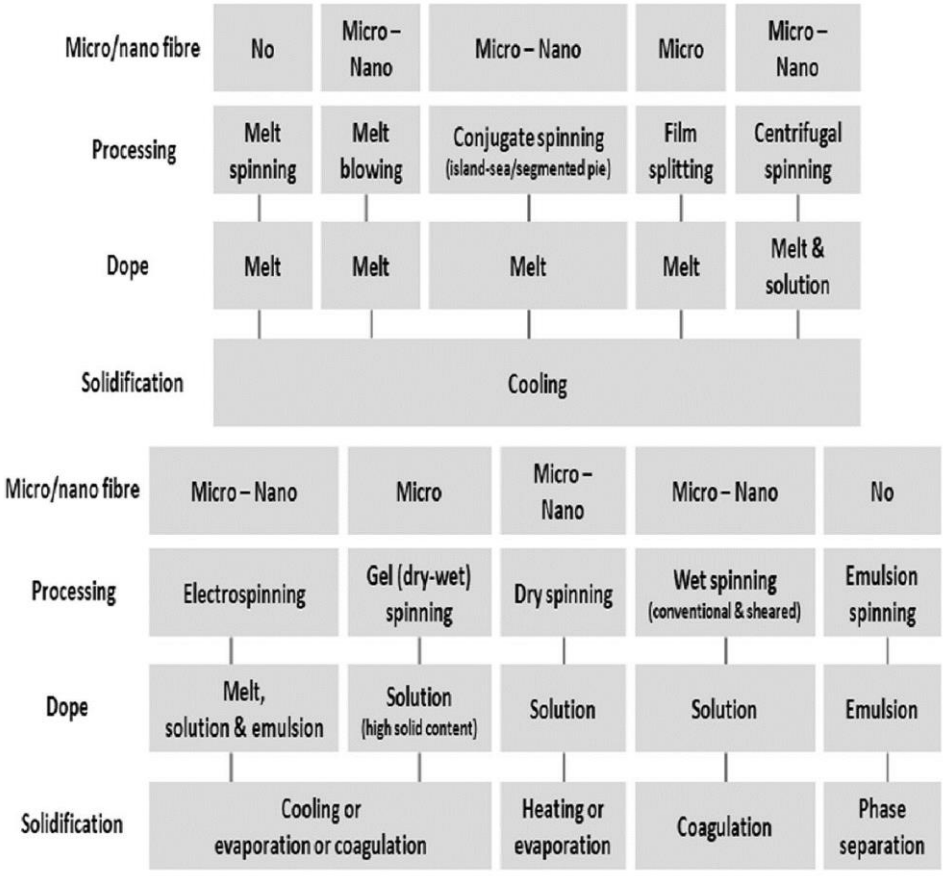

Figure 2-34 A concise comparison of fibre spinning processes[107].

The materials used for fibre formation have been developed to facilitate the incorporation of fibres with biodegradable[16,17], antibiotic properties[18] and even those that include living tissue[19–21]. Extensive progress has also been made in the scale-up of such materials targeting industrial applications[22]. Despite the wealth of research conducted, such micro or nano fibres have not yet, however, made it to the clinical trial stage of biomedical applications. This can be attributed to multiple factors, from mass production to long-term stability of the fibres *in-vivo*. For example, electrospinning, which is the main synthesis method of fibre formation, poses many challenges to their sustained usage in medical applications. Solution polarity needs to be concerned as its principle uses an electric field to drive the jet[92]. The lack of control over fibre diameter and pore sizes, as well as the random, non-woven nature of the fibres produced, cause difficulty in cell-penetration, which is a key factor in sustained use of scaffolds for tissue engineering[108,109]. While electrospinning is effective in producing microscale fibres, smaller diameters are difficult to obtain[110]. Attempts at customizing fibre morphology *via* this technique are complicated and lead to lower yields[111]. Moreover, electrospun fibres have inherently weaker mechanical strength than cast fibres and the solvents and cross-linking agents involved in the process often lead to toxicity and non-compatibility in biological systems[112].

Alternative spinning techniques have been developed to counteract some of the drawbacks of electrospinning[113]. These, however, are not without flaws themselves. For example, electrospinning has a needle clogging problem for some polymer solutions which is not observed with pressurised gyration[114].

Biospinning is a technique suitable for producing fibres with greater mechanical strength, such as scaffolds for tendons or bones[115]. Nevertheless, this method is

hampered by high cost, difficulty in scale up, longer production times and lack of customizability. Meltspinning can create fibres by extruding a heated polymer through a spinneret with textural-control for cell applications[116,117]. Yet, high energy costs, expensive equipment and difficulty in producing cell-incorporating fibres are considerable impediments. The latter issue can be solved *via* an interfacial complexation process, to encapsulate cells, which is also cheaper[118]; despite this, limitations in scale up, materials and dimension control are significant disadvantages. Overall, a technique to produce such biocompatible fibres in a facile, fast, and cost-effective manner, with controllable sizes and the potential for scale up, is highly desirable. If the above is also coupled with the ability of remote actuation, it can lead to significant advancements in drug delivery and tissue engineering.

2.3 Controlled Drug Delivery by Fibres

In recent years, drug delivery has been researched making significant progress for clinical use. Different kinds of materials have been studied and tested for better performance. This includes improving the drug volume load and controllable release. For the controlled part, it separates into trigger mechanism (switching on and off) and release rate adjustment. Researchers use specific material and innovative methods to develop drug delivery systems with different condition response. A large part of the systems is polymer based with pH-responsive control[119], temperature control[120], ultrasonic control[121] or magnetic control[122]. They produced gel beads[123] or bio-film[124] to load more drug. Some research uses porous material, having a better capacity for absorbing particles, as a scaffold to carry and release drugs[125].

Fibre in micro or nano scale is excellent material for loading drugs because of its extreme high surface-to-volume ratio[1]. One has been reported being used for lowering the environmental pollution. This nanocomposite is designed to release herbicide particles by temperature enhancing the utilization efficiency[126].

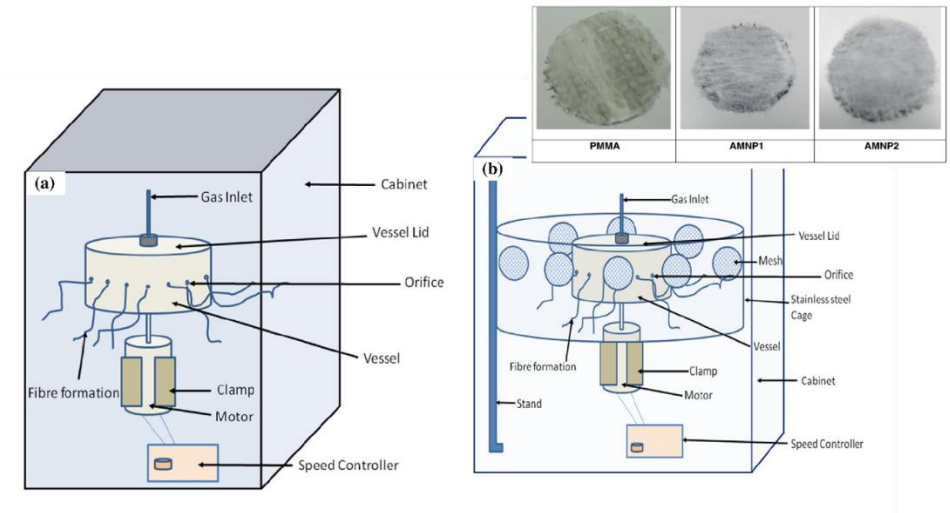

Figure 2-35 (a) Schematic of conventional pressurised gyration rig. (b) Schematic of modified rig to deposit fibres on meshed metallic discs for making filters.[127]

Some use electro-spun copolymer fibre mats for wound dressing like curing burn skin[128]. For other purposes, antibacterial fibres with special nanoparticles were successfully produced[127](Figure 2-35). However, without control function, it still has limited applications. To achieve this, movement controllable material is introduced as promising materials in a lot of areas. Some research shows active polymer film moving like waves driven by light[129] (Figure 2-36). Except for the design of movement control, many polymers have been researched to use for drug release[130]. That somehow confirms the potential of polymers which is safe for the human body and capable of delivering drugs as well. A comparison of electrospinning and pressurised gyration for drug release study using Amphotericin B and itraconazole loaded PVP fibres concludes that the pressurised gyration is a promising method with rapid production of fibres compared to electrospinning[114] (Figure 2-37).

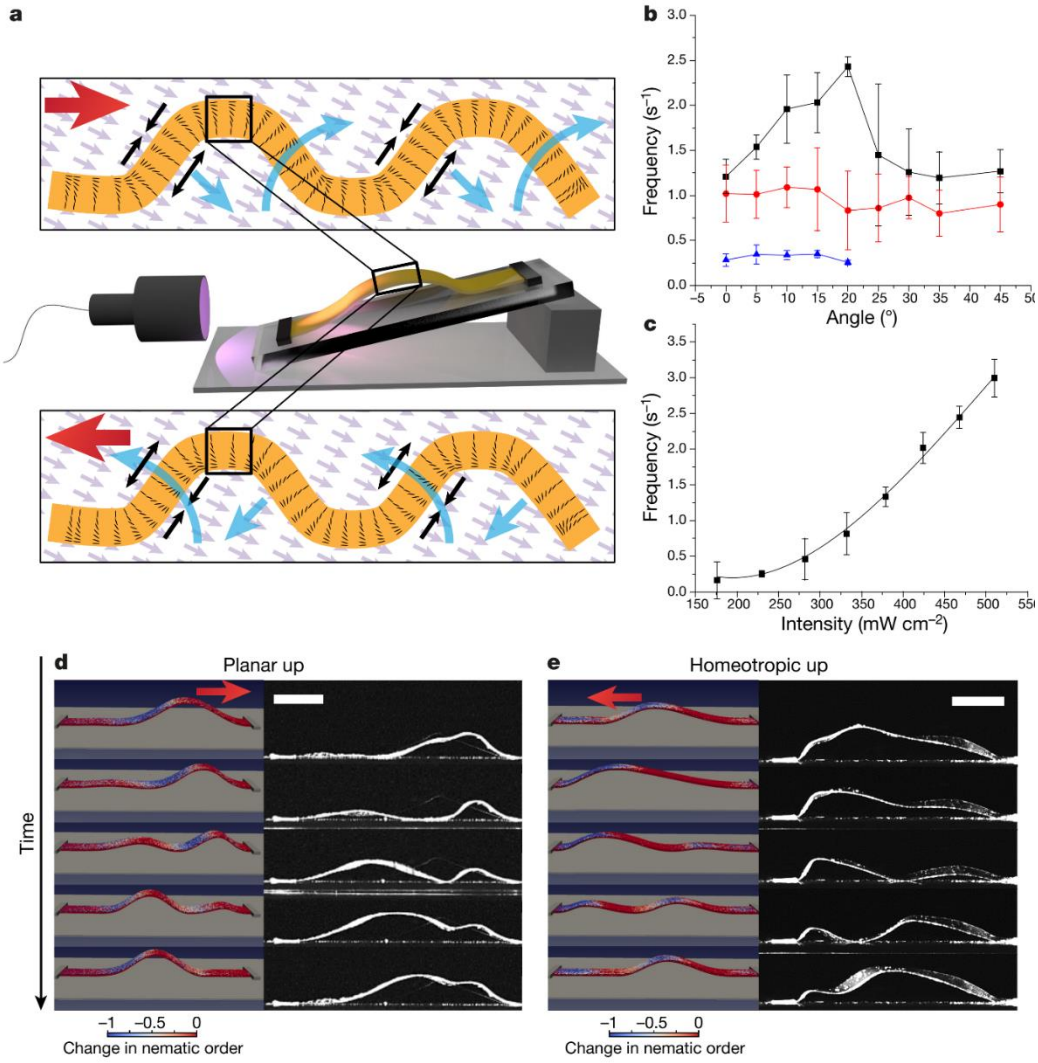

Figure 2-36 Mechanism of wave propagation and parameters that influence the propagation speed[129].

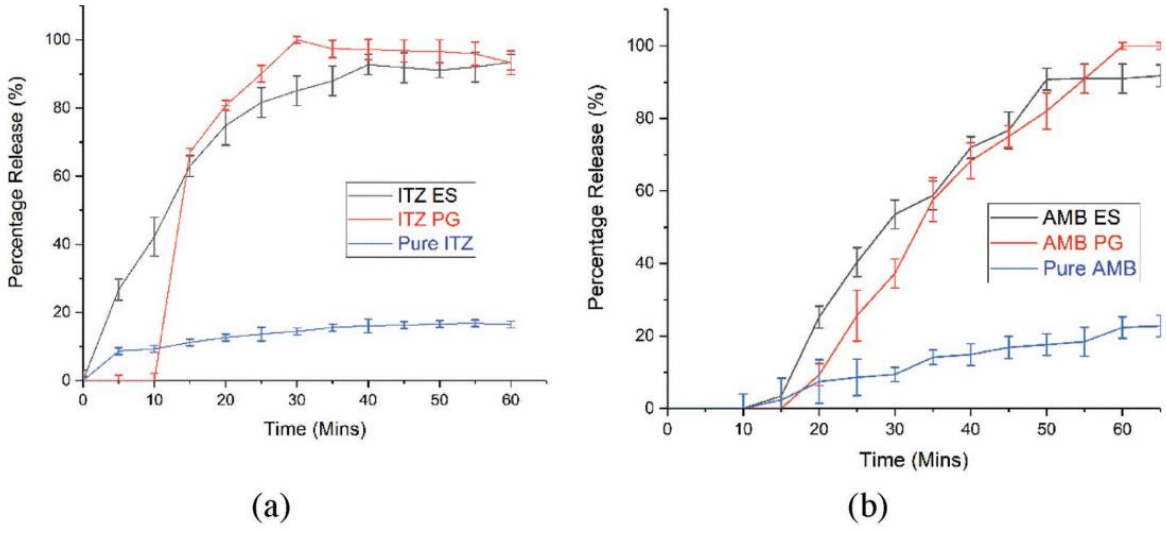

Figure 2-37 Drug dissolution profiles a) Itraconazole-loaded fibres and b) amphotericin B fibres[114].

Chapter 3.

Experimental details

3.1 Materials

All reagents and chemicals were used as received, without further modification. The information of materials and suppliers are provided.

3.1.1 Polyethylene oxide

Polyethylene oxide (i.e. PEO) is a non-ionic homopolymer of ethylene oxide units with CH_2CH_2O. It is biocompatible with extreme low toxicity and commonly used in the food and pharmaceutical industry.

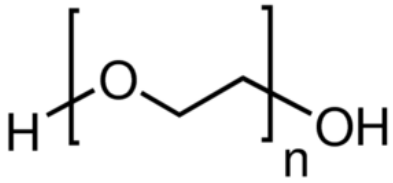

Figure 3-1 Chemical structure of Polyethylene oxide.

PEO was chosen to dissolve in water as the base spinning polymer solution regarding its safety (for the engineered protein to be used in the experiment) and well fibre formation by gyration such as pressurised gyration from the literature review.

Polyethylene oxide (PEO, powder, molecular weight: 200000 g/mol) from Sigma-Aldrich (Poole, UK) was used. To find the suitable PEO concentration of its aqueous solutions to spin by infusion gyration, 5%(wt), 10%(wt), 15%(wt) and 21%(wt) PEO-water solutions were tried and studied.

3.1.2 Poly(vinyl alcohol)

Poly(vinyl alcohol) (i.e. PVA), linear formula $(C_2H_4O)_X$, is a water-soluble synthetic polymer which is ideal bio-material reported being used in food and medical applications. It is often used to form thin films or as a surfactant, but due to its rheological property, it is rarely spun into fibres by gyration series approaches.

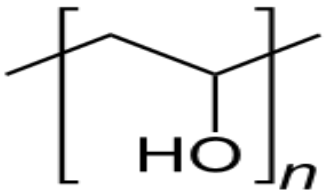

Figure 3-2 Chemical structure of Poly(vinyl alcohol).

In this study, three types of PVA polymer powder, with different molecular weights, were obtained from Sigma-Aldrich (Gillingham, UK): (1) PVA (363170, Mw 13,000-23,000, 87-89% hydrolyzed), (2) PVA (363138, Mw 31,000-50,000, 98-99% hydrolyzed), (3) PVA (363065, Mw 146,000-186,000, 99+% hydrolyzed).

3.1.3 Fluorescent gold binding fusion protein

Fluorescent proteins (DsRed_AuBP2, MBP-DsRed-AuBP2 and GFPuv-AuBP) are all made from Bioengineering Research Center (BERC), Department of Mechanical Engineering, University of Kansas (KU) (Lawrence, KS 66045, USA). To easily track the integration of Au-BP or Au-BP2 (with sequences WAGAKRLVLRRE or WALRRSIRRQSY) peptide into the polymer fibres, the gold binding peptide is genetically conjugated to a biomarker protein, i.e. red/green fluorescence (DsRed/GFPuv). The resulting protein with gold binding peptide tag (DsRed-AuBP2, MBP-DsRed-AuBP2 or GFPuv-AuBP) is hypothesized to blend into fibre formation by providing well-defined organic-inorganic surface interactions to decorate gold

nanoparticles embedded along the fibres while keeping its biological function, i.e. fluorescence property, intact.

3.1.4 Gold nanoparticles

Gold nanoparticles (average particle size: 10nm in diameter, stabilized suspension in 0.1mM PBS, reactant free) used for binding the peptide from the fluorescent proteins are from Sigma-Aldrich (Poole, UK).

3.1.5 Magnetic nanoparticles

Fe_3O_4, iron oxide, is a natural magnetic material which has strong magnetism and low toxicity. Its other forms, particles for example, keep the same magnetic property which is to be utilized in this study (fibre drug release part) for remote actuation and mobility control. If the iron oxide particle is within nano-size as that used in the experiment, it has the potential for embedding in nanofibres. The Fe_3O_4 magnetic nanoparticles (20nm, average diameter), i.e. MNPs, which were used are from US Research Nanomaterials, Inc. To prevent agglomeration, citric acid (Sigma-Aldrich, ACS grade >99.8%) has been used to process the particle powder.

3.1.6 Acetaminophen

Acetaminophen (analytical standard, powder) was purchased from Sigma-Aldrich (Poole, UK) which is an analgesic drug widely used to moderate pain in treatment. Its linear formula is $CH_3CONHC_6H_4OH$ and the molecular weight is 151.16.

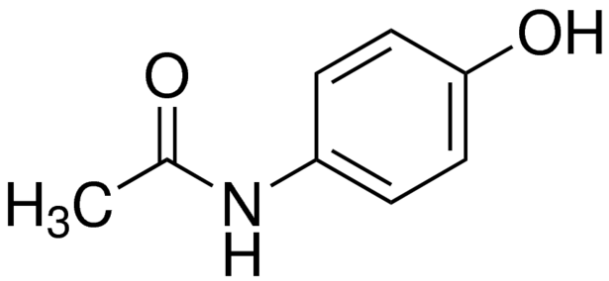

Figure 3-3 Chemical structure of Acetaminophen.

It was chosen as a model drug for this study due to its high solubility in ethanol[131] and its characteristic UV-Vis absorption[132]. The acetaminophen powder is to be loaded on to the PVA-MNP fibres for release study with or without magnetic actuation.

3.2 Preparation Methods

3.2.1 Protein expression and purification

The pDsRed-Monomer expression vector (Clontech) was used for cloning and expression of the *dsred* gene in *Escherichia Coli 2507 (E. coli 2507) cells*. Both the coding sequence of DsRed and Au-BP2 peptide were inserted into the pMal-c4x vector (NEB) to obtain MBP-DsRed-AuBP2 protein. The cells harbouring the expression vector were cultured in LB (Luria-Bertani) medium (10 g/L tryptone, 5 g/L yeast extact and 5 g/L NaCl, pH 7.0) supplemented with 100 µg/ml ampicillin. The cells were grown at 37^{o}C to an optical density of 0.6 at 600nm at which point the protein induction was initiated by the addition of IPTG (Isopropyl β-D-1-thiogalactopyranoside, Sigma-Aldrich, Milwaukee, WI) (0.4 mM) and for 48 h incubation.

Following the expression of protein, cells were harvested by centrifugation at 4000 ×g (times gravity) for 30 minutes at 4 ^{o}C. The centrifuged cell pellet was re-suspended in column buffer (20 mM Tris-HCl, 200 mM NaCl, 1 mM EDTA, pH 7.4) and disrupted by

sonication at 200 W for 1.5 min (pulsed on/off 10 s each) using Branson Digital Sonifier with a double stepped micro-tip. Cell debris was removed by centrifugation (15000 ×g for 30 min at 4 ^{o}C) and the supernatant was collected. The supernatant was sterile filtered as crude extract and 10 mL was loaded onto an amylose resin (New England Biolabs, Ipswich, MA) column (2.0 × 15 cm) equilibrated with column buffer. Following the removal of the unbound proteins, MBP-DsRed-AuBP2 fusion protein was eluted from the column with elution buffer (20 mM Tris-HCl, 200 mM NaCl, 1 mM EDTA, 10 mM Maltose, pH 7.4). Next, the maltose binding protein (MBP) tag was cleaved and removed (detailed procedure given below). The fusion protein was analysed by SDS-PAGE (sodium dodecyl sulphate polyacrylamide gel electrophoresis) on a 4 % stacking gel and 12 % separating gel. Gels were stained with Expedeon Instant Blue (Expedeon Inc., San Diego, CA) solution for 15 min at ambient temperature (20±1 ^{o}C) and destained with de-ionized water for 10 min.

The fusion of the gold binding peptide, AuBP2, to the full-length DsRed-Monomer protein was accomplished using complete gene synthesis. A MBP tag was used to facilitate protein purification. To construct the fusion proteins and expression vector, an exoproteolytic restriction site was localized between the malE gene and N-terminus of fusion protein for subsequent cleavage using Factor Xa protease enzyme. The desired vector was created by designing the oligonucleotides and their primers based upon the known AuBP2 peptide sequence, “CGP-WALRRSIRRQSY-GPC”, with the addition of a spacer sequence, “SGGG”, inserted between the peptide and the DsRed-Monomer on the expression vector (Figure 3-4). DsRed-AuBP2 encoding gene was cloned into the expression vector, pMALc-4X, harbouring malE gene. Next, the pMALc-4X-DsRed-AuBP2 plasmid was transformed into *E. coli* 2507. The transformed cells were used to express and purify the multifunctional proteins using an MBP-tag

which was later cleaved from the DsRed proteins by Factor Xa proteolytic enzyme. Further purification was accomplished using copper chelating affinity chromatography to remove the cleaved MBP tag and DsRed proteins (Figure 3-4).

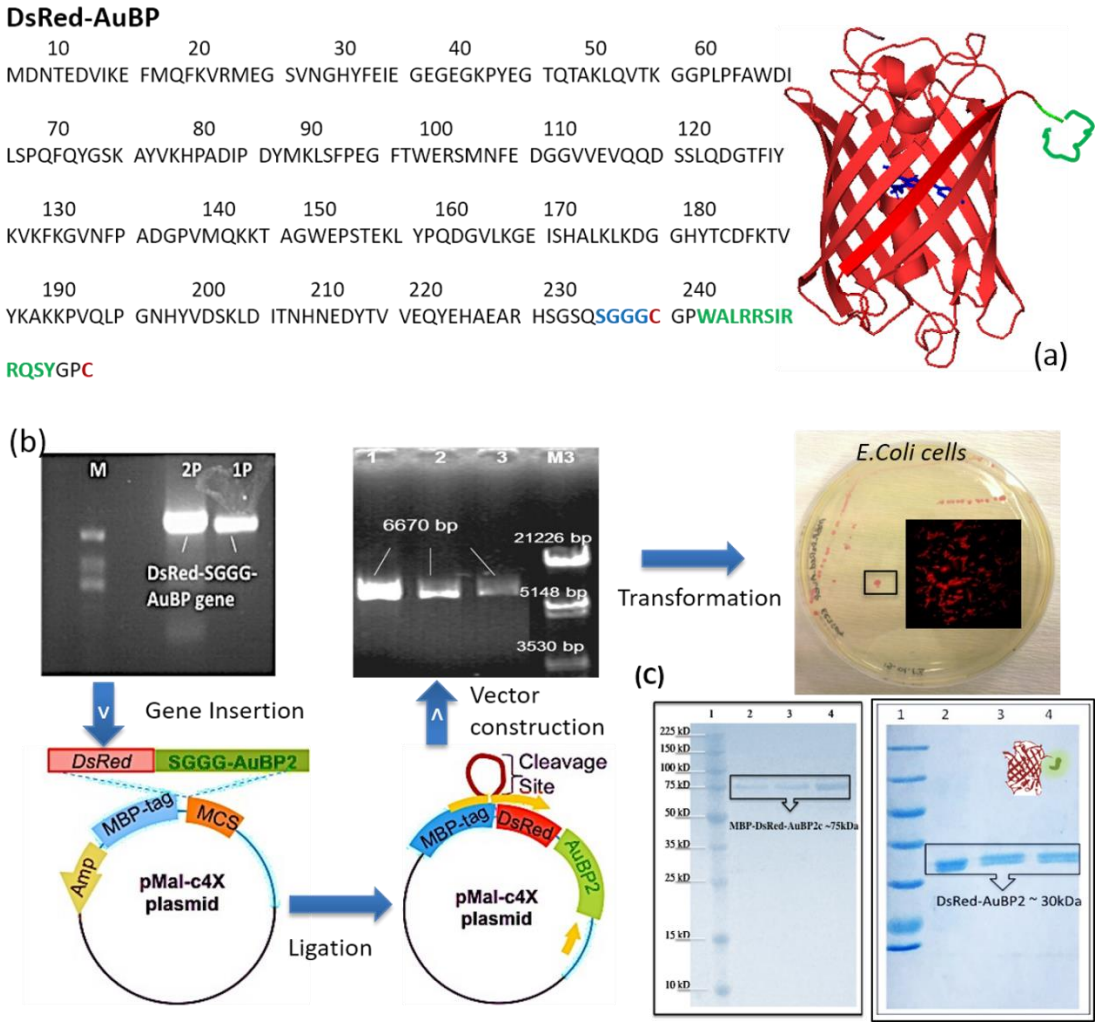

Figure 3-4 Vector Design and Expression of DsRed-AuBP2 protein. (a) Functional domains of the engineered protein, DsRed protein combined with gold binding peptide through a spacer, (b) Schematic of vector construction, (c) SDS-PAGE result of DsRed-AuBP2 following the affinity column purification.

Purified proteins yielded a maximum red fluorescence when the protein was excited at 556 nm which follows the expected excitation and emission maxima of the DsRed-Monomer at 556 nm and 583 nm, respectively. The gold binding affinity of the fusion protein was also confirmed through AFM analysis carried out on a gold surface.

The engineered fusion protein contains two functional domains of red fluorescent protein (DsRed) combined with a highly specific AuBP2 peptide tag (Figure 3-4 a). The pMALc-4X expression vector that encoded the maltose binding protein (MBP) was chosen due to its ease of cloning, over-expression, and purification. The DsRed-AuBP2 gene was cloned into pMALc-4X expression vector and transformed into an expression host cell, *Escherichia coli* ER2507 (Figure 3-4 b).

Positively identified clones were induced with 0.3 mM IPTG concentration to encourage over-expression of the DsRed-AuBP2 protein at 30 ^{o}C for 48 h. The expressed proteins were purified by applying two different column chromatography techniques. First, MBP-tagged affinity chromatography as used to purify MBP-DsRed-AuBP2. Pure protein fractions containing MBP-DsRed-AuBP2 were concentrated to 5 mg/ml of volume by 10000 MWCO of Amicon Ultra-15protein centrifugal filter (Merck Millipore, USA). Then, protein samples were transferred into 1X cleavage buffer containing 20 mM Tris-HCl, 100 mM NaCl, 2 mM $CaCl_2$ (pH 8.0) by ultrafiltration using the same centrifugal filter tube. 40 µl of 1 mg/ml Factor Xa (New England Biolabs, USA) was added to 2.5 mg/ml of fusion protein in 1X cleavage buffer. The cleavage reaction was performed overnight at 16 ^{o}C. The second affinity chromatography technique was used for further purification of the DsRed_AuBP2 bifunctional protein.

The red fluorescent protein, DsRed, has a unique binding affinity for copper ions, therefore a copper chelating affinity chromatography was utilized for the final purification step. On the basis of this interaction, the purification method was performed using copper immobilized column to remove unbound MBP- tags as well as Factor Xa enzymes following the cleavage reaction. As the crude protein was passed through the copper immobilized column, DsRed-AuBP2 bound to the resin whereas other interfering proteins did not bind to the column and hence were removed.

DsRed-AuBP2 was eluted using a competitive ligand imidazole that binds strongly to copper ions within the column, displacting our purified protein. The purity of DsRed-AuBP2 was analysed by SDS-PAGE and gave a single sharp band for DsRed-AuBP2 (Figure 3-4 c).

3.2.2 PEO-protein(+Au NPs) solution

All reagents were used without further purification and buffers were filtered and degassed before using. The polymer solution was prepared in an air-tight bottle using de-ionised water as solvent to dissolve the PEO powder under magnetic stirring at ambient temperature (20±1°C) for at least 24 hours until powders are well dissolved. Solutions with various concentrations of PEO were prepared, however, the 10wt% of PEO solution was used to integrate the proteins.

Phosphate buffer saline (PBS, BioPerformance certified, pH 7.4, Sigma-Aldrich, Poole, UK) solution with a pH~7.4 was prepared at ambient temperature and added to the prepared MBP-DsRed-AuBP2 engineered protein (molecular weight ~73 kDa) using a micropipette. Adding 410 µl of PBS solution to the protein in the tube achieved a working stock solution (410 µl) of 50 µM (micro molar) protein. 50 µl concentrated gold nanoparticle solution which was added to the gently shaken protein solution.

40g of PEO solution was taken in an air-tight bottle and 0.4 ml of the gold nanoparticle-protein mixture was added while sonicating in a water bath using an ultrasound sonifier (Branson sonifier 250) at a power output of 60% for 15 minutes. This prevented aggregation in the gold nanoparticle-protein-polymer solution.

3.2.3 PVA-MNP solution

Three types of PVA polymer powder with different molecular weights were taken in the following weight ratios to obtain three viscous solutions (Table 3-1)

PVA type	*Molecular weight*	*Weight %*
1	13000 – 23000	22
2	31000 - 50000	10
3	146000 - 186000	7

Table 3-1 Molecular weights and weight ratios of PVA polymers used for fibre fabrication.

The three solutions were made by mixing in the relevant weight of each type of PVA powder with distilled water and heating under magnetic stirring at 90 °C (for faster dissolution), for 5h, to achieve homogeneous mixtures.

Next, the three solutions were mixed in a volume ratio of 1:1:1, to make a total of 30 ml of 7.3wt% (type 1), 3.3wt% (type 2) and 2.3wt% (type 3) PVA aqueous solution. This mixture was magnetically stirred at the ambient temperature (~23 °C) for 24 hrs and then stored in sealed glass vials until use.

This specific combination, which delivers the optimum output of PVA fibres for infusion gyration, was studied and then fixed through attempting a different mixture of polymers with a different ratio in experiment practice. The Individual PVA aqueous solutions of each molecular weight were tried at the early study of material selection and preparation which hardly generate fibres while spinning.

To research the limitation of infusion gyration spinning capacity for a different polymer system, PVA was considered for fabrication as a kind of polymer which is still water-

soluble but not dissolving too quickly as PEO which was tested and used for carrying protein (requiring non-toxic solution condition). However, PEO powder can dissolve in water at the ambient temperature (~23 °C) fast and, for the PEO fibres made, the dissolution is even faster in practice. The stability of fibres sometimes plays an important role because it decides the product application. In contrast, the PVA aqueous solution requires a higher temperature to dissolve the polymer powder well and completely, which may have a stronger resistance to humidity and act as a smooth shifting attempt of the polymer system for infusion gyration promising a change to a non-water-soluble one in the future. Moreover, the MNPs to be loaded in the next step have fewer requirements of solution condition than protein and PVA has been used generating fibres by other researchers (see Chapter 2), for example, through pressurised gyration[6].

To fulfil the appropriate viscosity of solution for spinning, a different concentration was tried. However, each of the solutions had negative results of fabrication which also had been the reason for attempting different molecular weight PVA polymers. The higher the molecular weight of PVA is, the more viscous the solution at the same concentration (weight%) would be and the longer time it takes to fully dissolve the PVA powder from the experimental preparation experience. As individuals with different molecular weight, they cannot spin into fibres themselves which have been tried many times, so the idea of combining them came up from the successful experience of fluorescent protein integration onto PEO fibres (see Chapter 4). The smaller protein structure can attach on the long chemical chain of PEO polymer in solution as well as in final fibres. Therefore, the different molecular weight PVA polymer with different chain length in chemical structure may offer a similar mechanism of nano-scale

assembly which can be used to strengthen the connection between each other and further to form fibres.

Each specific molecular weight PVA was made into its aqueous solution first. The solution mixture of all three molecular weight types was tried which developed to the combination used for loading MNPs at ratio listed. However, during the trial, any two types from the three selections mixed to each other (three mixture varieties tested in total) were abandoned because of low fibre yield. Prior to putting MNPs into PVA for mixing, MNPs were subject to acid coating which is a nanoparticle aggregation prevention process to ensure effective dispersion in the aqueous-polymer solution.

In the last section, an ultrasound sonifier was used for PEO-protein solution to prevent aggregation. The sonication works with the polymer-protein mixture to prevent aggregation because the main attraction from the protein macromolecular and nano-particles would be the intermolecular force which includes van der Waal force and hydrogen bonding regarding the aqueous solution in use. Intermolecular force exists all the time but aggregation takes time as well. Therefore, if the ingredients disperse well in solution and this dispersion lasts until spinning, the aggregation can be prevented from forming composite nanofibres. However, due to the nature of magnetic nanoparticles in this study which gives a stronger and more immediate aggregation force, the ultrasound sonifier is no longer suitable for processing in the same way. To overcome the strong magnetic force of the particles, the citric acid coating of MNPs is introduced which covers MNP surface and raise mobility.

Citric acid was dissolved in deionized water in a ratio of 0.5 g/l, at 90 °C for 1 hour, under magnetic stirring. Then, the stirrer was removed and a calculated weight of Fe_3O_4 MNPs was added to the solution and mixed for another 1 hour. Afterwards, the

acid coated MNPs were precipitated by placing a magnet under the bottom of the vessel, and the solution was decanted. The collected MNPs were then washed twice, with 100 ml of deionized water, and dried at 80 °C in the oven, for 3 hours or until a constant weight was obtained. Subsequently, the PVA solution was mixed with 3%(wt), 4%(wt), 5%(wt) Fe_3O_4 magnetic nanopowder (~20 nm), coated with citric acid, and vigorously vortexed (VWR Analog Vortex Mixer) to obtain PVA-MNP solutions.

3.2.4 Experimental set-up for fibre generation

The experimental set-up of the infusion gyration process is shown in Figure 3-5. It consists of a rotary aluminium cylindrical vessel containing 20 small round orifices on the face (Figure 3-6).

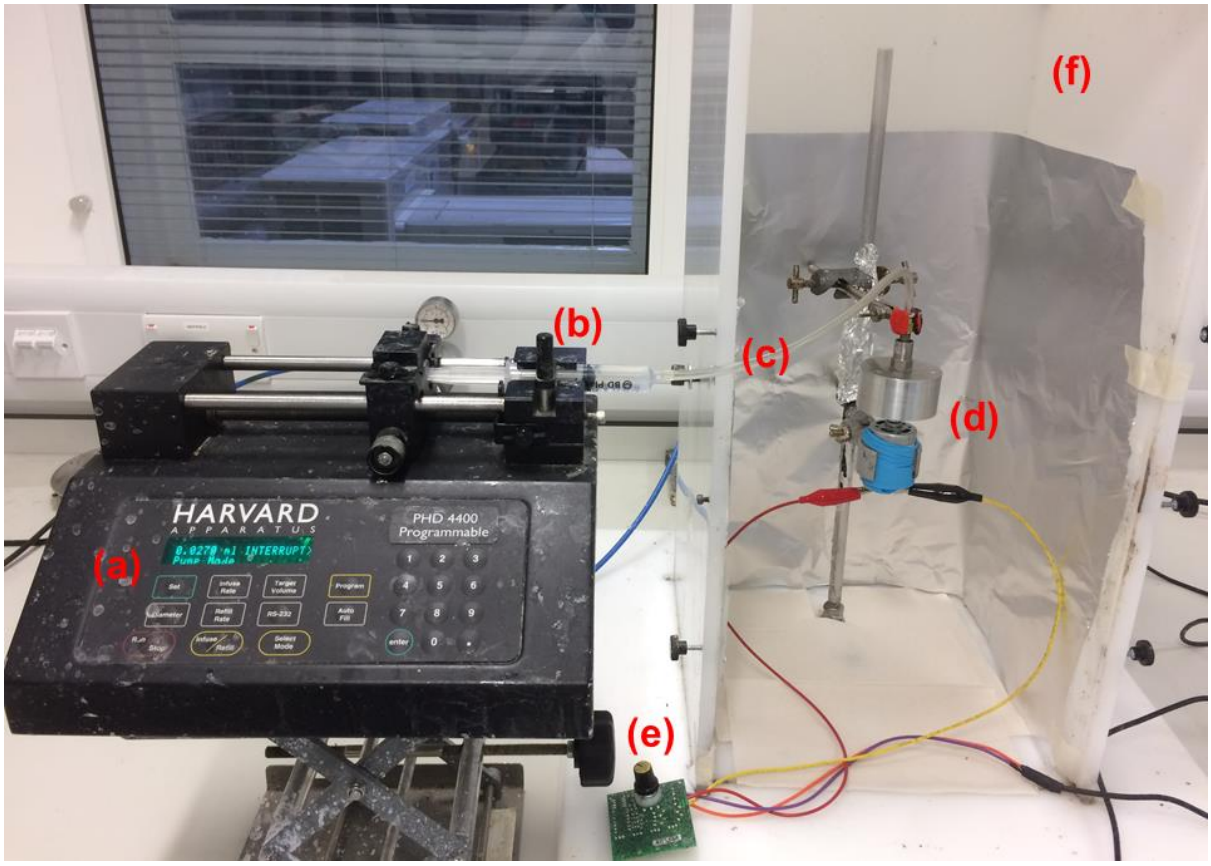

Figure 3-5 Infusion gyration set-up. (a) Syringe pump, (b) Syringe, (c) Solution tube, (d) Cylindrical vessel, (e) Speed controller and (f) Protection case.

The dimensions of vessel are 60 mm in diameter with a height of 50 mm. The orifices (20 in total) are 0.5 mm in diameter shared the same height of 25mm from the vessel bottom. One end of the vessel is joined to a syringe pump (PHD 4400 Programmable, Harvard Apparatus) through a rotary joint, which can control flow of the protein-polymer mixture or control the polymer solution into the vessel.

The bottom end of the vessel is connected to a DC motor, which can produce variable speeds up to 36,000 rpm (Figure 3-6). Because of the centrifugal force and the hydrostatic force, which overcome the surface tension force at the orifice, a jet is formed. The flow in the vessel is kept constant to minimize the hydrostatic force effect during gyration.

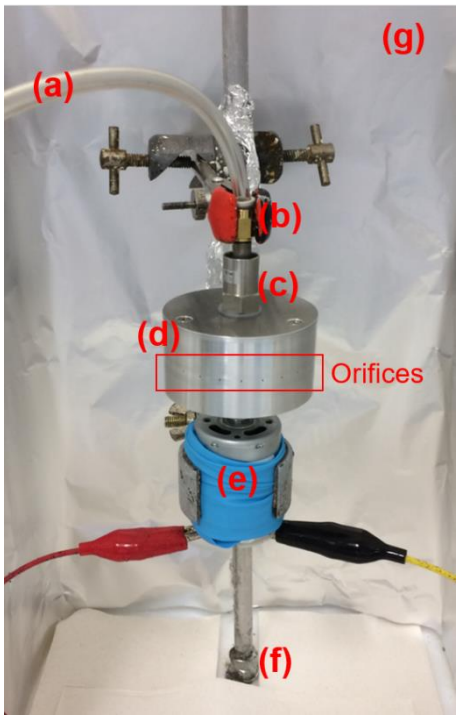

Figure 3-6 Spinning system of infusion gyration. (a) Tube, (b) Connector, (c) Rotary joint, (d) Cylindrical vessel, (e) DC motor, (f) Crank and (g) Aluminium foil.

A gradual increase of the rotating speed will elongate the formed jet when it comes out via the orifices and subsequently solvent evaporates occur to form solid micro and nano fibres. This unit is placed in a transparent plastic container to collect the polymer

fibres conveniently. The polymer fibres were collected using a stationary aluminium foil within the container.

3.2.5 Fibre spinning

3.2.5.1 PEO-protein

In order to investigate the fibre size and size distribution under different conditions, three types of fluorescent protein(s) PEO combined solutions were spun at different flow rates (5000 µl/min, 4000 µl/min, 3000 µl/min, 2000 µl/min, 1000 µl/min and 500 µl/min) under a constant rotating speed (36,000 rpm) at the ambient temperature (20±1 °C) and relative humidity (42±1%) (Table 3-2).

Protein(s) type used	Spinning solution composition		Rotational speed
DsRed_AuBP2	40g 10wt% PEO-water solution	0.4ml DsRed_AuBP2 (with gold nanoparticles)	36,000rpm
GFPuv_AuBP2	40g 10wt% PEO-water solution	0.4ml GFPuv_AuBP2 (with gold nanoparticles)	36,000rpm
MBP-DsRed-AuBP2 & GFPuv_AuBP2	80g 10wt% PEO-water solution	0.8ml mixture made by 0.4ml GFPuv_AuBP2 (+ Au NPs) & 0.4 ml MBP-DsRed-AuBP2(+ Au NPs)	36,000rpm

Table 3-2 Parameters of fabrication (PEO-protein).

3.2.5.2 PVA-MNP

All the pure PVA and PVA-MNP solutions, i.e. 0%(wt), 3%(wt), 4%(wt) and 5%(wt) MNPs in PVA aqueous solutions, were then spun into fibres, according to procedures described. During fabrication of the fibres, the rotational speed of infusion gyration was fixed at 36,000rpm for this study. The flow rate of the solution to the vessel was tried at 1000µl/min, 2000µl/min, 3000µl/min, 4000µl/min and 5000µl/min referring to the previous study. It was held at 4000µl/min during fabrication because it delivered the highest quantity of fibres. A stationary steel mesh was placed 120 mm away from the rotating vessel to help collect the fibres. The solutions were spun at the ambient conditions of 23±1 °C and 40±1% relative humidity (Table 3-3).

Rotational speed	Flow rate	Mesh distance	Ambient temperature	Relative humidity
36,000rpm	4000µl/min	120mm	23±1 °C	40±1%

Table 3-3 Fabrication parameter of PVA and PVA-MNP solutions.

After the spinning was completed, all samples were transferred to sealed containers for further characterization.

3.2.6 Collection of fibres

3.2.6.1 Natural organization

At the early stage of using gyration, no specific tools were used for collection because a fibre sample can form a network itself around the motor and crank in the container. Careful transfer of the sample from the network to a glass slide or aluminium piece is

the only step needed. However, the sample cannot form a uniform shape and for some polymers, they do not grow nets. Many fibres are wasted while spinning because they stick on the protection paper or aluminium foil from the inner wall rather than attach to each other. This method is suitable for small scale trail of samples when the characterization does not require large amount (Figure 3-7).

Figure 3-7 Natural organization of fibres.

Two prototypes of the container were used for gyration. One is a sealed box with openable acrylic glass door to observe motor condition and fibre formation. It provides protection from solution spray but with less air flow for ventilation which is essential for fibre formation. In practice, a small gap (2-3 cm) is always left. Then, the other prototype has a sliding acrylic glass door which can be half open during spinning and covers the rotating part as protection. Sufficient air is for solution evaporation. However, strong solvent destroys acrylic glass which becomes less transparent and fragile after several times of use. PEO fibres were tried to collect using this method.

Therefore, some collectors were developed. The material is crucial as some solution with strong solvent can break the collector or corrode it causing the target sample to be disturbed. Metal is the priority choice regarding the requirement for most experiment.

3.2.6.1 Collecting mesh

To collect more fibres from each spinning, a stationary steel mesh was introduced placed 120mm away from the rotating vessel. One old version with each cell 75×15mm was used which gave a much better collection of fibres than natural organization but the small cell size caused inconvenience of getting fibres out.

This situation happens on copper net collector as well which was used but later abandoned in laboratory due to difficult cleaning although the softness of copper makes it possible to form desired shapes for collection (Figure 3-8).

Moreover, in order to catch more flying fibres around the spinning cylinder, a smaller cell is applied which also brings the inconvenience of fibre transfer.

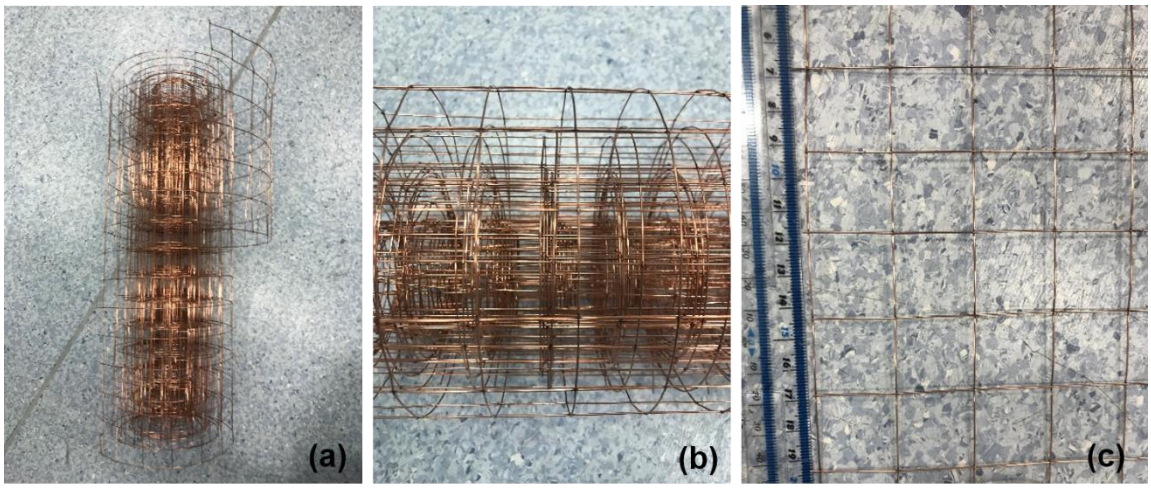

Figure 3-8 Copper net collector (a), (b) and (c) with cell size 25mm×25mm.

Therefore, a mesh with cell size 75×25mm is used for faster collection which speeds up the whole experiment process (Figure 3-9 a and b). After spinning, fibres on the mesh are easy to transfer. By this method, most of the fibres can be collected even to form a shape such as a mat, a ball or a sponge. It has been tested many times for collecting the magnetic PVA fibres which, afterwards, functions well for drug release test. (Figure 3-9 c)

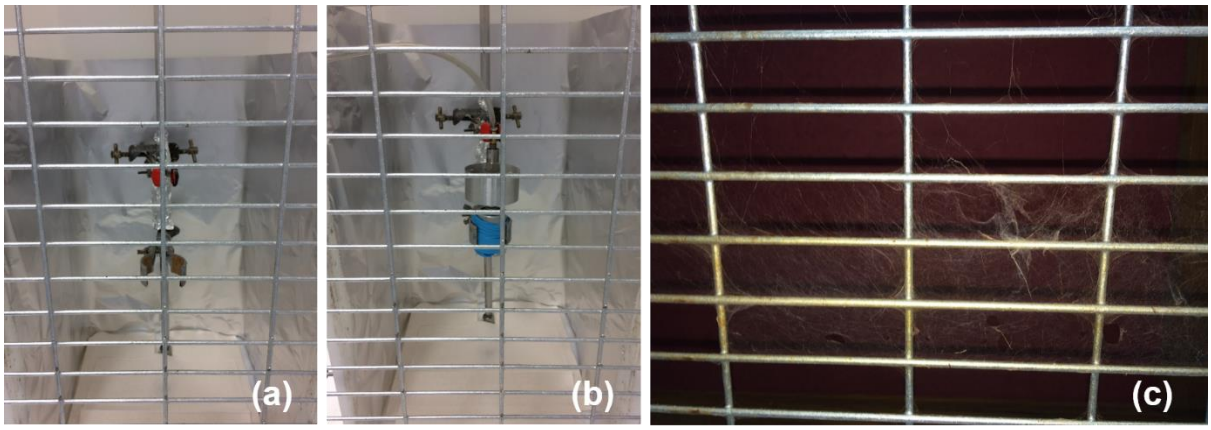

Figure 3-9 Steel mesh (a) without and (b) with spinning cylinder. (c) PVA-MNP fibres collection.

3.3 Characterization Methods

3.3.1 Solution properties

As a review of the former chapter, the properties of the spinning solution need to be characterized either for electrospinning or gyration whose fibre forming process and outcome are influenced. The basic ones are quality controls for solution preparation so that the solutions can be ensured stable and under same conditions for each experiment.

When the polymer requires temperature control during dissolving into solvent, a thermometer is used. The pH meter is for solutions requiring pH control such as PBS buffer.

The physical or mechanical properties of the solution are also important because they are directly related to the performance of spinning. Through the measurement and comparison of the solution properties, the principle of polymer solution converting to fibres stands out. The surface tension and the viscosity of spinning solution are crucial in gyration fibre forming.

To research the relationship between solution physical properties and the Berry number (a dimensionless index relates to fibre size), the measurements of surface tension and the viscosity for 5%(wt), 10%(wt), 15%(wt) and 21%(wt) PEO-water solutions were undertaken through a KRUSS K9 tensiometer (Figure 3-10 a) and a Brookfield DV-3 Ultra programmable rheometer (viscometer) (Figure 3-10 b), respectively, at ambient temperature (20±1°C). The meters are always calibrated before using.

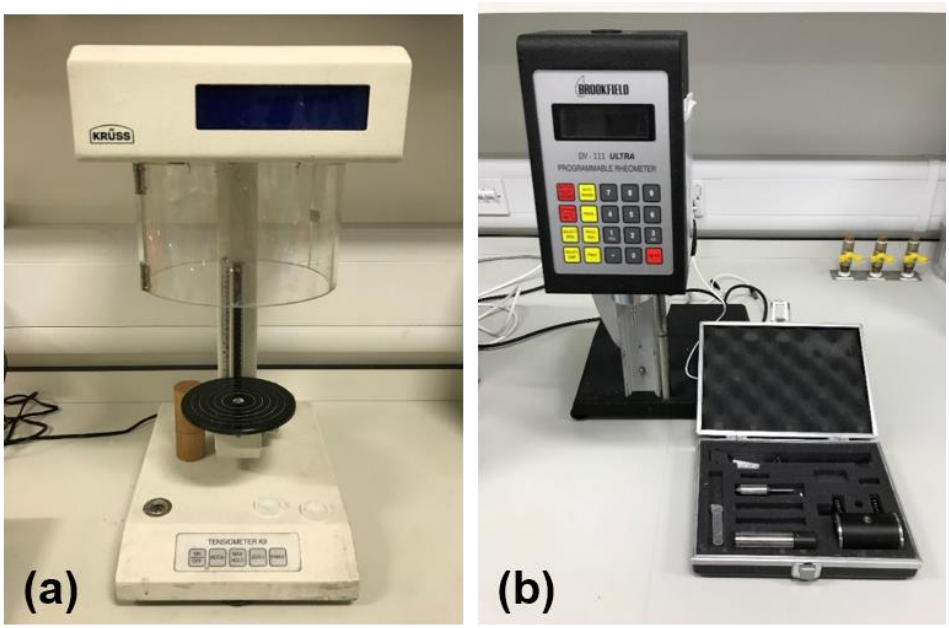

Figure 3-10(a) KRUSS K9 tensiometer (b) Brookfield DV-3 Ultra programmable rheometer (viscometer).

3.3.2 Environmental properties

The environment is important for spinning and characterization. Humidity and ambient temperature are recorded by a humidity meter and a thermometer. These properties affects the formation of fibres because the evaporation is an indiscrete part during spinning. Moist fibres are difficult to collect. A sample desiccator is usually used if the fibre requires the drying process after collection.

3.3.3 Optical microscopy

Optical microscopy is for the morphology study of fibres generated such as shapes, size and diameter. PVA and PVA-MNP fibre samples were observed under a Nikon Eclipse ME 600 optical microscope, fitted with a Micropublisher 3.3 RTV, 3.3-megapixel CCD Colour-Bayer Mosaic, Real Time Viewing camera (Media Cybernetics, Marlow, UK). These fibres were checked through an optical microscope with general larger scale rather than SEM because, for the following drug release test

demonstration, the shape of the fibres collected in its entirety exhibits more structure information for drug loading.

3.3.4 Fluorescence microscopy

A fluorescence microscope (EVOS FL Cell Imaging System, Life Technologies Limited) was used for detecting fluorescence along PEO-protein fibres. Images were taken both in transmitted light and red/green fluorescence for comparison. The fibres were characterized on the same position of the sample with fluorescence mode on and off to verify the integration of the peptides in the fibres.

3.3.5 Scanning electron microscopy (SEM)

The characteristics and the morphology of PEO-protein fibres with high magnification were studied using field emission scanning electron microscopy (Hitachi S-3400N Scanning Electron Microscope). The images were obtained with secondary electrons where the fibre samples were coated with gold using a sputtering machine (sputter time ~75s) before loading to the microscope.

High and low magnification images were acquired at randomly selected positions (>20) within a sample. The fibre diameter was obtained using ImageJ software. About 150 measurements per sample were made at random locations along the fibre to plot the fibre diameter distribution.

The size and morphology of PVA and PVA-MNP fibres were analysed using field-emission scanning electron microscopy (FESEM) with a JEOL JSM6310F instrument. All samples were coated with carbon prior to imaging, using a Quorum K975X turbo-pumped thermal evaporator (Quorum Technologies Ltd., East Sussex, UK).

3.3.6 Energy-dispersive X-ray spectroscopy (EDX)

EDX (Energy dispersive X-ray) spectroscopy which was used in this study of fibre research is a technique for chemical elemental analysis of specified sample area. EDX analysis was performed through an INCA X-sight EDAX system (Oxford Instruments) which was used with a Hitachi S-3400N. Surface elemental analysis with EDX spectrum and element dot mapping has been done on PVA-MNP fibres.

3.3.7 High-speed camera

To better understand the process of spinning, a high-speed camera system was used which can detect small changes in a very short time. Through high speed imaging of the rotating cylindrical vessel, the moment of the spinning solution coming out via the orifices can be captured which provides more detailed information of the production process. Spinning videos of infusion gyration were captured using FASTCAM SA1.1 (PHOTRON, Bucks, United Kingdom) (Figure 3-11).

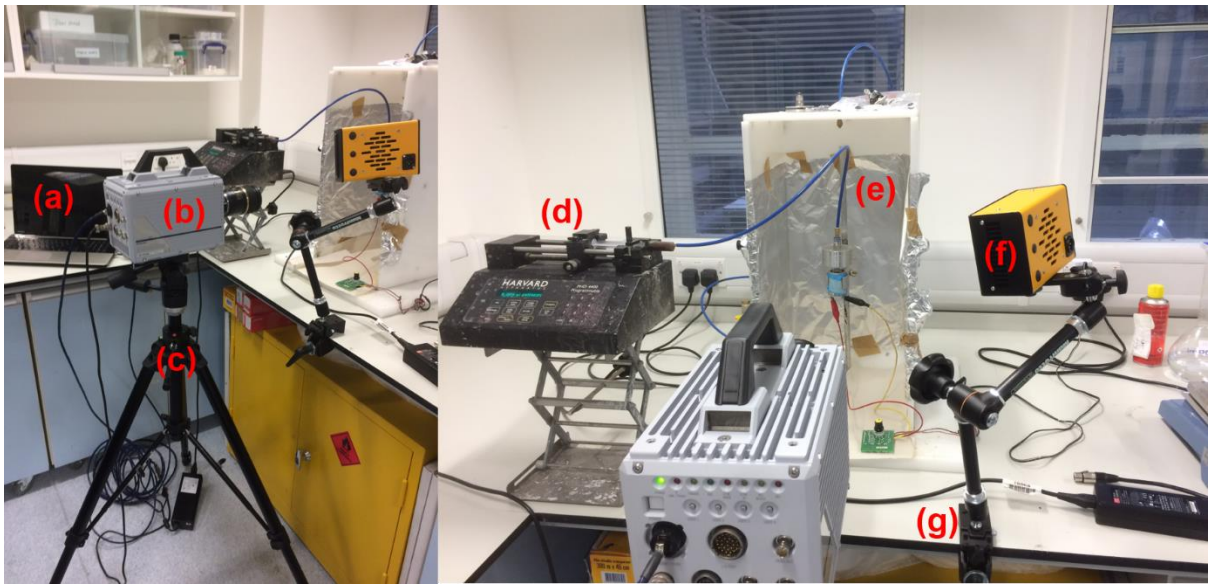

Figure 3-11 High speed camera set up. (a)Laptop, (b)Camera, (c)Tripod, (d)Syringe pump, (e)Infusion gyration set up, (f)Light, (g)Light crank.

The lens used is TAMRON SP Di AF 90mm F/2.8 MACRO 55 272E which stays 0.5 m to 1 m distance to the spinning cylinder depending on image and focus control while filming.

By Photron FASTCAM Viewer (PFV) 3.6.7.0, the capturing software supplied by the high-speed camera company, the video can be played back at slow motion at a variable frame rate and saved by the cable connected laptop.

3.3.8 UV-Vis spectroscopy

The concentration of acetaminophen released into the solution through PVA-MNP fibres was measured via ultraviolet−visible spectroscopy (UV−vis) at a characteristic absorbance wavelength of 248 nm using the absorbance mode of a BioTek Synergy H1Multi-Detection Reader. These measurements were compared to a calibration curve, and the acetaminophen (model drug used in this study) concentrations of the experimental samples were determined by the Beer−Lambert law.

Stability of the composite fibres (PVA-MNP) was also studied. Fibres were immersed in an absolute ethanol solution for 4 weeks to test Fe_3O_4 leaching via UV-Vis spectroscopy (Agilent Technologies Cary 4000 UV-Vis spectrophotometer).

3.3.9 Fourier transform infrared spectroscopy (FTIR)

Fourier transform infrared spectroscopy (FTIR) is used to detect the chemical composition of samples. The infrared spectra of PEO-protein fibres were recorded on Perkin Elmer Spectrum-400 FTIR spectrometer between 4000 cm^{-1} and 650 cm^{-1} with

a resolution of 4 cm^{-1}. To obtain a reasonable signal-to-noise ratio, the average of 20 scans was taken. Samples were analysed directly by single-bounce diamond ATR.

The chemical composition of the PVA-MNP fibre sample was analysed using FTIR. This characterization was achieved via FTIR spectroscopy, with a Bruker Vertex 70 instrument. Examination of the FTIR peaks allowed the identification of all the typical peaks for PVA and citric acid.

3.3.10 SQUID analysis

In order to correctly quantify the amount of MNPs loaded on to fibres, the material was subject to superconducting quantum interference device (SQUID) analysis. Magnetization measurements were performed using a Quantum Design MPMS SQUID-VSM magnetometer. Samples were weighed and mounted within polycarbonate holders and subsequently measured (±1 T, 796 kAm^{-1}, at 300 K).

3.3.11 Copper binding assay

Significant quenching of the red fluorescence activity occurred from studies in the presence of copper ions. Thus, the potential of using the fibres for rapid monitoring for the presence of copper ions has been explored, a major component in heavy metal pollution.

To understand the quenching mechanism of fibre, the metal ion binding study was carried out against copper ions. Different concentrations of copper solution were added to fibre samples in 100 µL of 3-(*N*-morpholino)propanesulfonic acid buffer. The

fluorescence intensity was measured (Varian Cary Eclipse Fluorescence Reader) by recording the resulting emission at 590 nm wavelength after the excitation of the samples at 558 nm wavelength.

3.3.12 Localized surface plasmon resonance spectroscopy (LSPR)

The effect of proteins on the plasmon excitation wavelength for gold nanoparticles (Au NPs) was analysed by measuring the light absorbance of Au NPs in the absence and the presence of protein-conjugated Au NPs in the fibre using a Cytation 3 Imaging Multi-Mode Plate Reader (BioTek Instruments, Inc., Vermont, USA). Each spectrum is an average of three individual samples recorded twice. Herein, LSPR bio-sensing measurement was based on the resonant interaction induced by the biomolecules binding onto the nanoparticle surface. The change in the local dielectric owing to molecule recognition and binding was measured by a shift in the LSPR λ_{max}.

3.4 Controlled Drug Release Experiment

Drug release experiments were conducted in absolute ethanol medium, with acetaminophen (Sigma Aldrich, analytical standard) chosen as a model drug for this study due to its high solubility in ethanol[131] and its characteristic UV-Vis absorption[132]. For each experiment, 5.0 mg of acetaminophen powder was weighted and transferred on to 60.0 mg of magnetic fibres prepared. The fibres were wetted with three drops of absolute ethanol, prior to transfer of acetaminophen on to them (Figure 3-12). To ensure that the drug was effectively immobilized in the fibre network, the acetaminophen powder was spread throughout and pressed against the fibres with a spatula.

This system was then transferred to a glass vial containing 10.0 ml of absolute ethanol. Both control experiments and actuation experiments were conducted in duplicate, to

measure the release of acetaminophen into the solution with time. For the actuation experiments, the fibre-drug system was continuously moved via four stacked external neodymium magnets (emagnets UK, EP336, 20 mm dia x 5 mm - N42 - NiCuNi plated – 1.4 T) (Figure 3-12 C). Samples of 500 µl of the ethanol solute were taken out from the system, first after every minute, up to 5 minutes, and then, at every 5 minutes, for a total period of 30 minutes. Subsequently, the samples were analysed via UV-Vis spectrophotometry, to determine the concentration of acetaminophen released via magnetic actuation. The 500 µl taken out for sampling was replaced with new ethanol each time, in order to keep a total constant volume of 10 ml of ethanol throughout the experiment. The same procedure was followed to conduct control experiments, with the exception of the magnetic actuation.

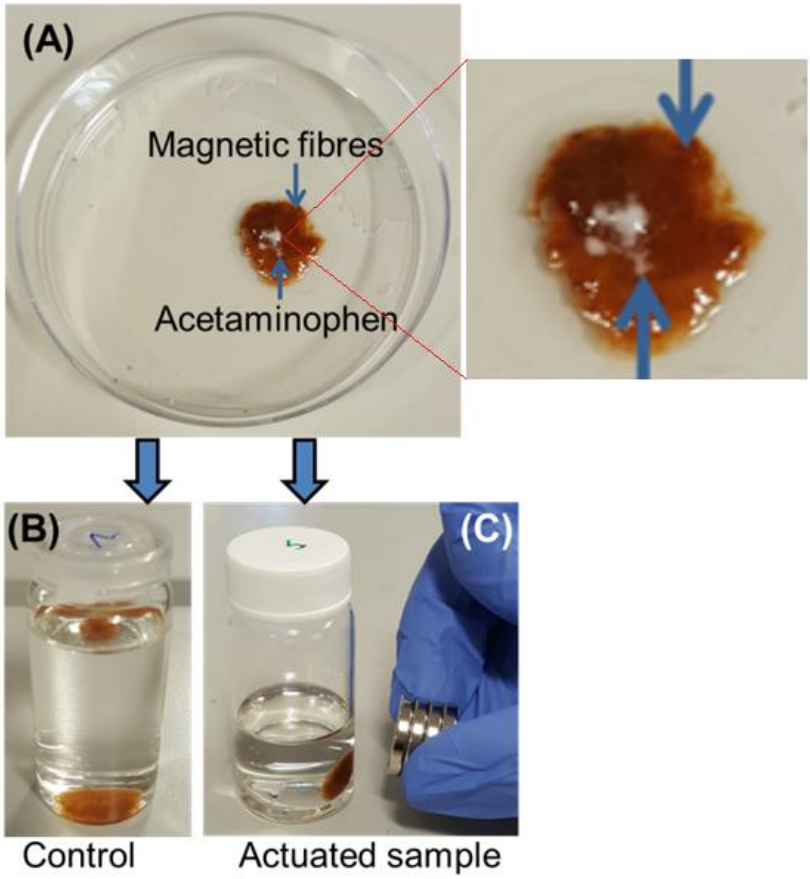

Figure 3-12 Drug release experiments using magnetic fibres. (A) Loading of acetaminophen onto the fibres, (B) control experiment without any actuation, (C) fibre-drug system actuated via an external magnet.

Chapter 4.

Fabrication of PEO fibres with fluorescence protein using infusion gyration

4.1 Introduction

The infusion gyration method resulting in the formation of bio-hybrid fibres containing the genetically engineered protein and gold nanoparticles (AuNPs) was developed.

(1) Gold nanoparticles (AuNPs) were functionalized with DsRed-AuBP2 in which the DsRed protein was fused with gold binding peptide. (2) Polyethylene oxide (PEO) polymer solution was mixed with DsRed_AuBP protein functionalized AuNPs. (3) Through the infusion gyration method, bio-hybrid fibre was produced which is embedded with functional protein and nanoparticles as depicted in Figure 4-1.

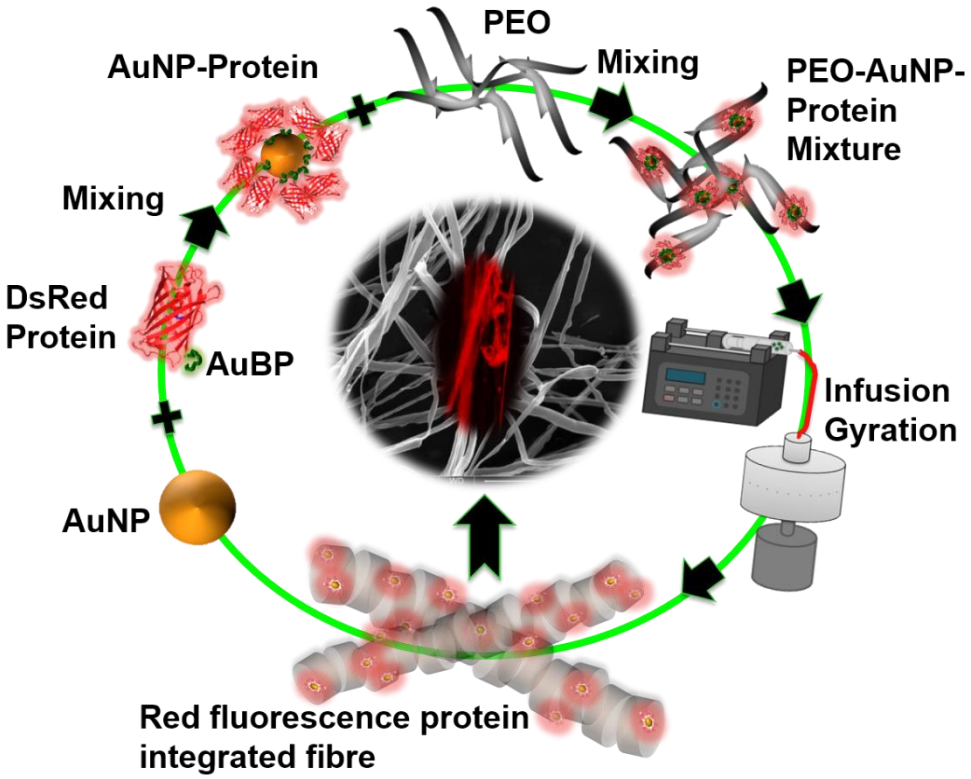

Figure 4-1 Schematic illustration of the formation of engineered fluorescent protein (DsRed) integrated fibres.

GFP_AuBP2 was used for green fluorescence, and a mixture of red and green fluorescence proteins was tried to test the compatibility of the fibre system.

4.2 Berry Number

In fibre forming processes, the physical properties of polymer solution (viscosity and concentration) influence the resulting fibre size and fibre morphology[3,5]. It has been shown that the fibre size obeys a power law relationship relative to the viscosity and the concentration of the polymer solutions[134].

$$d = \eta^a \quad \text{---------} \quad (1)$$

$$d = C^b \quad \text{---------} \quad (2)$$

Where d is the fibre size, η is the viscosity, C is the concentration, a and b represent constants (experimental).

Combining equations (1) and (2) will result in the power law relationship that is,

$$\eta = C^c \quad \text{---------} \quad (3)$$

Where c is the scaling exponent.

In a typical pressurised gyration process not only the viscosity and polymer concentration influences the fibre size but also the polymer chain entanglement, which is a prerequisite to form the nanofibres[5]. To verify this in the infusion gyration process an analysis procedure was adopted using the Berry number, which is a dimensionless index used to control and indicate the fibre size in fibre processing methods.

$$Be = [\eta]C \quad \text{--------} \quad (4)$$

In equation (4) above, Be is the Berry number, $[\eta]$ is the intrinsic viscosity and C is the concentration.

Table 4-1 shows the solution physical properties and the Berry number obtained for various concentrations of PEO (in water) polymer solution.

Polymer concentration (wt%)	Viscosity (mPa s)	Surface tension (mN/m)	Berry number (Be)
5	75±4	50±1	1.6
10	390±23	51±1	3.2
15	2200±75	52±2	4.8
21	3000±86	57±2	6.72

Table 4-1 Polymer concentration, viscosity and Berry number for PEO solutions at ambient temperature (20±1°C).

To derive the Berry number, the intrinsic viscosity of the PEO is taken as 0.32 dl/g (measured and calculated in laboratory). Figure 4-2 (a) shows the relationship between the polymer concentration and the viscosity of the PEO-water solution.

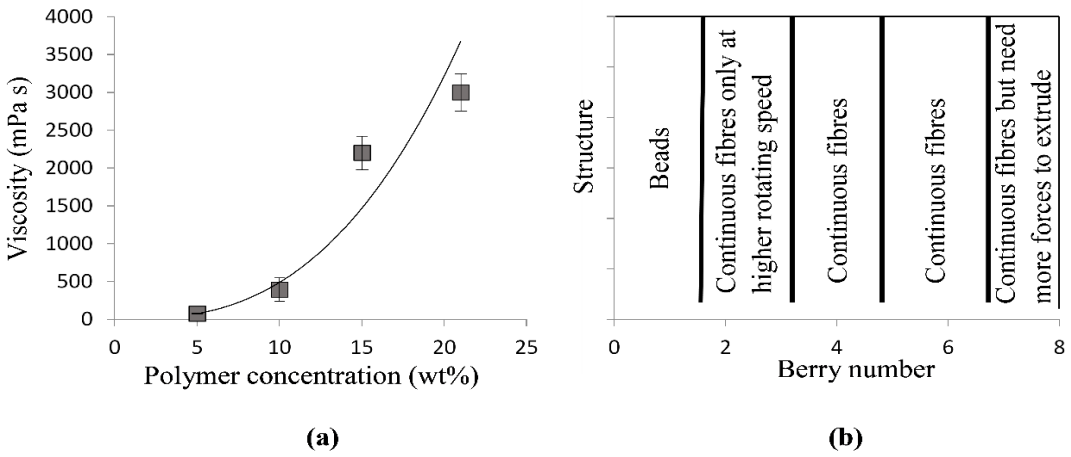

Figure 4-2 Relationship between (a) the viscosity and polymer concentration and (b) the Berry number and structures (36,000rpm).

It is clearly seen that when the concentration is low the viscosity is also low. When the concentration increases the viscosity increases gradually until a specific value is reached, after which the viscosity increases considerably. The non-linear behaviour is attributed to the relationship between the polymer concentration and the viscosity and for the PEO-water solutions equation (3) above gives $\eta=0.92C^{2.73}$ (determined from Figure 4-2 (a)).

For linear polymers in a good solvent, $\eta \sim C^{1.0}$ in the dilute regime, $\eta \sim C^{1.25}$ in the semidilute unentangled regime, $\eta \sim C^{4.8}$ in the semidilute entangled regime, and $\eta \sim C^{3.6}$ in the concentrated regime.[27] The scaling dependence for PEO solutions is much lower than that for linear poly(ethylene terephthalate co-ethylene isophthalate) and similar to branched poly(ethylene terephthalate co-ethylene isophthalate) in chloroform/dimethylformamide where $\eta \sim C^{6.0}$ and $\eta \sim C^{2.73}$, respectively[135]. In addition, it is closer to the value, $\eta \sim C^{3.28}$, reported for Gelose 80 starch in the semidilute entangled regime[136]. In the semidilute, unentangled region, the polymer chains overlap each other, but does not form entanglement. In the semi-dilute entangled region polymer chains sufficiently overlap each other and form entanglement, resulting in a network structure.

The linear polymer has extended coils and form strong entanglements whereas the branched polymer forms weaker entanglements[3]. Figure 4-2 (b) shows the relationship between the Berry number and structures formed in the process under the condition of 36,000rpm (maximum stable rotating speed due to the motor performance). In dilute polymer solutions, Be < 1.6, fibres could not be formed due to insufficient polymer chain entanglement. When the 1.6 < Be < 3.2 the fibres formed only at a rotating speed of 36,000 rpm. This is due to the increase of the time constant of forces acting on the polymer solution and a more viscous response of the polymer solution. Thus, it

requires a minimum rotating speed of 36,000 rpm to initiate the fibres[5]. When the 3.2 < Be < 4.8 there is sufficient amount of chain overlap and entanglement to form the fibres. However, when the Be > 4.8 much thicker fibres are obtained. Therefore, a 10wt% PEO polymer solution was selected for integration of Ds-Red-AuBP2 protein in the fibres.

4.3 Fibre Yield

Fibre yields at the six different flow rates with same polymer solution of 10wt% PEO-water are shown in Table 4-2. The yield is calculated from both the flow rate (which gives the mass transfer per unit time) as well as the weight of the final products.

Infusion rate (µl/min)	5000	4000	3000	2000	1000	500
Weight of polymer solution (g)	6.20	6.17	6.16	4.95	6.55	7.13
Weight of PEO (g)	0.620	0.617	0.616	0.495	0.655	0.713
Weight of PEO (mg)	620	617	615	495	655	713
Weight of fibres collected (mg)	27.3	19.7	5.5	3.0	3.9	3.7
Input-output ratio (%)	4.4	3.2	0.9	0.6	0.6	0.5
Yield (g/hr)	1.45	0.86	0.18	0.08	0.04	0.02

Table 4-2 Yield of peptide integrated fibres at various infusion rates (10wt% PEO-water solution).

Moreover, the yield is plotted (Figure 4-3). It is clearly seen that the yield nearly doubles with doubling the flow rate until the value of 3000µl/min was reached, after which, the yield increased dramatically when compared to the lower flow rate yields. The yield obtained for the infusion gyration method was lower than that achieved through traditional pressurised gyration. This may be due to the absence of blowing in the former[5]. However, rather than the run-to-stop process of pressurised gyration which

spins in a very short time after solution adding, infusion gyration provides a more stable output through flow rate control which also restricts fibre yield due to controlled mass delivery.

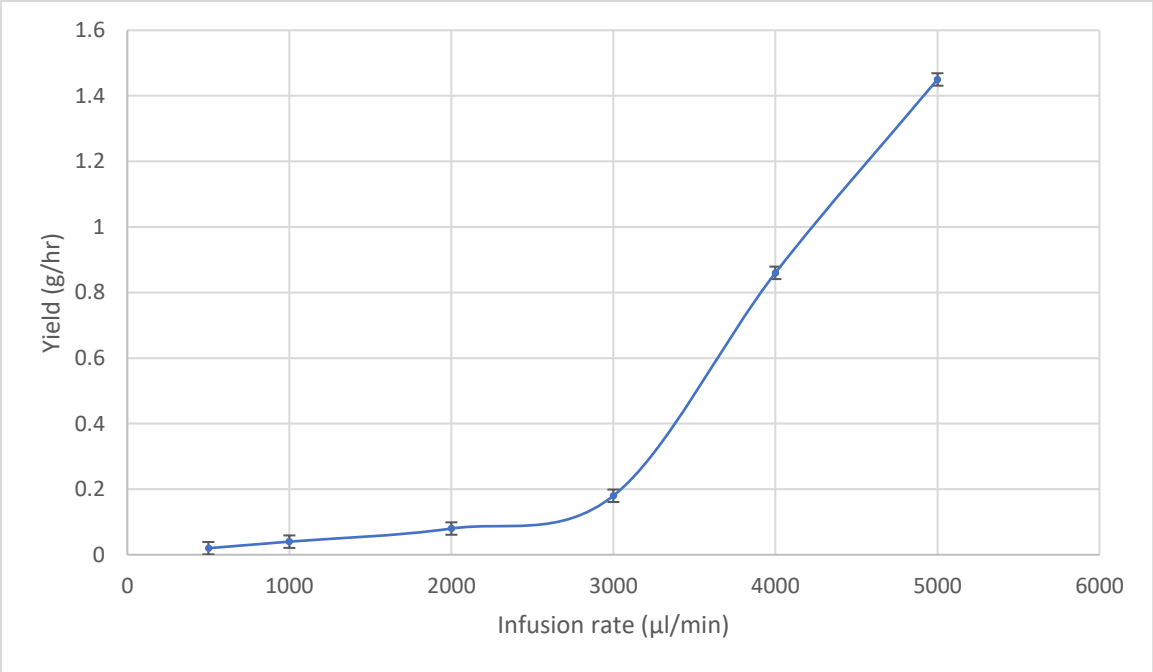

Figure 4-3 Infusion rate effect on fibre yield.

When collecting the fibres from the spinning container, there is always a loss because some fibres may strongly attach to the collector or form in the places where to pick with difficulties such as corners as well as working parts with an irregular surface. Furthermore, some spray drops were observed which means part of the solution did not spin into fibres. However, these fibres were collected strictly following the same procedure which reveals the actual relationship between each other for production and collection in manufacturing process.

As the flow rate controls the yield (which controls the mass output per unit time), for the results, linear change is divided into two phases which are from 500µl/min to 2000µl/min and from 3000µl/min to 5000µl/min. The ideal change should be always

linear, for example, with flow rate increasing from 2000μl/min to 4000μl/min which doubles the former, the yield should also double. Because as flow rate doubles, the volume of solution doubles in unit time which means doubled mass is spun. However, the real yield of 2000μl/min is far too low compared to the one expected. A conclusion can be made that, for lower flow rate, the converting efficiency of solution into fibres is lower. Here, the concept of input-output ratio for fibre spinning is introduced which represents the solution-fibre transform efficiency of the system (Figure 4-4).

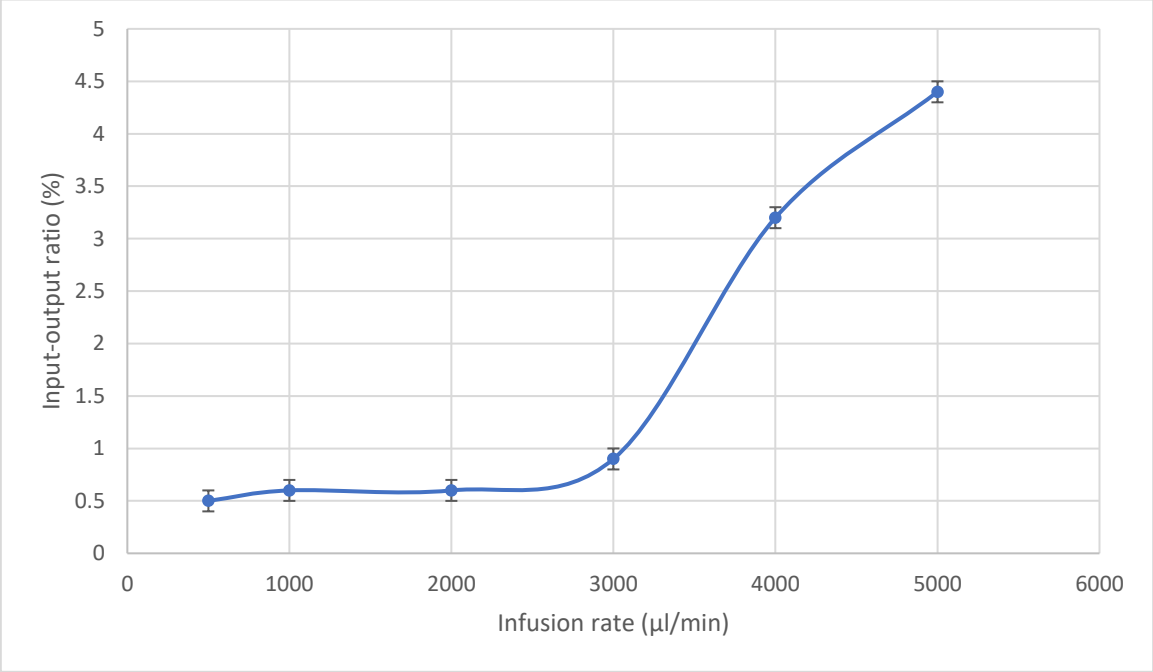

Figure 4-4 Infusion rate effect on Input-output ratio.

It is seen that at lower flow rates, the ratio is extremely low. Therefore, by following the principle of yield performance, either high flow rate is adopted for large scale manufacturing, or low flow rate can be applied for a combined production of fibres with other products like spay particles, in the future.

4.4 Addition of DsRed-AuBP2 to 10wt% PEO-water solution

4.4.1 Self-assembly of DsRed_AuBP2 on Au substrate

To assemble the fusion protein onto a gold surface, a gold surface was generated using micro-contact printing (μCP), onto where the proteins were directly applied. An AFM image (Figure 4-5) was recorded in tapping mode with a silicon cantilever at a 1 Hz scan rate and shows that DsRed-AuBP2 strongly binds exclusively to the gold region of the patterned surface. The AuBP2 peptide tag was confirmed to provide self-immobilization on the gold surface with consequential direction for the engineered fluorescence protein to self-assemble and develop a protein-based pattern.

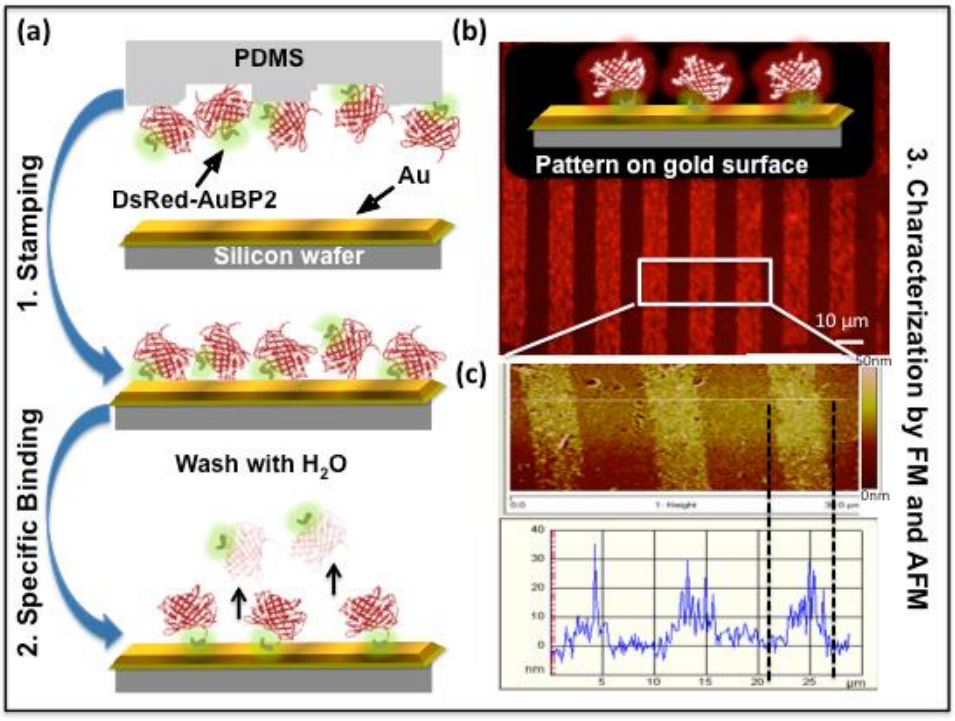

Figure 4-5 Schematic representation of (a) the generation of two-dimensional arrays of immobilized proteins on a patterned substrate fabricated through μCP and (b) fluorescence microscopy (FM) image of gold substrate following self-assembly of DsRed-AuBP2. (c) AFM image of gold substrate following self-assembly of DsRed-AuBP2 with height profile of the arrays.[133]

4.4.2 Fibre morphology

The gold nanoparticles attachment to the fibres are verified through SEM (with focused ion beam) using a dual beam (Helios) machine. The fibrous sample is cut through a section using low beam current (40 pA) and the dispersion of nanoparticles on the surface (indicated by arrows) was observed (Figure 4-6).

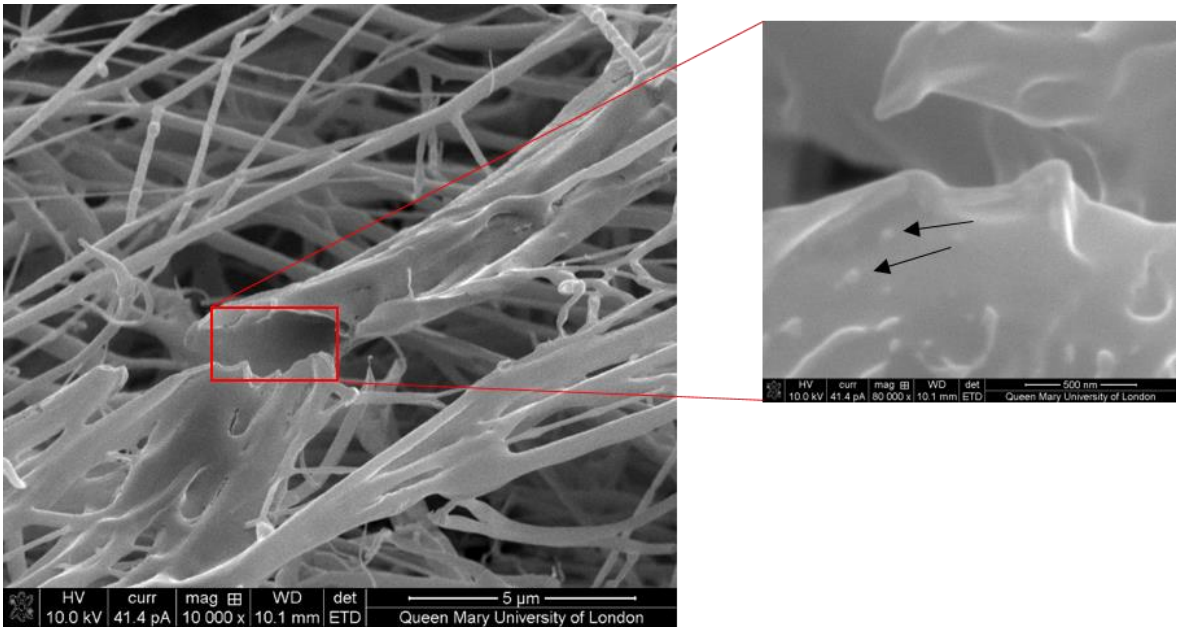

Figure 4-6 Focused ion beam SEM images.

Figure 4-7 - Figure 4-12 provide details regarding the fibre size (diameter) and size distribution of the protein-integrated fibres produced. These ranged from 117 to 216nm in average diameter for the six different flow rates studied. At the lowest flow rate, 500µl/min, the mean fibre size diameter was 117nm. When the flow rate was doubled to 1000µl/min the mean fibre size was 161nm. Surprisingly, the flow rate of 3000µl/min resulted in a reduced mean fibre size of 132nm and this is explained below. The initial size increasing trend continued at higher flow rates, however, at 4000µl/min size was 190nm, and at 5000µl/min 216nm.

The polydispersities of the fibre size distributions were 47, 32, 19, 26, 25, & 23% for flow rate values of 500, 1000, 2000, 3000, 4000, and 5000µl/min, respectively, with

the rotating speed remaining constant at 36,000 rpm. The morphology of fibres revealed continuous, uniform structures. Single strand pore-free fibres were bundled together and it was also possible to form well-aligned structures due to the high stretching force experienced during gyration. Compared to pressurised gyration, the ability to use higher flow rates allows increased hydrostatic pressure which was kept constant for flow rates at a fixed rotating speed by ensuring continuous flow. However, the hydrostatic pressure is much lower than the centrifugal force at the orifice.

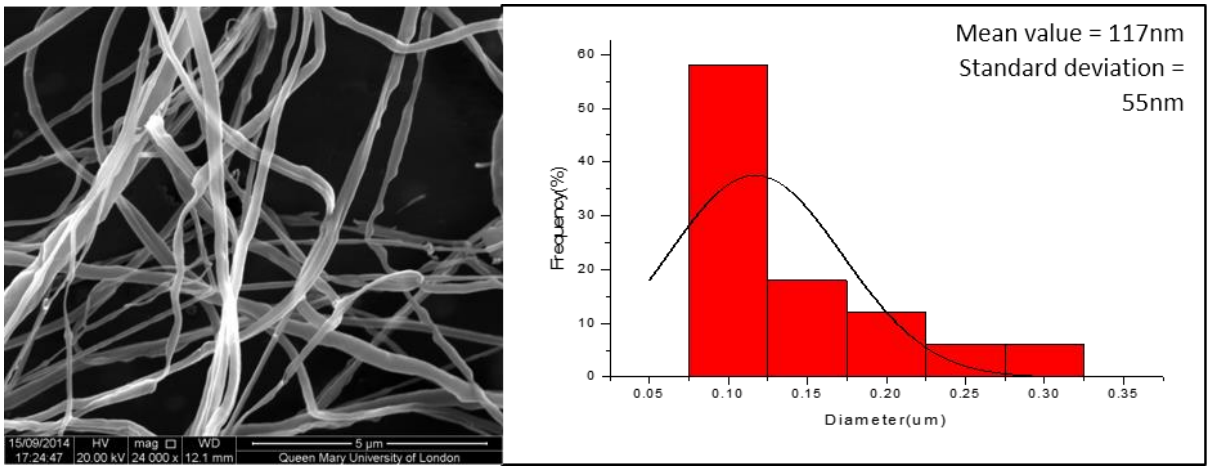

Figure 4-7 Fibre diameter distribution and the corresponding SEM image of fibres at 500 µl/min.

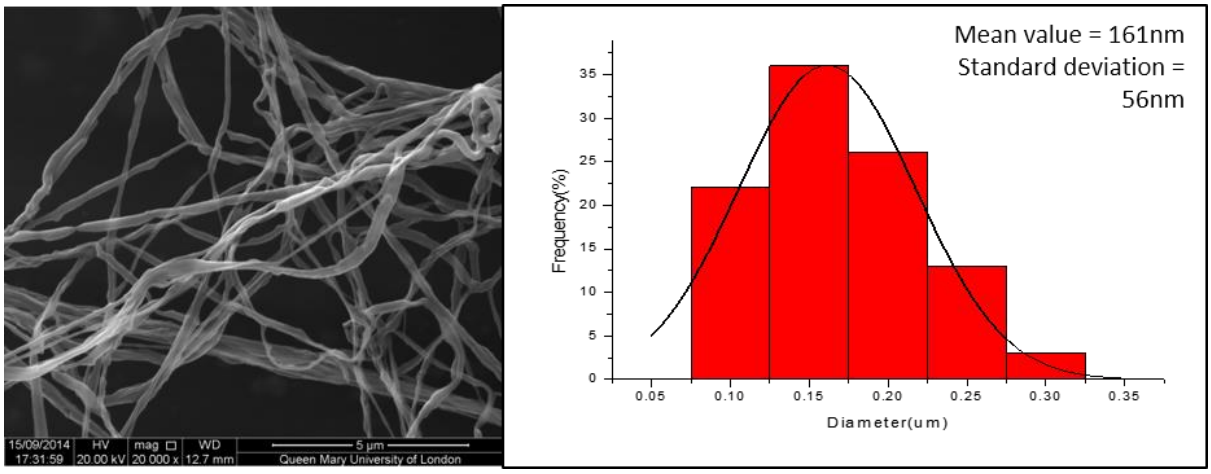

Figure 4-8 Fibre diameter distribution and the corresponding SEM image of fibres at 1000 µl/min.

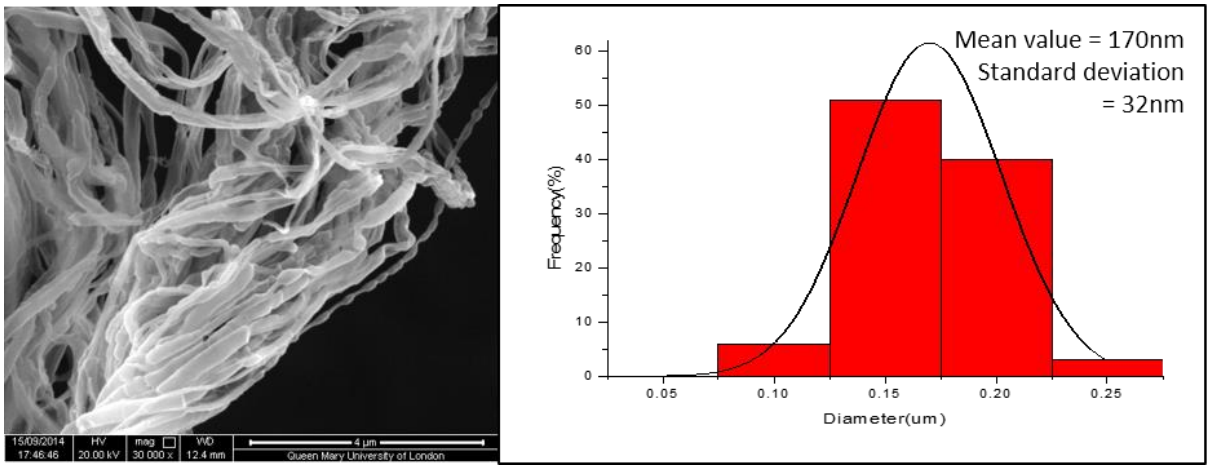

Figure 4-9 Fibre diameter distribution and the corresponding SEM image of fibres at 2000 µl/min.

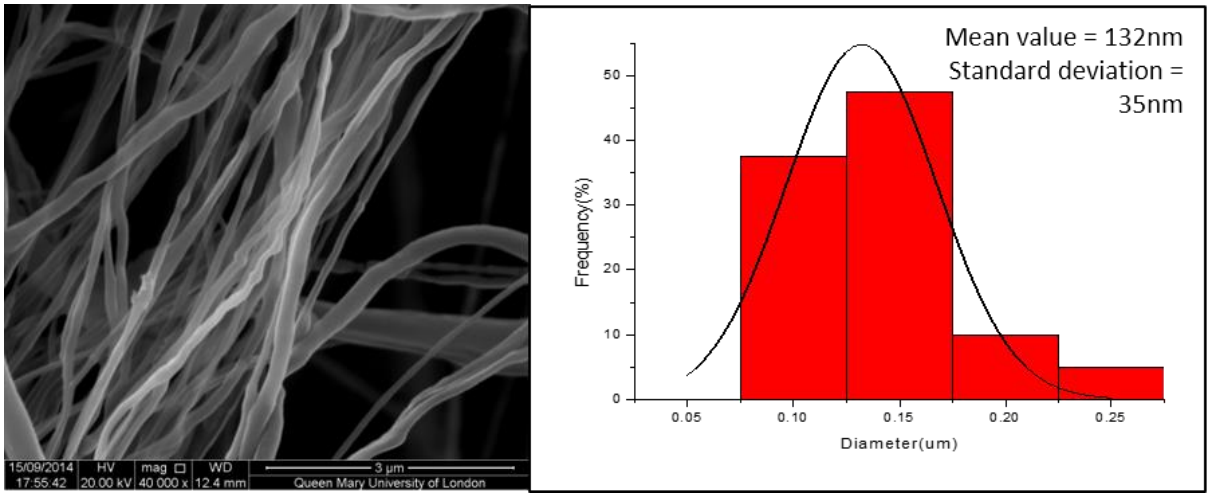

Figure 4-10 Fibre diameter distribution and the corresponding SEM image of fibres at 3000 µl/min.

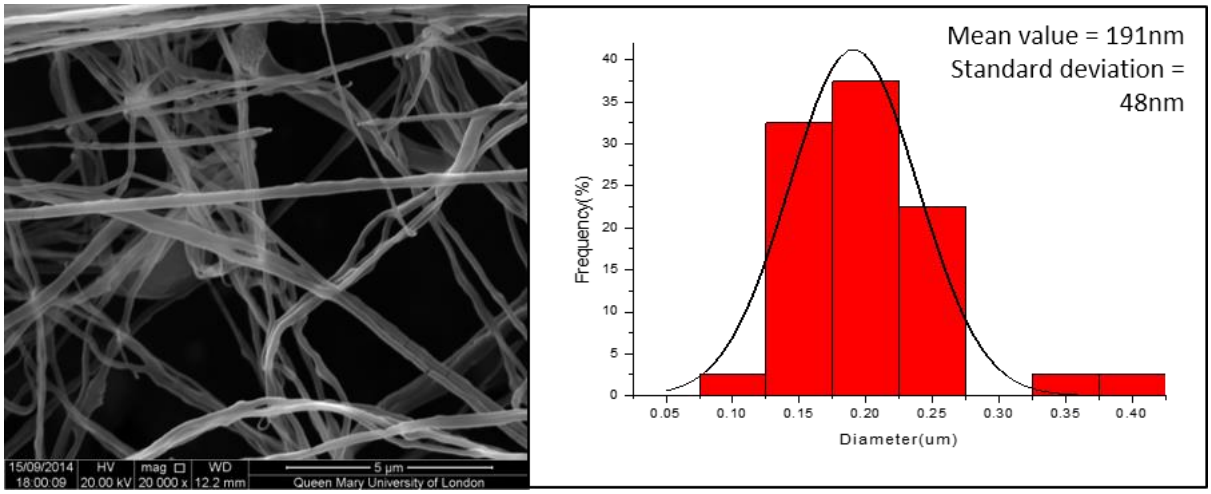

Figure 4-11 Fibre diameter distribution and the corresponding SEM image of fibres at 4000 µl/min.

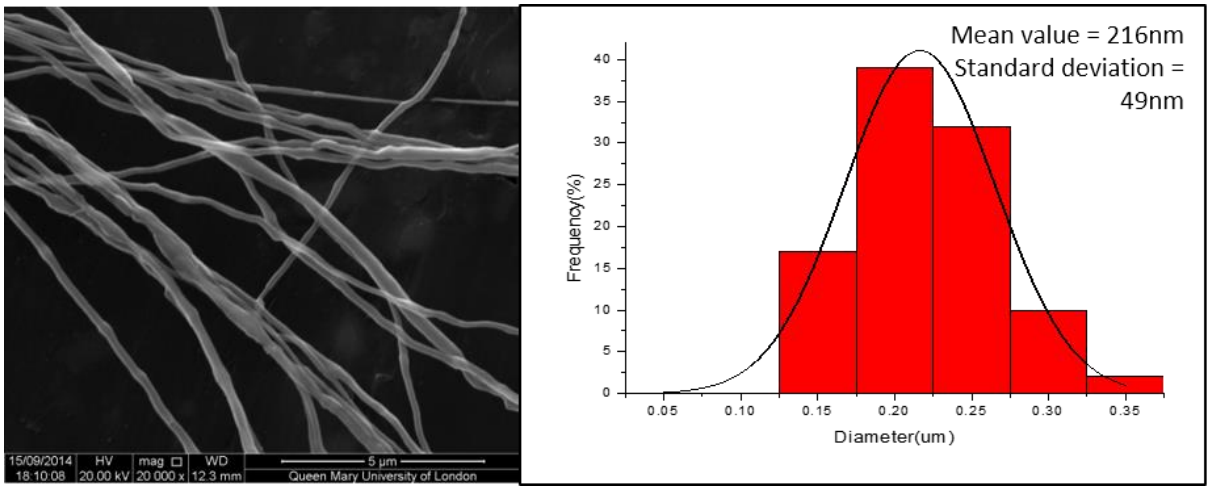

Figure 4-12 Fibre diameter distribution and the corresponding SEM image of fibres at 5000 µl/min.

This allows the destabilizing centrifugal force and the withholding surface tension force to determine the final size and size distribution of the fibres. Moreover, the flow rate regulates the volume of material and the mass transfer across the orifice. Then the relationship between the infusion flow rate and the fibre mean diameter can be drawn in Figure 4-13.

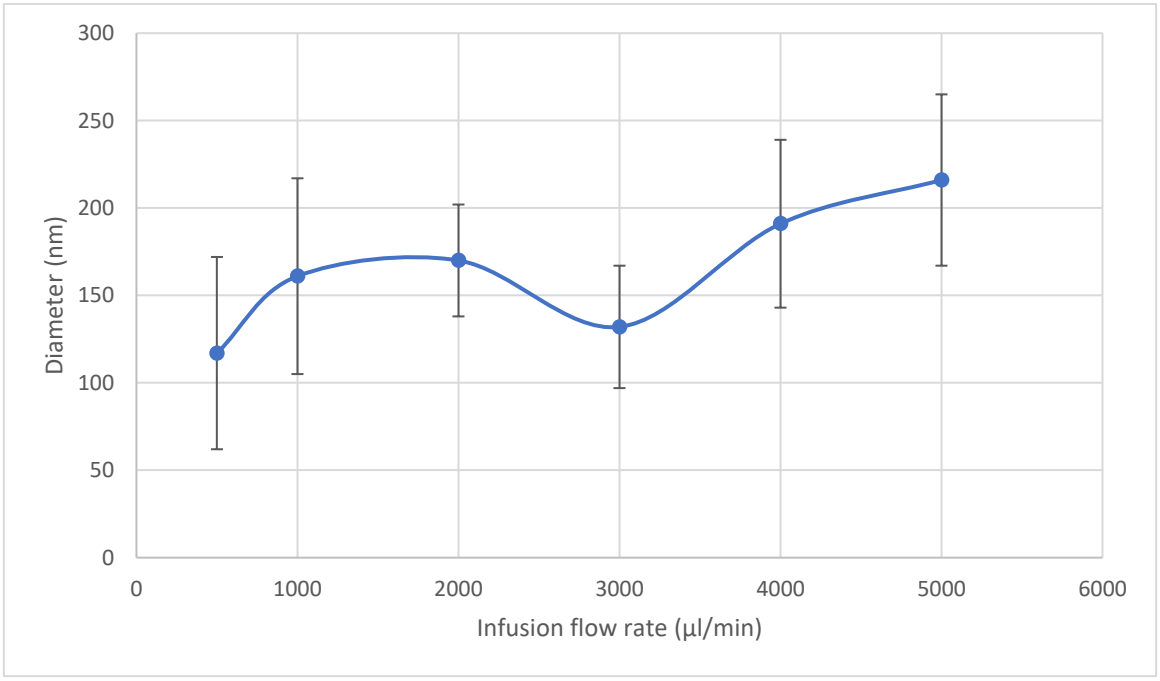

Figure 4-13 Infusion flow rate effect on the fibre mean diameter. DsRed-AuBP2.

The overall increase of fibre diameter with increasing flow rate is attributed to this phenomenon. The drop in fibre diameter observed at 3000µl/min, and subsequent increase at higher flow rates may be attributed to the balance of solvent evaporation and change in the volume of material at the orifice. At lower flow rates, the solvent has enough time to evaporate, allowing the polymer jet more time to stretch which results in the formation of finer fibres. At higher flow rates, the solvent does not have sufficient time to evaporate before reaching collection. Therefore, a coarser fibre is formed[137,138]. Additionally, in infusion gyration the volume and shape of the polymer droplets vary for different flow rates at the orifice which could cause differences in fibre size and size distribution. Finally, during spinning, the travelling polymer jet experiences aerodynamic forces that may impact the stretching of the jet and, thereby further alter the final size and size distribution.

4.4.3 Fluorescence microscopy

The fluorescence contrast image shows the attachment of protein-AuNP mixture dispersed in the fibres (Figure 4-14).

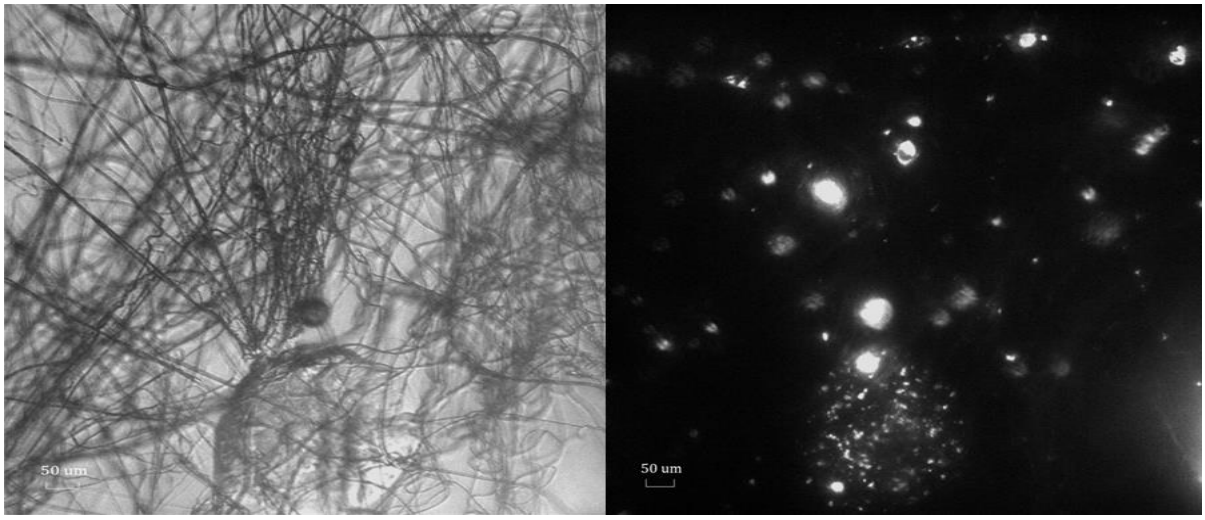

Figure 4-14 Ds-Red-AuBP2 proteins attached to the fibres fluorescence contrast images.

Moreover, the fluorescence microscopy images obtained for various conditions are shown in Figure 4-15 - Figure 4-20. The pictures on the left show the optical images whereas those on the right display the corresponding fluorescence images for various flow rates.

In each instance red fluorescence is a document to reveal a smooth structure. These images indicate the excellent integration of engineered protein with gold binding peptides in the fibres and the flow rate variation does not violate their performance on this level. The excellent alignment of the peptide integrated fibres may be due to tension experienced by fibres and the interaction of the gold binding peptides to the surface of the fibres which aid to prevent slippage of the bonds that may otherwise arise from shearing action.

It is also suggested that the method could be utilized to make various structures that could be tuned physically or chemically without significant variation along the fibrous structures.

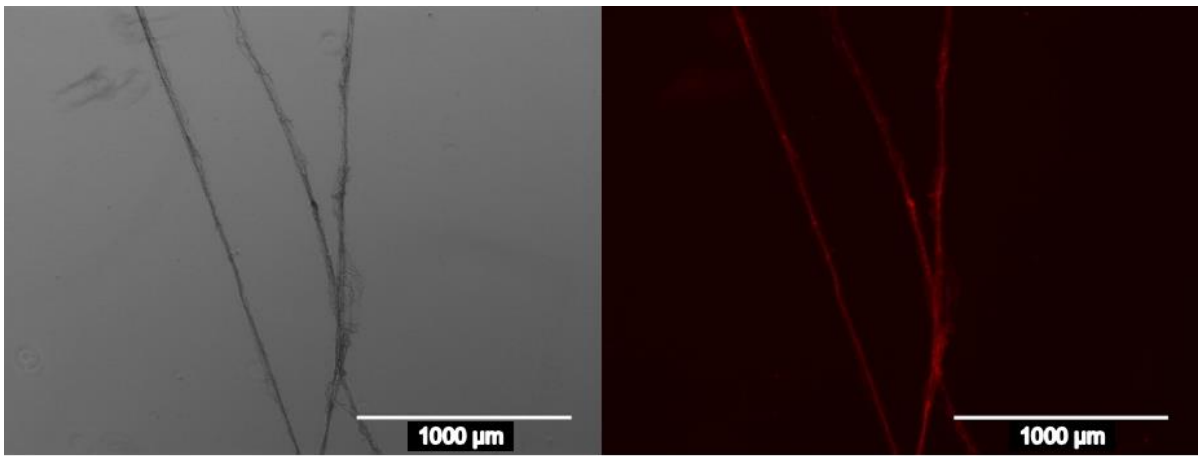

Figure 4-15 Fluorescence microscopy images of the products at 500 µl/min.

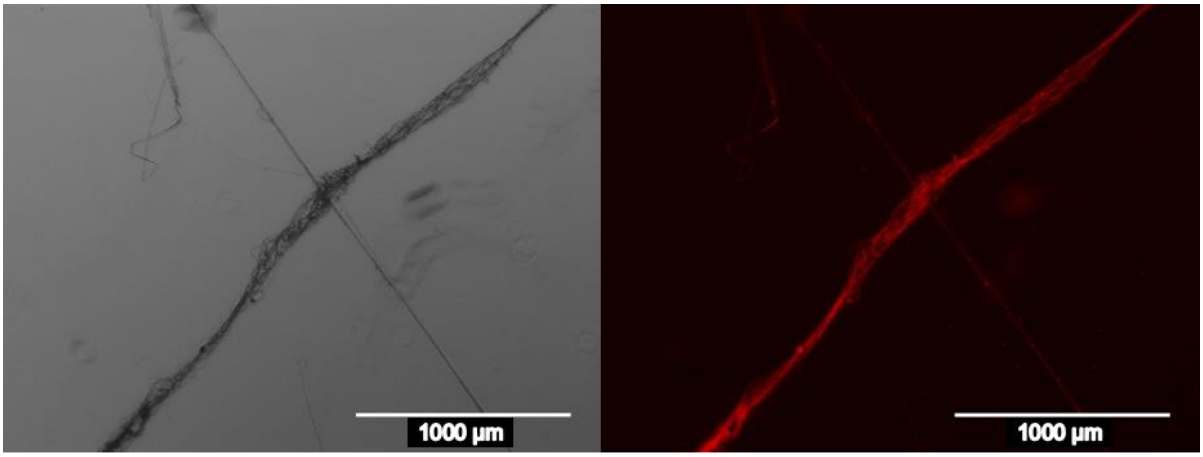

Figure 4-16 Fluorescence microscopy images of the products at 1000 µl/min.

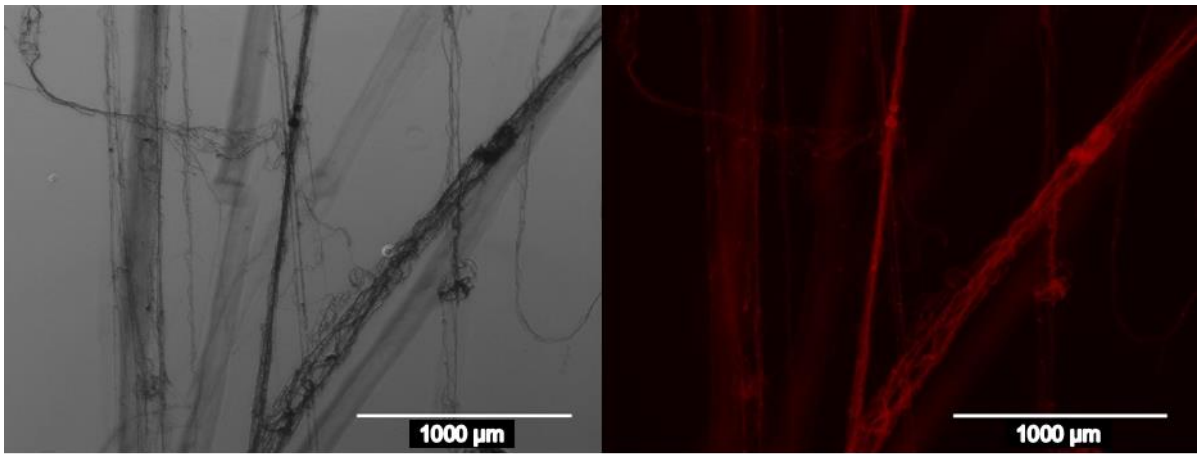

Figure 4-17 Fluorescence microscopy images of the products at 2000 µl/min.

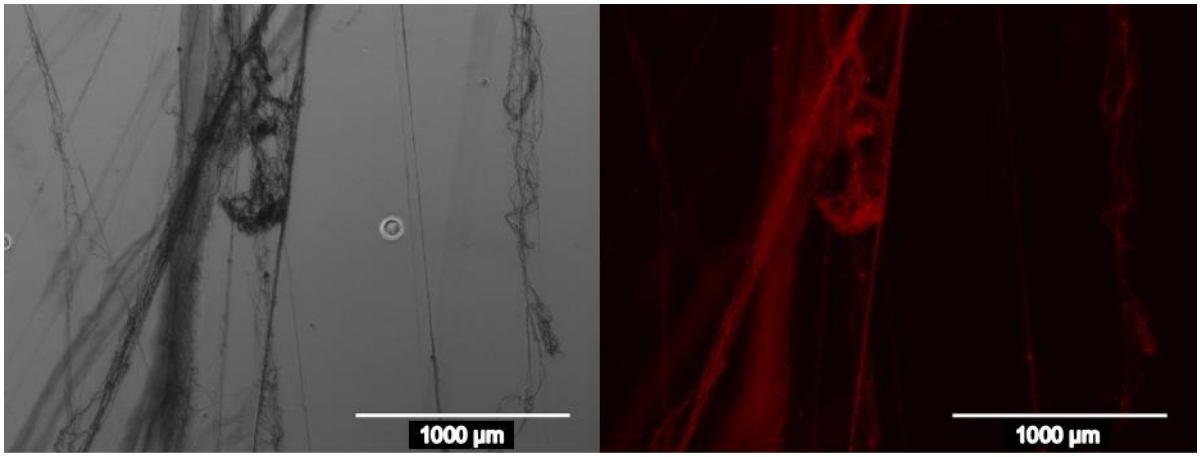

Figure 4-18 Fluorescence microscopy images of the products at 3000 µl/min.

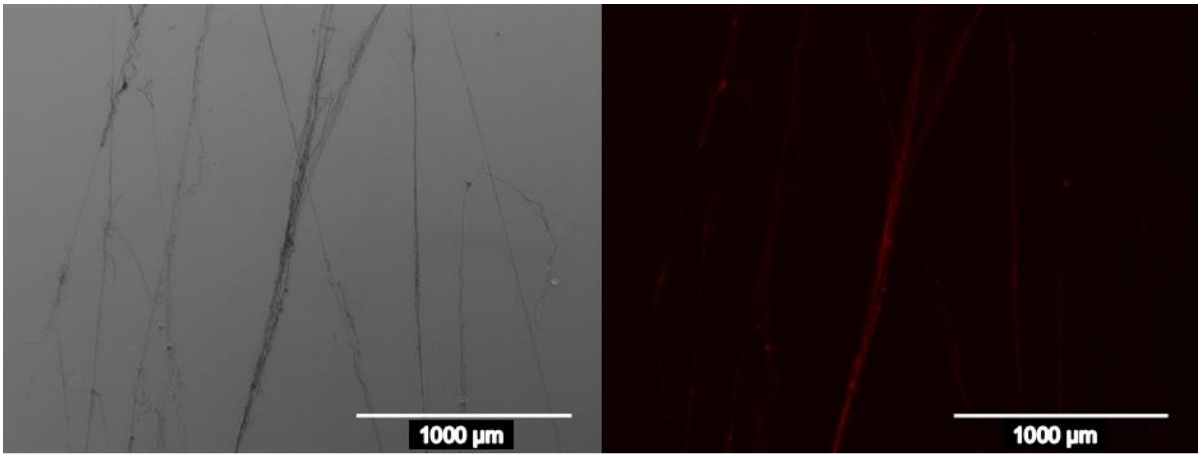

Figure 4-19 Fluorescence microscopy images of the products at 4000 µl/min.

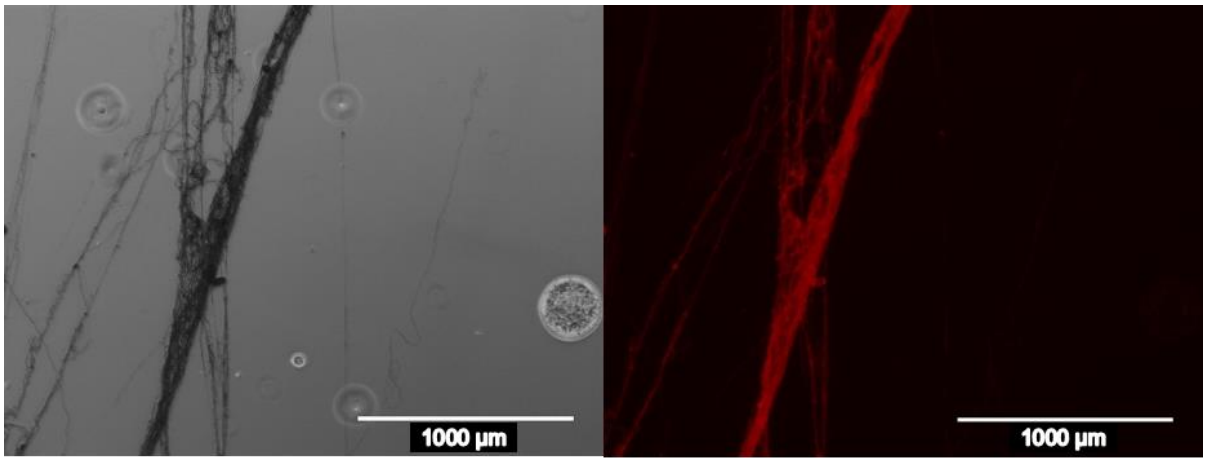

Figure 4-20 Fluorescence microscopy images of the products at 5000 µl/min.

Additionally, bio-hybrid mats composed of micro and nano fibres were analysed in both dry and wet conditions using a cell imaging multi-mode reader and indicate that protein-integrated samples did not dissolve in aqueous environments and that similar fluorescent images were obtained in both dry and wet forms (Figure 4-21). Thus, protein-based fibres did not show any leakage of protein into the PBS buffer which was verified through fluorescence analysis of the buffer solution after the fibres were removed. Interestingly, as expected, PEO fibres that were not integrated with proteins dissolved completely when exposed to an aqueous environment, suggesting a stabilizing role of the protein nanoassemblies on the fibres. Here, engineered DsRed-AuBP2 proteins

were utilized due to their low autofluorescent potential given their excitation and emission wavelengths in the near far-red region of the spectrum which allow for a higher signal to noise ratio.

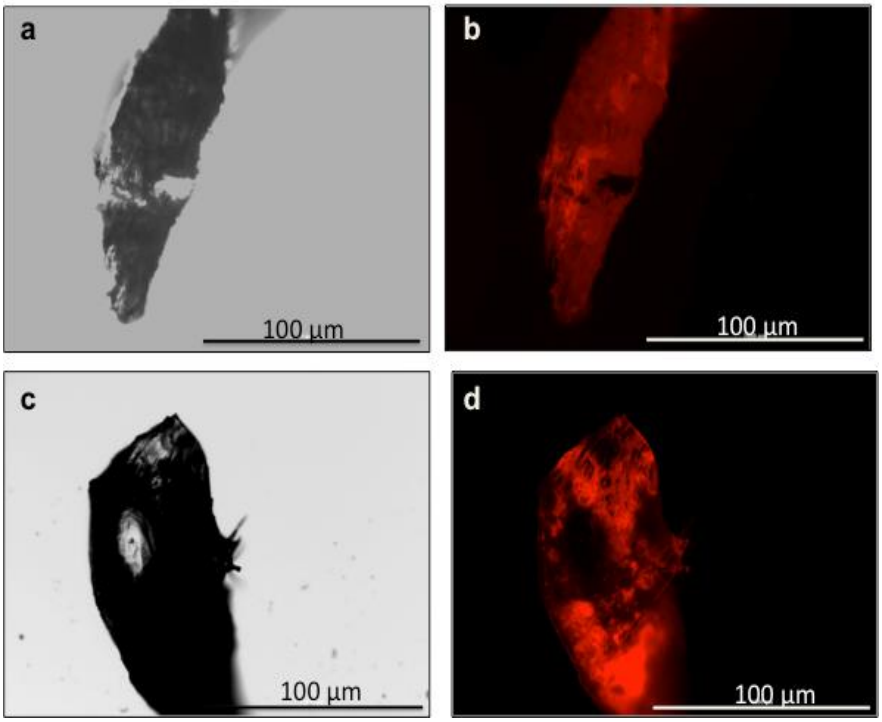

Figure 4-21 Fluorescence Microscope image of protein integrated fibres (a-b) samples were in PBS buffer, (c-d) samples in dry condition.

4.4.4 FTIR

FTIR (Fourier transform infrared spectroscopy) analysis conducted on the PEO and bio-hybrid (PEO/Protein) fibres confirmed the presence of the protein. Figure 4-22 depicts the characteristic peaks of PEO are observed at 2900 cm^{-1} (methylene group CH_2 molecular stretching), and at 1100 cm^{-1} and 960 cm^{-1} (C-O-C group stretching), [139–141]. A change in bandwidth for the absorption centred around 2880 cm^{-1} also occurred and changed further with protein integration.

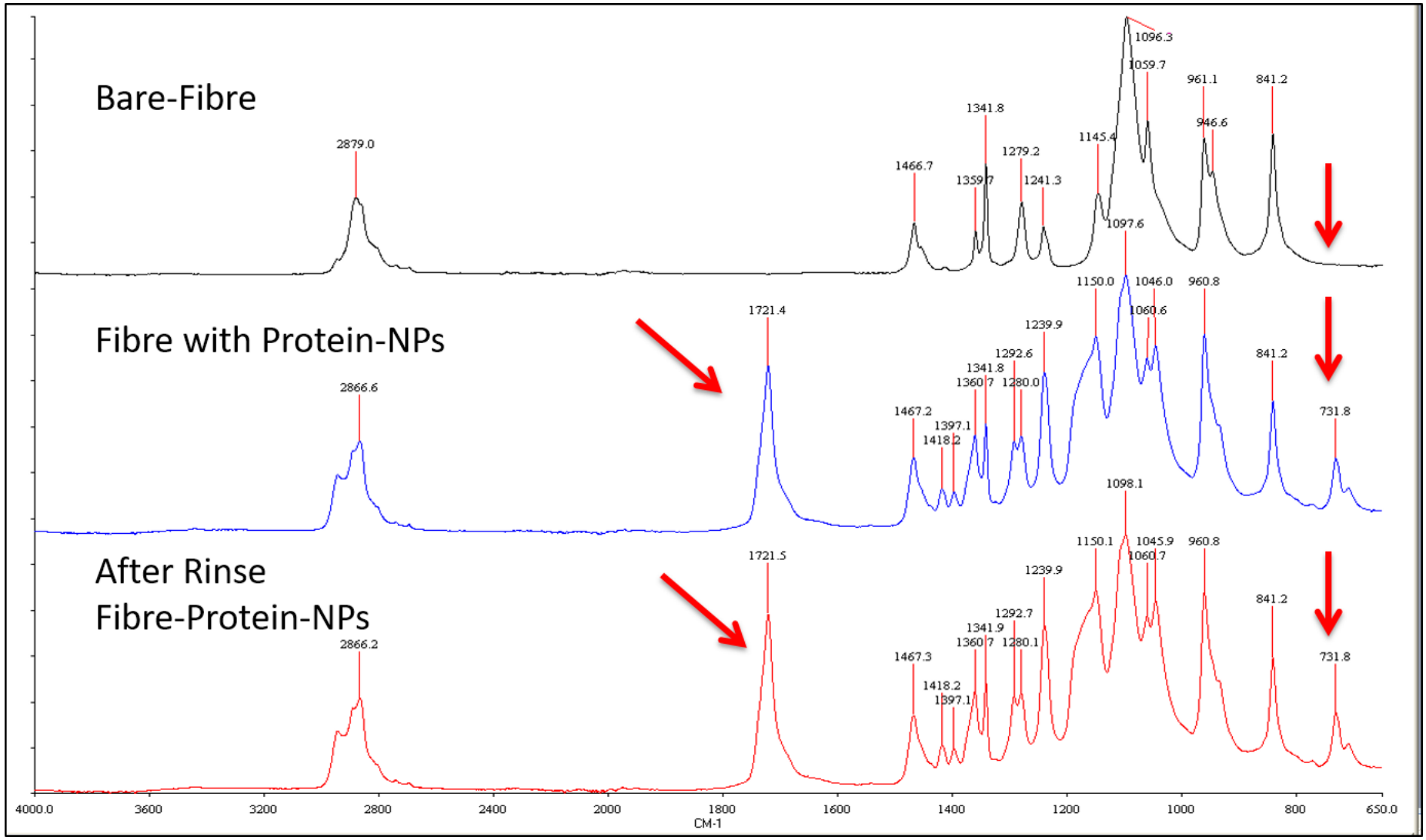

Figure 4-22 FTIR spectra of the samples. X-axis is wavenumber (cm-1).

Engineered proteins in the PEO/Protein fibres resulted in an FTIR peak at 1720 cm^{-1}, representing the characteristic amide bonds of protein. After washing the PEO/Protein fibres with PBS, the same FTIR peak was still observed. The maintained carbonyl peak suggests that the protein remained bound to the surface of the AuNPs which were integrated in the PEO fibres, even following a washing step. This is remarkable protection of the water soluble PEO polymer and is discussed further below.

Integrating discrete AuNPs into the hybrid fibres may significantly alter their inherent optical properties which were evaluated by UV-Vis and fluorescence spectrophotometry. The integration of AuNPs onto the surface of the fibres had a significant effect which was observed, when compared to non-protein integrated fibres. Hybrid fibres in PBS buffer exhibited a strong fluorescence emission band at wavelength 570nm (Figure 4-23). Interestingly, protein based fibres did not dissolve in PBS buffer and did not show any leakage of protein to the buffer. When fibres were removed from the PBS buffer, the fluorescence intensity of PBS buffer alone was completely mitigated confirming that the red fluorescent protein did not leak into PBS buffer (Figure 4-24).

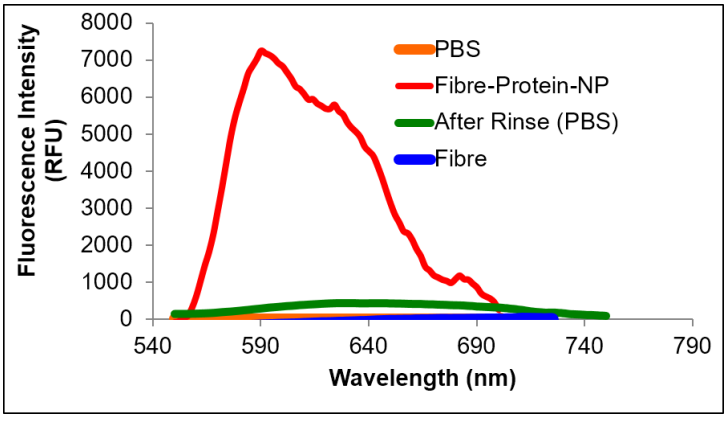

Figure 4-23 Optical characteristics of PEO and PEO/Protein fibres measured by fluorescence spectrophotometry. Fibres containing red fluorescence protein in PBS buffer.

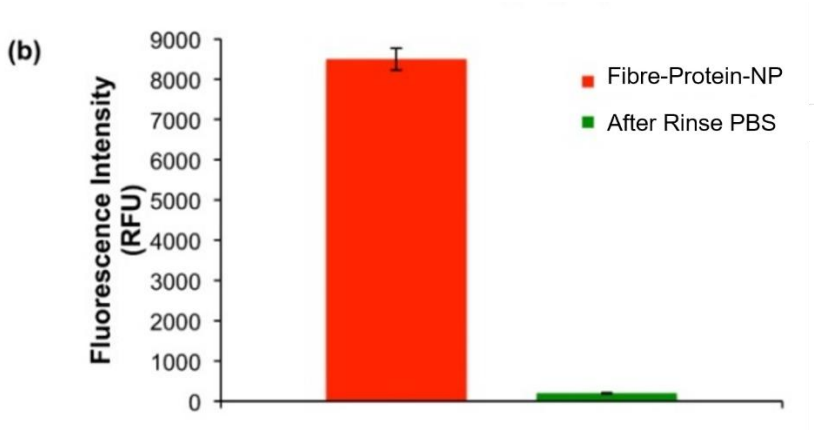

Figure 4-24 Optical characteristics of PEO and PEO/Protein fibres measured by fluorescence spectrophotometry. The removal of the PEO/Protein fibres from PBS buffer diminishes fluorescence intensity demonstrating no significant protein leakage into the solution.

4.4.5 Copper binding assay

The PEO-protein fibres were investigated if they would demonstrate the selective binding to copper ion once they are placed in solution having copper ion. Based upon the fluorescence intensity plotted against the wavelength, the fibres were demonstrated quenching around 70% through 50μM copper concentration (Figure 4-25).

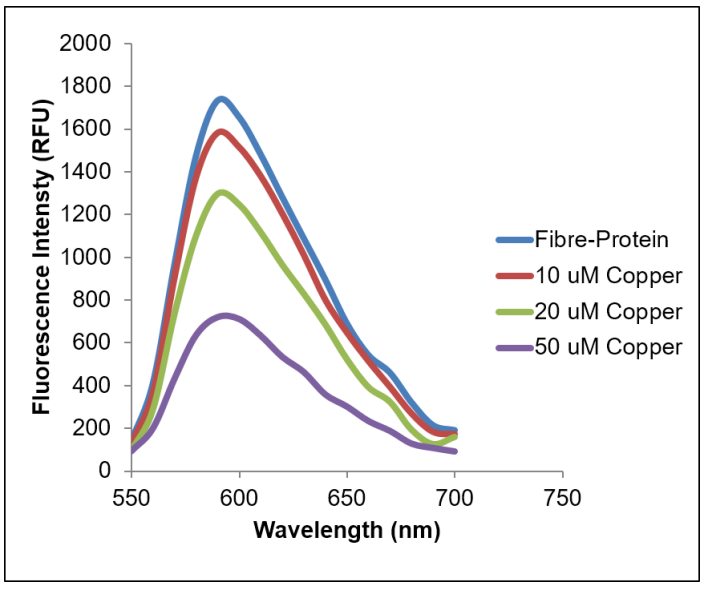

Figure 4-25 Titration of DsRed-AuBP2 integrated fibre with Cu^{2+}. Emission spectra was obtained by excitation at 558 nm in the presence of 10, 20, 50μM Cu^{2+}.

With the increasing amount of copper ion, the fluorescence intensity decreases which means part of the protein in the fibre binds the copper ion and lose fluorescence. This promising result not only demonstrates the potential of protein-integrated fibres to monitor the presence of copper ions in solution, but also establishes the potential environmental impact that may be achieved through further tuning of the system to detect biological and chemical changes in the environment.

The results provide evidence that the red-fluorescence activity of the engineered proteins embedded in the fibres maintain full functionally and can respond to various dynamic conditions.

4.5 Addition of GFPuv-AuBP2 to 10wt% PEO-water solution

4.5.1 Fluorescence microscopy

Figure 4-26 - Figure 4-31 display the fluorescence microscopy images of the fibre samples in experiment sequence from low flow rate (500µl/min) to high flow rate (5000µl/min). Every fibre sample with different infusion flow rate was photographed at the same position of fibres in transmitted light mode and in fluorescence mode for comparison. Two levels of scale were recorded during observation.

For both 100µm scale and 1000µm scale images, individual fibre grows straight and smoothly through transmitted light for all different flow rates.

In fluorescence mode, all images confirm the fluorescence along fibres at both scales which display the red colour (the red only indicates the fluorescence not represents the actual colour of the protein) in dark field. At these scales, there is no detectable difference by morphology between the six fibre samples of different flow rate.

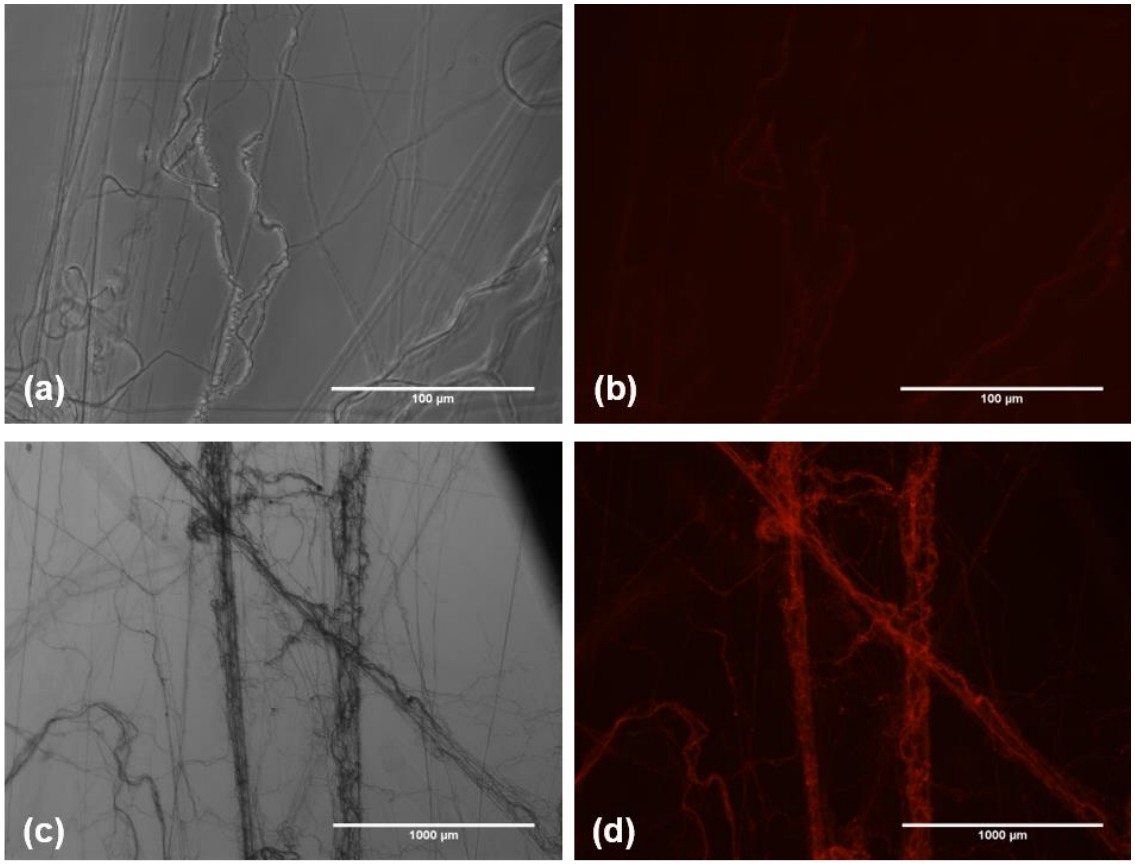

Figure 4-26 Fluorescence microscopy of GFPuv-AuBP2 PEO fibres (500µl/min).

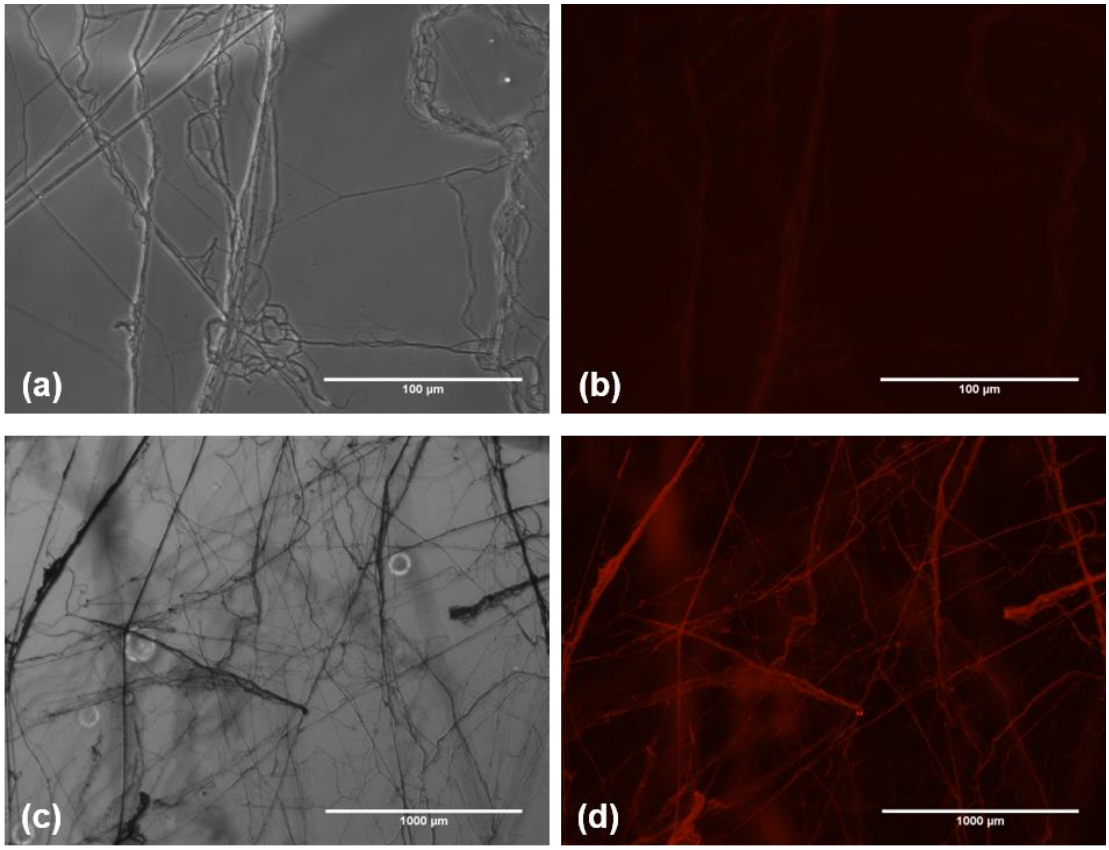

Figure 4-27 Fluorescence microscopy of GFPuv-AuBP2 PEO fibres (1000µl/min).

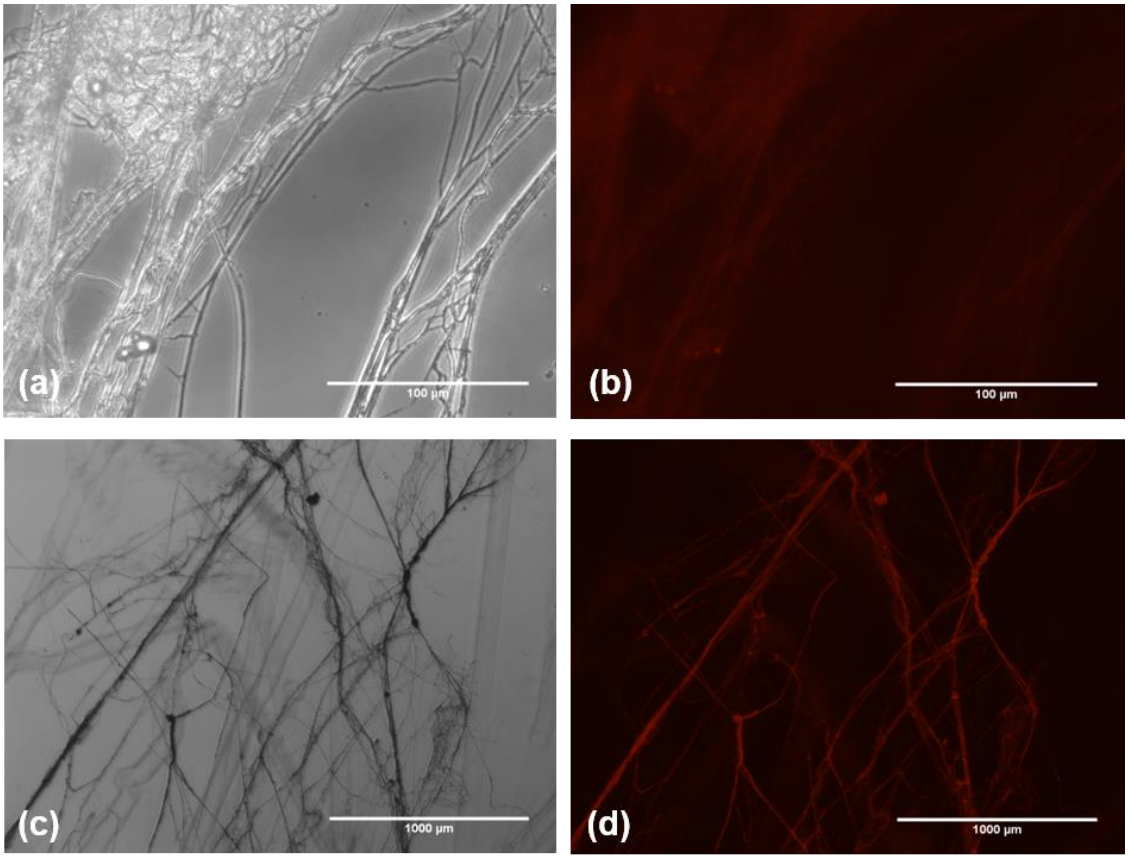

Figure 4-28 Fluorescence microscopy of GFPuv-AuBP2 PEO fibres (2000µl/min).

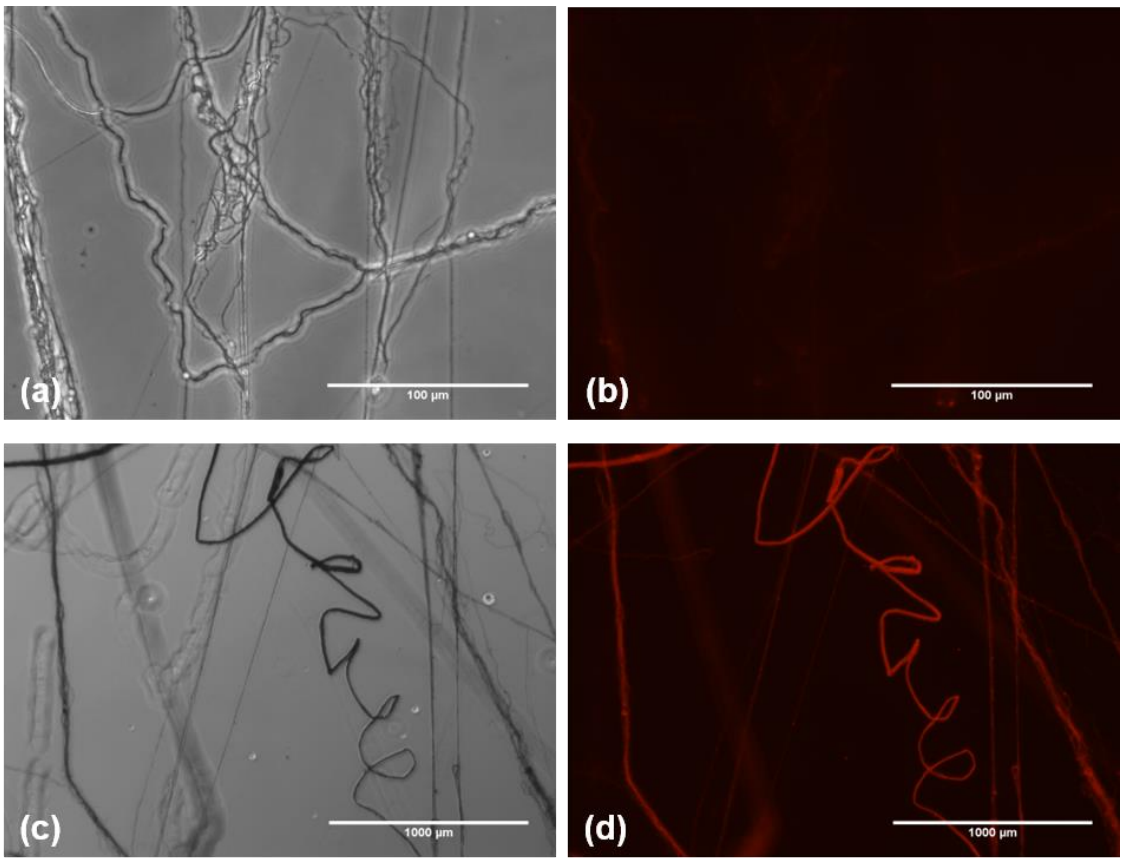

Figure 4-29 Fluorescence microscopy of GFPuv-AuBP2 PEO fibres (3000µl/min).

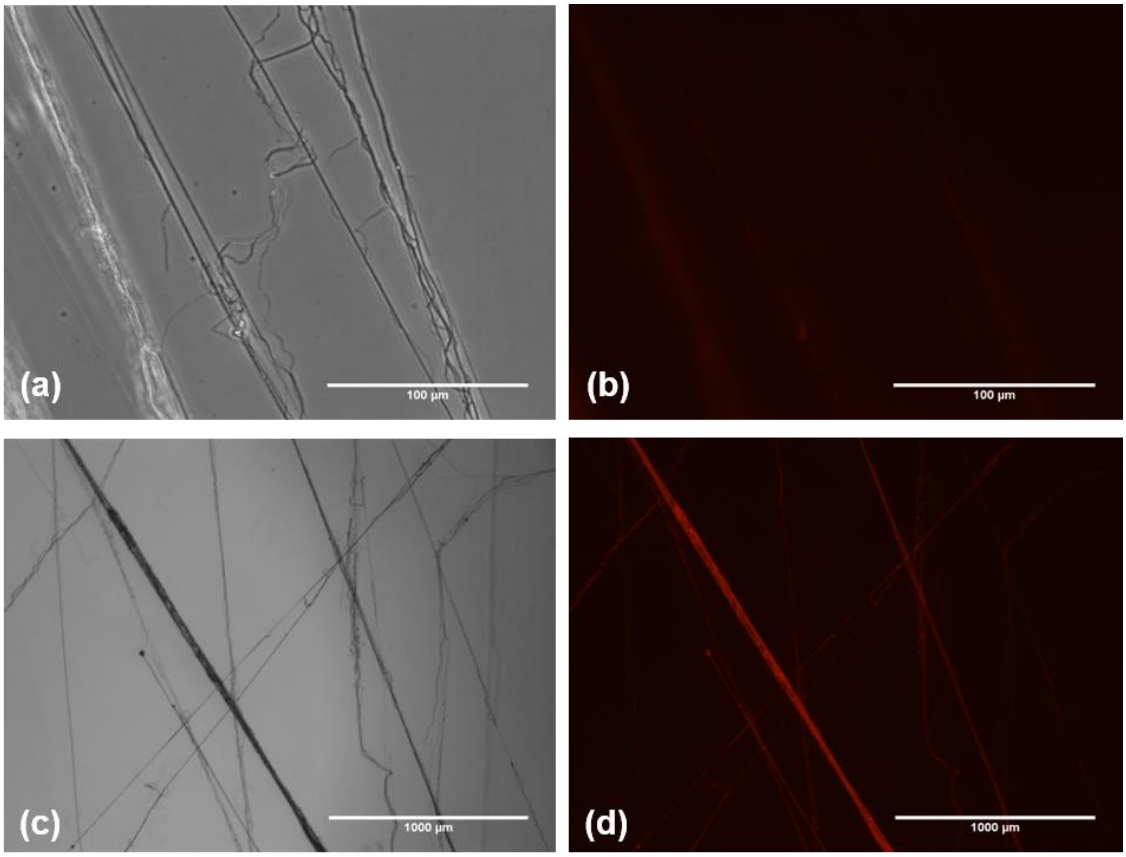

Figure 4-30 Fluorescence microscopy of GFPuv-AuBP2 PEO fibres (4000µl/min).

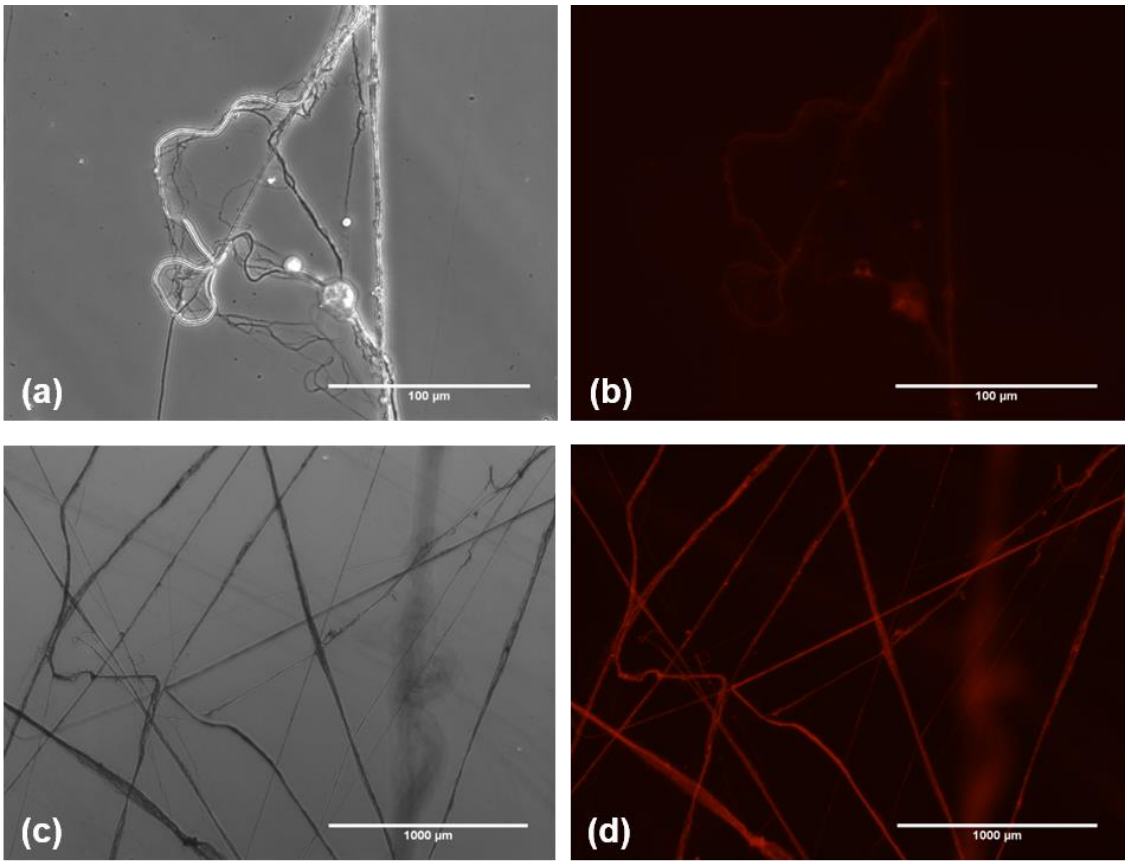

Figure 4-31 Fluorescence microscopy of GFPuv-AuBP2 PEO fibres (5000µl/min).

The effect of infusion flow rate on fibre shape is hard to be observed from the fluorescence images due to low magnification. However, this will be discussed in the next section where SEM is used at nanometre level with higher observation capacity. The protein is well-distributed in the fibres because all fibres show uniform fluorescence compared to the same positions observed through transmitted light. Compared to the results of previous addition, similar fluorescence outcome confirms the integration of engineered protein with gold nanoparticles to the polymer fibres.

The function of fluorescence protein works well after the fibre produced using this method. The 1000μm scale images show brighter colour due to more focus in a small field giving stronger fluorescence to the sensor of the microscope which submits better results of protein presence and distribution in fibres.

4.5.2 Fibre morphology

Figure 4-32 - Figure 4-37 show the SEM images along with the fibre diameter distributions. Images were recorded for each fibre sample produced at a flow rate of 500μl/min, 1000μl/min, 2000μl/min, 3000μl/min, 4000μl/min or 5000μl/min. Measurement was taken for the calculation of the average fibre diameter as well as size distribution.

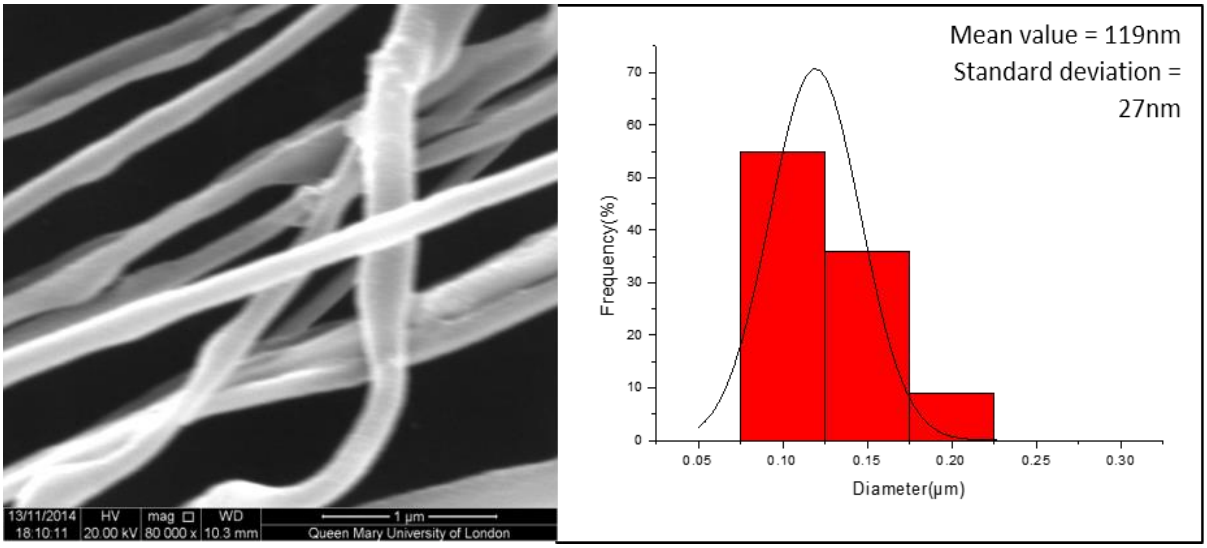

Figure 4-32 Size distribution of GFPuv-AuBP2 PEO fibres (500μl/min).

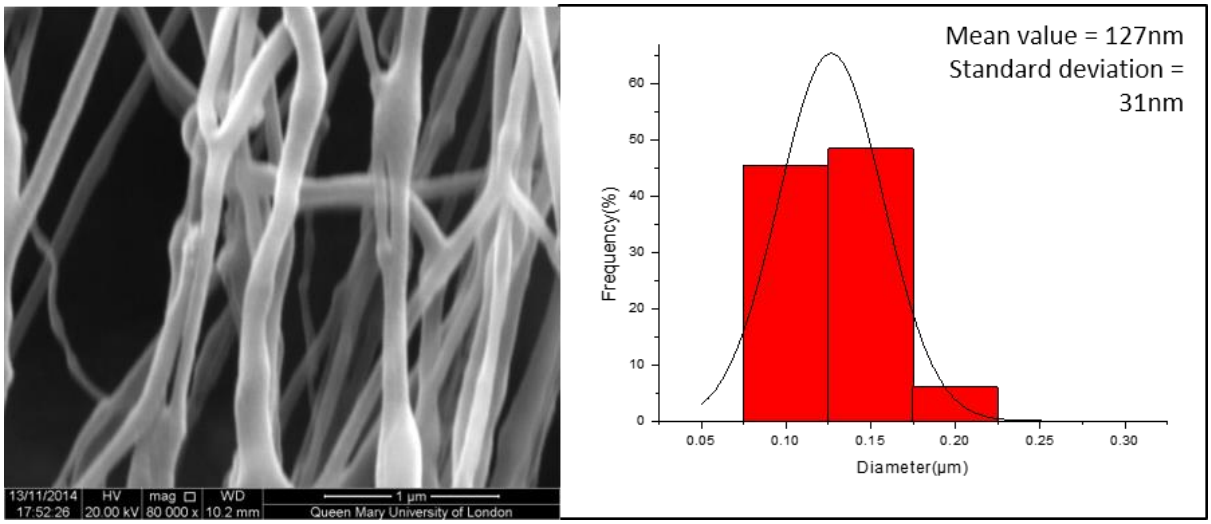

Figure 4-33 Size distribution of GFPuv-AuBP2 PEO fibres (1000µl/min).

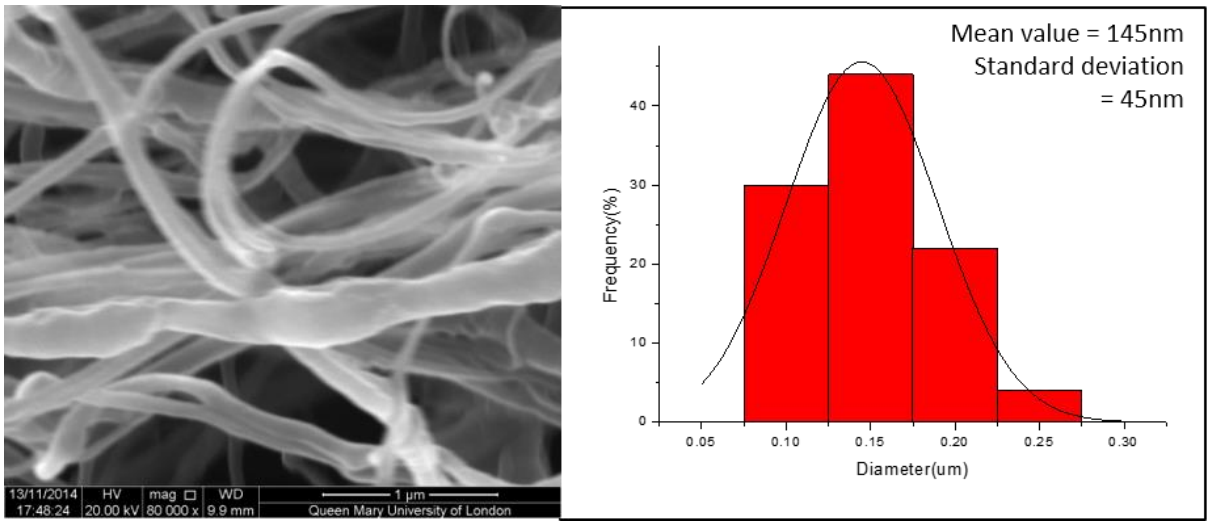

Figure 4-34 Size distribution of GFPuv-AuBP2 PEO fibres (2000µl/min).

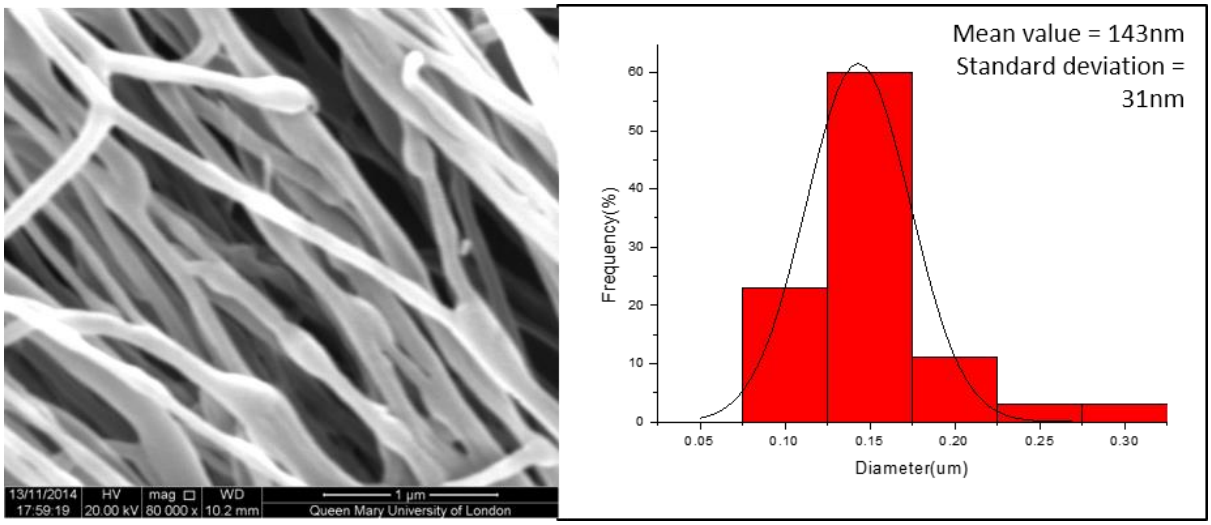

Figure 4-35 Size distribution of GFPuv-AuBP2 PEO fibres (3000µl/min).

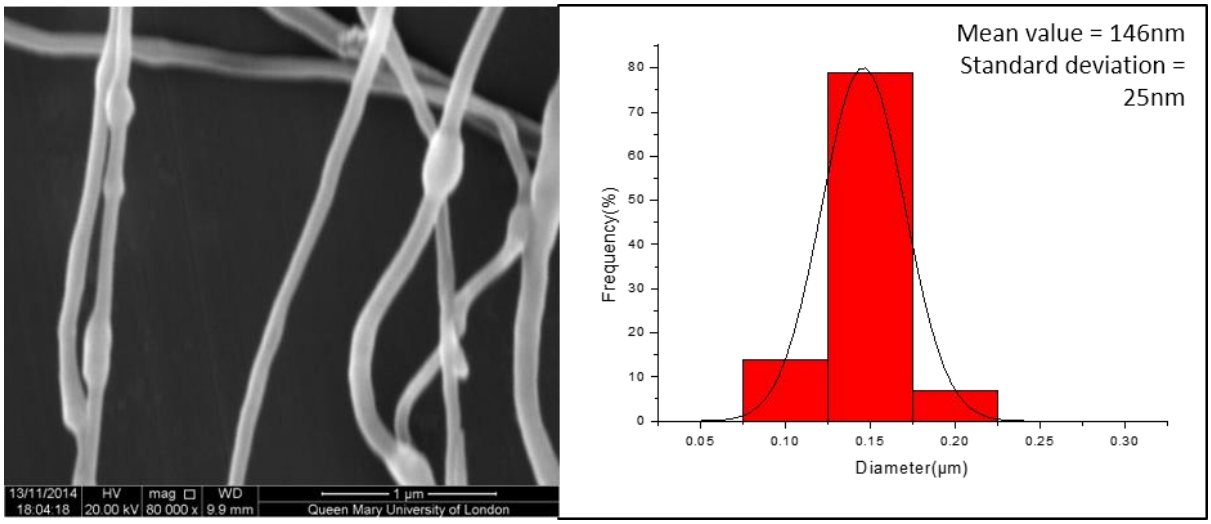

Figure 4-36 Size distribution of GFPuv-AuBP2 PEO fibres (4000µl/min).

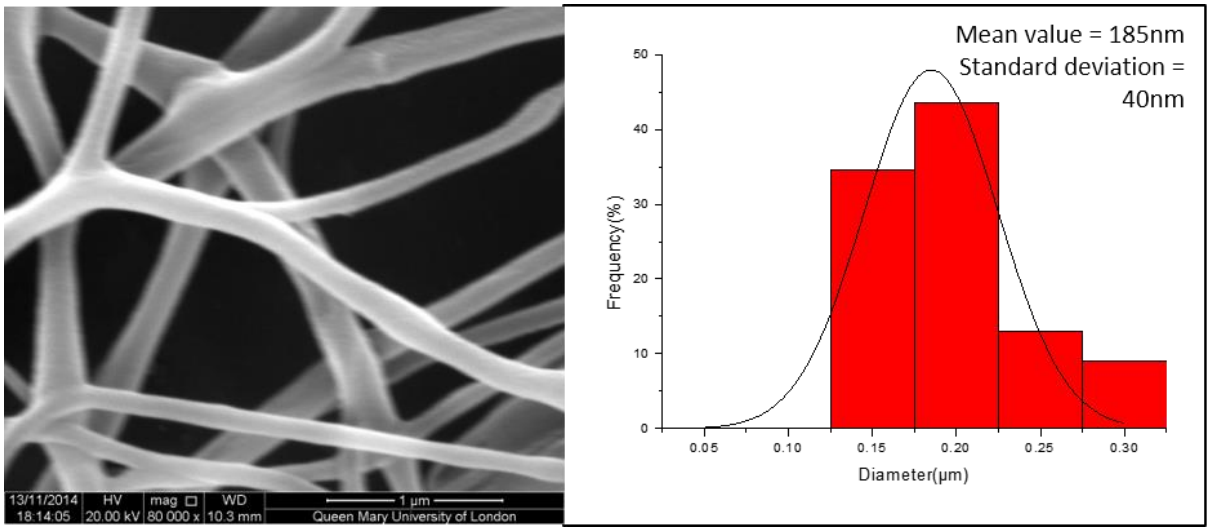

Figure 4-37 Size distribution of GFPuv-AuBP2 PEO fibres (5000µl/min).

The fibres display smooth shape without beads at this level. The plotted graph shows a trend of diameter increasing as flow rate grows (Figure 4-38).

The mean value of fibre diameter increases from 119nm to 185nm as the flow rate goes up from 500µl/min to 5000µl/min. However, from 2000µl/min to 4000µl/min, the curve is quite flat and the point at 3000µl/min decreases a little bit in the trend which also appeared in previous addition with DsRed-AuBP2 even at the exact 3000µl/min. The possible reason has been proposed in the last section (addition of DsRed-AuBP2) where the same idea may be shared.

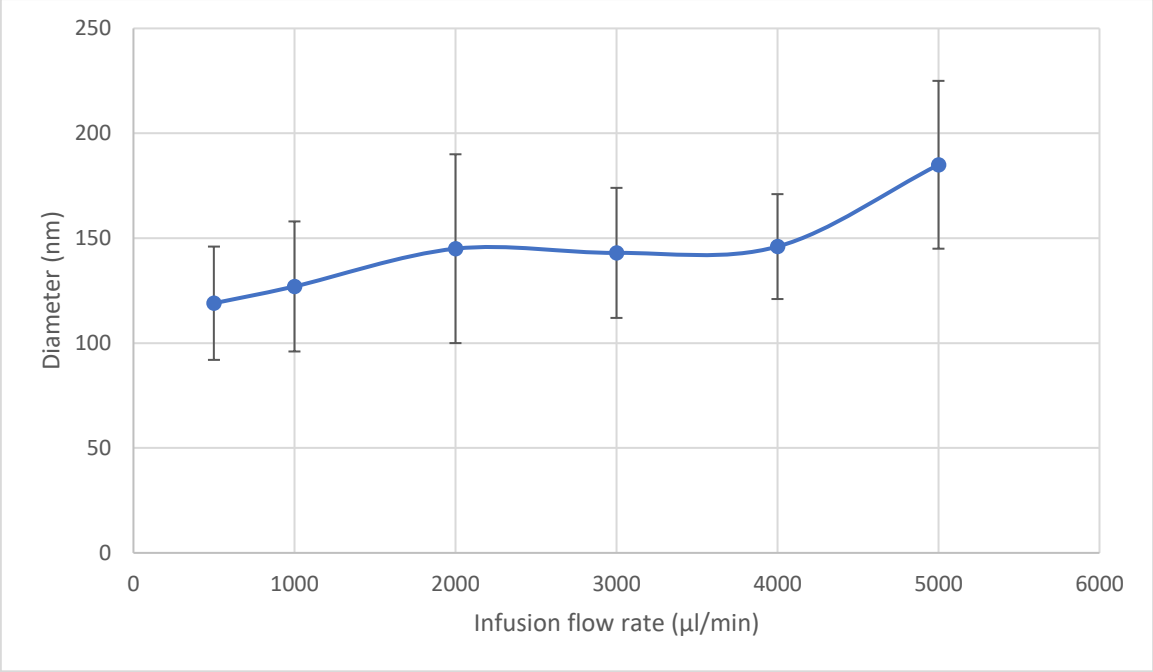

Figure 4-38 Infusion flow rate effect on the fibre mean diameter. GFPuv-AuBP2.

At or around this point, the balance may occur between the solvent evaporation and the volume of material change at orifice. The source of this balance needs to be analysed and will be discussed in Chapter 6. This phenomenon is confirmed because it happens in two additions with the same process conditions (flow rate, gyration speed and etc.) but different mixture materials (one is DsRed-AuBP2 and another is GFPuv-AuBP2). A repeat study will be in the next section. Moreover, this trend information is useful on flow rate selection for spinning in the future.

4.6 Addition of GFPuv-AuBP2 & MBP-DsRed-AuBP2 to 10wt% PEO-water solution

4.6.1 Fluorescence microscopy

Table 4-3 - Table 4-8 show the compared fluorescence microscopy images of fibre with two mixed proteins following an increasing flow rate with the same order as the past two additions from 500µl/min to 5000µl/min. Every fibre sample with different infusion flow rate was photographed at the same position of fibres in transmitted light mode, green fluorescence mode and red fluorescence mode for comparison. Two levels of scale (100µm and 400µm) were recorded during observation.

Similar to the previous addition of GFPuv-AuBP2, the fibres of all batches show continuous and uniform structure on apparent morphology through transmitted light with undetectable difference on shapes between each other at these scales.

Moreover, both green fluorescence images and red fluorescence images for the same batch support the present evidence as well as the working status of GFPuv-AuBP2 and MBP-DsRed-AuBP2 proteins in fibre because of the positive fluorescence sign shown in both pictures. It also confirms that these two proteins function well with no disturbance on each other when they are mixed together at the same volume in PEO-water solution.

They did not lose their respective fluorescence after being processed into fibres. This means these two proteins can be used together as composite materials for fibre which will enhance its complexity and flexibility. The same volume mixture of the proteins is noticed in this addition. The ratio of protein mixture may deliver a different level of red or green fluorescence for presenting fibres with designed proportion of light intensity on different wavelengths in some application.

MBP-DsRed-AuBP2 & GFPuv-AuBP2 Mixture-PEO fibres (500µl/min)		
Transmitted light image	Red fluorescence image	Green fluorescence image
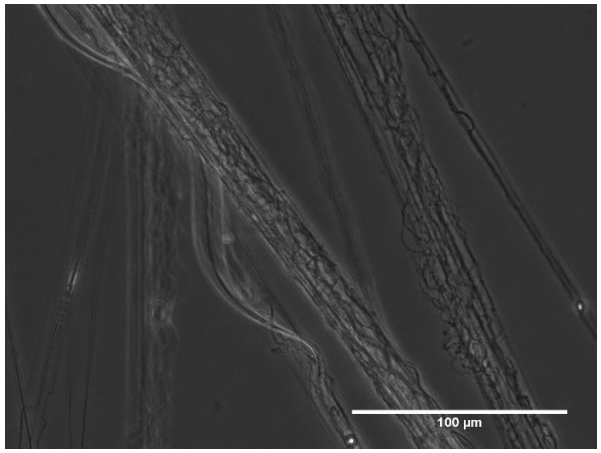	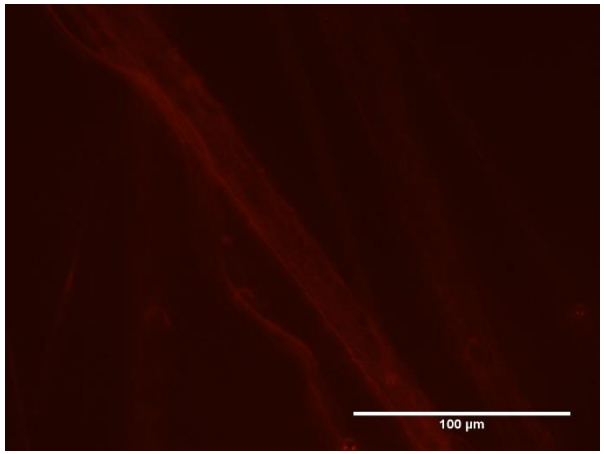	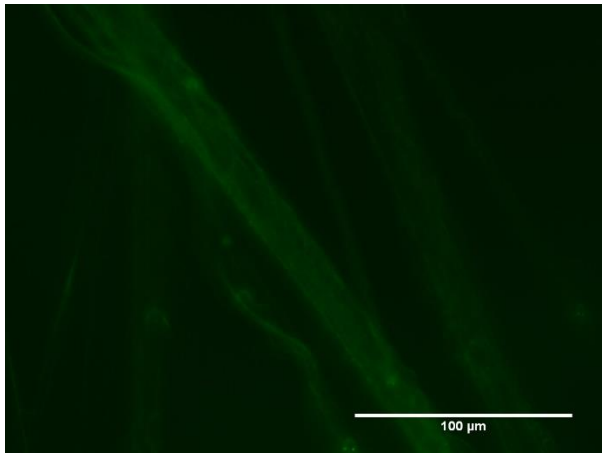
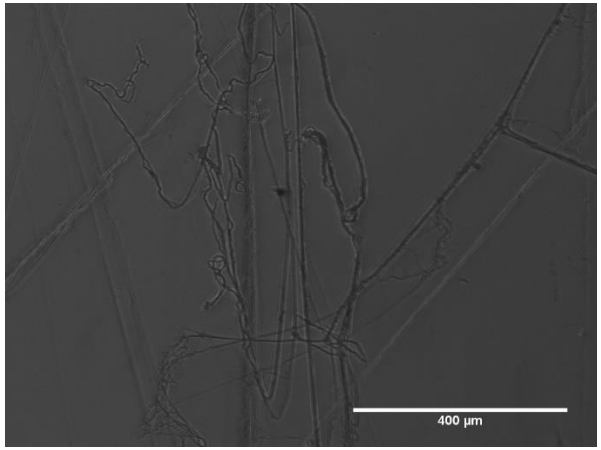	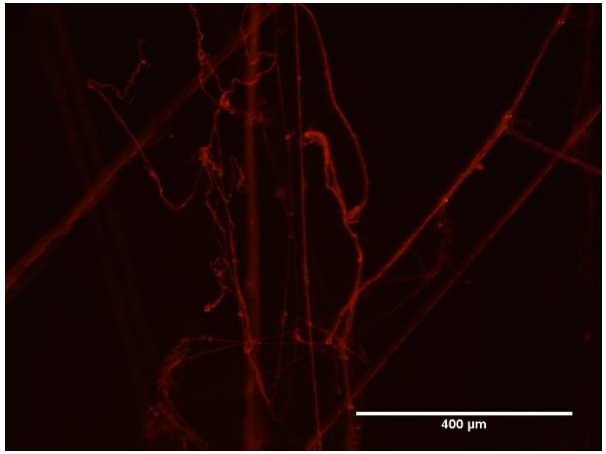	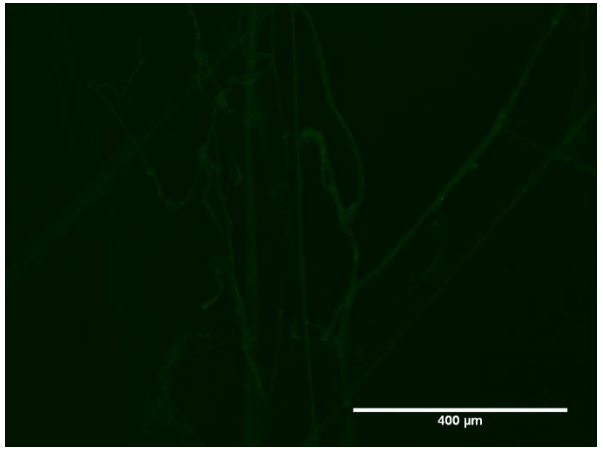

Table 4-3 Fluorescence microscopy images of mixed protein PEO fibres at a flow rate of (a) 500µl/min.

MBP-DsRed-AuBP2 & GFPuv-AuBP2 Mixture-PEO fibres (1000µl/min)		
Transmitted light image	Red fluorescence image	Green fluorescence image
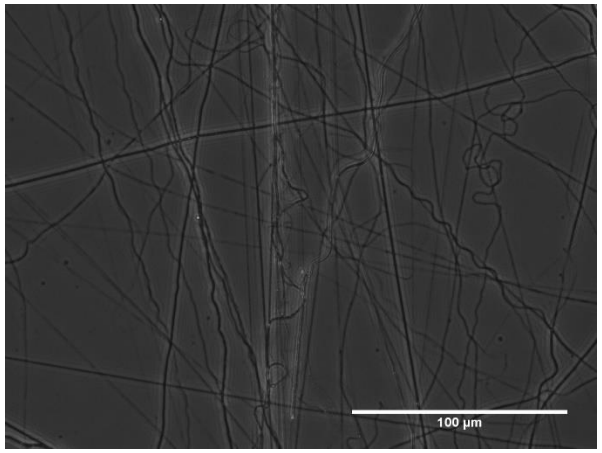	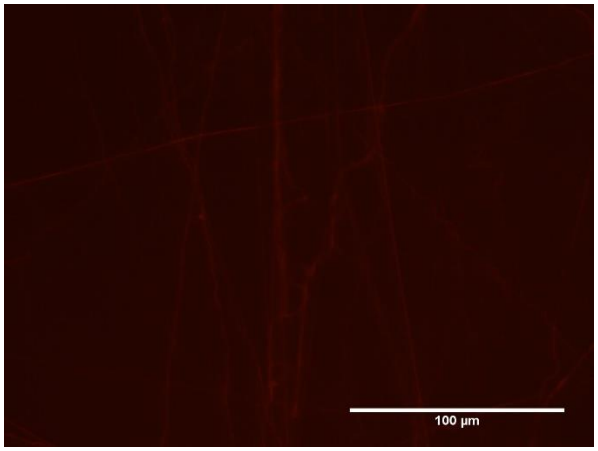	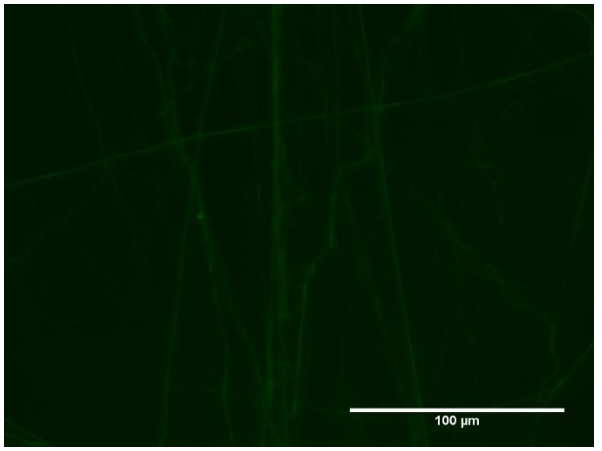
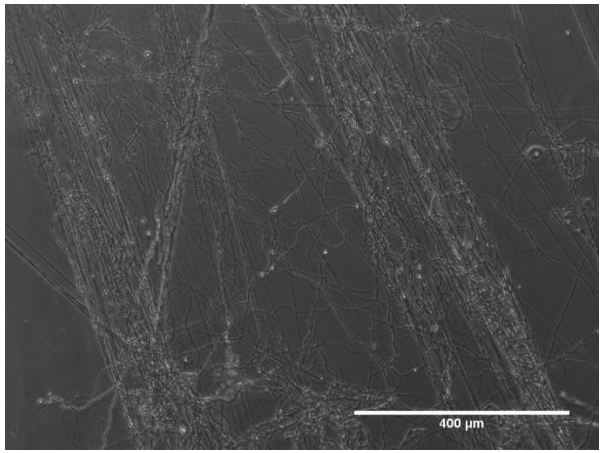	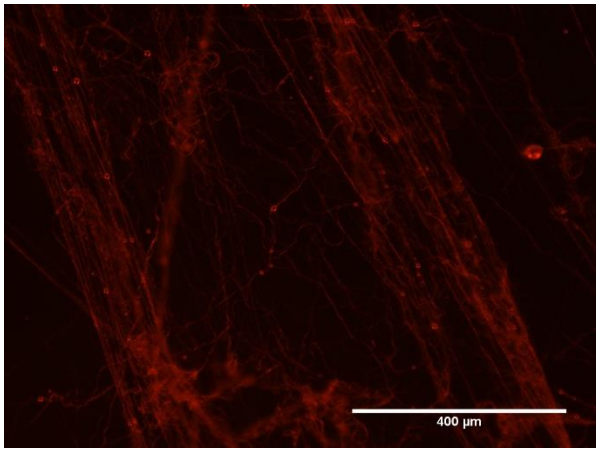	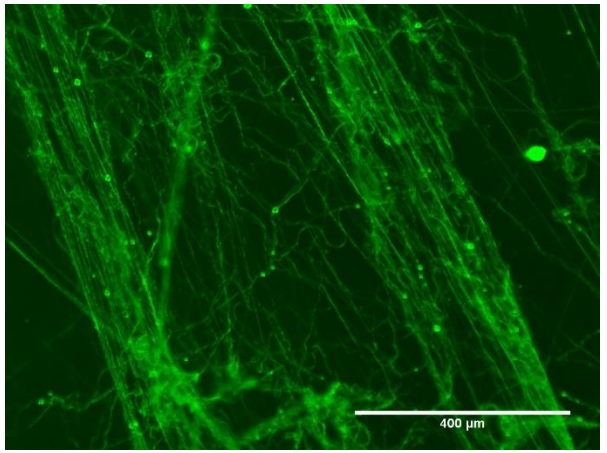

Table 4-4 Fluorescence microscopy images of mixed protein PEO fibres at a flow rate of (b) 1000µl/min.

MBP-DsRed-AuBP2 & GFPuv-AuBP2 Mixture-PEO fibres (2000µl/min)		
Transmitted light image	Red fluorescence image	Green fluorescence image
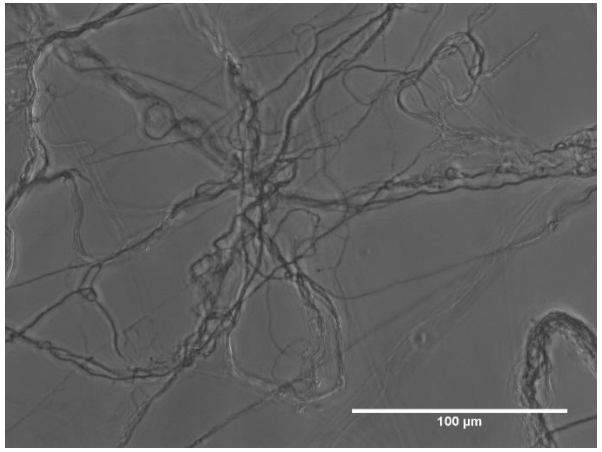	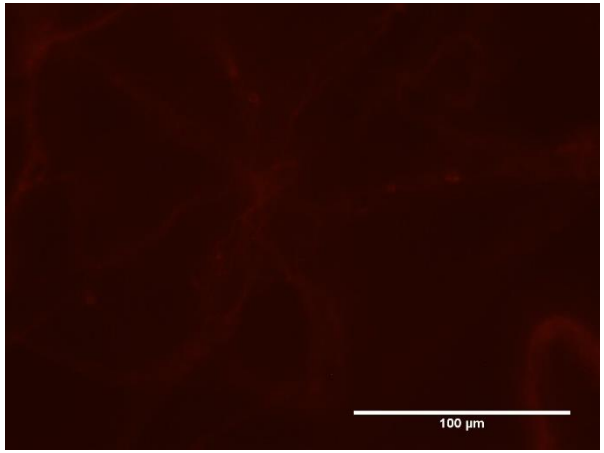	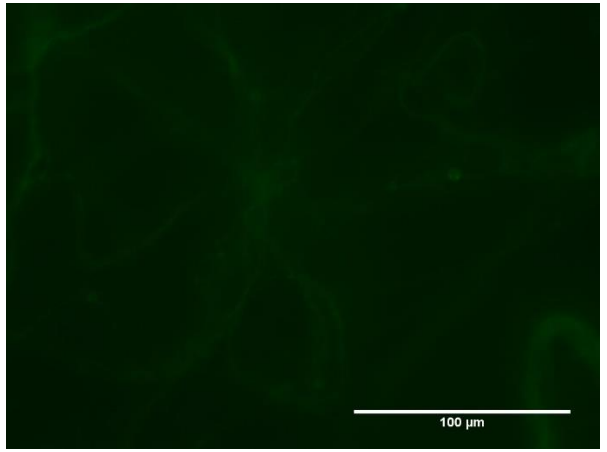
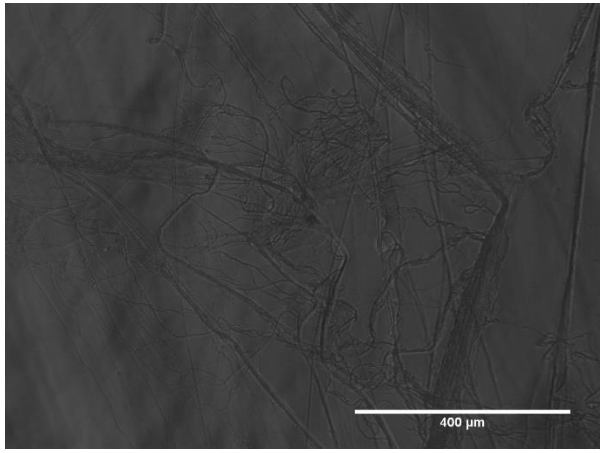	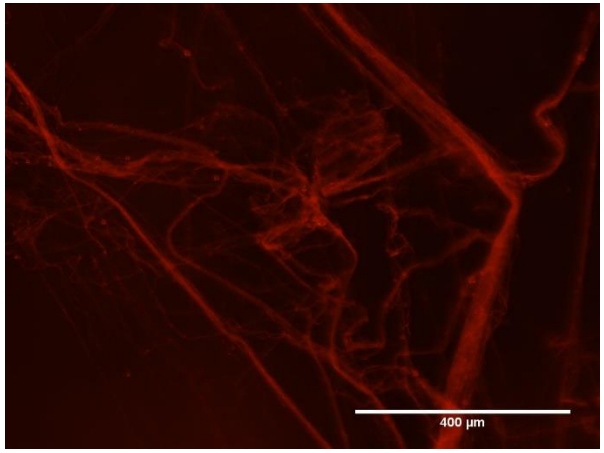	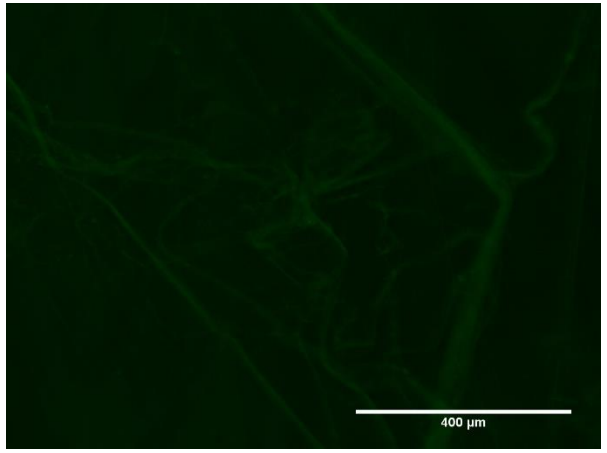

Table 4-5 Fluorescence microscopy images of mixed protein PEO fibres at a flow rate of (c) 2000µl/min.

MBP-DsRed-AuBP2 & GFPuv-AuBP2 Mixture-PEO fibres (3000µl/min)		
Transmitted light image	Red fluorescence image	Green fluorescence image
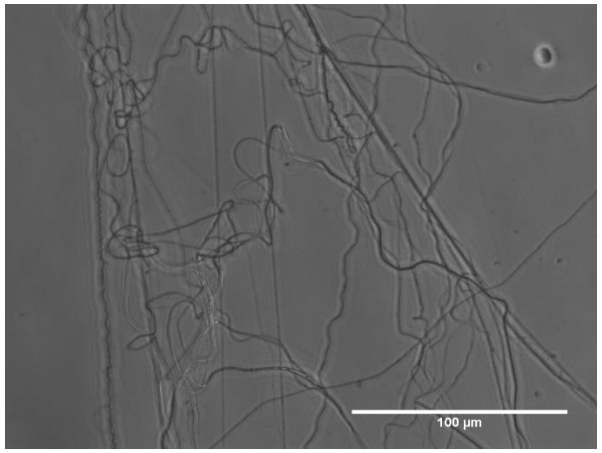	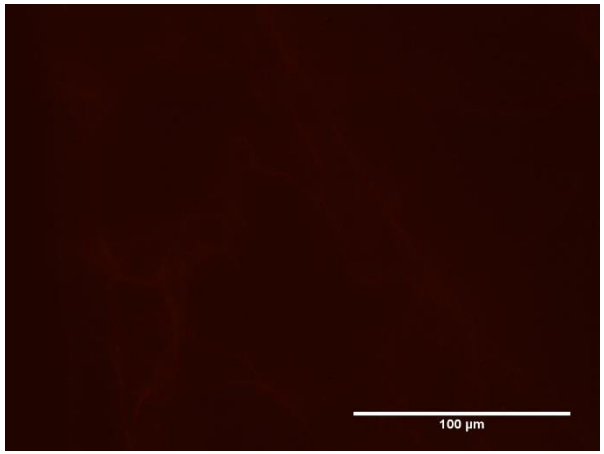	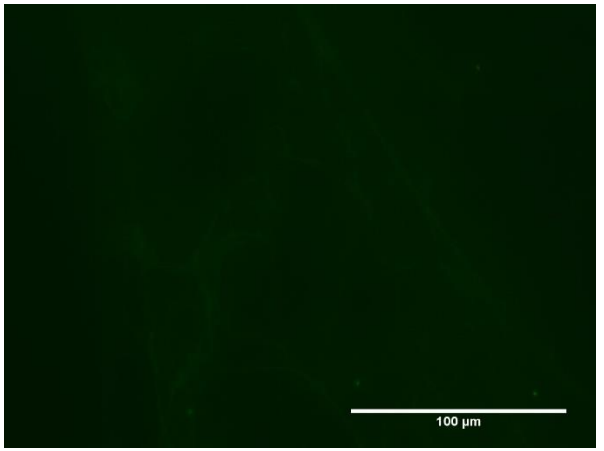
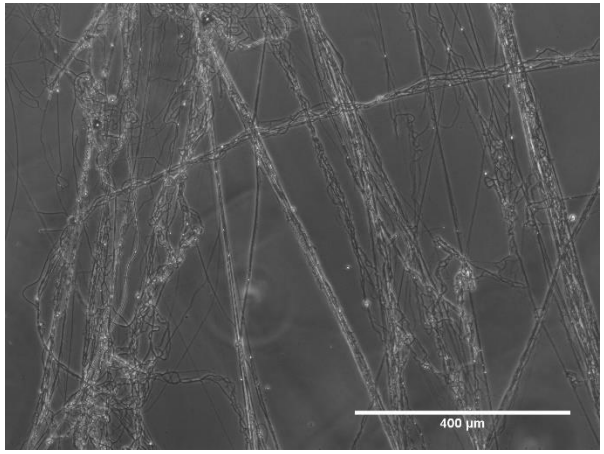	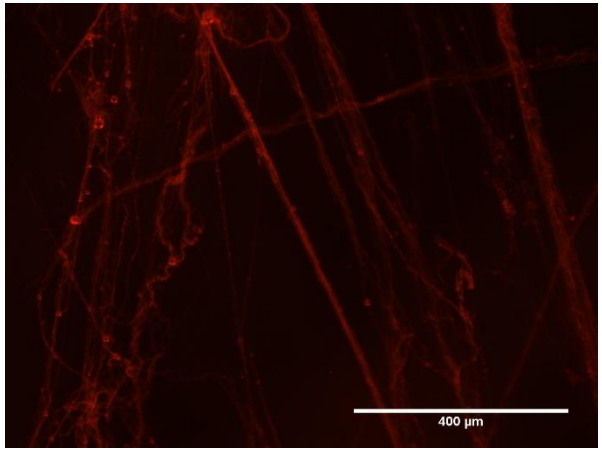	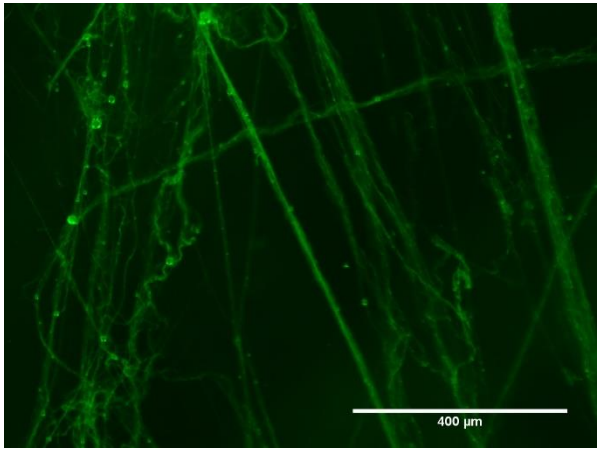

Table 4-6 Fluorescence microscopy images of mixed protein PEO fibres at a flow rate of (d) 3000µl/min.

MBP-DsRed-AuBP2 & GFPuv-AuBP2 Mixture-PEO fibres (4000µl/min)		
Transmitted light image	Red fluorescence image	Green fluorescence image
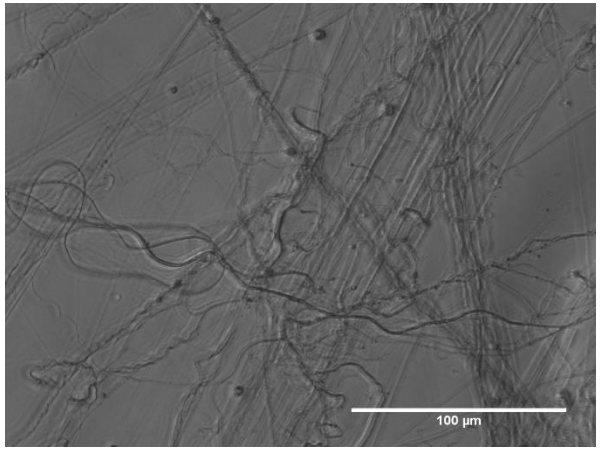	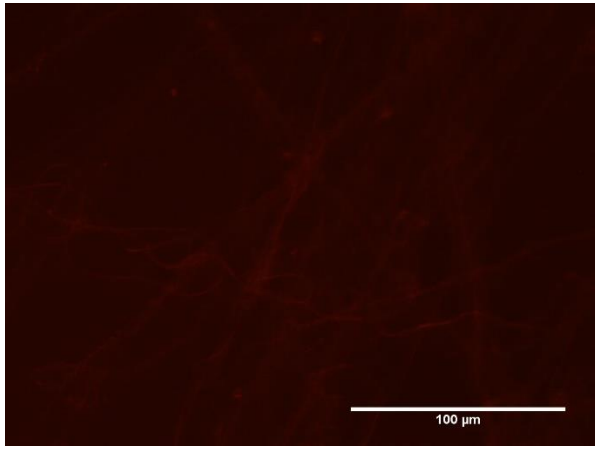	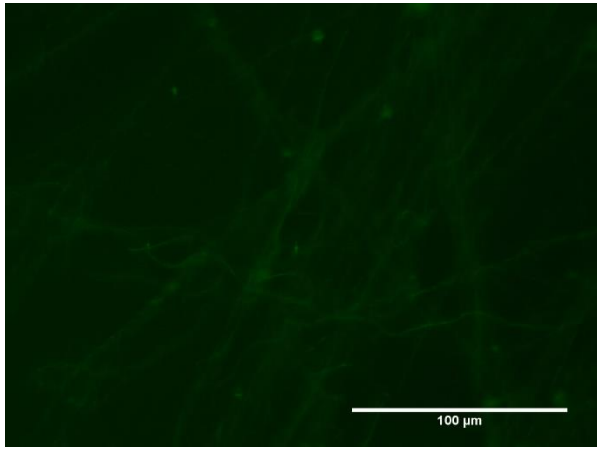
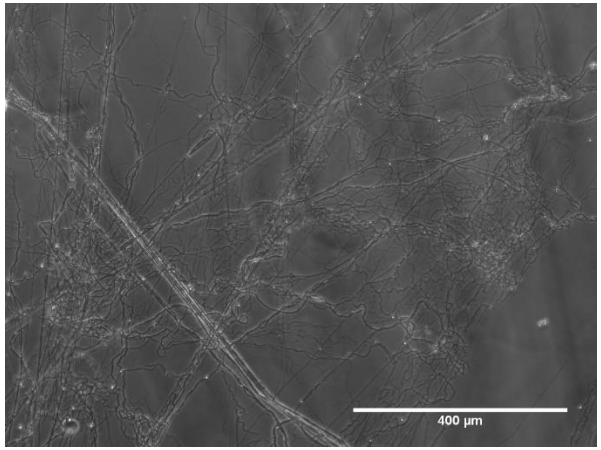	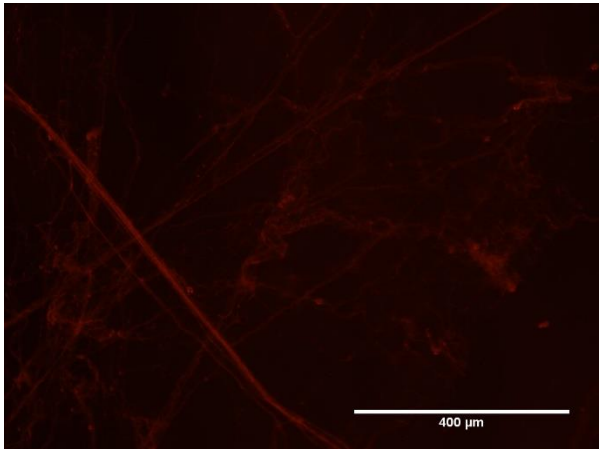	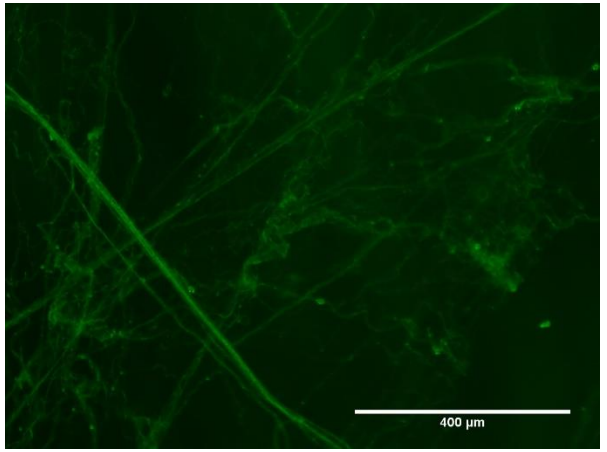

Table 4-7 Fluorescence microscopy images of mixed protein PEO fibres at a flow rate of (e) 4000µl/min.

MBP-DsRed-AuBP2 & GFPuv-AuBP2 Mixture-PEO fibres (5000µl/min)		
Transmitted light image	Red fluorescence image	Green fluorescence image
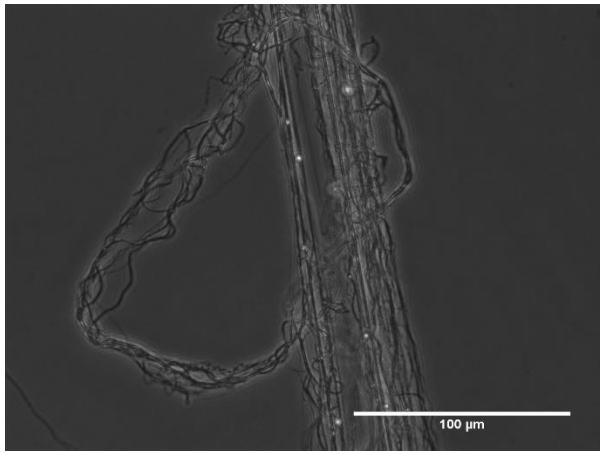	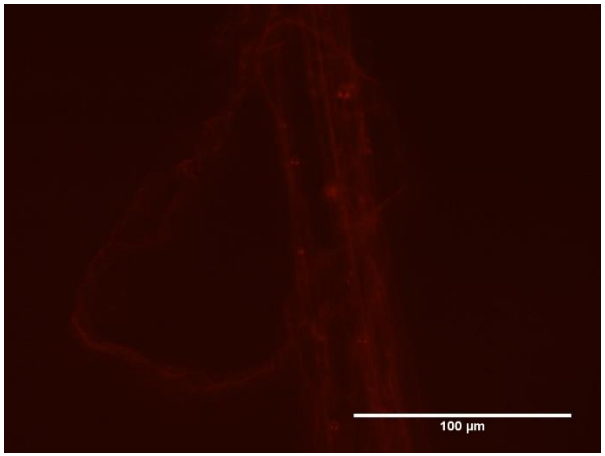	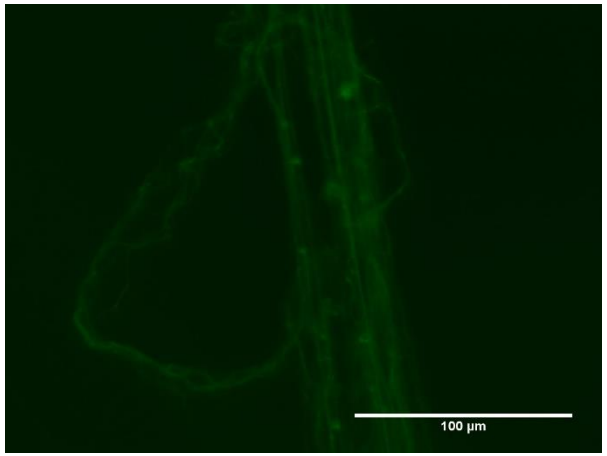
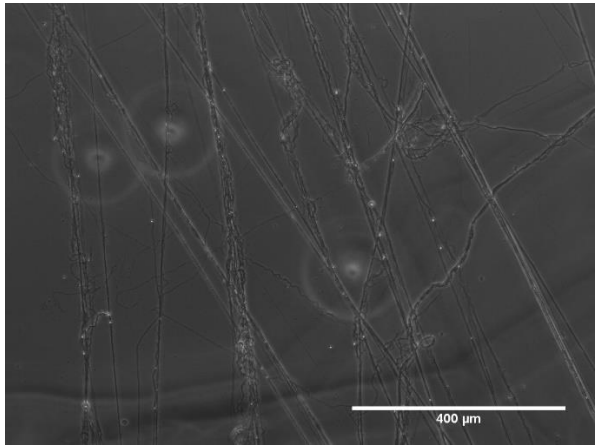	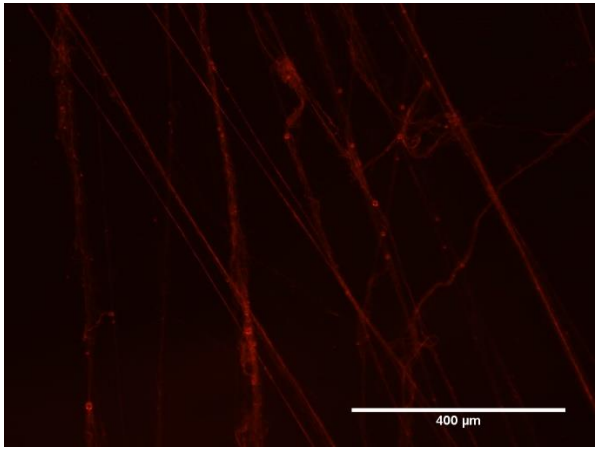	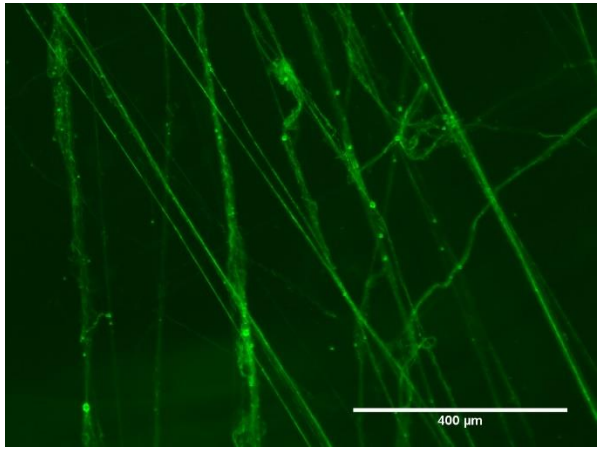

Table 4-8 Fluorescence microscopy images of mixed protein PEO fibres at a flow rate of (f) 5000µl/min.

4.6.1 Fibre morphology

Figure 4-39 - Figure 4-44 give the SEM images of fibre samples with different infusion flow rate by the same value and order of the previous addition (GFPuv-AuBP2). The average diameter of the fibres was measured and recorded for the size distribution calculation. The fibres are still smooth and uniform. The mean values of the fibre diameter show a decreasing trend (138nm, 125nm, 137nm, 133nm, 124nm and 117nm) as the flow rate increases (500μl/min, 1000μl/min, 2000μl/min, 3000μl/min, 4000μl/min and 5000μl/min) except the one of 1000μl/min (125nm).

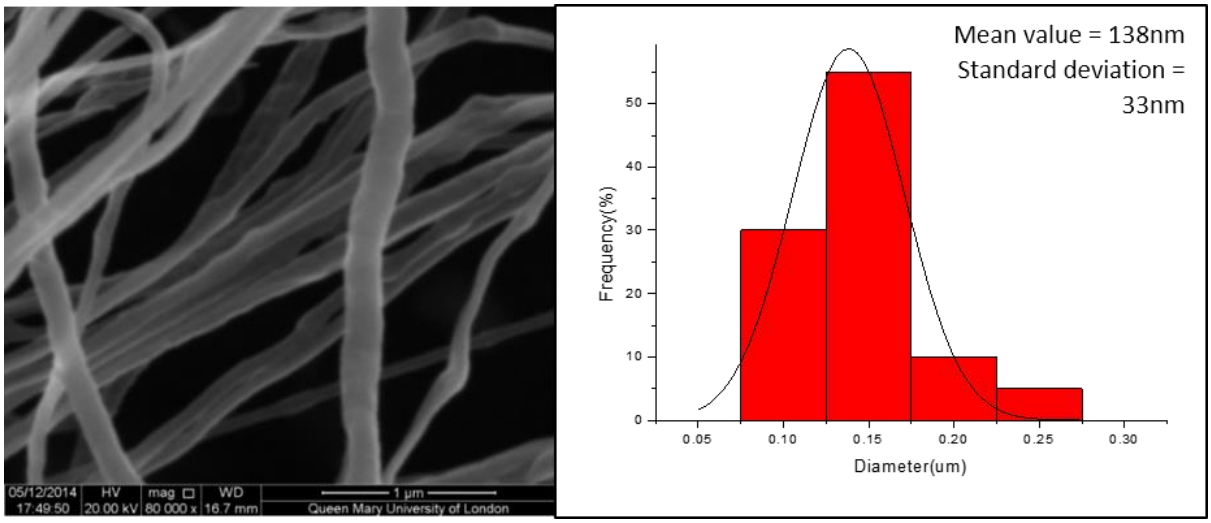

Figure 4-39 Size distribution of GFPuv-AuBP2 mixed with MBP-DsRed-AuBP2 PEO fibres (500μl/min).

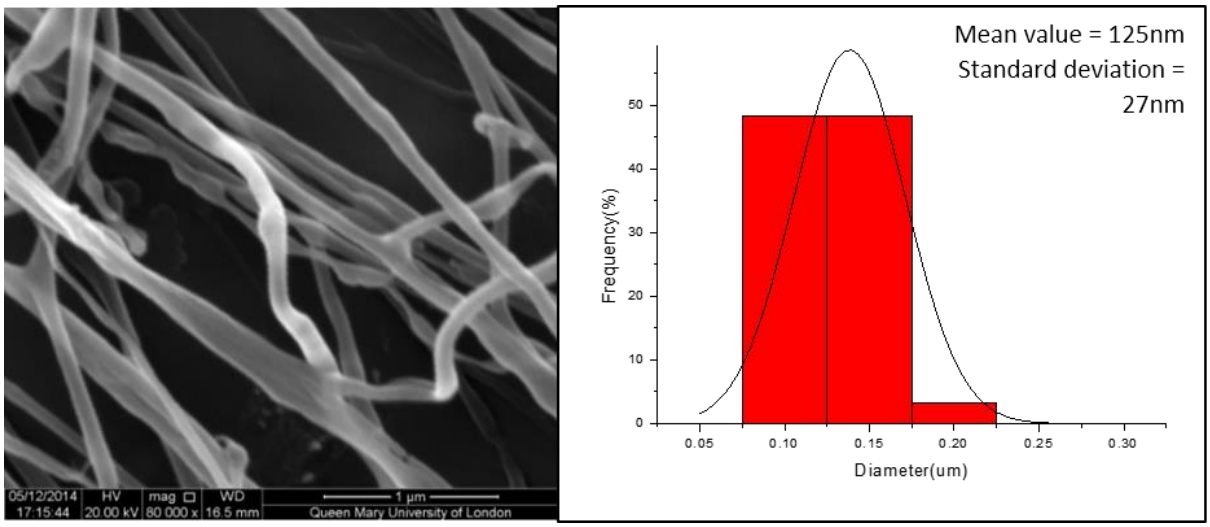

Figure 4-40 Size distribution of GFPuv-AuBP2 mixed with MBP-DsRed-AuBP2 PEO fibres (1000μl/min).

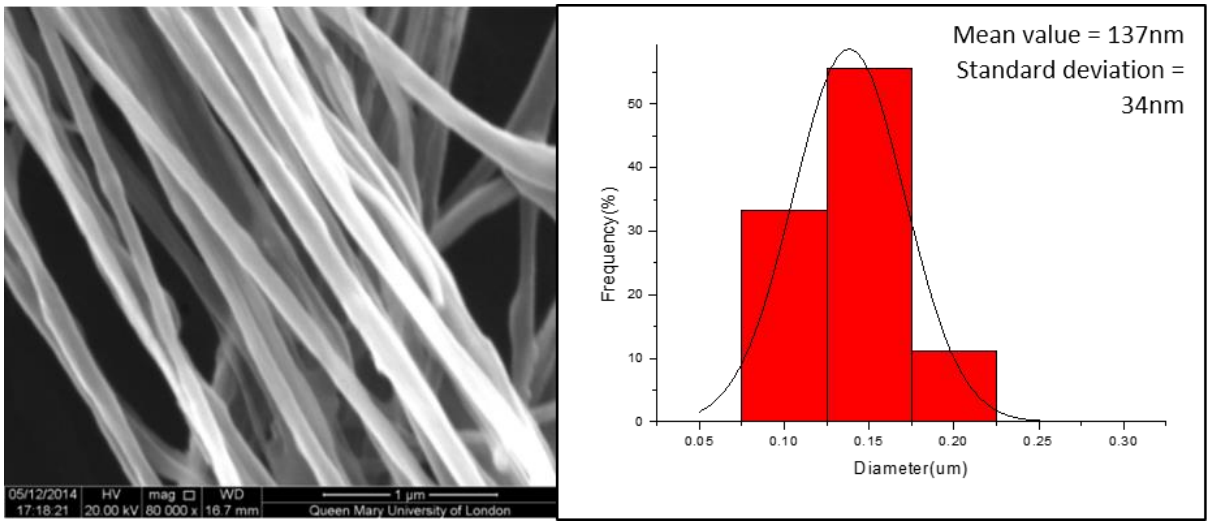

Figure 4-41 Size distribution of GFPuv-AuBP2 mixed with MBP-DsRed-AuBP2 PEO fibres (2000µl/min).

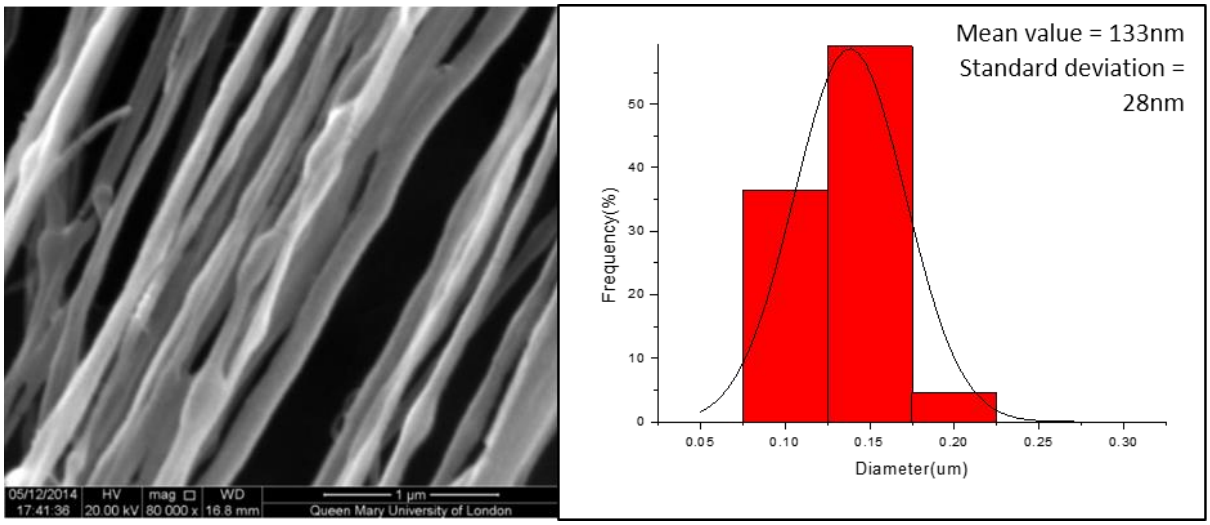

Figure 4-42 Size distribution of GFPuv-AuBP2 mixed with MBP-DsRed-AuBP2 PEO fibres (3000µl/min).

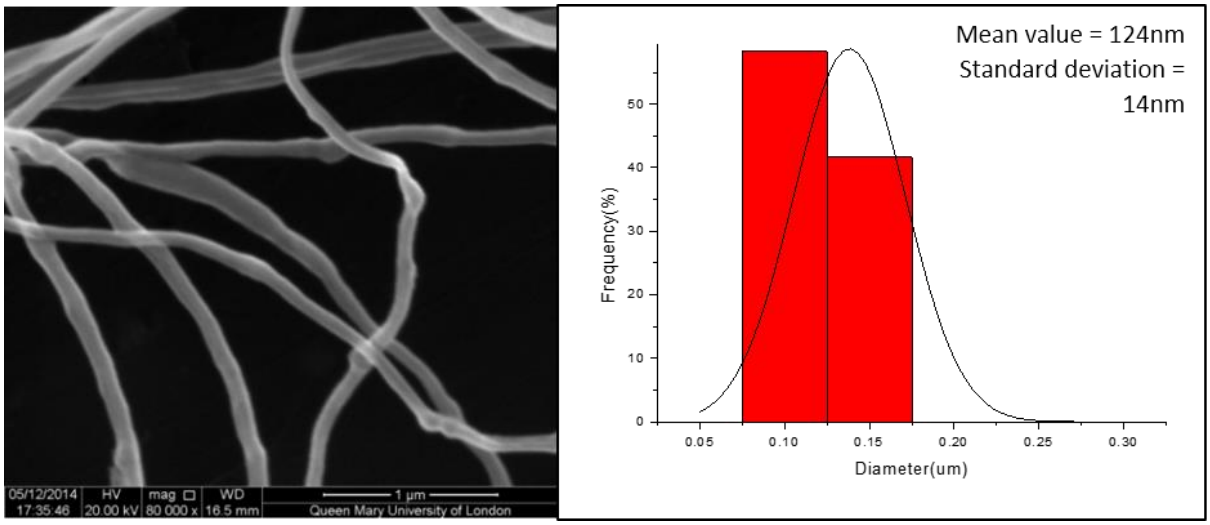

Figure 4-43 Size distribution of GFPuv-AuBP2 mixed with MBP-DsRed-AuBP2 PEO fibres (4000µl/min).

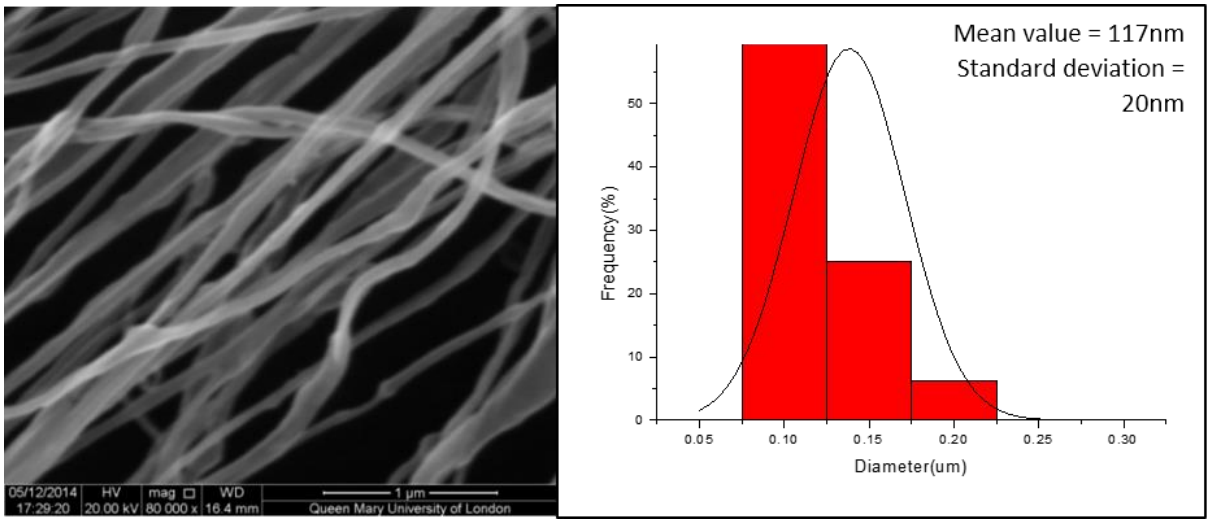

Figure 4-44 Size distribution of GFPuv-AuBP2 mixed with MBP-DsRed-AuBP2 PEO fibres (5000µl/min).

From plotted Figure 4-45, it is seen that there are two differences for this part compared to the previous additions. One is the trend on mean diameter of this addition which has an opposite direction to both previous ones with the same increasing fibre size in general. Another is the flow rate 'dropping point' (1000µl/min), which has been discussed in the last section, of this addition which differs from the other two which share the same point of 3000µl/min.

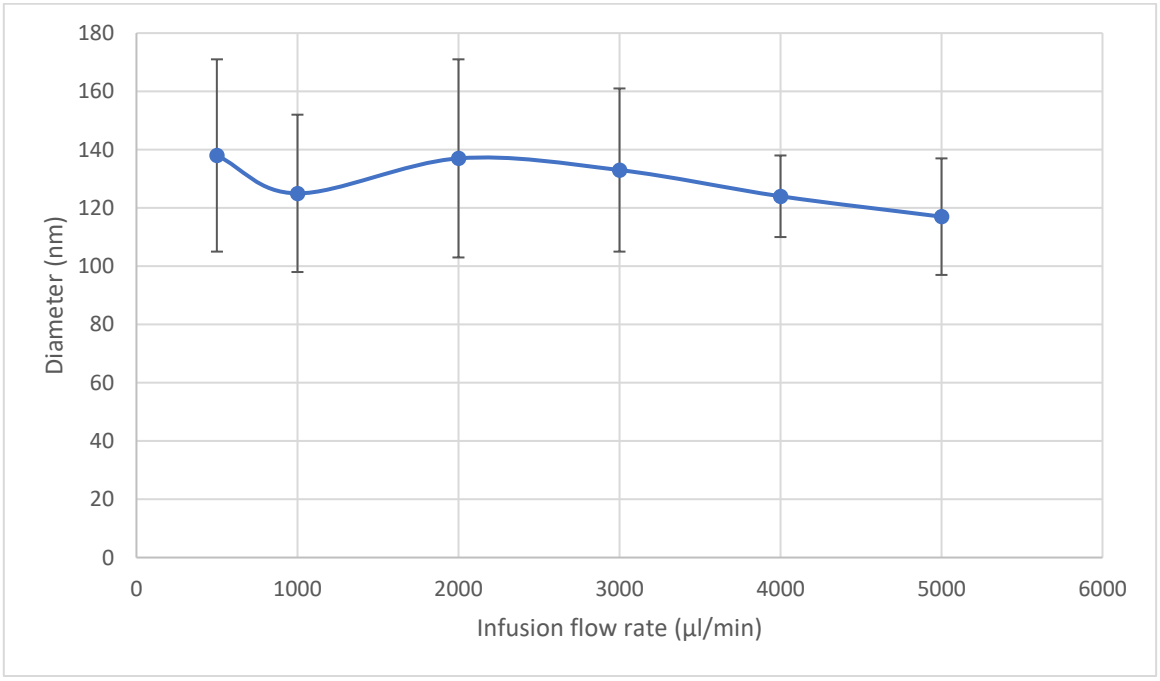

Figure 4-45 Infusion flow rate effect on the fibre mean diameter. Mixed proteins.

The concentration of the solutions and the gyration conditions for all three additions are the same. However, this one has two types of protein mixed in the polymer solution which clearly affects the process of fibre forming. The mixture may change the property of the solution and shift the trend. The phenomenon of a lower point in between the values still exists in this addition. Therefore, in this fibre process system, the 'dropping point' regarding the particular flow rate always exists in general which can be influenced by the solution property. This needs to be taken into consideration when a desired fibre size is decided to achieve through controlling the flow rate during the experiment. The discussion will be made depending on the results from all additions.

4.7 Effect of Flow Rate

From all three types of fibre formation outcome, the data can be combined illustrating the effect of flow rate on the fibre size (Figure 4-46).

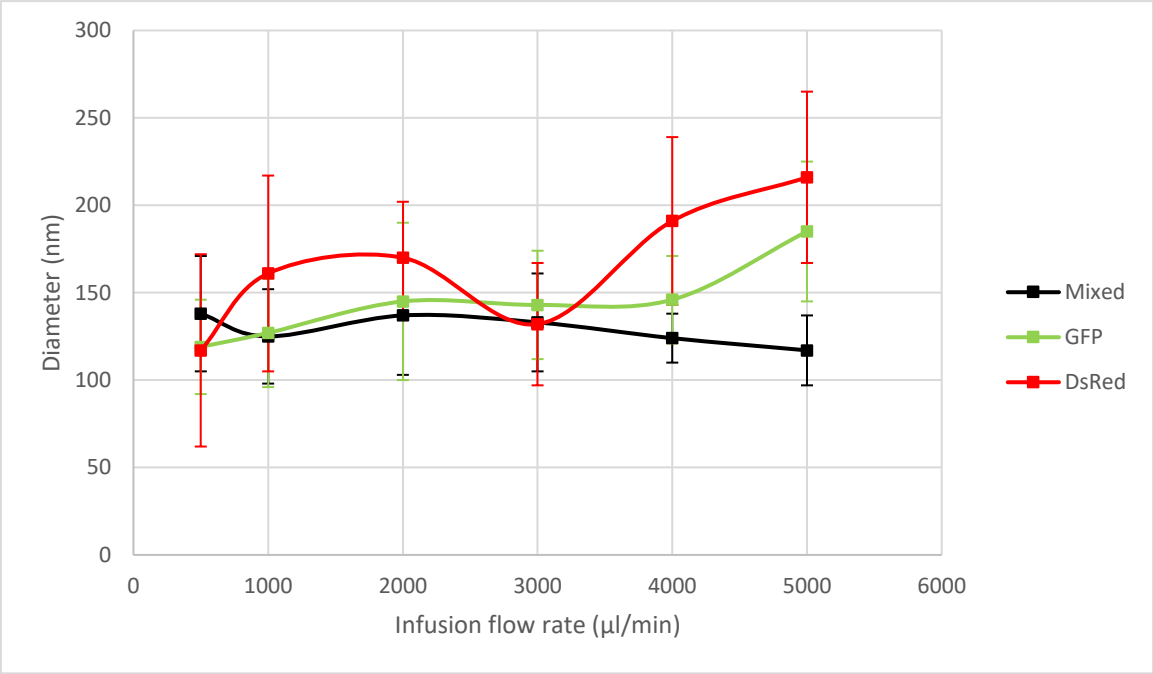

Figure 4-46 Infusion flow rate effect on the fibre mean diameter.

Firstly, the change for all samples on fibre size is not large (50nm – 280nm) which promise the applications requiring size control on this level. Then, the size of three samples is observed very close on 3000μl/min which makes this point ‘strange’. The huge drop for DsRed sample happens at this flow rate point which was also recorded for pressure coupled infusion gyration (see Chapter 2). It is noted that pressure coupled infusion gyration uses different concentration of PEO-water (5%, 10%, 15% and 21% in weight) for comparison, however, the variety of pressure and rotating speed shows no influence on this ‘strange point’ which means this point only relates to flow rate. As the point comes along with the infusion flow rate factor, this interesting phenomenon has not been reported in other methods such as pressurised gyration which will be fully discussed in Chapter 6 delivering possible explanation.

Chapter 5.

Fabrication of PVA fibres with magnetic nanoparticles for remote-controlled drug release

5.1 Introduction

The goal of this study is to demonstrate a magnetically actuated drug delivery system, based on PVA-MNP fibres, generated *via* infusion gyration (Figure 5-1). The fibres are made of biocompatible components targeting biomedical applications, specifically, drug release. The ability of these fibres to be actuated *via* an external magnetic field is demonstrated, along with extensive characterization of its physical-chemical properties. The release of controlled quantities of acetaminophen, *via* magnetic actuation of this material, is explored. Furthermore, the advantages and potential scope of application, beyond drug-delivery, are discussed.

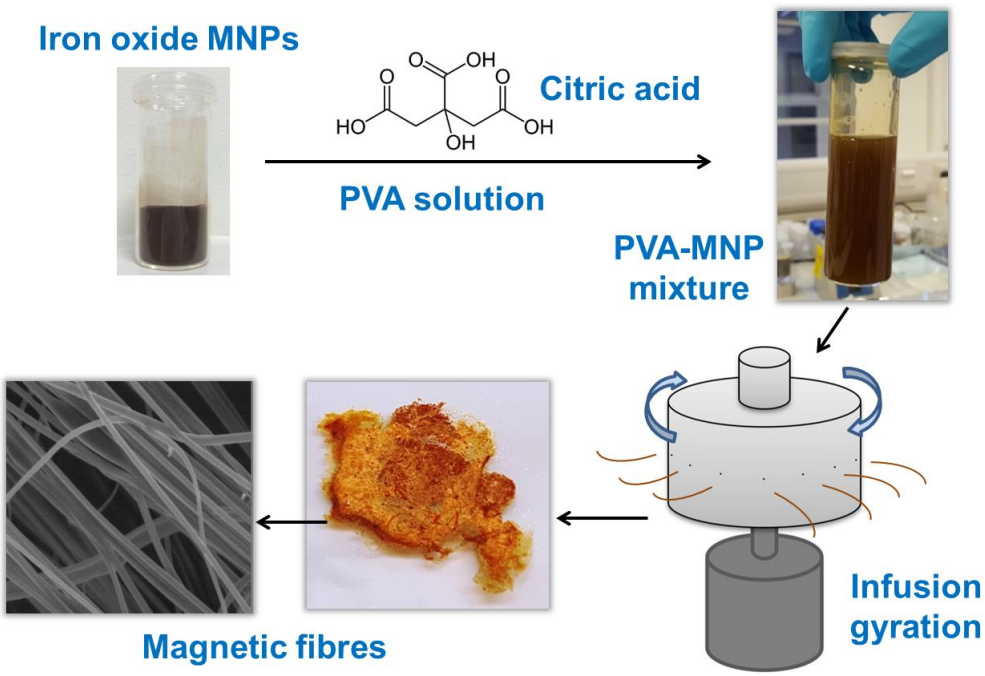

Figure 5-1 Fabrication of PVA fibres with magnetic nanoparticles.

5.2 High Speed Camera

Figure 5-2 shows the snapshot images of the video which records the fibre formation of PVA aqueous solution around the spinning cylinder. Moreover, Figure 5-3 indicates the moment of the polymer solution jet coming out of the vessel orifice. From these images, it is known that infusion gyration is functioning well and stable.

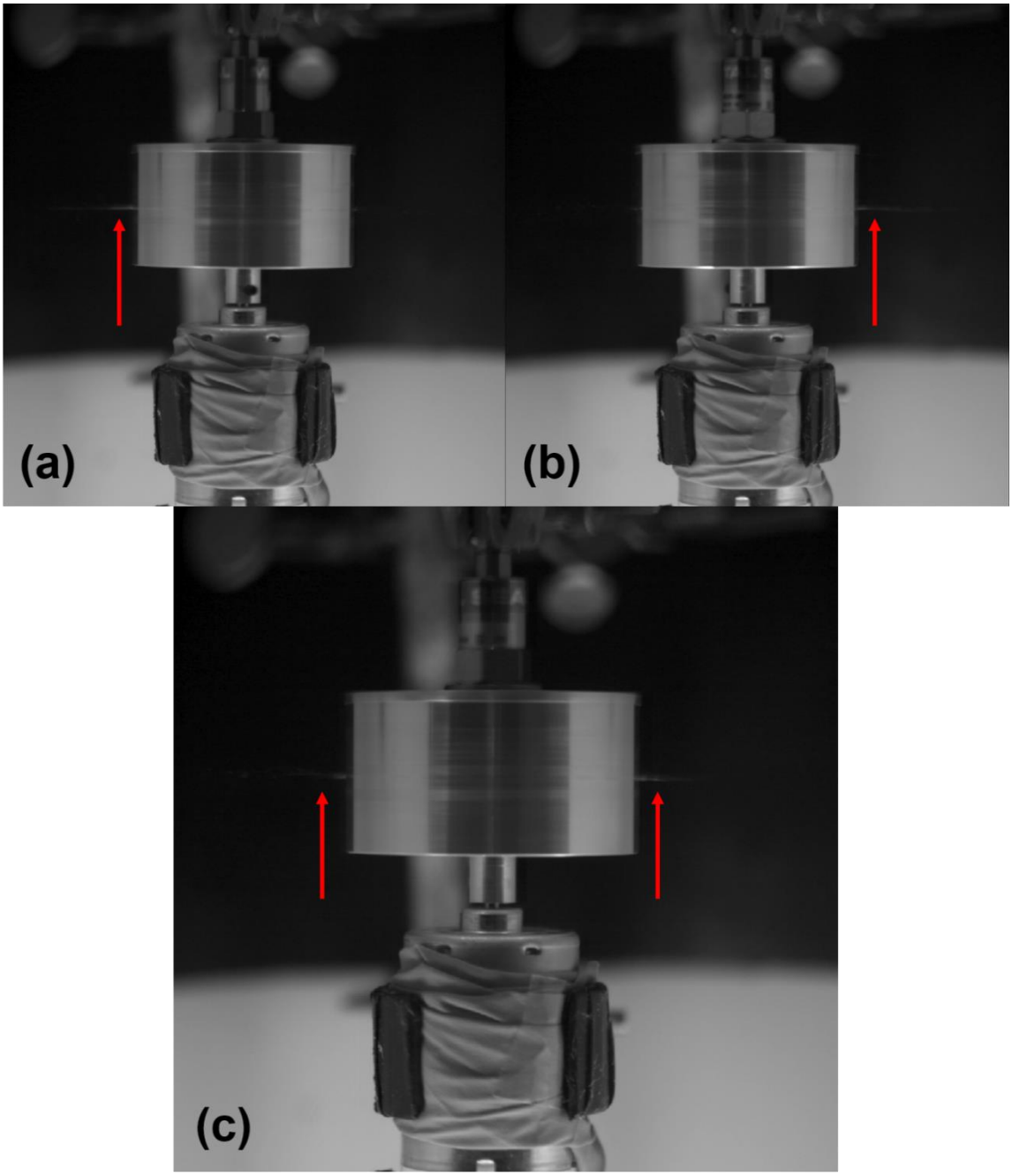

Figure 5-2 High-speed camera snapshot images of the spinning cylinder showing fibre formation during the infusion gyration process. The red arrow indicates the solution jet (a)(b)(c).

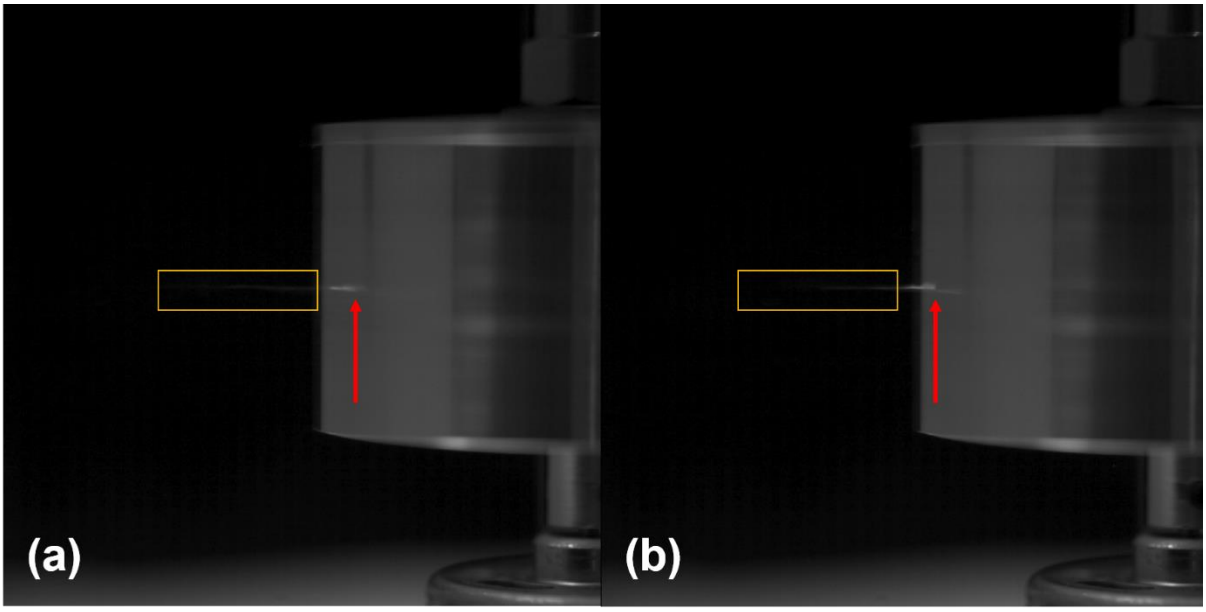

Figure 5-3 High-speed camera snapshot images of the spinning cylinder showing fibre formation during the infusion gyration process. The red arrow indicates the solution jet and the yellow square indicates jet dragging (a)(b).

The drag of the polymer solution jet which is included in the fibre formation process theoretically is confirmed by practice.

5.3 SEM and Fibre Morphology

Four different solutions were made and spun for study which are pure PVA solution (0%), 3%(wt), 4%(wt) and 5%(wt) of MNPs under the same conditions of 36,000rpm and flow rate 4000µl/min. In the practice of solution mixture making, 5 % (wt) MNPs in PVA solution is close to the limit of mixing. Beyond 5 % (wt), the solution reaches a 'saturation' status which starts having MNPs in the bottom of the bottle as precipitate. To research the MNP concentration effect on the final fibre product, four samples were studied by SEM and EDX. The results can not only reveal the rule of MNP loading in fibre, but also improve the design of the mixture.

Furthermore, for different applications, a better selection of concentration can be made. Fibres made from both PVA and PVA-MNP appeared to have a distribution of 100-300 nm in diameter determined by ImageJ (Figure 5-4-Figure 5-7).

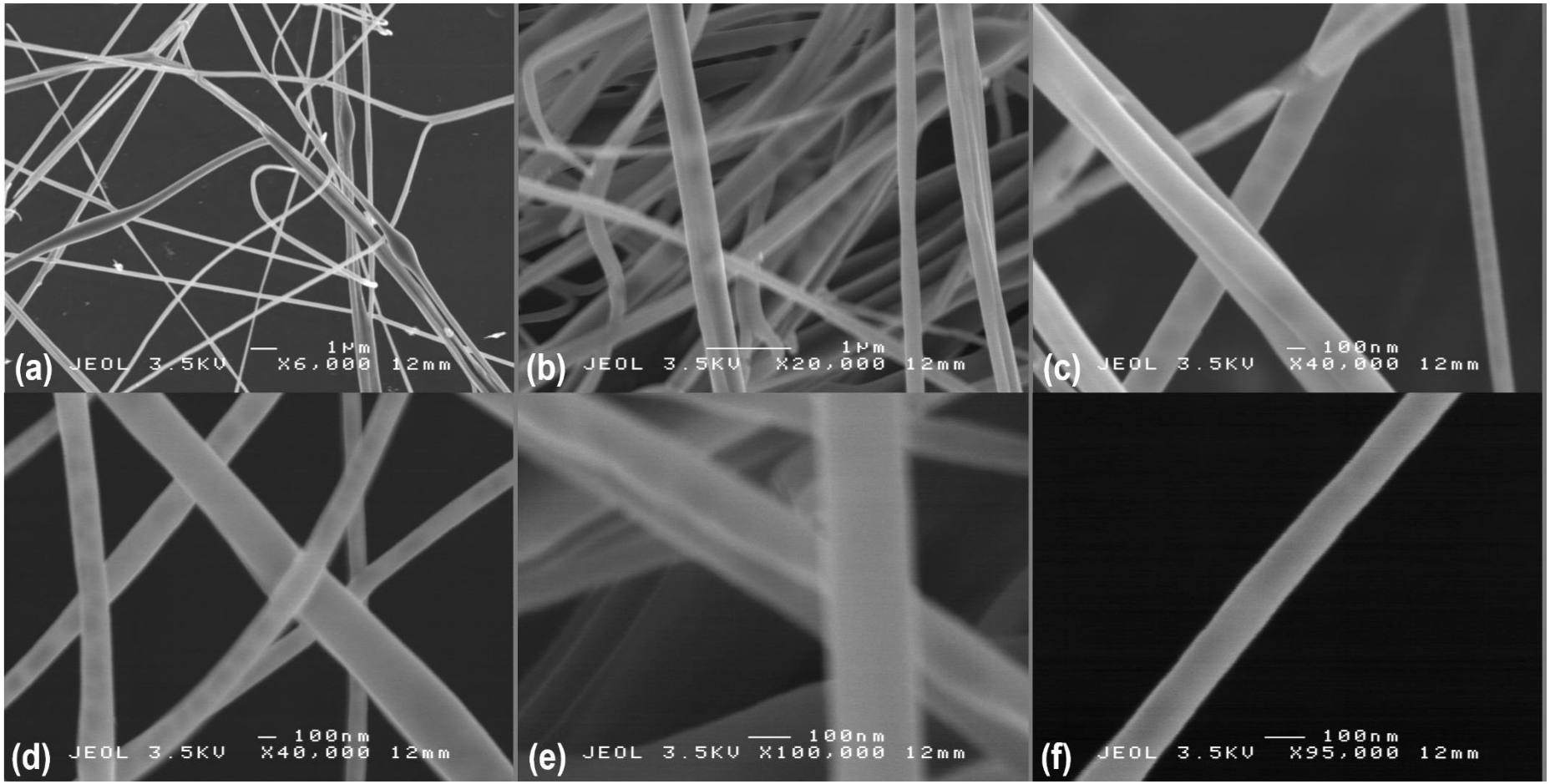

Figure 5-4 SEM images of pure PVA fibres.

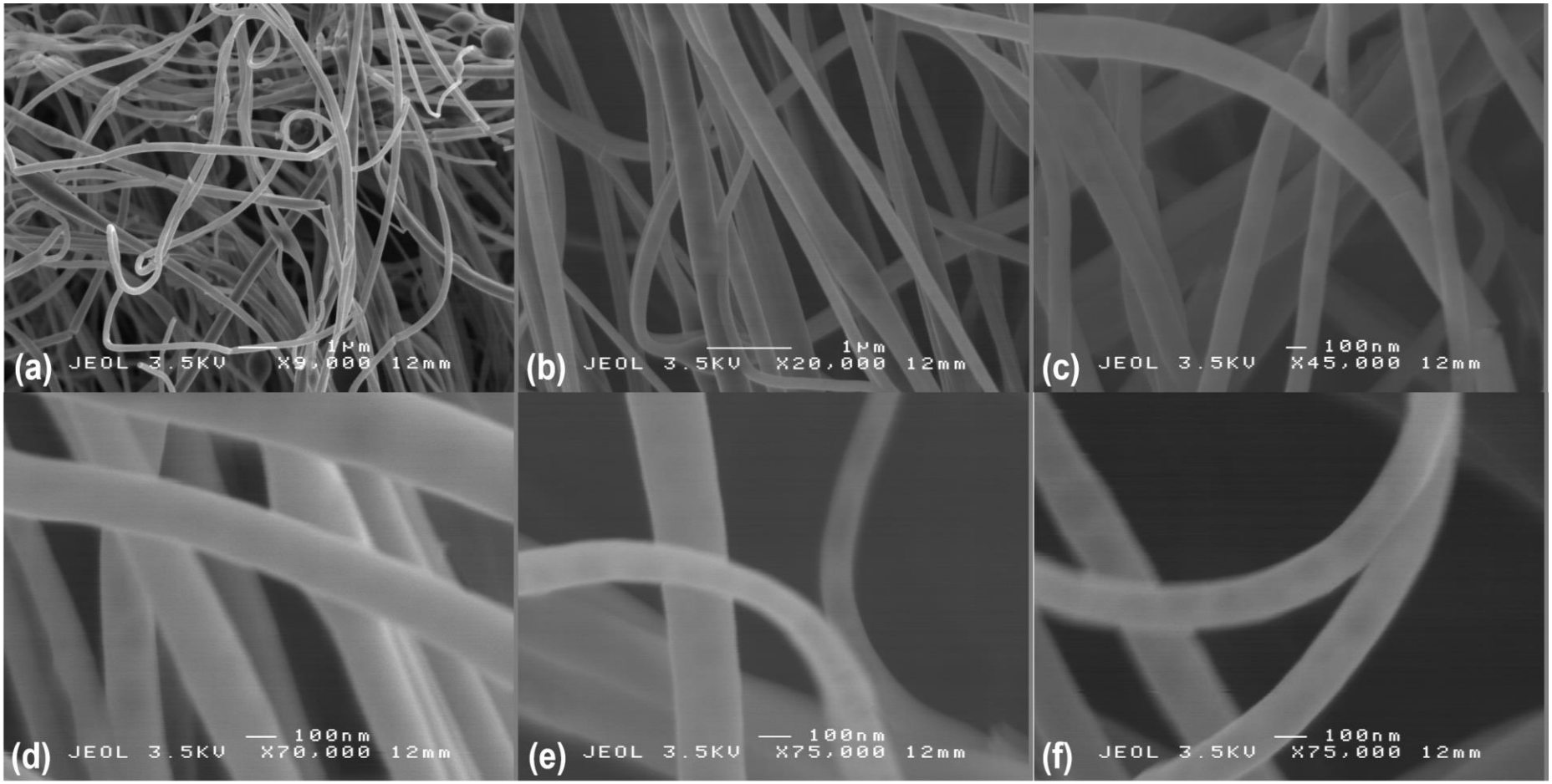

Figure 5-5 SEM images of 3%(wt) PVA-MNP fibres.

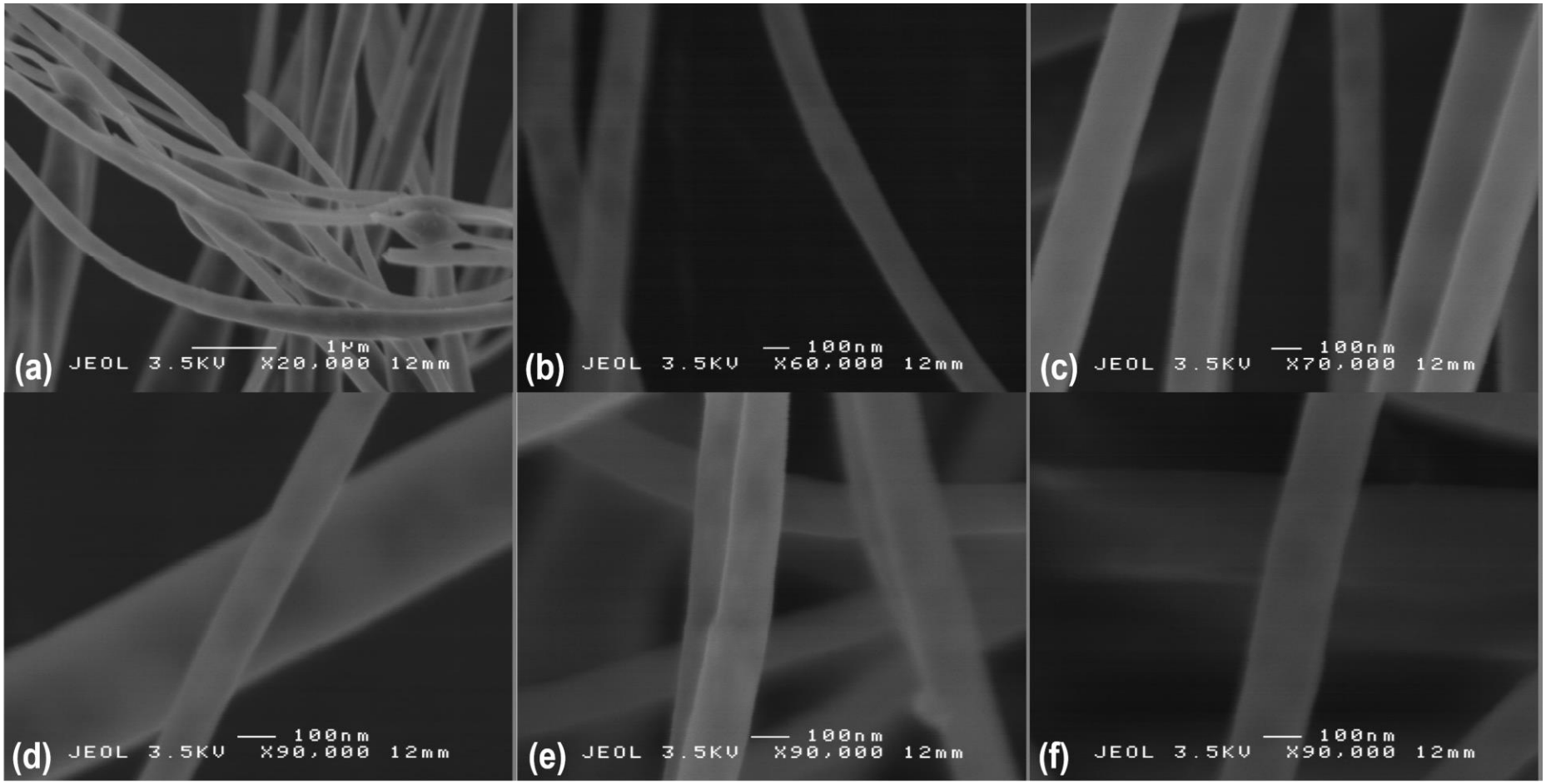

Figure 5-6 SEM images of 4%(wt) PVA-MNP fibres.

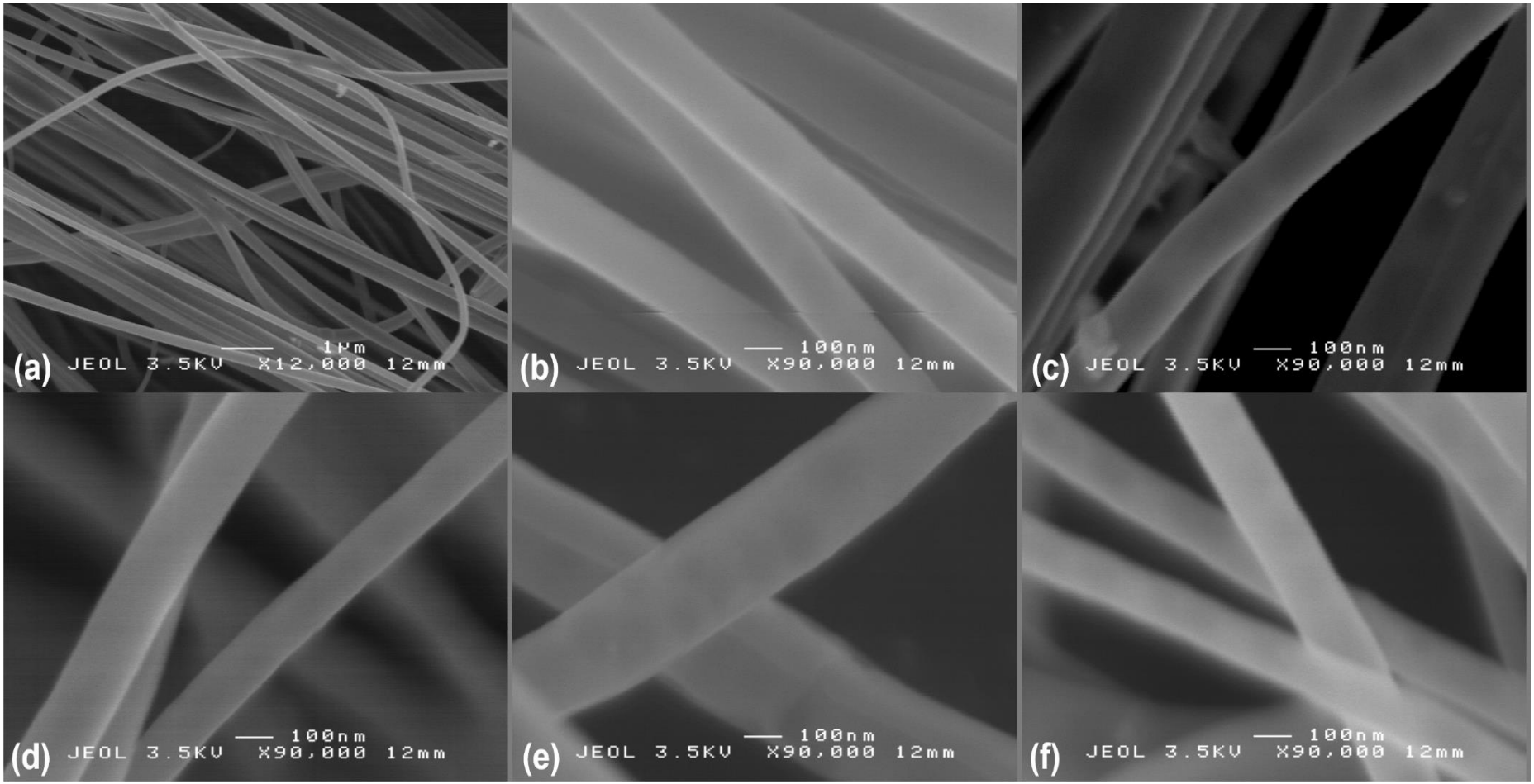

Figure 5-7 SEM images of 5%(wt) PVA-MNP fibres.

5.4 EDX Analysis

5.4.1 Element dot mapping

The incorporation of Fe_3O_4 MNPs into the fibres was visualized *via* EDX dot mapping, which can reveal if the iron oxide powder is distributed homogeneously on the fibres. Apart from Fe, C, O and S are also taken in element analysis as a reference. The white dots on the black background represent their position compared with SEM image in the same area.

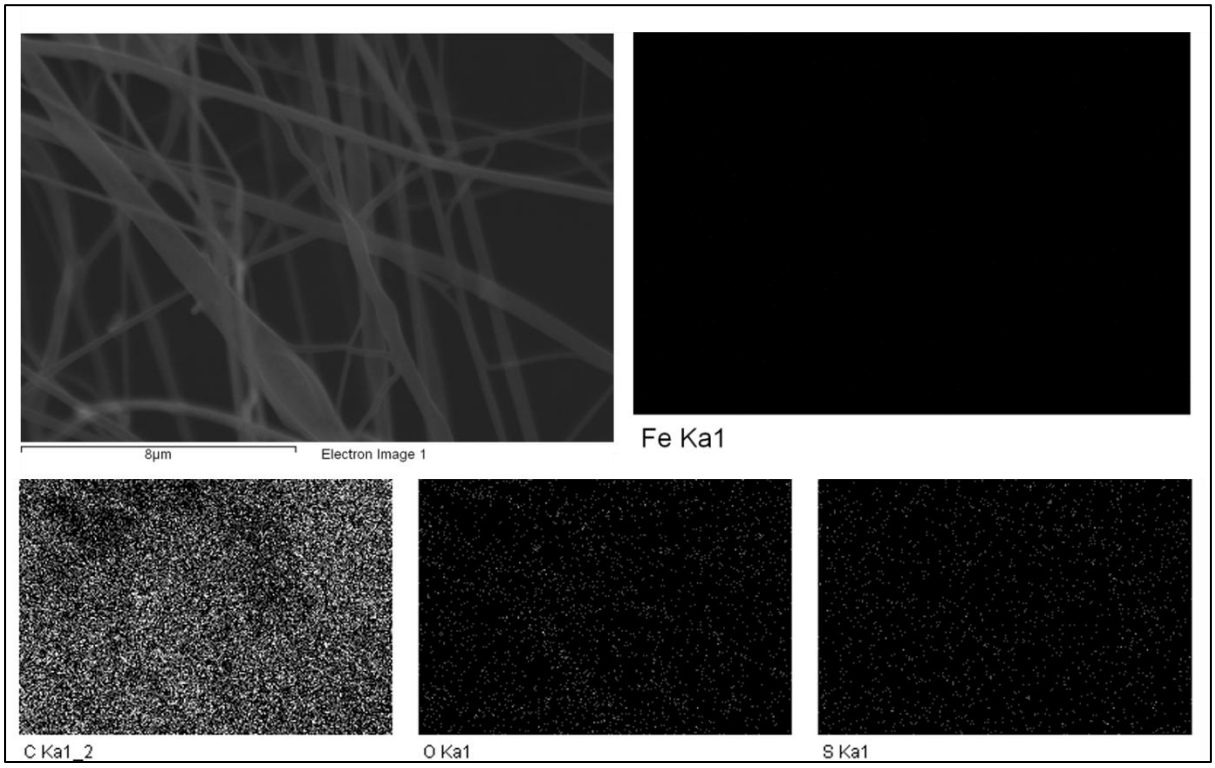

Figure 5-8 SEM-EDX dot mapping images. Pure PVA fibres.

To indicate the presence of Fe element (from Fe_3O_4) on selected areas of samples, the spectroscopy system needs to run more times (10-15) on the same area to detect clear elements for dot mapping because even for 5% (wt) PVA-MNP fibres, the content level of Fe is low from the whole sample background for the analysis system used.

However, due to the system sensitivity, too many repeating scans cause a lot of noise on mapping which becomes an error in the image (Figure 5-8 -Figure 5-14).

Four samples were analysed for test and future selection which are pure PVA fibres, 3% (wt) PVA-MNP fibres, 4% (wt) PVA-MNP fibres and 5% (wt) PVA-MNP fibres. As MNPs percentage in PVA increases, their behaviour on EDX analysis changes which are to be studied and if the trend exists, the improved design of fibre composition can be used for future experiment.

Pure PVA fibres are done first for a comparison as the control sample to others (Figure 5-8). Because without Fe, the sample should give no response to the Fe element. For the Fe element dot mapping on the top right of Figure 5-4, the nearly pure darkness confirms pure PVA fibres have no Fe can be speculated.

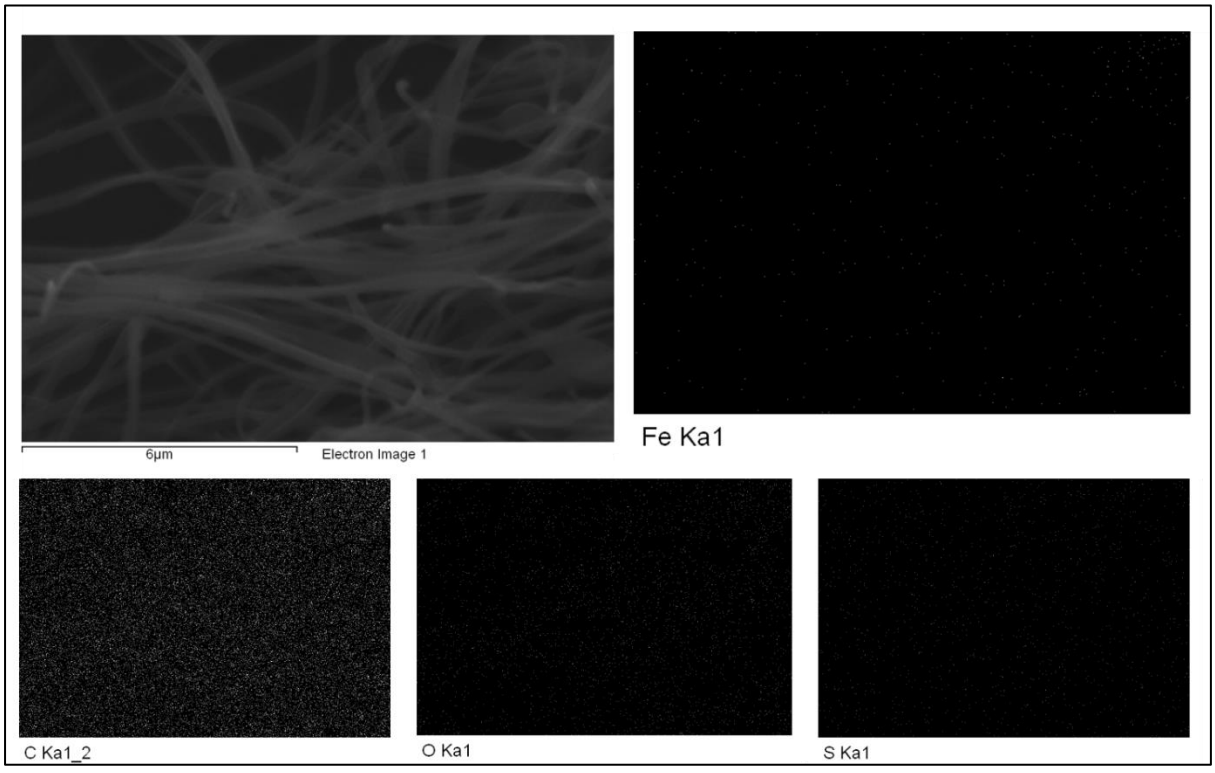

Figure 5-9 SEM-EDX dot mapping images. 3%(wt) PVA-MNP fibres (a).

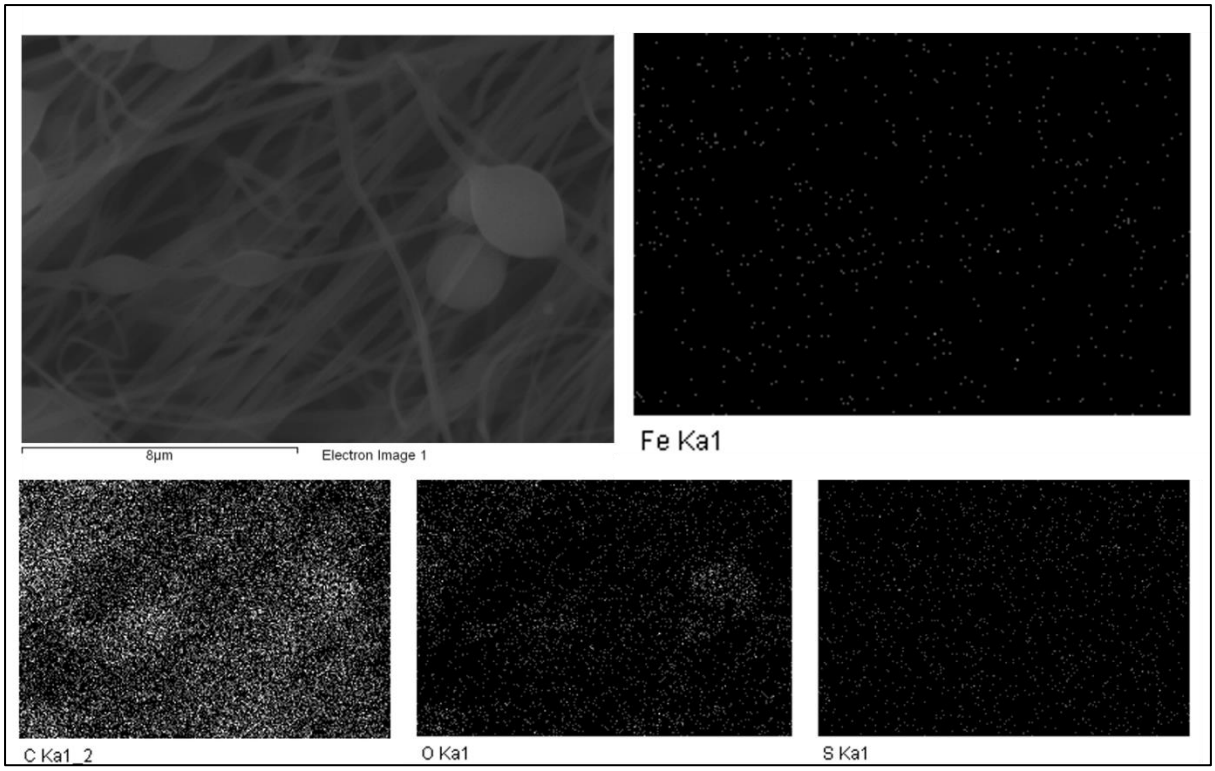

Figure 5-10 SEM-EDX dot mapping images. 3%(wt) PVA-MNP fibres (b).

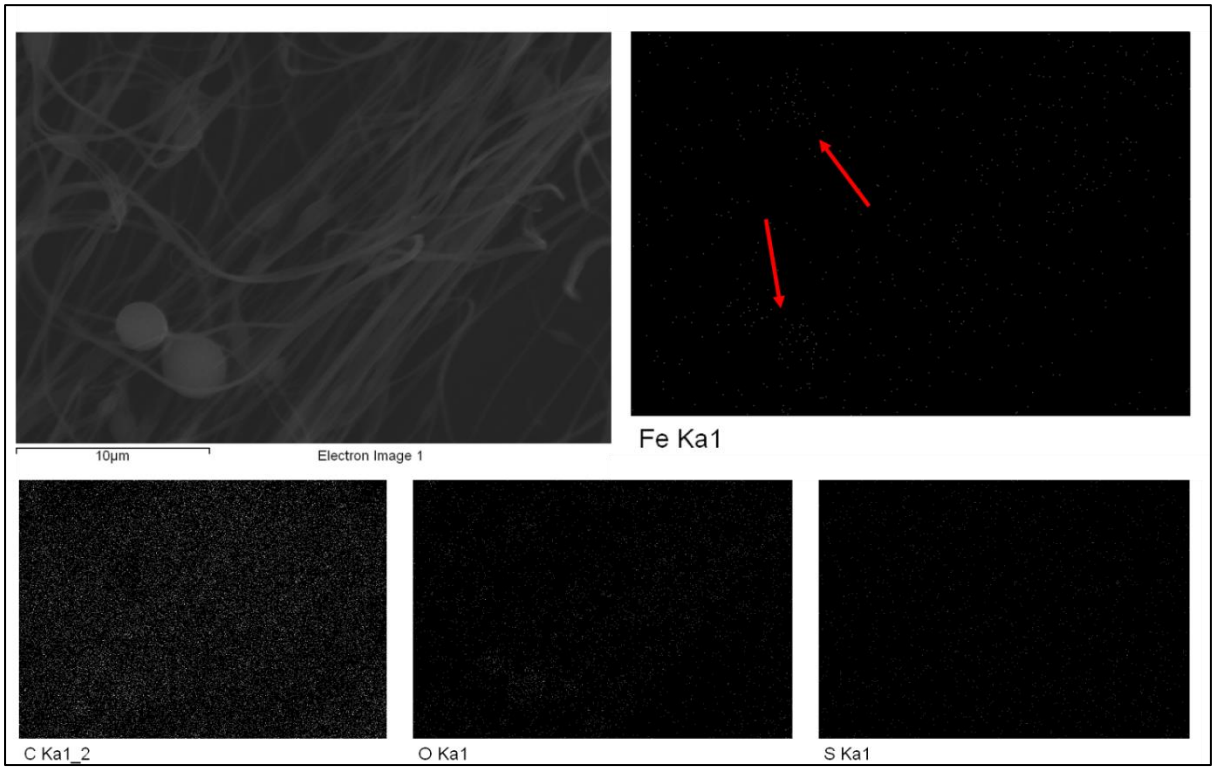

Figure 5-11 SEM-EDX dot mapping images. 4%(wt) PVA-MNP fibres (a).

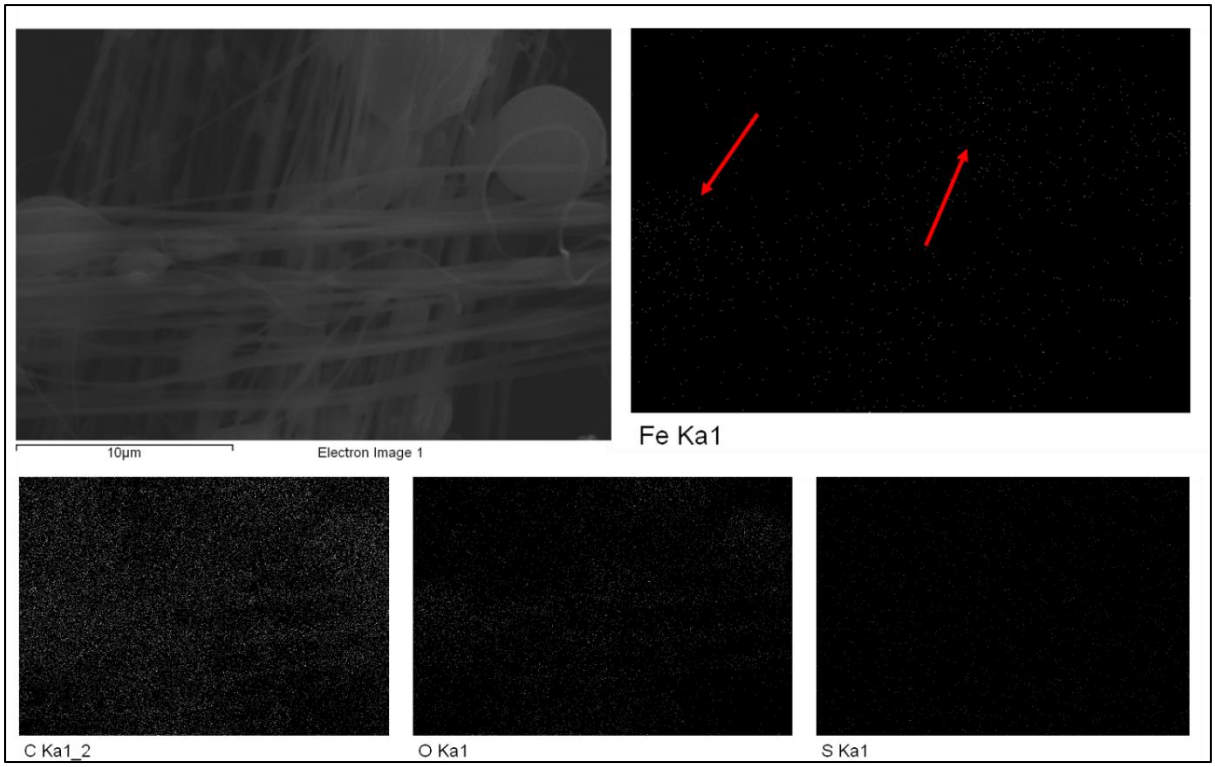

Figure 5-12 SEM-EDX dot mapping images. 4%(wt) PVA-MNP fibres (b).

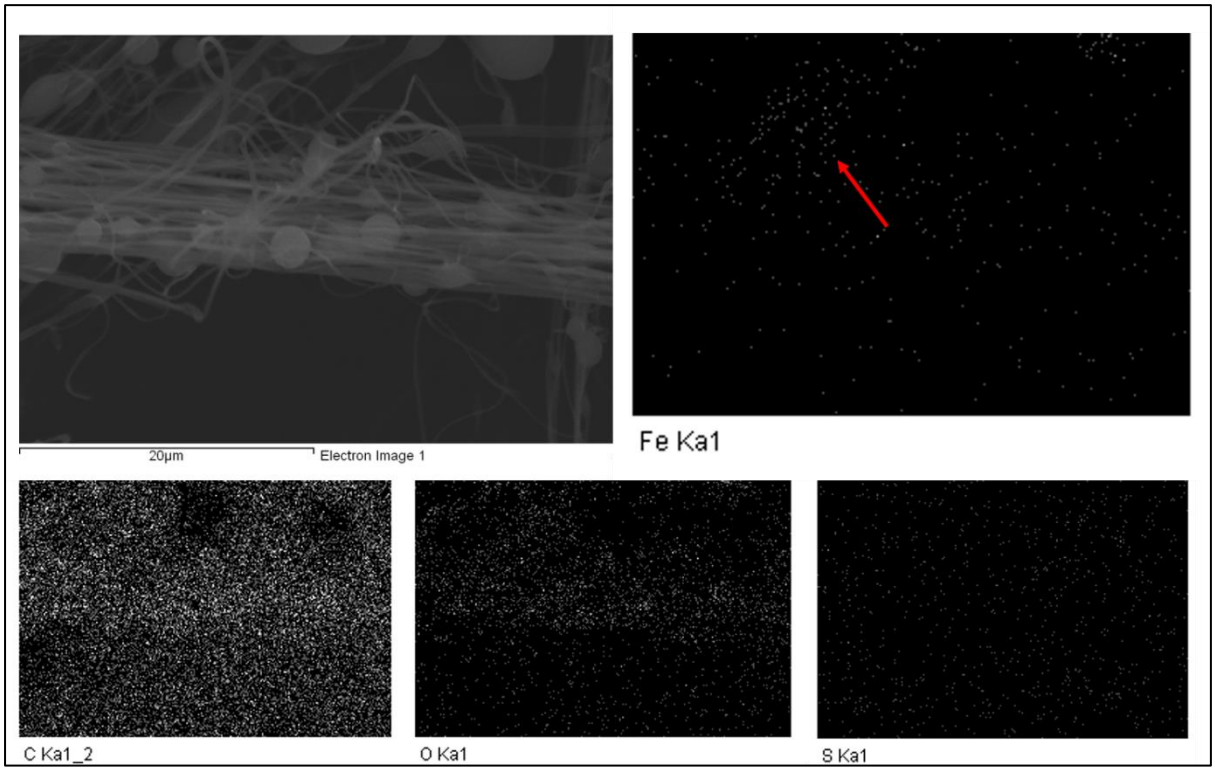

Figure 5-13 SEM-EDX dot mapping images. 5%(wt) PVA-MNP fibres (a).

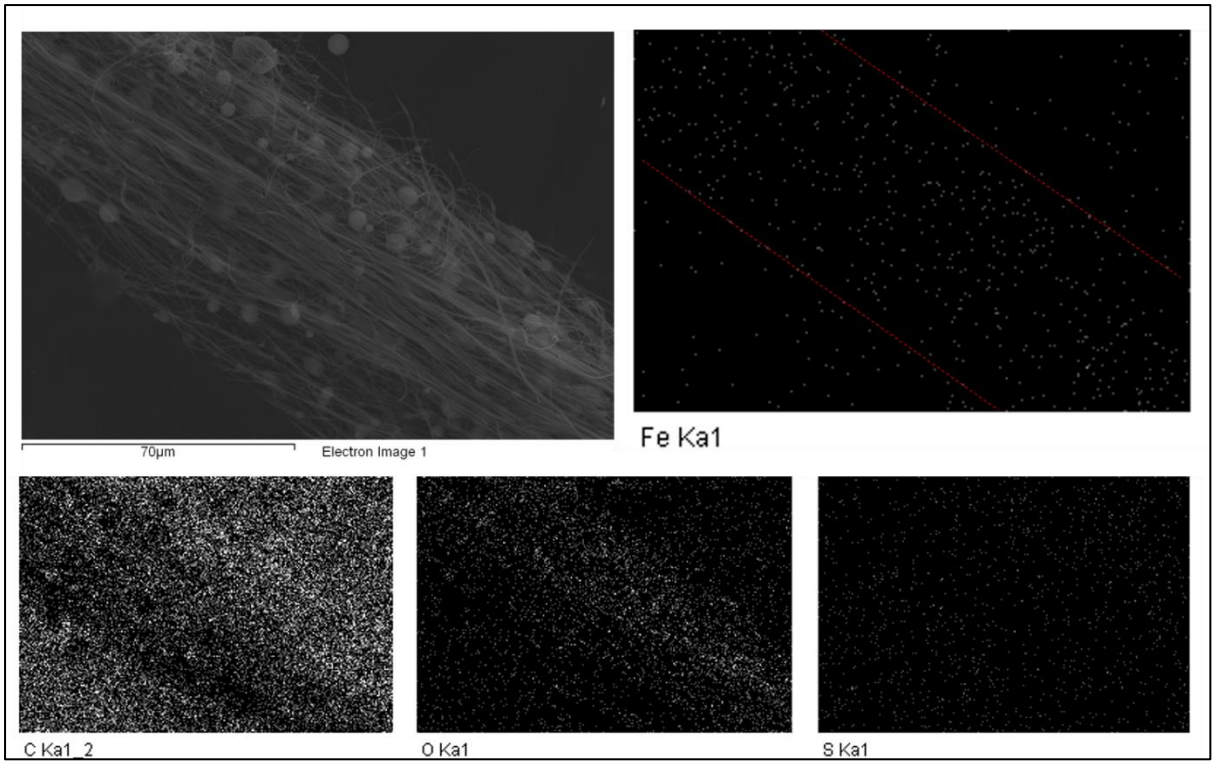

Figure 5-14 SEM-EDX dot mapping images. 5%(wt) PVA-MNP fibres (b).

C, O and S act normally as they are mostly from the background but C and O show more information because PVA has C and O which may show concentration in the images if the fibres are constructing a shape. S is from the electric conductive sticker used for fixing the sample on the metal base for SEM. Therefore, S should always show an average dispersion on mapping.

For 3% (wt) PVA-MNP fibres, the results show that the Fe element exists (Figure 5-9,Figure 5-10). However, the weak signal, due to low Fe concentration for the sample, causes the dots to be mapped not in the position as coming along with fibres in SEM image. As a comparison, 4% (wt) ones are better on performance which the red arrows in the images indicate the dot group giving a stronger response (Figure 5-11,Figure 5-12). This also accords with the principle that more MNPs are added to the PVA solution and more MNPs will be loaded into final fibres.

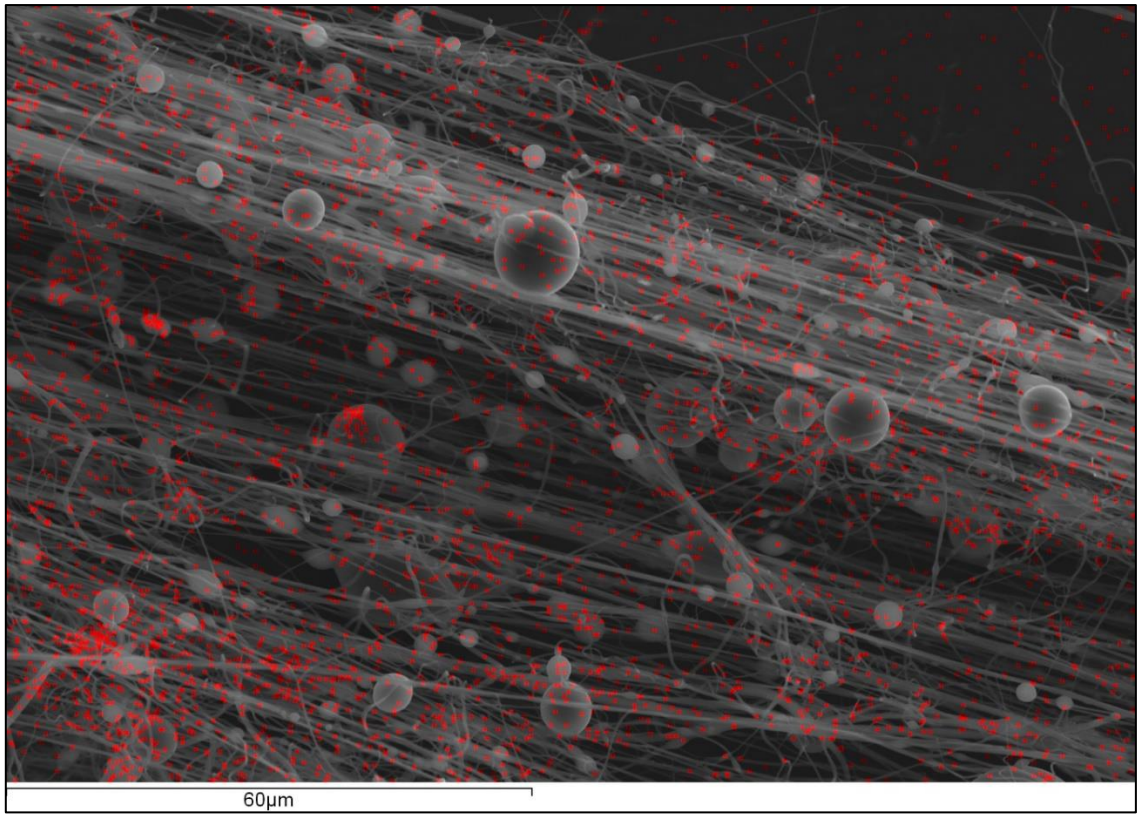

Figure 5-15 SEM dot mapping: red dots indicate the presence of Fe in fibres (a).

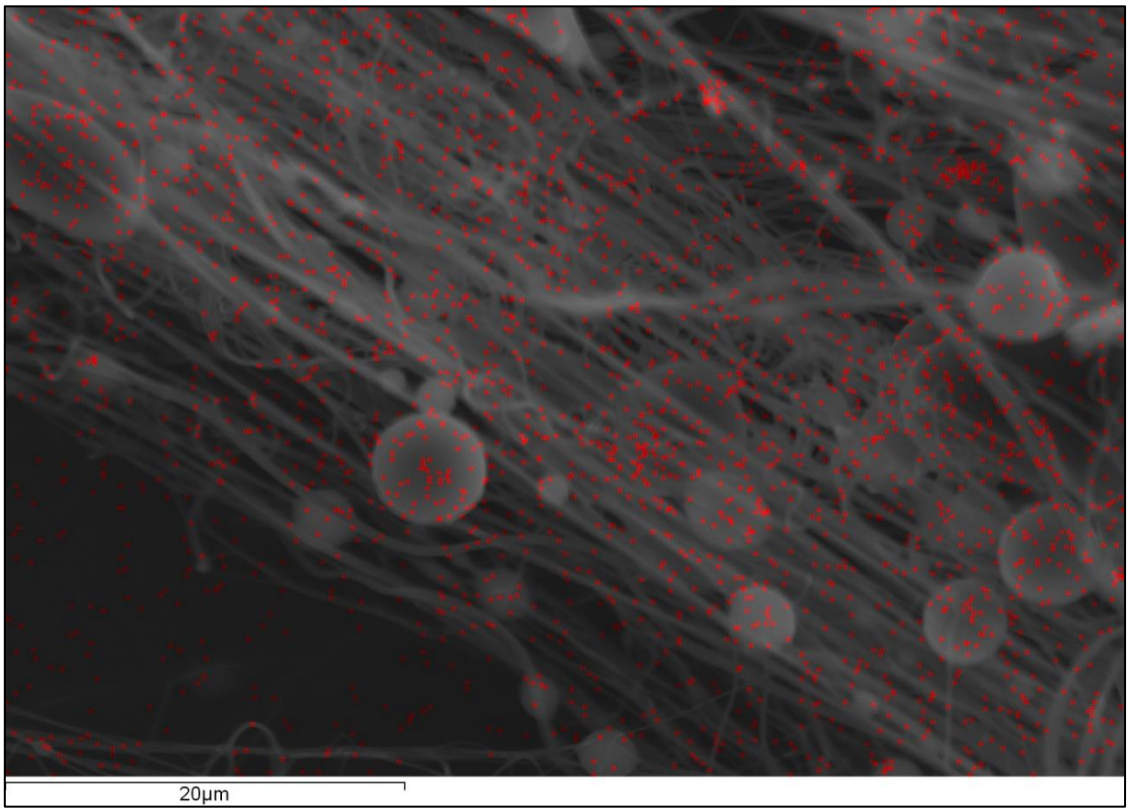

Figure 5-16 SEM dot mapping: red dots indicate the presence of Fe in fibres (b).

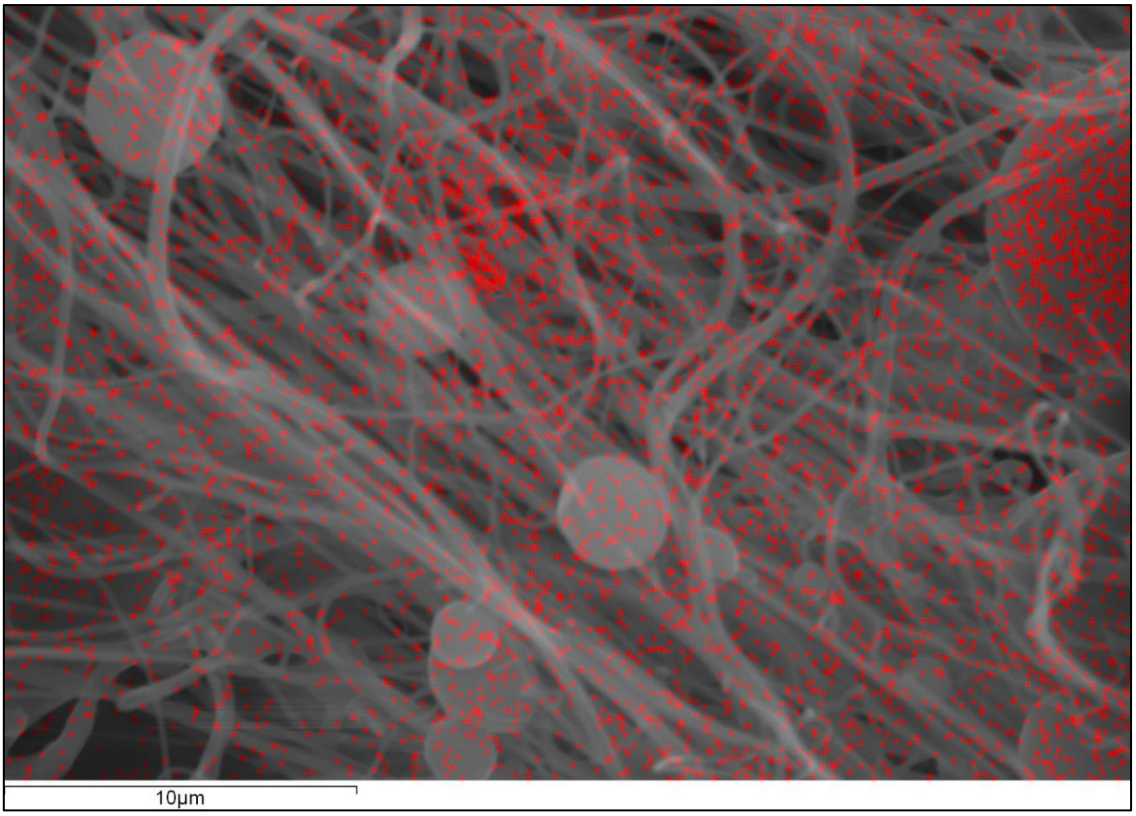

Figure 5-17 SEM dot mapping: red dots indicate the presence of Fe in fibres (c).

The 5% (wt) sample (with red arrow and guidance line) supports this principle by showing the dots in a pattern compared to fibres themselves from SEM images (Figure 5-13,Figure 5-14). Moreover, C and O element dot mapping results are a good reference for this pattern.

As can be seen, with the weight percentage of MNP increasing from 3% to 5%, the number of dots from corresponding SEM-EDX mapping images also increases.

Although due to the capacity of element detecting, the instrument delivers much noise to the final results, the loading of MNPs on PVA fibres is confirmed. For a better demonstration of the Fe element in existing positions in the scanning area, another three mapping functions were run by EDX program on 5% (wt) PVA-MNP because of its higher-level response. Those images show the combination of Fe (red dots) and sample SEM image (Figure 5-15 - Figure 5-17).

5.4.2 Surface elemental analysis

To detect a more specific volume of Fe on PVA-MNP fibres, the surface elemental analysis using EDX was done, where the selected area of fibre sample subject to EDX analysis was studied.

The samples for EDX are all placed on the sticker designed for microscopy and spectroscopy. To exclude the interference of the elements of the sticker, a blank area scan for the pure sticker with the same carbon coating as fibre samples was done (Figure 5-18). The sticker has Na, S, O and C (C is removed from the list in the figures by a software setting because of carbon coating) as main elements, therefore these elements will also appear in fibre sample results of EDX.

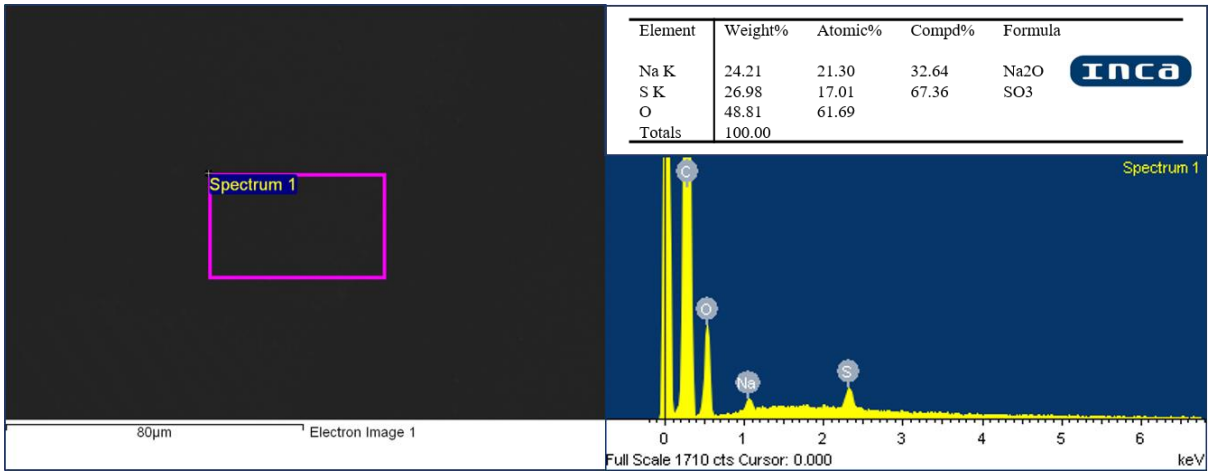

Figure 5-18 SEM-EDX images. Sticker.

To study the effect of different MNPs weight percentage solution mixture on MNPs' actual loading on the final product, four PVA-MNP fibre samples (with MNPs concentration increasing in PVA solution for spinning) are used as in the former section.

The pure PVA (0%) fibre sample is for control. 3%(wt), 4%(wt) and 5%(wt) PVA-MNP fibres were made forming progressive levels for analysis. All samples were studied in

the same condition. For each sample, three different areas, which are general fibre area, the fibre bead and the fibres in the same area near the bead, were fully characterised to get the volume of Fe loaded. Moreover, three areas rather than one can reduce the error of the area selection factor (Figure 5-19 - Figure 5-30). Red arrows are drawn in the spectrum images indicating Fe peak. The Fe element was also highlighted in the table of element analysis with its concentration.

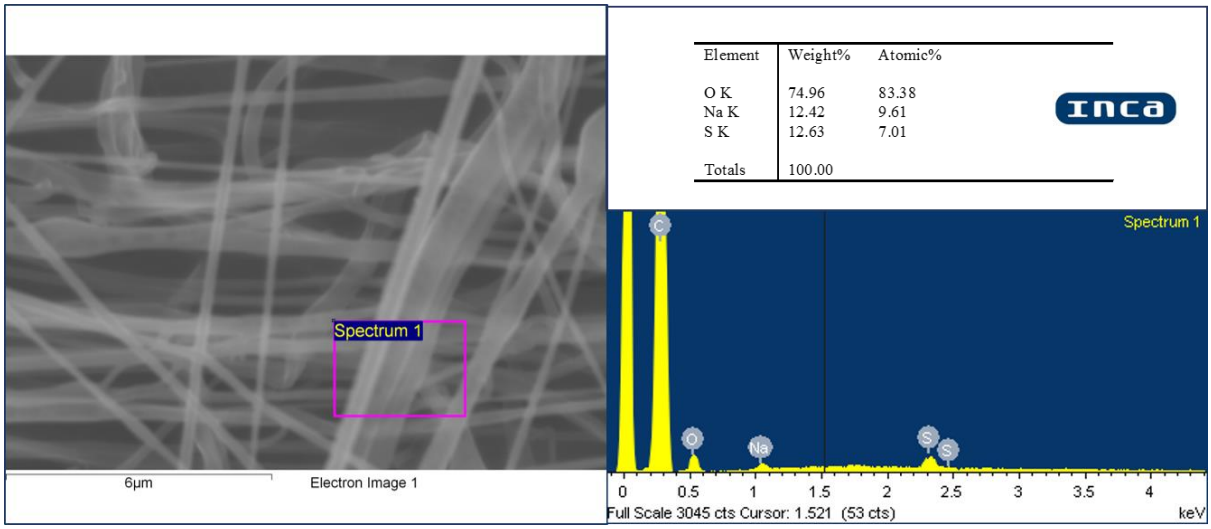

Figure 5-19 SEM-EDX images. Pure PVA (a).

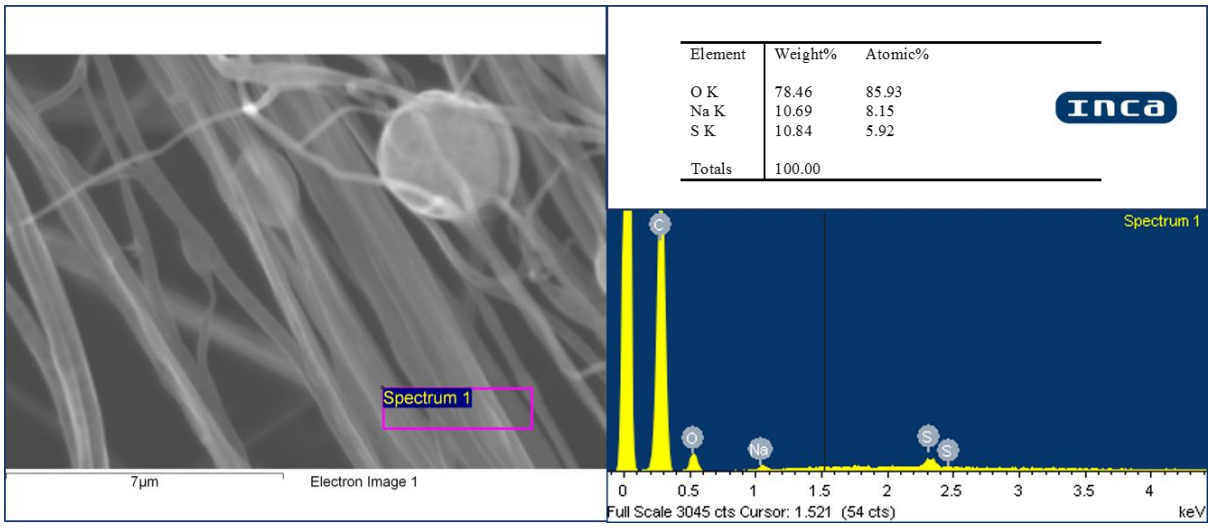

Figure 5-20 SEM-EDX images. Pure PVA (b).

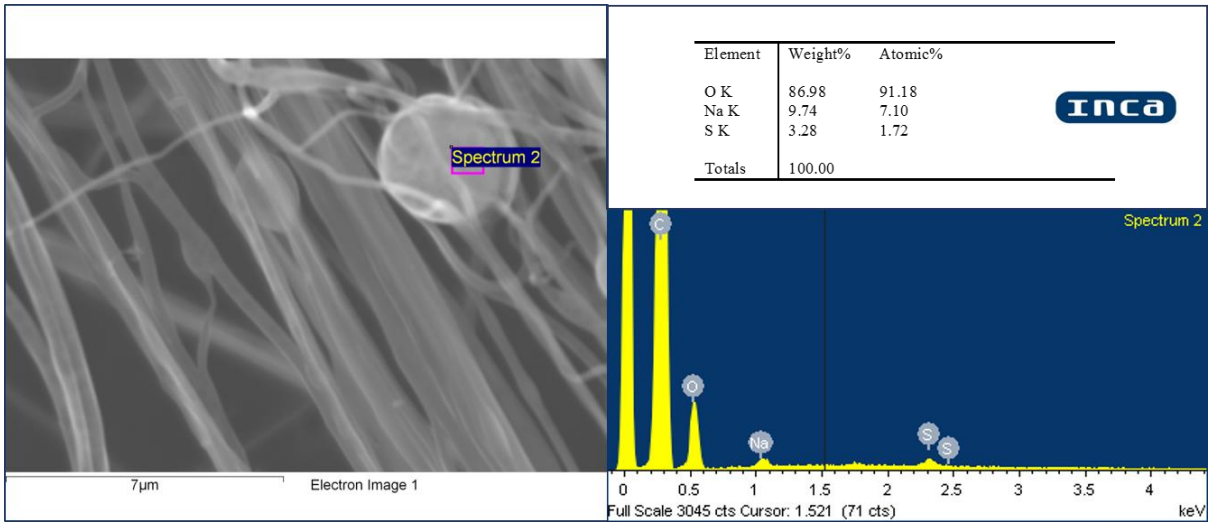

Figure 5-21 SEM-EDX images. Pure PVA (c).

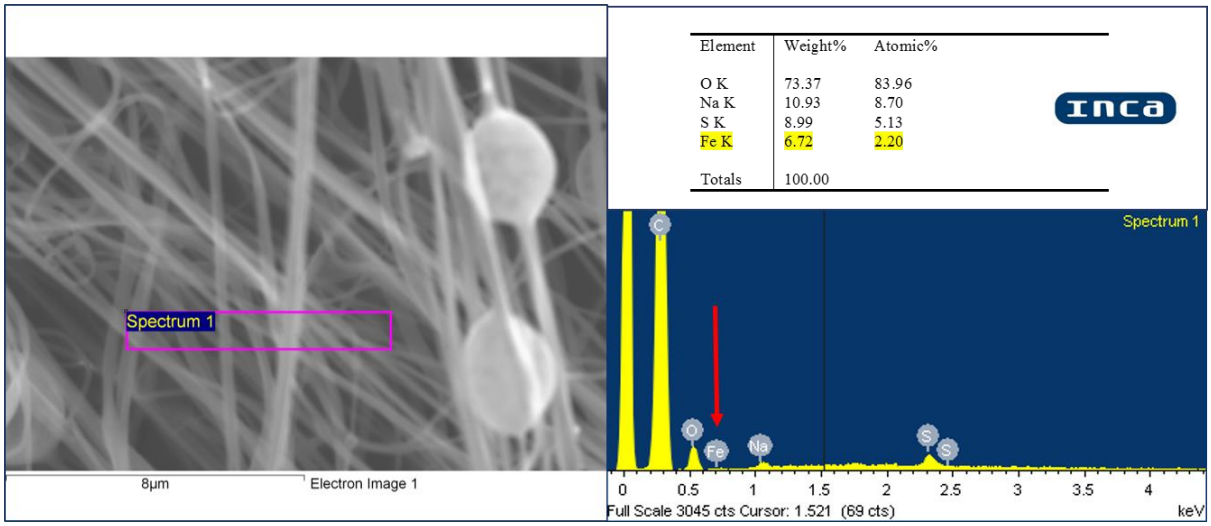

Figure 5-22 SEM-EDX images. 3%(wt) PVA-MNP fibres (a).

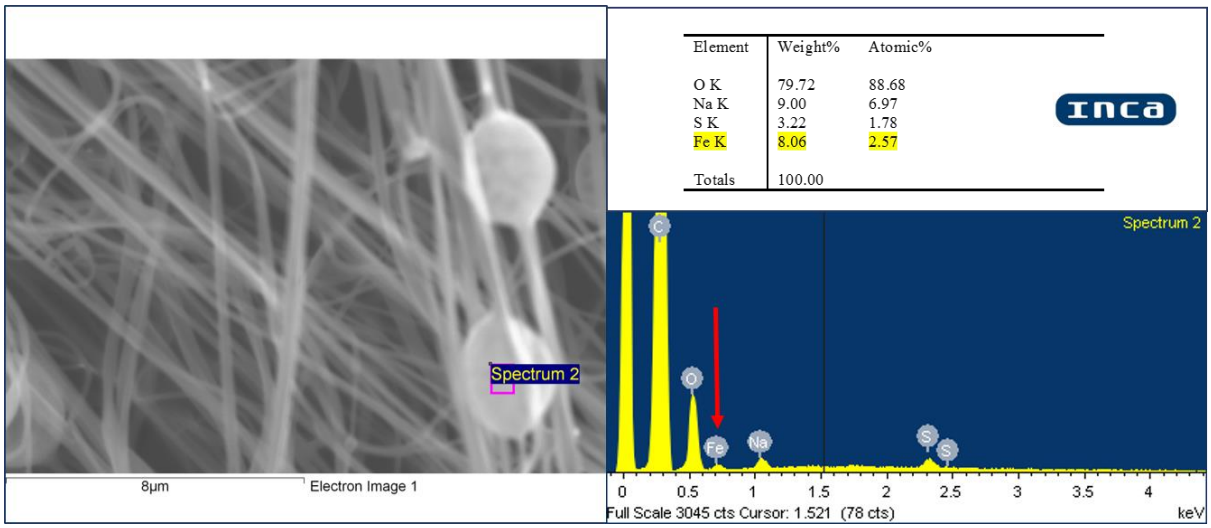

Figure 5-23 SEM-EDX images. 3%(wt) PVA-MNP fibres (b).

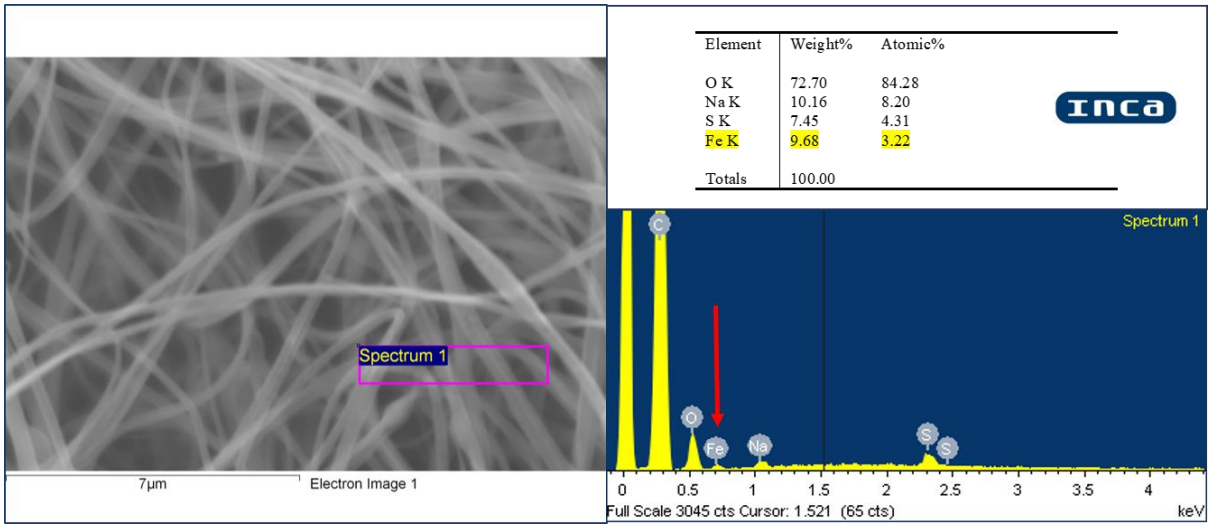

Figure 5-24 SEM-EDX images. 3%(wt) PVA-MNP fibres (c).

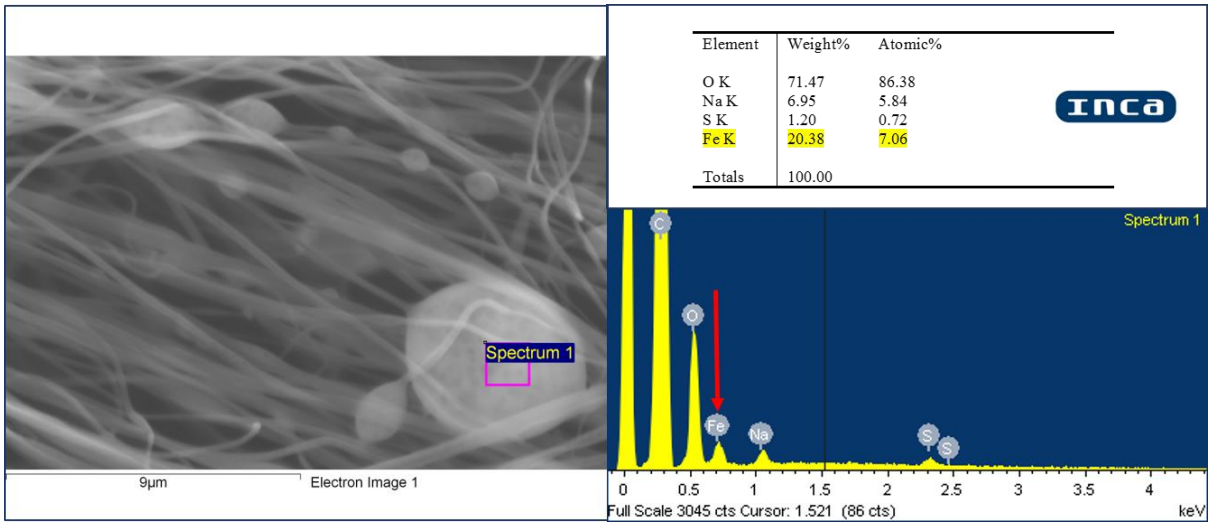

Figure 5-25 SEM-EDX images. 4%(wt) PVA-MNP fibres (a).

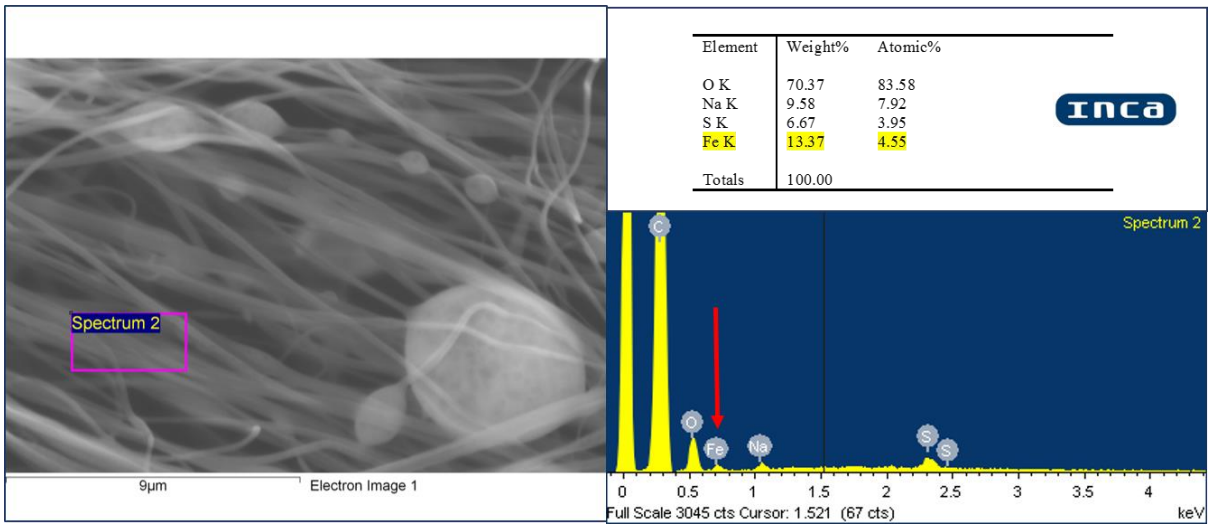

Figure 5-26 SEM-EDX images. 4%(wt) PVA-MNP fibres (b).

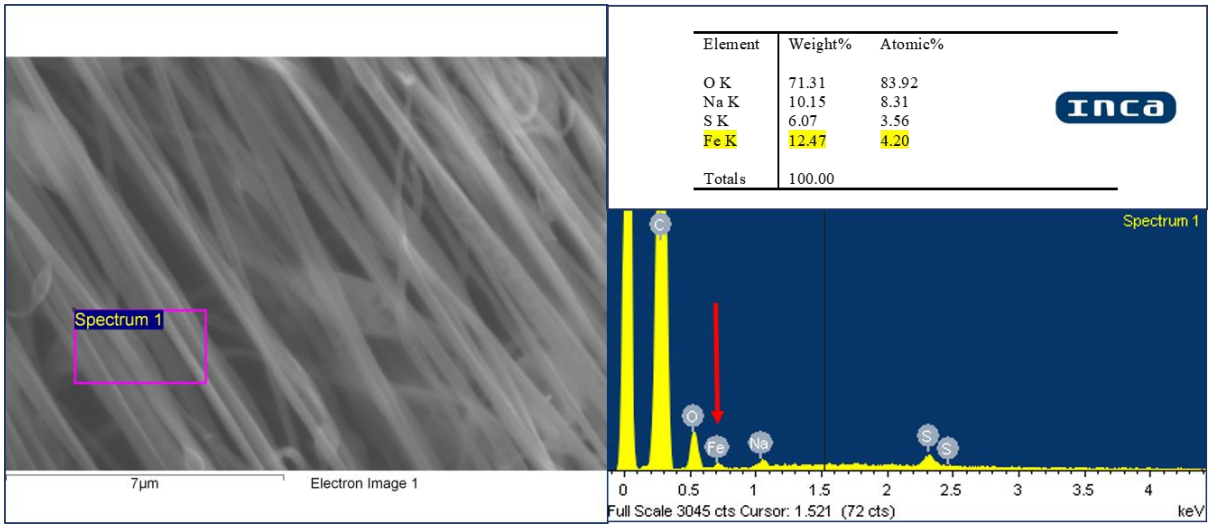

Figure 5-27 SEM-EDX images. 4%(wt) PVA-MNP fibres (c).

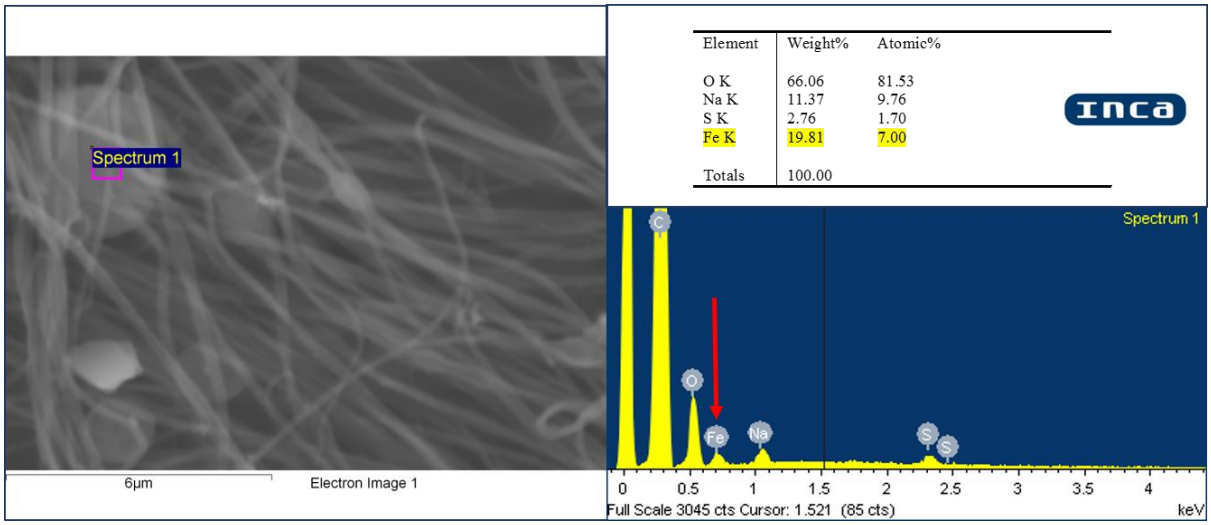

Figure 5-28 SEM-EDX images. 5%(wt) PVA-MNP fibres (a).

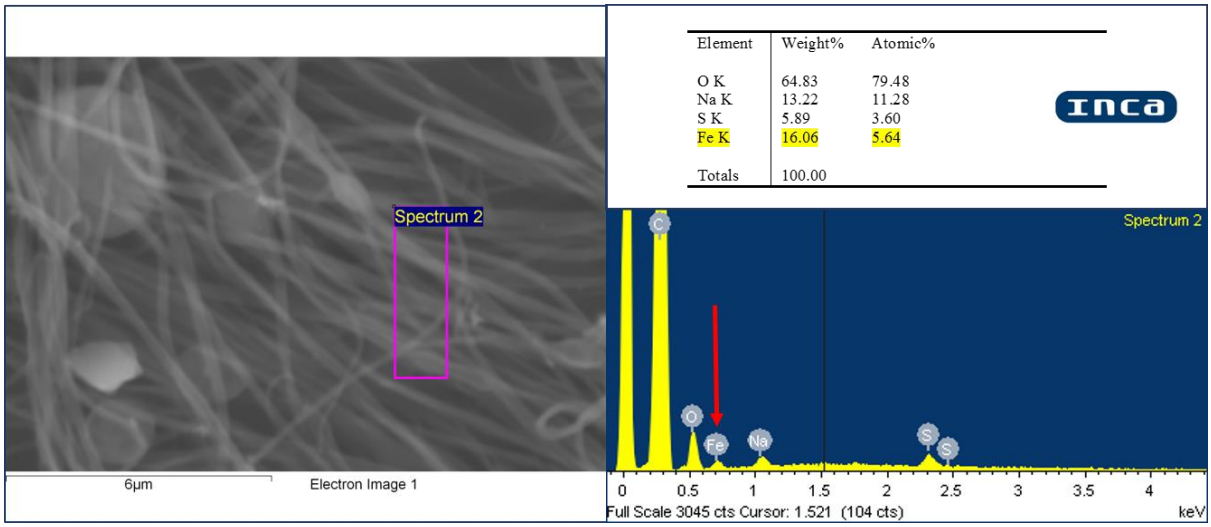

Figure 5-29 SEM-EDX images. 5%(wt) PVA-MNP fibres (b).

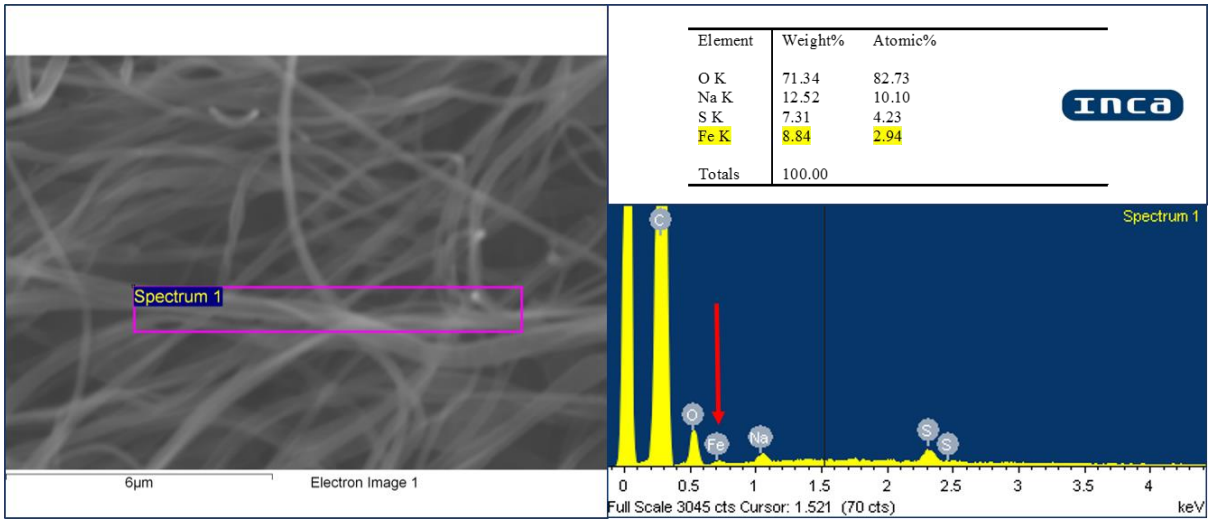

Figure 5-30 SEM-EDX images. 5%(wt) PVA-MNP fibres (c).

The presence of surface Fe was successfully detected using EDX. For 3%(wt) PVA-MNP sample, the recorded readings of Fe weight percent are 6.72% and 9.68% on fibres, and 8.06% on bead. Beads Fe content for 4%(wt) and 5%(wt) is 20.38% and 19.81%. Fibre area Fe content for 4%(wt) shows 13.37% and 12.74%. This content becomes 16.06% and 8.84% for 5%(wt). The beads have higher Fe volume because beads have larger thickness giving more materials, but this is not much more than in fibres which means the dispersion of MNPs in the whole fibre sample is quite average. The average Fe loading volume in fibres for 4%(wt) is close to 5%(wt). As stated in the former section, 5%(wt) solution making in practice is close to the limit of the mixture. Higher (over 5%) additional volume of MNPs to the PVA solution cannot make the absorption better. Therefore, MNPs loading to fibres can be increased by adding more MNPs into PVA solution during preparation. However, 5%(wt) is the restriction for not exceeding the limit of the PVA-water system which is important because this information can be used for solution design and preparation. As 5%(wt) may apply the most loading of MNPs which deliver stronger magnetism and do not break the mixture, it was chosen to be used for the following test of controlled fibre moving and drug release.

5.6 FTIR

The typical peaks for PVA and citric acid were identified through FTIR (Figure 5.33). These include the broad peaks at: 3300 cm^{-1} from the stretching mode of inter- and intra- molecular hydrogen bonds of O–H; 2920 cm^{-1} and 2850 cm^{-1} from the C–H vibrational mode of alkyl groups; 1735 cm^{-1} from the stretching mode of C=O of the carbonyl groups; 1085 cm^{-1} from the C–O–C stretching mode; a shoulder at ~1141 cm^{-1} from C–O stretching of crystalline PVA; and, at 1242 cm^{-1}, from the symmetric stretching mode of citric acid[142–144].

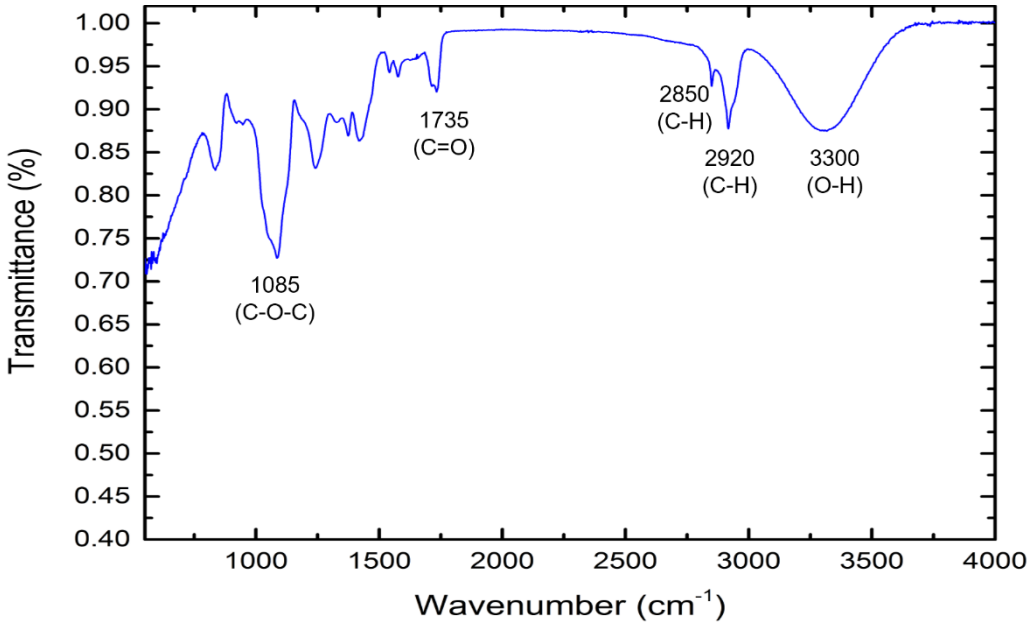

Figure 5-31 FTIR spectrum.

Figure 5.33. Characterization of chemical composition and magnetic content of the PVA-MNP fibres. (A) FTIR spectrum.

However, the characteristic vibrational bands of Fe_3O_4, usually found at 634, 582 and 397 cm^{-1} characteristic of magnetite[145] were not discernible *via* the instrument used.

5.7 SQUID analysis

The SQUID analysis is to measure the magnetization of the materials tested, through which, the MNPs amount in the fibres can be determined. It was found that the fibres were comprised of 4.9 % magnetic component by weight (due to Fe_3O_4 MNPs), as determined by the fraction of the mass magnetization for the PVA-MNP fibres (M = 2.6 Am^2kg^{-1}) and the pure MNP nanoparticles (M = 53.8 Am^2kg^{-1}) (Figure 5-32).

Since the polymer solution fed to the spinning apparatus consisted of 5 % of MNPs by weight, this shows that the process of infusion gyration is highly effective in generating fibres with minimal loss of the magnetic material.

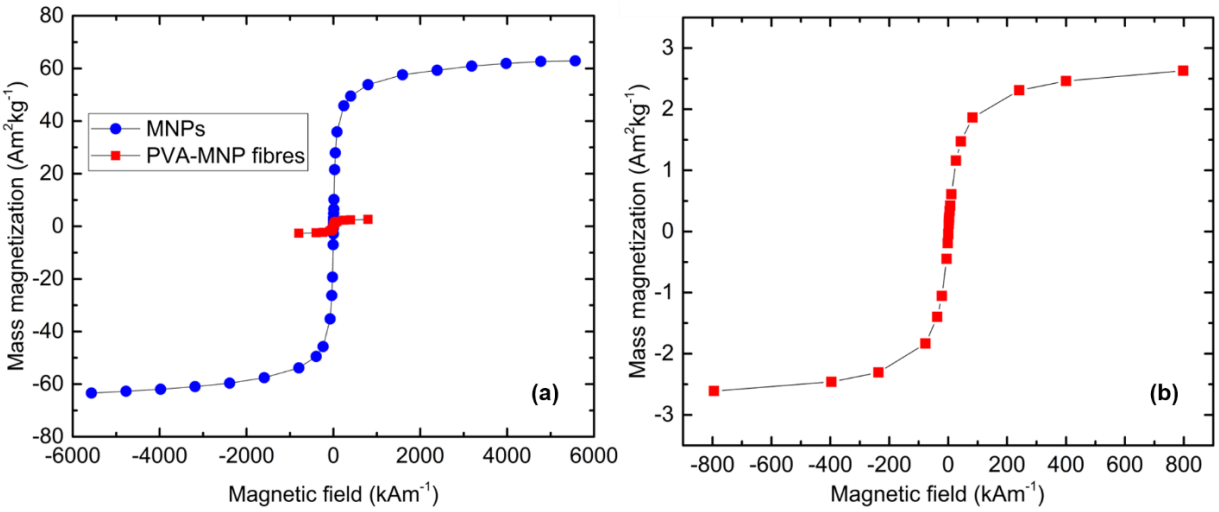

Figure 5-32 Mass magnetization behaviour of (a) both pure MNP and 5%(wt) MNP-PVA fibre samples, (b) 5%(wt) MNP-PVA fibre samples.

This observation, coupled with the previously investigated efficacy of the gyration process[133] renders the potential for scaled up production of magnetic fibres using this technique.

5.8 Optical Microscopy

Optical microscopy revealed a fibre matrix containing small amounts of beads distributed in the matrix, for both pure PVA (Figure 5-33) and PVA-MNP (Figure 5-34) samples. The general fibre structure with three scales were observed and recorded.

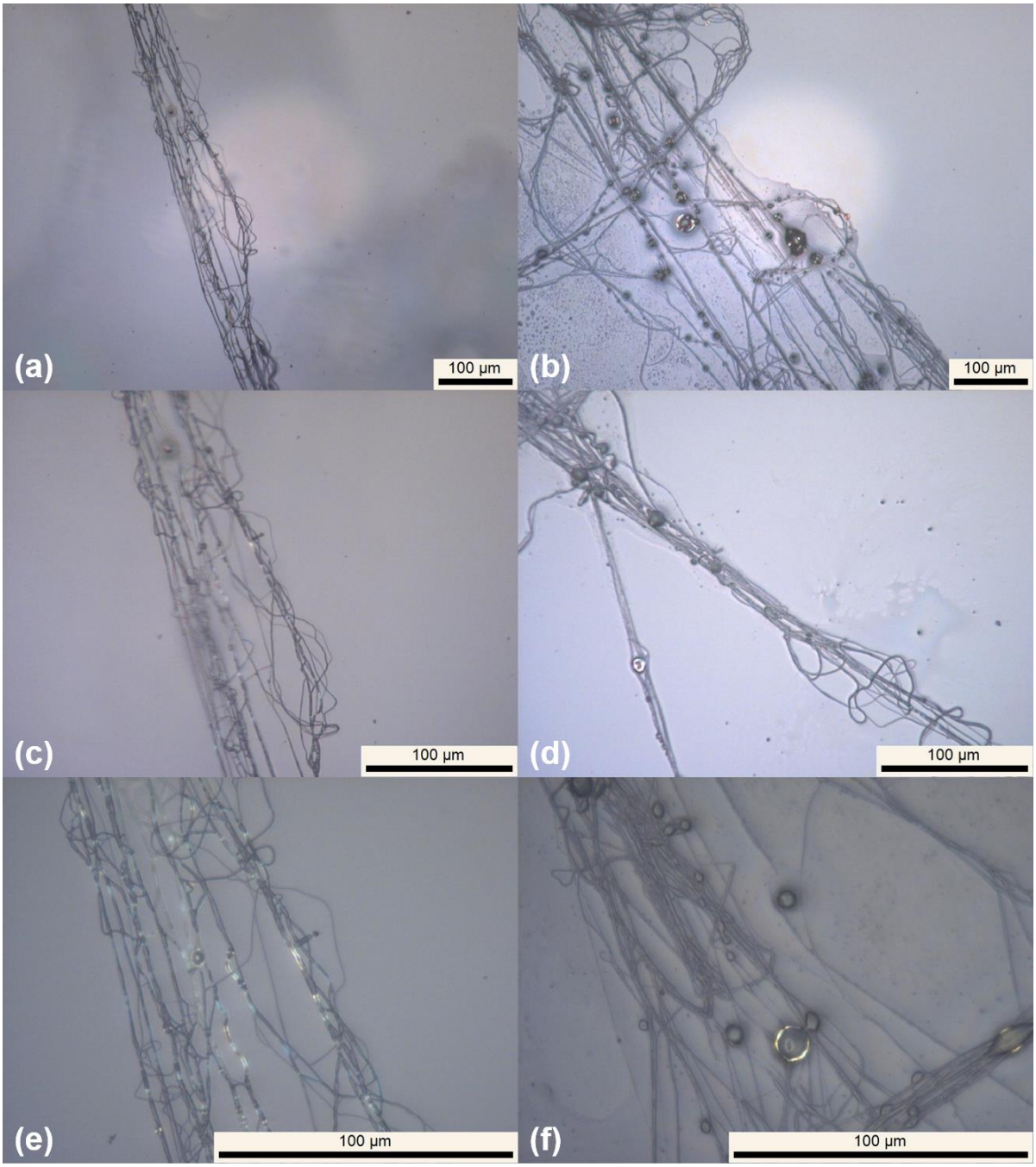

Figure 5-33 Optical microscope images. Pure PVA.

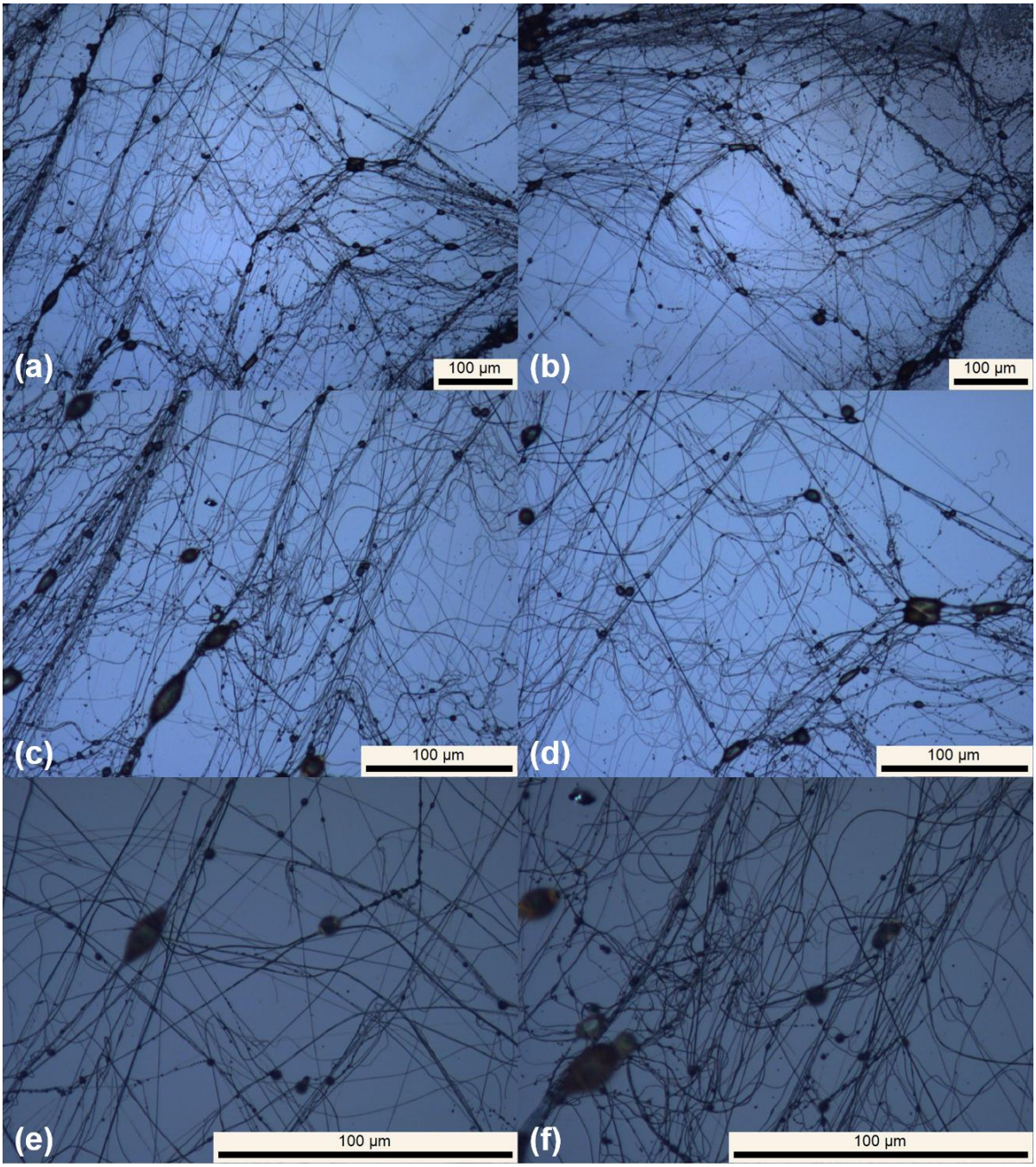

Figure 5-34 Optical microscope images. 5%(wt) PVA-MNP fibres.

The pure PVA fibres show transparent structure and PVA-MNP ones are darker along the fibre which is because it loads the MNPs.

5.9 Drug Release Experiment

Acetaminophen was effectively immobilized onto the PVA-MNP fibres, following which, the drug-fibre system was transferred to an absolute ethanol medium and studied for the release of acetaminophen with time, both with and without magnetic actuation. Separate experiments were conducted in duplicate, for the control (i.e., without actuation) and actuated studies.

Samples were taken out at relevant time intervals (1min for the first 5 and 5min for the rest until 30min complete) and subject to UV-Vis analysis. The ethanol volume was kept constant for all samples throughout the study by replacing the sampling volume. The fibres effectively responded to the external magnetic field, while contained in glass vials open to the air, or in glass vials containing absolute ethanol (Figure 5-35). The fibres could also easily be guided in a channel containing ethanol (Figure 5-36).

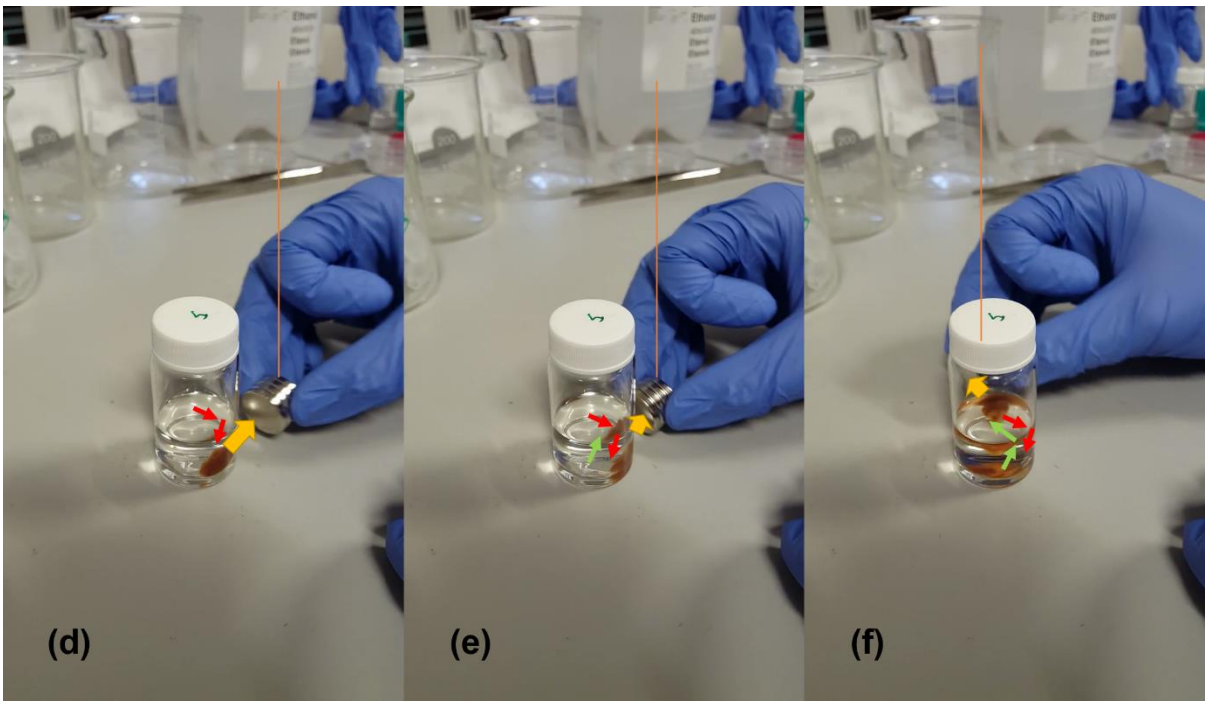

Figure 5-35 Procedure for magnetic actuation of fibres loaded with acetaminophen.

The ability to release controlled quantities of drugs *via* application of an external stimulus onto the carrier platform is a highly advantageous feature for drug delivery. This was successfully demonstrated by the controlled release of acetaminophen loaded on the PVA-MNP fibres, *via* an external magnetic field. Absolute ethanol was chosen as the medium for these experiments, in which the magnetic fibres were stable.

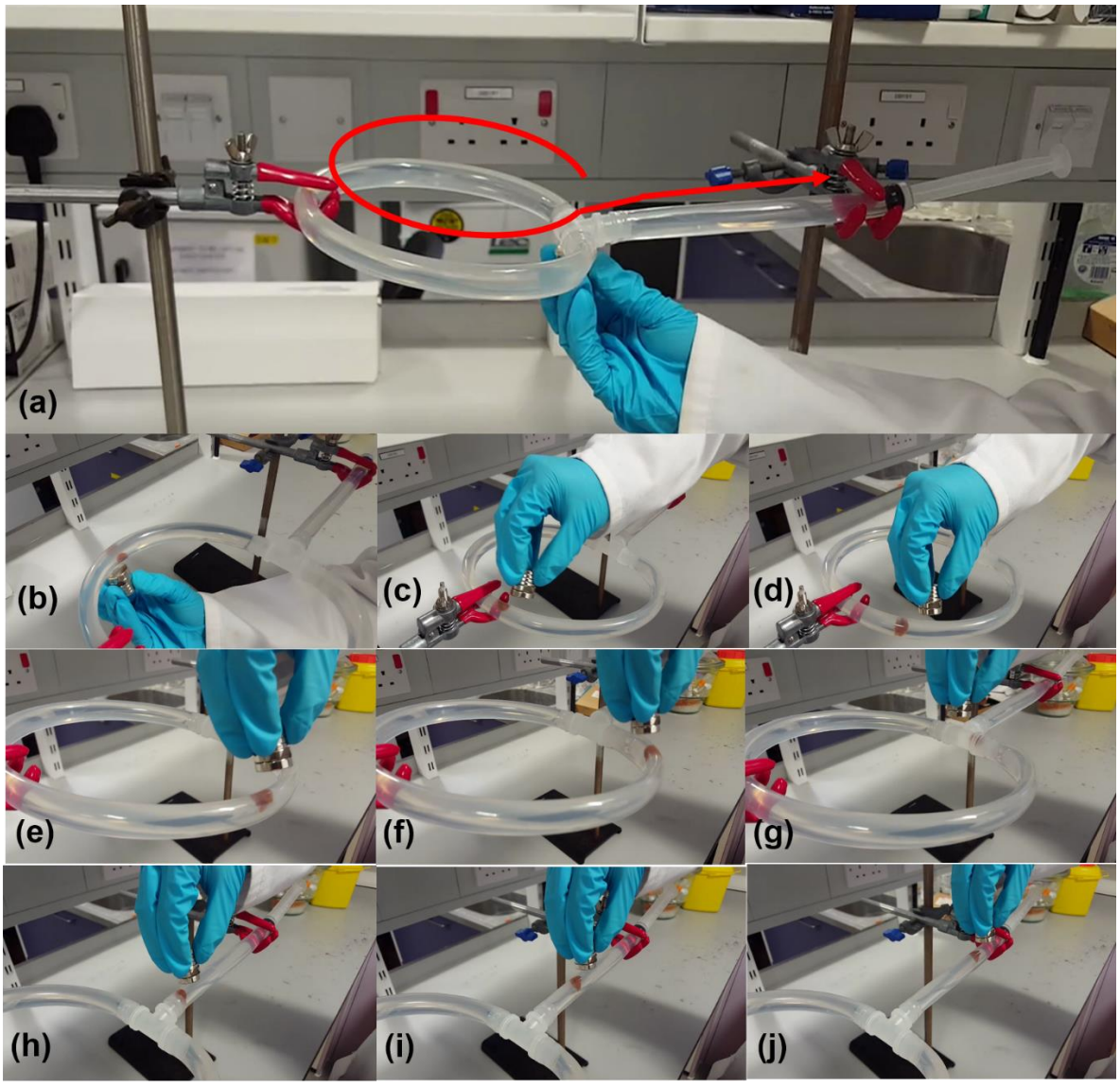

Figure 5-36 Transportation of the magnetic fibres along a tube, using magnetic actuation, demonstrating the scope of actuation.

5.9.1 UV-Vis & release study

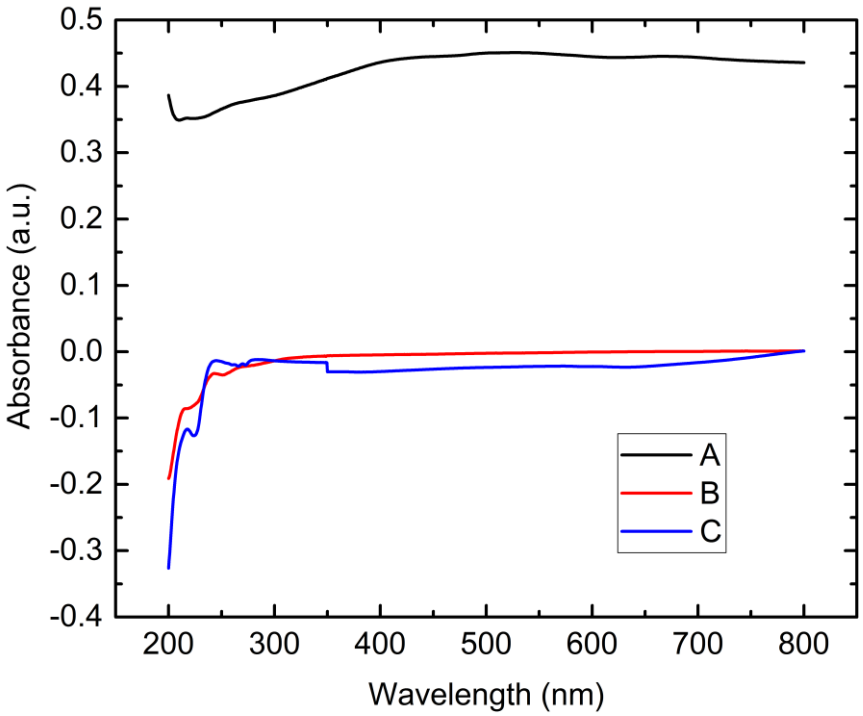

Figure 5-37 MNP leaching studies for PVA-MNP fibres conducted via UV-Vis absorbance of supernatant solutions of the following: (A) 5 % (w/v) MNPs dispersed in ethanol, (B) 5 % PVA-MNP fibres stored in ethanol for 4 weeks, (C) Ethanol (blank).

UV-Vis experiments conducted on the supernatant of PVA-MNP fibres stored in absolute ethanol for 4 weeks, showed no traces of Fe_3O_4 leaching which confirms the stability of the composite fibres (Figure 5-37).

Acetaminophen has strong UV absorption with a prominent peak at 243 nm and a broad shoulder around 290 nm, in water[146]. In absolute ethanol these peaks were observed at 248 nm and 295 nm, respectively (Figure 5-38).

A calibration curve for acetaminophen was obtained using standard solutions and was used to determine the concentration of its quantities released during the control and actuation experiments of the acetaminophen loaded fibre system (Figure 5-39).

Based on the above results, the concentration and the cumulative % of acetaminophen released were plotted against time (Figure 5-40 and Figure 5-41, respectively).

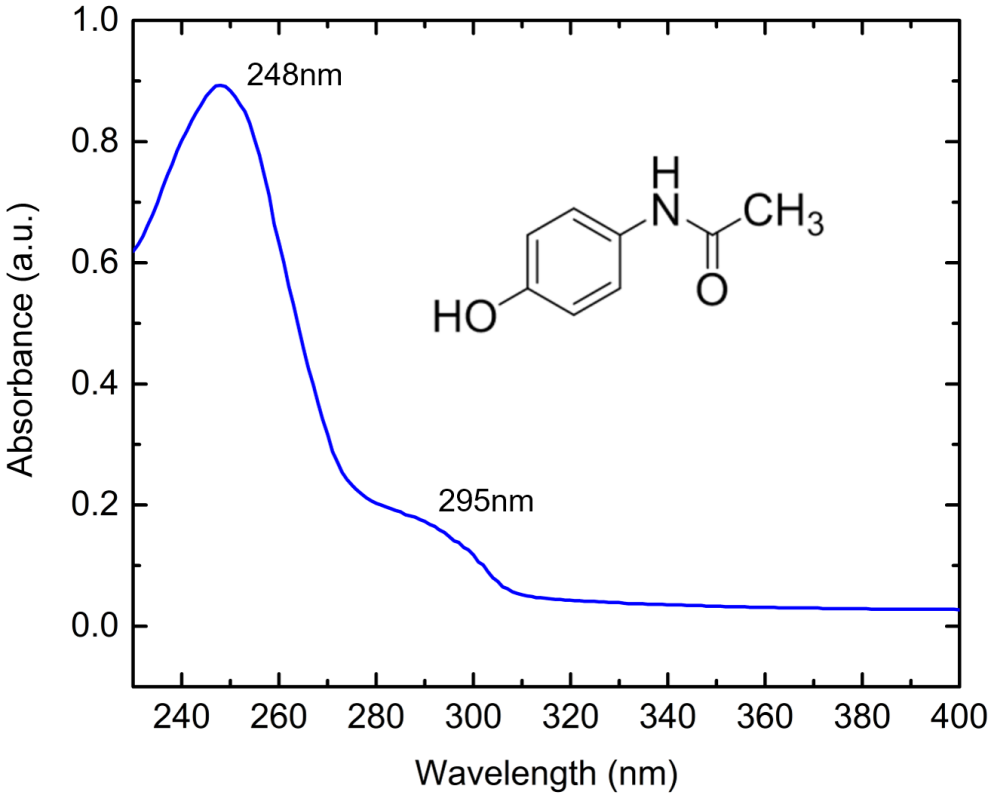

Figure 5-38 Chemical structure and UV-Vis absorption spectrum of acetaminophen.

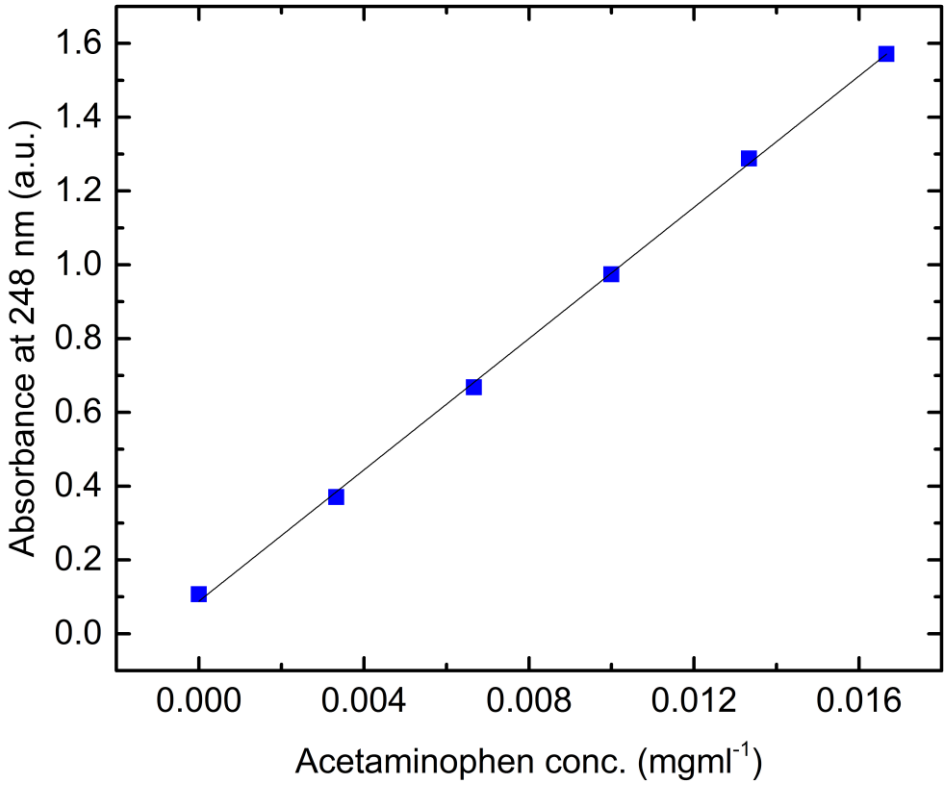

Figure 5-39 Calibration curve for acetaminophen, prepared at a 100x dilution.

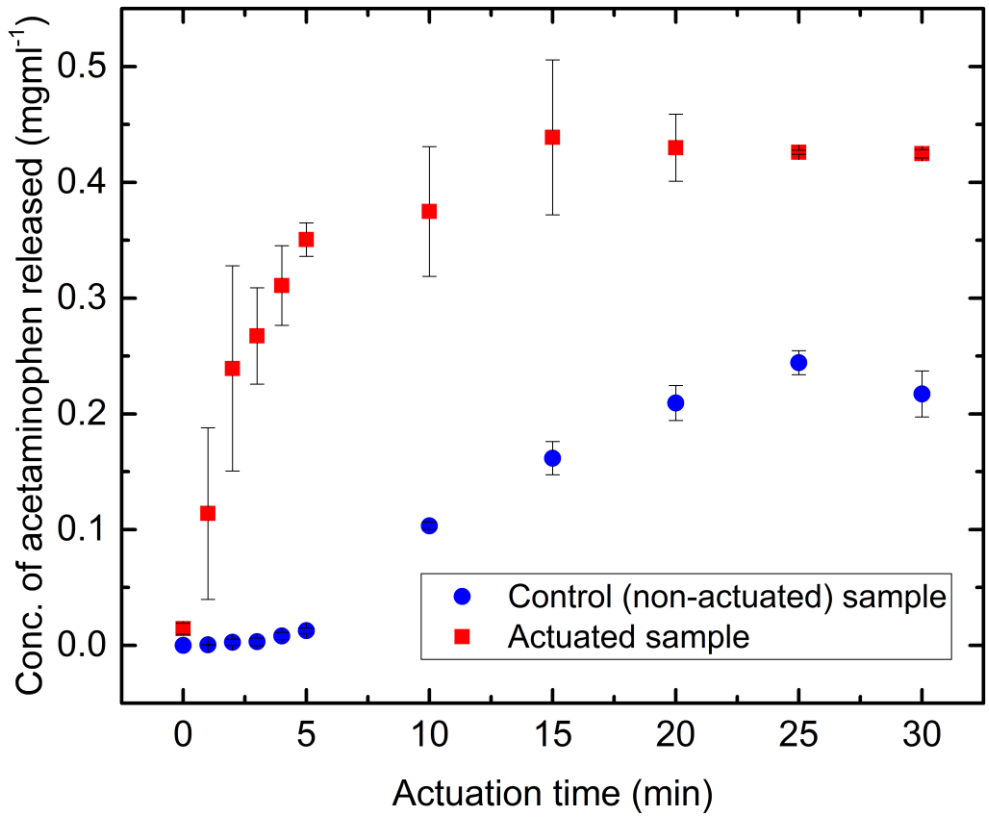

Figure 5-40 Concentration of acetaminophen released with time.

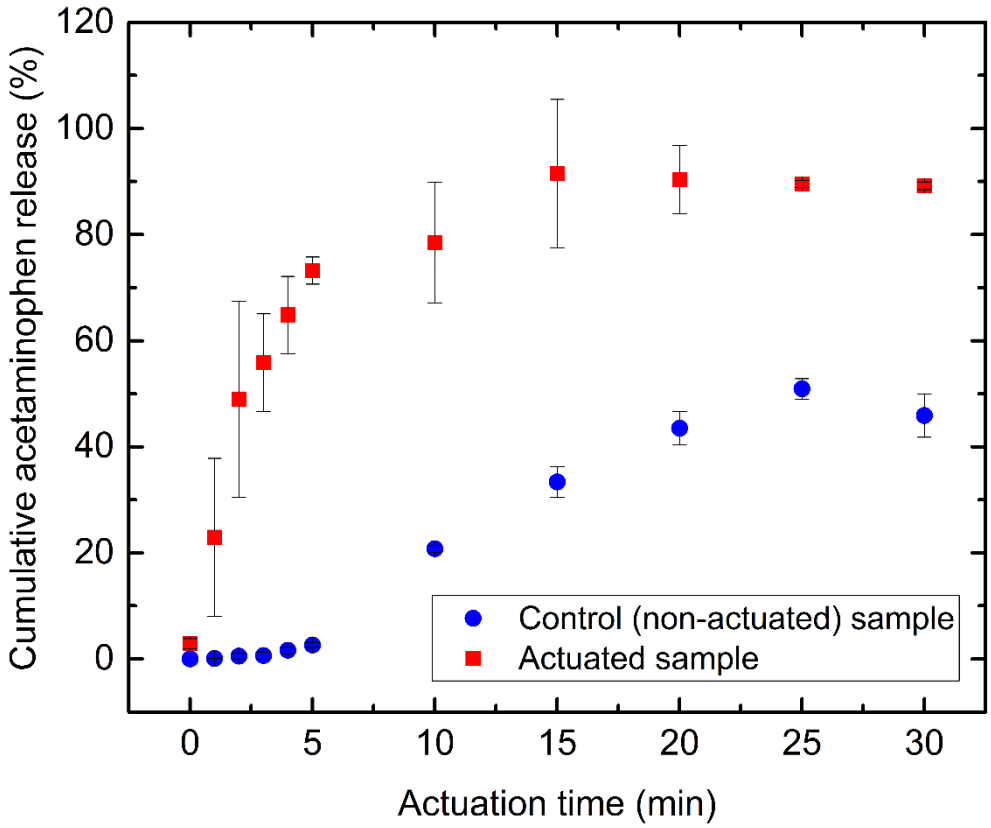

Figure 5-41 Cumulative weight percentages of acetaminophen released with time. The control experiment represents the equivalent release of acetaminophen without magnetic (or any other type of) actuation.

It was evident that the magnetically actuated fibre system released significantly more acetaminophen with time, compared to the non-actuated system. For the actuated samples, a rapid release of acetaminophen was observed during the first 5 min, followed by a gradual increase, up to 15 min, following which the release plateaued until the 30-min experimental time frame.

This behaviour is consistent with a 'burst-release' mechanism[147]. Over 90 % of the drug is already released by the end of 15 min of actuation, and the release appeared to be slightly reduced after this point. A possible explanation for the above is that the drug release had stopped due to entrapment of the remaining drug within the fibre matrix, resulting in an overall reduction of concentration. Hence, the drug release based on magnetic actuation appears to consist of two main phases: a 5-min initial burst release, and then a relatively slower but steady release up to 15 min.

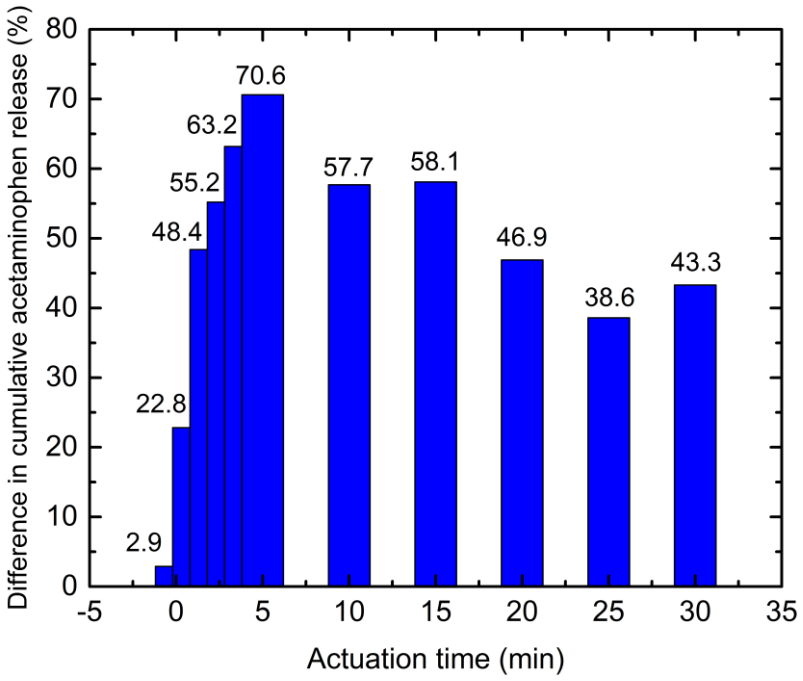

Figure 5-42 Effect of magnetic actuation on drug release with time: the difference between actuated and non-actuated cumulative release curves.

It is also noteworthy that since the drug release is triggered by movement (i.e., magnetic actuation), the acetaminophen concentration cannot be ensured

homogeneous throughout the test solution. This may result in greater differences in duplicate experiments conducted for actuated samples compared to the controls, hence, bringing about larger experimental errors for the former. In contrast, the control samples released significantly lower amounts of drug during the first 5 min, followed by a slower gradual increase of drug release over the next 20 min, and finally showing a slight decrease in the last 5 min. This behaviour can be attributed to simple diffusion of the immobilized acetaminophen powder from the fibre network.

The difference between the cumulative % of acetaminophen released over time, from the actuated and control experiments is depicted in Figure 5-42. By the end of the first 5 min, approximately 71 % of acetaminophen is released, compared to the control, followed by a decreased, yet steady difference up to 15 min, and even smaller differences by the end of 30 min. This is clear evidence that remote magnetic actuation can bring about significant release of drugs from the PVA-MNP fibres.

5.9.2 Summary

Based on the above results, it is evident that the PVA-MNP fibres are capable of fast drug release during smaller time scales and slower, consistent rates of drug release over time, *via* magnetic actuation. This novel, biocompatible, cost effective and controllable technique has the potential to be used clinically, as an effective tool for triggered drug release. Application of this mode of drug delivery is particularly attractive in wound care, due to several reasons: 1) it can be used in the community by tissue viability nurses, 2) repeated drug delivery can be effected, without necessarily changing or removing the dressings, 3) chemical debridement of wounds (as opposed to surgical debridement for which one needs an anaesthetic, theatre time

and, often, a physician to conduct the procedure) can be carried out if the relevant drug is incorporated into the PVA-MNP fibres. Moreover, there is increasingly a focus to move the management of wound care into the community, which achieves two important NHS objectives: (a) it relieves hospital bed pressures, and (b) patients can be managed in the convenience of their own homes, and are not subjected to the challenges of being an in-patient.

This technology also has potential applications for “site-specific” treatment, due to its customizable properties. For example, the sensitivity of magnetic actuation of the fibres, namely, the minimum depth and distance from the magnetic source needed for actuation, can be improved by either increasing the MNP concentration or the power of the magnet. Then, the material can possibly be applied in treatment of atherosclerotic plaque in the carotid artery, or, in simpler terms, for prevention of a stroke. In this instance, the magnetic fibres could be administered intravenously, and then the magnetic actuation could be directed to the carotid artery in the neck, so that the drug would be released only at this specific site. If deeper penetration of the magnetic force can be achieved safely, then one could envisage widening the portfolio of use within the body, in a number of conditions, for example, acute conditions such as sepsis, and chronic diseases, such as inflammation in arthritis, inflammatory bowel disease, and in a range of oncological therapies.

Chapter 6.

Infusion gyration analysis

6.1 Set-up Analysis

The infusion gyration system is developed from the gyration system. For each gyration system, an infilling tube on top of the cap is designed either delivering continuous gas pressure which forms pressurised gyration which was introduced in Chapter 2 or continuous spinning solution at some flow rate which forms infusion gyration.

Regarding Figure 6-1 of the fibre spinning gyration system, the whole system can be treated as functional blocks combined in a different way. For example, if we choose pressure block and gyration block, it is pressurised gyration.

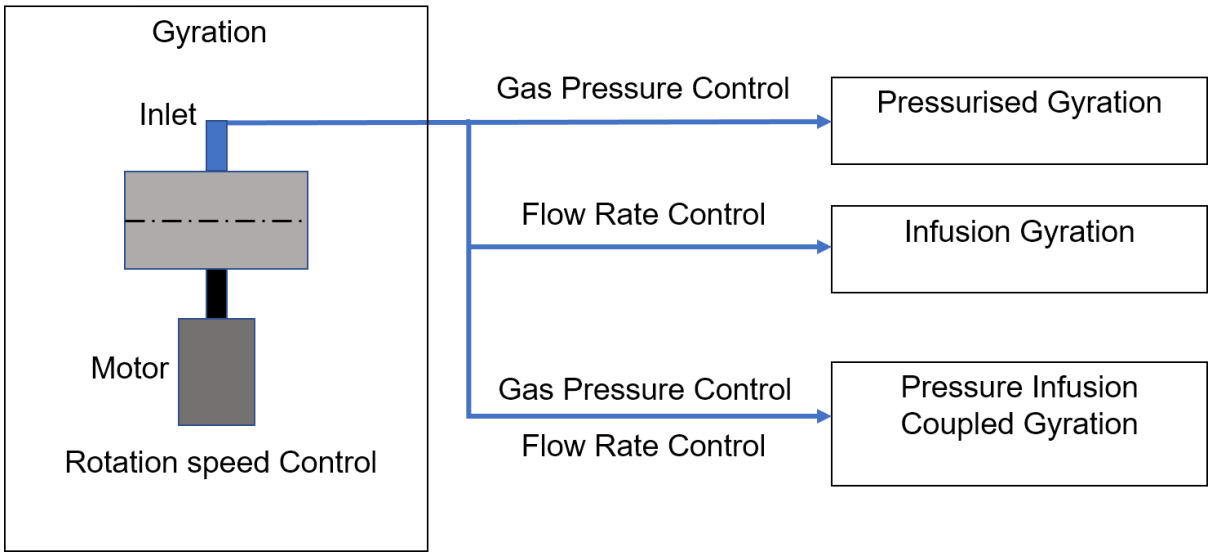

Figure 6-1 Analysis of gyration system.

A high-pressure nitrogen supply is used because of its low cost and nitrogen barely reacts with chemicals which may be a kind of protection to the spinning solution. If the experiment requires low complexity of its surrounding, nitrogen provides a purer gas environment for the spinning process. Moreover, this gas supply can vary depending

on other experiment designs. If a new design requires another gas environment because the solution needs the reaction with the specific gas during the spinning process, the nitrogen cylinder can be replaced by hydrogen or oxygen. Or, if the solution is safe to the air, which means the solution only requires pressure, a stable air turbocharger with enough pressure providing capacity is also acceptable. Here, the important thing is that any kind of gas supply affects the environment outside around the pot. In this small area, humidity and temperature change quickly in a short time. Any gas supply change should be tested to narrow down the effect on the spinning process unless the effect is needed.

However, the solution needs to be added into the vessel prior to spin because the gas supply occupies the inlet from the pressurised gyration system to deliver pressure to the cylindrical vessel. Therefore, the volume of solution should be considered and the run is a start-stop process which means if every part is fixed preparing for a start, the change must be made after spinning completion.

Furthermore, solutions can also be spun at 0 gas pressure revealing the fact that rotation is the main power driving the formation of fibres. The results from Chapter 2 also confirms that gas pressure was used as a tuning tool of fibre shape.

The idea of inventing a novel infusion gyration system is to simplify the spinning process such as solution adding and to control the solution supply in order to control the spun fibre properties.

6.2 Time Analysis

Time is an important factor in laboratory experiment or industrial manufacturing. The time analysis of experiment completion is made from experiment experience which

provides recommendations of experiment planning (time control of completing experiment) and improvement in the future (Table 6-1).

Step	Actions	Time
1	Solution preparation. Some solution needs a longer time to dissolve.	Depends.
2	Set-up preparation including electric connection, tube connections, screws and seals.	~15min.
3	Trial. This may be done several times ensuring system is working well.	~5min.
4	Syringe pump setting and syringe preparation	~5min.
5	Spinning session (start to finish).	~10min.
6	Solution refill.	~2min.
7	Cleaning.	~15min.

Table 6-1 Time analysis of infusion gyration.

Step 5 and 6 can be repeated if needed. The preparing and cleaning process take most of experiment time except for solution making and spinning repeats.

6.3 Fibre Formation analysis

The centrifugal force driving the solution into tiny streams through orifices is from high speed rotating cylindrical vessel (Figure 6-2).

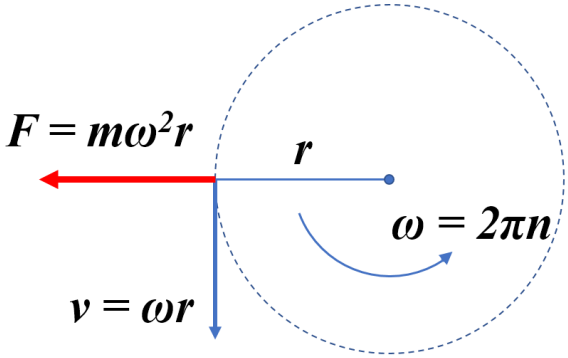

Figure 6-2 Centrifugal force.

This force directly relates to rotational speed ($\boldsymbol{n}$) of the vessel driven by the motor. Here, in calculation, the unit rpm needs to transfer to rad/s. For pressurised gyration introduced in the literature review, the centrifugal force also combines to the force from gas pressure (P, $Pa\ in\ unit$) which is supplied by the system where S (m^2) is cross-section area of the orifice.

$$F_{gas\ pressure} = \frac{P}{S}$$

When the stream is accelerated, it has the velocity to fly and stretch. The stream becomes thinner and longer at this stage (Figure 6-3).

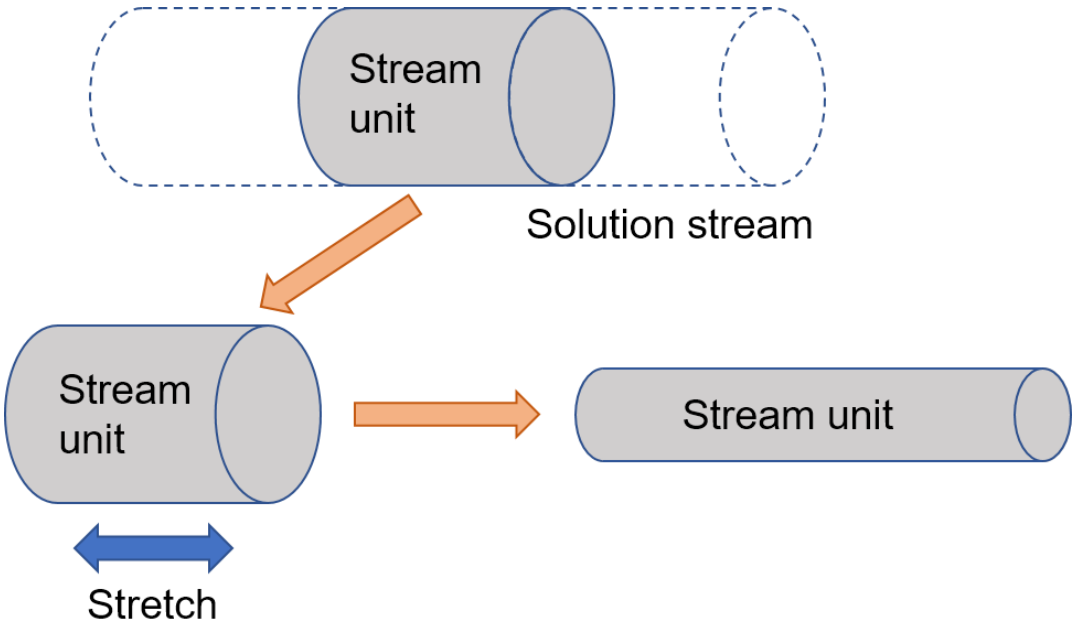

Figure 6-3 Stream stretching.

In this process, the solvent evaporates as well as the fibre forms (Figure 6-4). The formation of different fibre shape occurs in this stage connecting to the evaporation rate which is affected by polymer, solvent, concentration and environmental humidity.

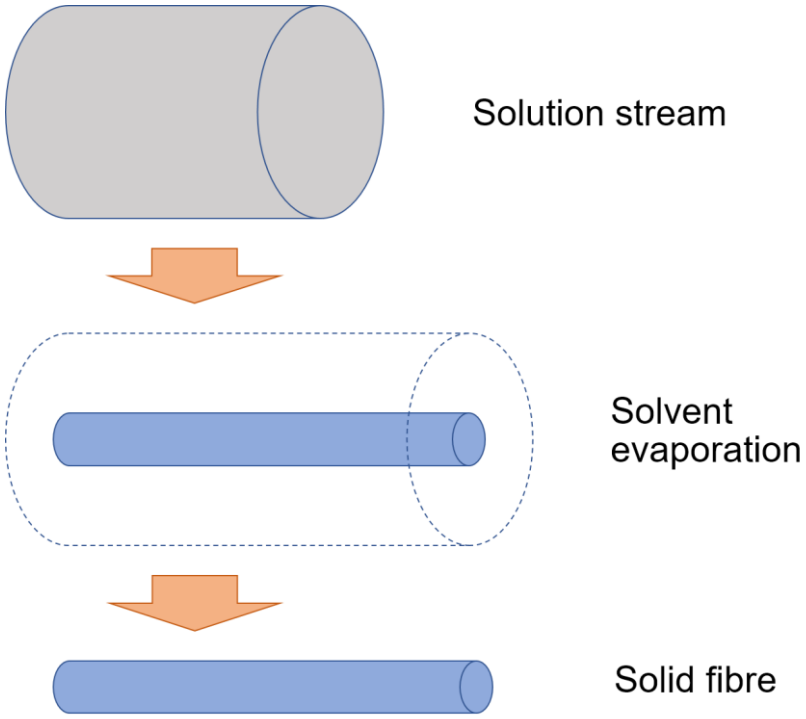

Figure 6-4 Fibre formation.

However, due to the difference of solution property (such as viscosity and surface tension), different formation happens to the stream. Some stream breaks before it gets thinner (Figure 6-5).

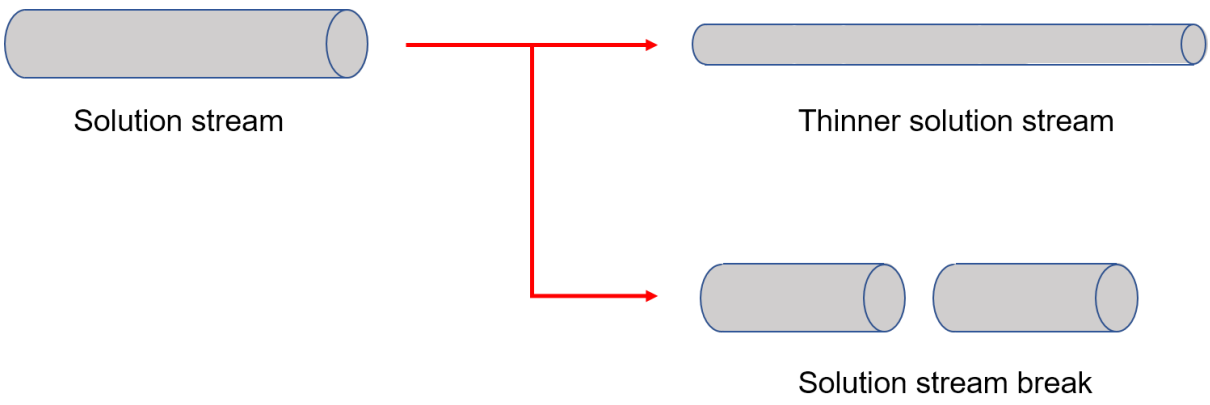

Figure 6-5 Stream break.

These broken streams either form large diameter fibres or form beads if the evaporation is slow (because surface tension directs liquid into a spherical structure).

6.4 Balance Point Conjecture

The ‘strange point’ of flow rate, which was introduced in Chapter 4, happens in the infusion gyration process. The average diameter of fibres decreases at some point at a flow rate in between a lower one and a higher one. Three repeats of experiment resulted the same. If the parameter changes from flow rate to pressure, the point cannot be observed any more (the pressurised gyration shows linear result[5]). This is because the pressure may only assist the centrifugal force to project by providing more pushing power. Moreover, the solution is all added prior to spin for pressurised gyration and the gas may influence the evaporation rate. These factors are all for stretching the stream.

However, as we control the flow rate in the process, the stream can no longer stretch freely. For infusion gyration, the centrifugal force is a constant value, if the rotating speed of the vessel is stable, which accelerates the stream to a velocity at early flying stage. If we multiply this velocity by the stream cross section area, we get another ‘flow rate’ value which is defined by volume over time. However, the initial flow rate (stream with velocity) is supplied and controlled by the infusion system. These two values exist in one continuous stream which would also cause stretch or press on itself influencing the fibre size. In other words, the infusion system can drag or push the flying stream from one side during spinning. At lower flow rate, all solution is spun into fibres as they have a smaller size. At higher flow rate, breaks decrease but more mass into the stream causes larger fibre size. However, in between, there is always a point, i.e. ‘balance point’, whose supply equals to the stretching mass which will extend the

fibre length to its limit. This point delivers a lower diameter of fibres which differs from polymer, solution concentration and other parameters.

6.5 Products

6.5.1 PVA fibres

In chapter 5, high magnification SEM of PVA-MNP fibres was studied. Here, images of a much lower one were taken for comparison (Figure 6-6 - Figure 6-9). Beads are observed within fibres with different size which were also recorded in optical microscopy images in Chapter 5. The content of MNPs does not obviously affect fibre morphology in large scale which accords with the results of high magnification images close-up to the single fibres.

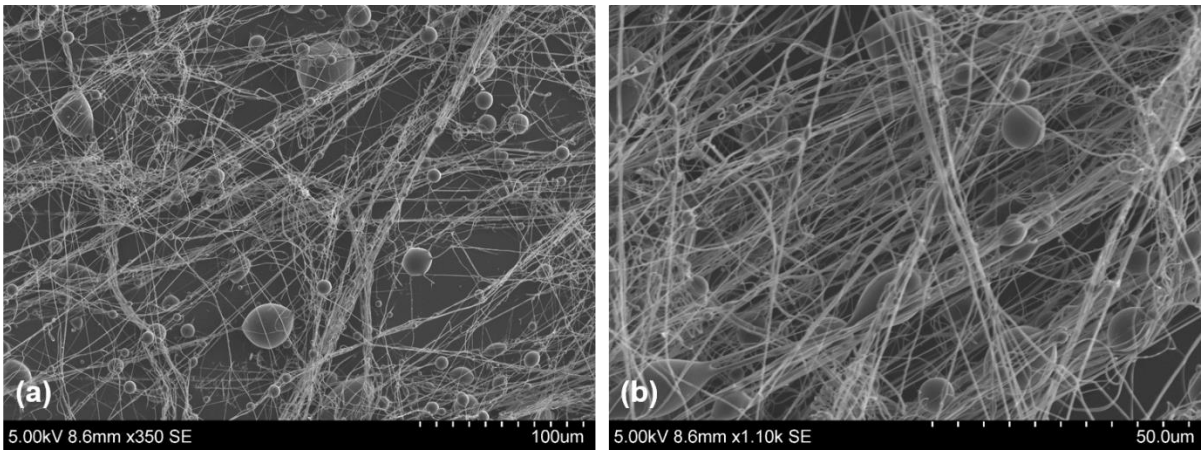

Figure 6-6 SEM images of pure PVA fibres.

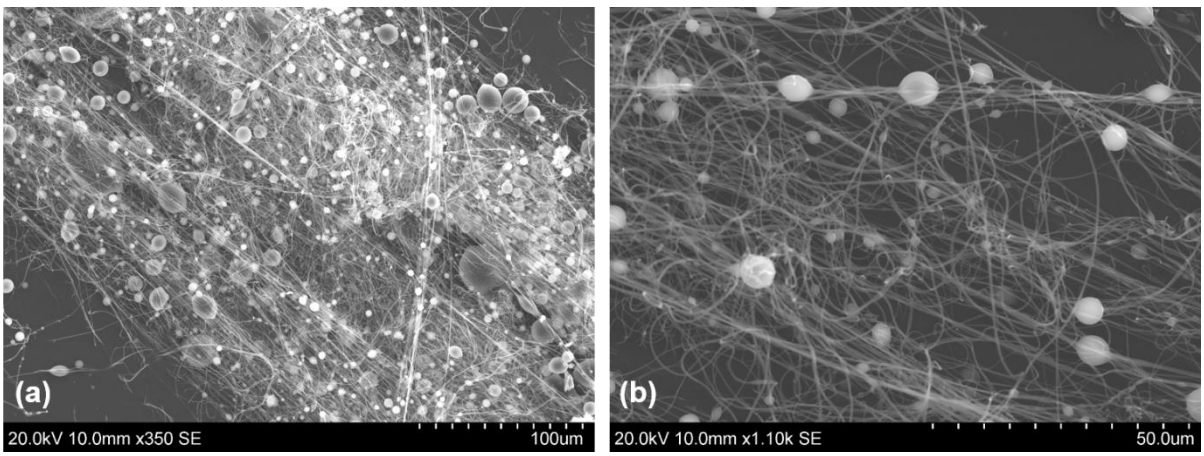

Figure 6-7 SEM images of 3%wt MNPs PVA fibres.

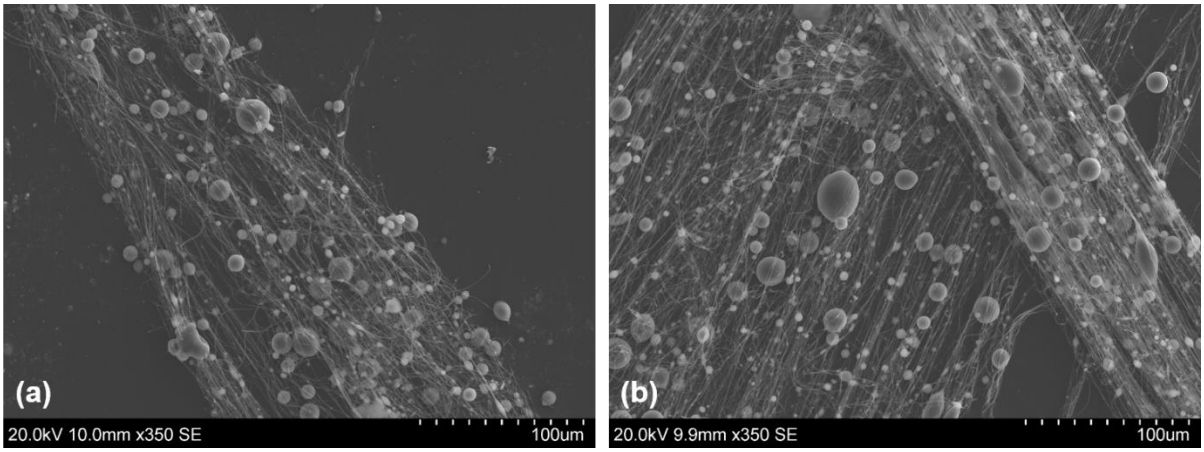

Figure 6-8 SEM images of 4%wt MNPs PVA fibres.

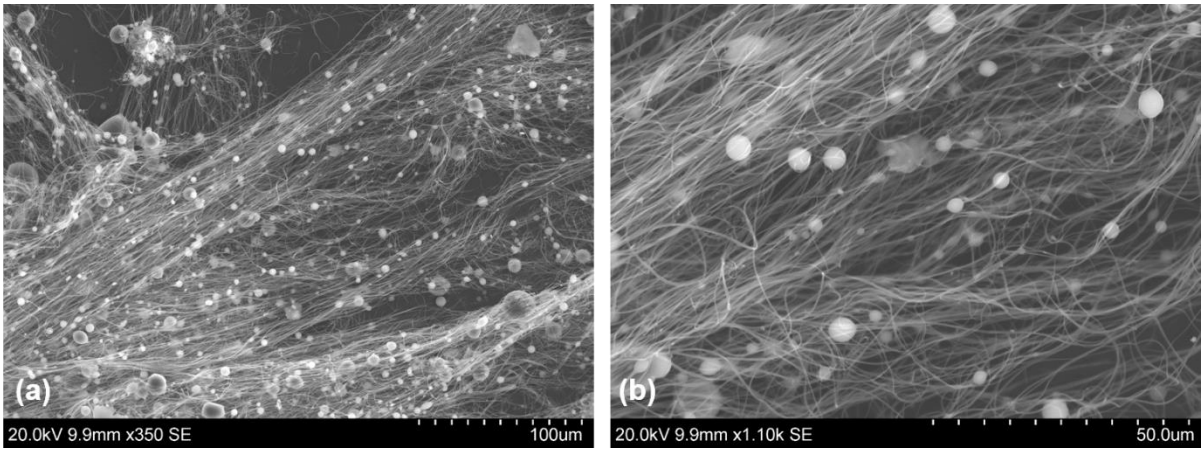

Figure 6-9 SEM images of 5%wt MNPs PVA fibres.

Beads existing in the final generated fibres by different method are quite common and they come along with the fibre formation process[99]. Some application may make use of them because of their properties such as increasing the loading or attaching ability of other media, for example.

6.5.2 PVA & PEO fibre comparison

Both as water soluble polymer successfully spun by infusion gyration, the morphology comparison of two fibres through SEM images can point out their similarities and difference providing recommendations for spinning other polymers in the future (Table 6-2).

PVA fibres	PEO fibres
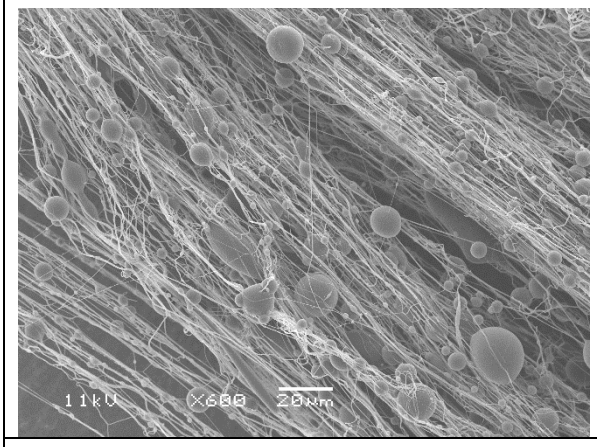	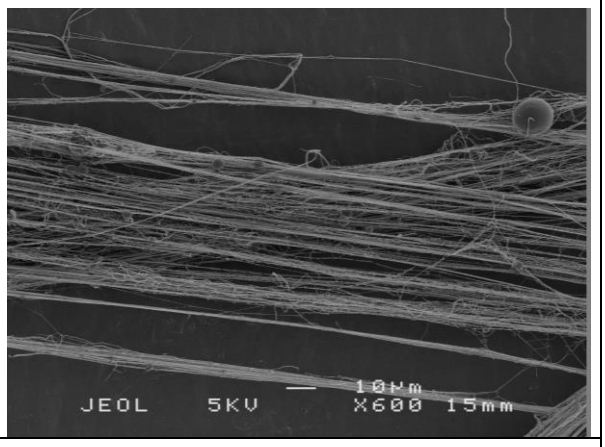
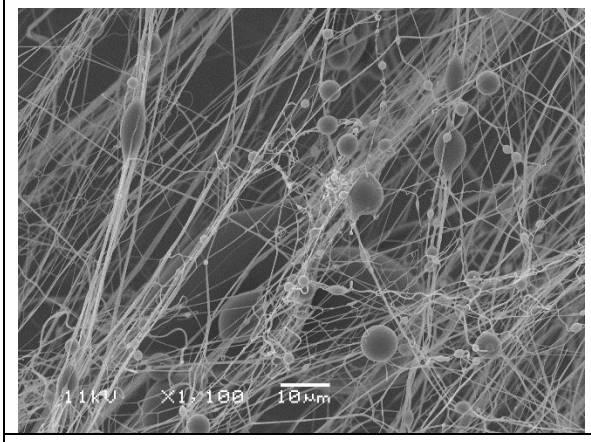	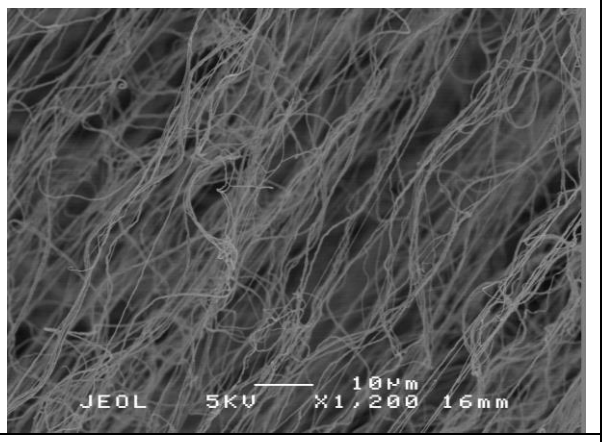
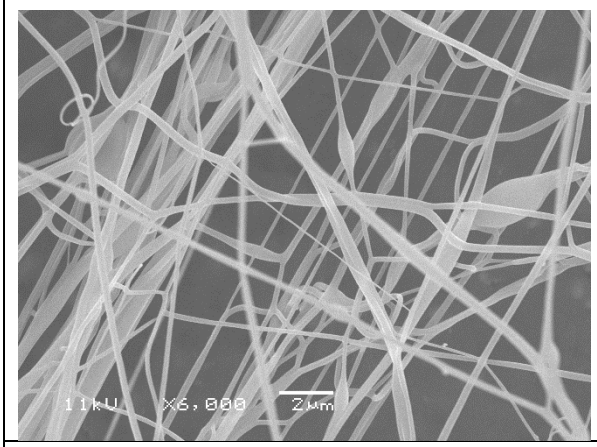	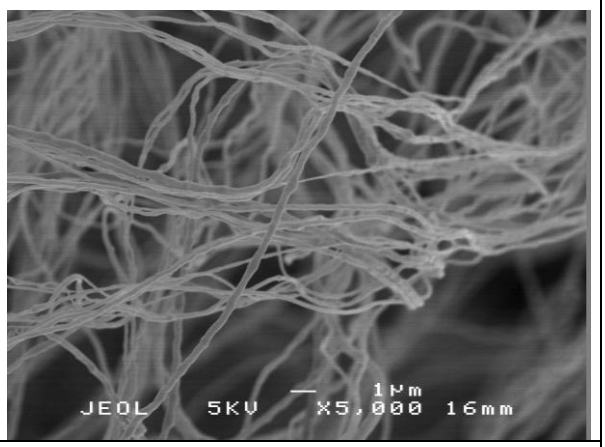
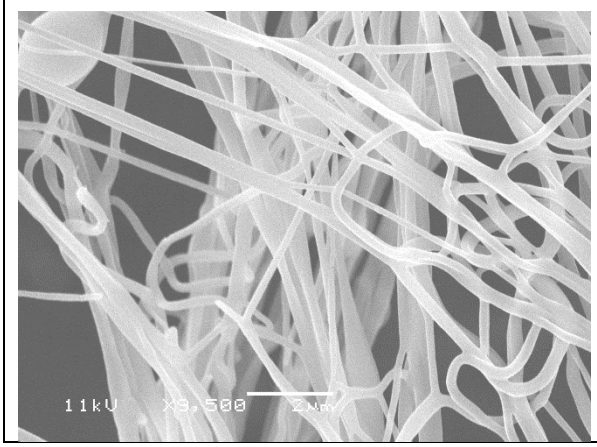	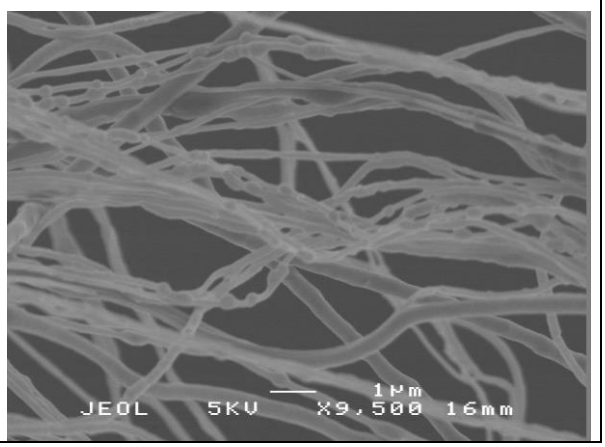

Table 6-2 SEM image comparison for PVA and PEO fibres.

From the comparison above, similar fibre size of them is observed and differences can be concluded as follows.

1. PVA fibres have more beads than PEO ones in general.
2. PVA fibre is smooth on its surface, however, it is rough for PEO.
3. PVA fibre tends to be straight. PEO fibre is curlier.
4. PVA fibres form a net structure. PEO fibre stands alone.

Therefore, the number of beads (or beads formation), fibre surface roughness and shape will not affect the fabrication process of infusion gyration. Polymer can be changed for controlling these factors depending on product requirement and application. Infusion gyration also has a potential of adapting different polymers.

6.5.3 PAN fibres

To test the capacity of infusion gyration spinning non-water-soluble polymer fulfilling the waterproof requirement for possible future applications, polyacrylonitrile (PAN) which does not dissolve in water but in strong solvent has been tried. PAN (polyacrylonitrile, 150,000 typical average molecular weight) powder and DMF (*N,N*-Dimethylformamide) solvent used are from Sigma-Aldrich (Poole, UK).

10wt% PAN-DMF solution was prepared for spinning:

18g of DMF was prepared in an air-tight glass bottle as solvent and 2g of PAN powder was added in the bottle. The solution was shaken for full mixture and kept stirring for no less than 48hrs until PAN powder is fully dissolved. 20g 10wt% PAN-DMF transparent solution was made. 5ml 10wt% PAN-DMF solution was added into a

syringe fixed on a syringe pump and spun by infusion gyration. Spinning speed was set to 36,000rpm and infusion flow rate was 2000ul/min. Spinning time is 3min and after spinning was stopped, the fibres were kept on aluminium foils for 10min to dry the fibres. Then the fibres were collected for SEM (Figure 6-10).

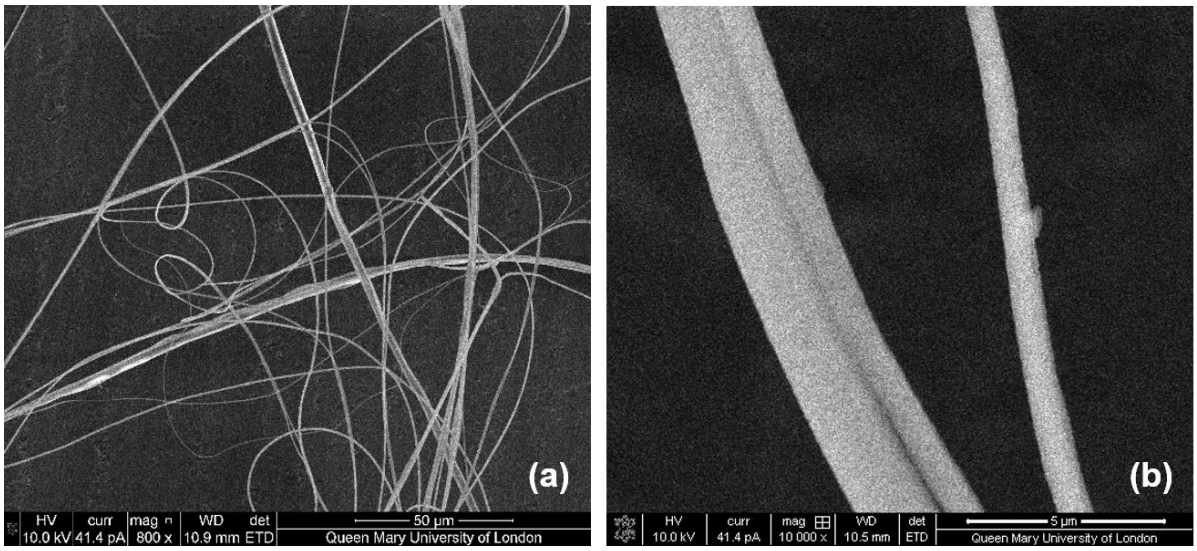

Figure 6-10 SEM images of PAN fibres.

The fibre surface is smooth and beads were not observed for PAN fibre sample which means bead-free waterproof fibre can be made through infusion gyration. This successful spinning of PAN fibres also broadens the type range of materials this method can process. Moreover, these polymers with different properties would serve more applications of fibre.

6.5.4 Microbubbles

In Chapter 2, it has been reported that polymer microbubbles can be generated through pressurised gyration. To gain the flexibility of infusion gyration, trial of microbubble production was applied.

5wt% PVA (Mw 31000) aqueous solution was prepared. The flow rate was set to be 6000 µl/min which is higher than usual mimicking the status of sufficient solution which

pressurised gyration provides. The rotating speed was kept the same as before on 36,000rpm. Microscope slides were placed on the inner wall of the spinning container. They were immediately transferred and observed after production, under an optical microscope (Nikon Eclipse ME 600) fitted with a camera (JVC KY-F55B). Images are as follows (Figure 6-11).

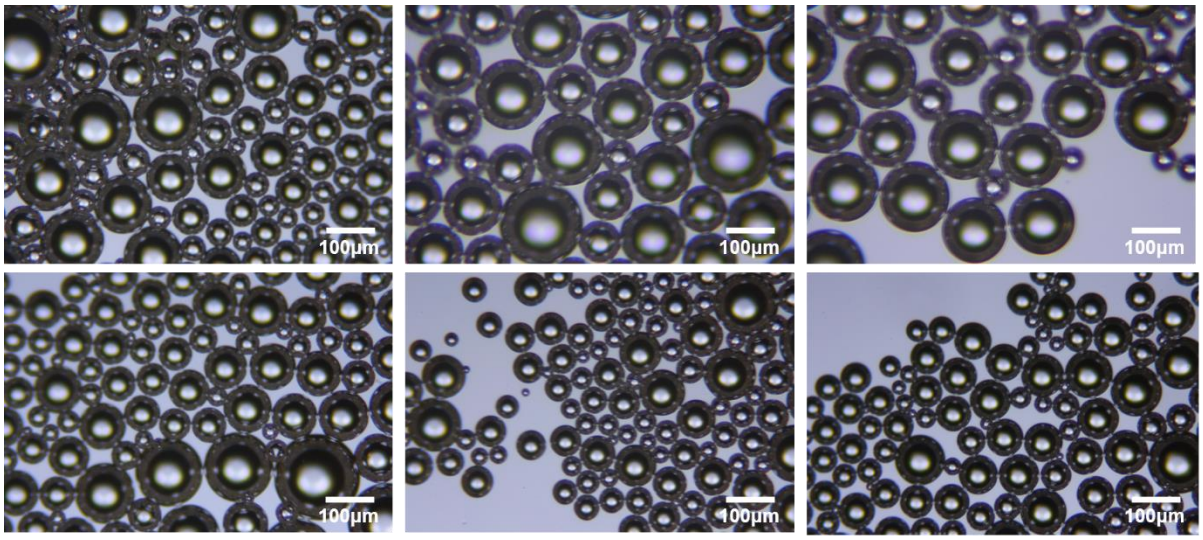

Figure 6-11 Microbubble generation by infusion gyration.

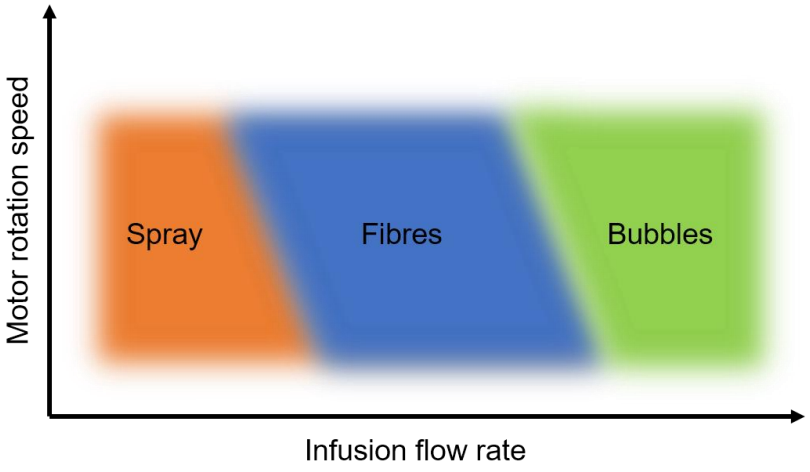

Figure 6-12 Products by infusion gyration.

It is seen that microbubbles were well formed and delivered by infusion gyration which extends the product range proving its high flexible process ability (Figure 6-12).

Chapter 7.

Conclusions and Future work

7.1 Conclusions

Micro and nano fibres composed of nano-assemblies show great promise as enabling constituents for diverse applications in areas ranging from tissue engineering, sensing, optoelectronics and nanophotonic devices due to their controlled organisation and architecture. This thesis provides an infusion gyration method that enabled a bio-fabrication process to form functional micro/nanofibres with inherent biological functions. This method (detailed in Chapter 3) allows tuning both the fibre size and distribution by adjusting the flow rate of the polymer solution without using an external pressure. The results have multiple implications.

In chapter 4, PEO fibre coupled engineered protein has been made showing fluorescence which is designed as the fibre function. A power law relationship between the polymer concentration and its viscosity, as well as a relationship between the Berry number (Be) and the formed structures are the principles that guide the formation of fibres. A sufficient amount of chain entanglement was obtained at Be > 1.6 for fibres integrated with proteins having 117-216 nm diameter range. Fibre morphology evaluated by field emission scanning electron microscopy demonstrated well fibre formation. The effects of processing parameters on fibre size, size distribution and morphology are analysed. Fluorescence microscopy analysis corroborated with FTIR data confirmed the integration of the engineered gold binding peptide within the fibres. The compatibility of proteins into fibres was tested. The assembly of the engineered proteins as an integrated part of the fibre could be followed using fluorescence protein. The integration of biological building blocks i.e. functional proteins and peptides to

fibre processing may allow harnessing the extraordinary diversity afforded by protein functions to generate smart bio-hybrid materials for imaging, bioelectronics, bio-sensing and tissue engineering applications.

In chapter 5, a new experimental system of controlled drug release was introduced. A PVA mixture ratio for infusion gyration was found. PVA fibres with iron oxide nanoparticles incorporated were prepared through this method which has been tested as potential for industrial mass production. From the SEM, EDX and other characterization method results, the nanoparticles are bonded into polymer structures as aggregation and dispersed in fibres uniformly. These fibres with sufficient magnetization can be noncontact controlled for movement and actuation showing strong magnetic field response via external magnets. They were shown to be stable when stored in ethanol, without any leaching of iron oxide nanoparticles. Moreover, the spongy structure of fibre mass is a good absorbent for drugs. This fibre with its magnetic activity shows great potential of target-controlled and sustained drug release for bio-medical purpose such as treatment of wound healing. An approach has been established in laboratory conditions to demonstrate the concept of controlled drug release. Acetaminophen, as a model drug used, was successfully released from the fibres when subject to magnetic actuation, bringing about over 90 % cumulative release in 15 min. Compared to non-actuated controls, the magnetic fibres showed over 71 % more release of the drug within 15 minutes, so the utility of the new drug delivery and controllable release platform has been illustrated. The above, coupled together with the facile, cost effective material synthesis, with proven ability to scale up, offers attractive opportunities in clinical application of the magnetic fibres.

In Chapter 6, a detailed analysis for an infusion gyration system is made theoretically and practically. A conjecture was proposed to explain the phenomenon which happened during the process. Different products were studied.

7.2 Future Work

Excellent functional composite micro/nanofibres have been made for potential applications and the novel infusion gyration system invented has demonstrated the capacity of generating products under control. As far as can be established by the whole functional fibre spinning using an infusion gyration experience, improvement can be made in two main parts.

1. If we face the product object, i.e., we would like to achieve some functions, objectives and application in practice on the fibres themselves, we can test and change the type of polymer as well as the different solvent system or functional adoptions.

2. If we face the generation process, i.e., we would like to increase the yield of production and improve the fibre shape, we can tune the parameters of the set-up such as flow rate and motor speed or even add other new parameters like temperature control to the system.

Therefore, by following these two key principles, these aspects of recommendations for the future work are as follows.

7.2.1 Change of the engineered protein

The integration of fluorescence protein to the fibres using an infusion gyration process demonstrates that the engineered proteins (i.e. biological building blocks) can contribute to bio-hybrid fibre formation by providing control over nanoscale assemblies. Fluorescence protein has a potential for bio-sensing as it is easy to track by fluorescence microscopy which, on the other hand, helped the trial in this study. Nevertheless, other engineered proteins with functions can be used in fibre spinning to achieve another kind of functional fibres, even different proteins are mixed. Therefore, designed functional bio-material may be performed by changing the engineered protein mixed to polymer solution.

7.2.1 Drug release test *in-vivo*

The PVA-MNP fibres used in the drug release test shows a good performance. However, it is just a validation of drug delivery. More planned tests of drug release experiment can be done to make the fibres closer to clinical application. The material (polymer and drug) can be changed (to a non-water-soluble one, for example) for the other areas extended by this system for different purposes.

7.2.2 PVA mixture theory developing

An important and interesting finding is that, for infusion gyration, only the mixture of three different PVA molecular weights in a specific ratio can deliver a higher volume of fibres during formation. One possible reason is that the crosslink occurs between

the chemical chains of the different size of PVA macromolecular. Research has been made to chitosan hydrogels on crosslinking network structure[148] (Figure 7-1).

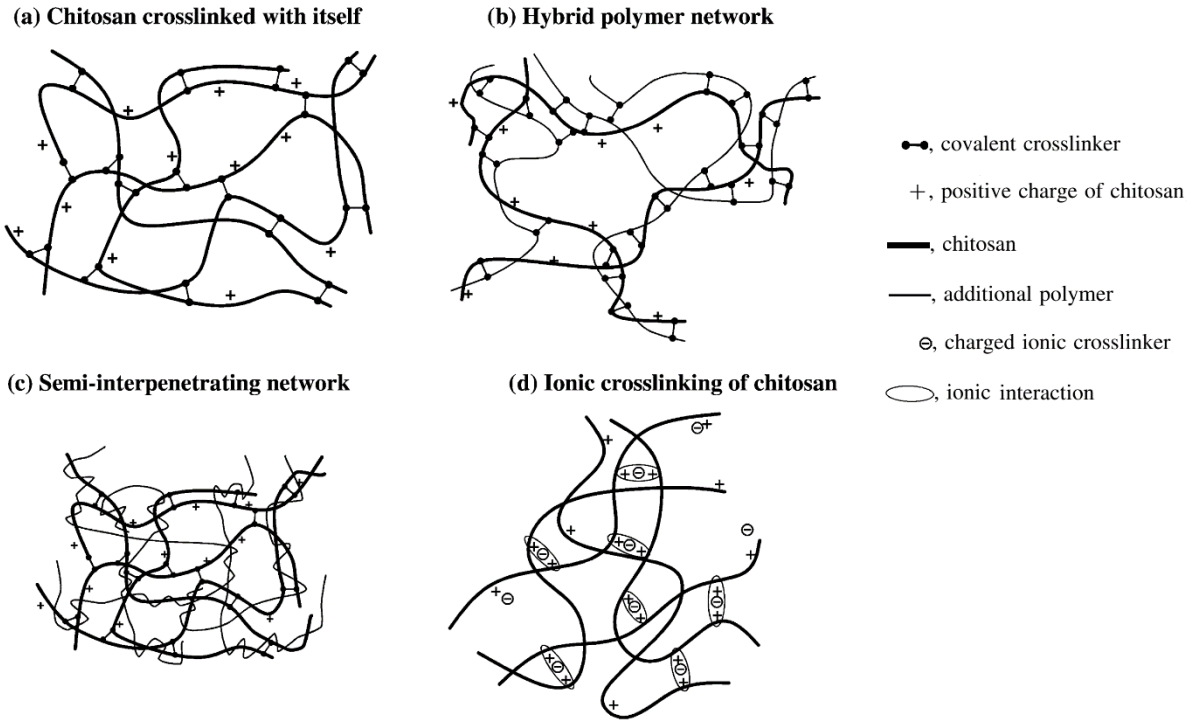

Figure 7-1 Schematic of chitosan hydrogel structure types[148].

Therefore, the theory of PVA mixing can be studied and developed to gain a better understanding of polymer fibre formation. Topology may be a useful mathematical tool for analysing as 'knot theory' is to study patterns of rope structure (which may have a similarity with a chemical chain) knotting, binding and attaching. Energy can also be a factor to be considered.

7.2.3 Study of infusion gyration

More polymers can be tested generating fibres through this method at a different flow rate. The relationship between fibre properties and spinning parameters can be concentrated for production and research in the future.

7.2.4 New system design

A better clean and closed protection collection system can be designed to improve the quality control of fibres. If a small climate control system is applied to the infusion gyration, the temperature, humidity and air flow can be purified and kept constant to reduce disturbance of the fibre formation. Moreover, the modularity can be enhanced if function block design is introduced. For example, a different performance motor or a collector can be changed for a different project and the collection distance can be modified every time which tunes the forming space. This design shortens the time span of experiment and even the repair sometimes which means changing or replacing parts is rapid. Even new function blocks for this system can be developed to improve the capacity for other applications.

7.2.4.1 New flow supply

Using a shunt connector can provide more flexibilities to the system (Figure 7-2).

Figure 7-2 Shunt connector.

Application 1: Fast shifting syringes (Figure 7-3). Through this method, a solution can be quickly refilled to the system doubling the volume of solution spun once and shortening refill time. When one syringe finishes a solution, the system is stopped to fix another into position.

Figure 7-3 Fast shifting syringes by shunt connector.

Application 2: Combining spinning solutions. Two liquids can be mixed (in different ratio) when delivered to the cylindrical vessel if the liquid requires mechanical mixture to spin in a very short time (like oil phase and water phase). In addition, mixed fibres may be spun through it where the composite material can be designed and made.

This idea can extend to three or more solutions mixing during spinning which may need more syringes system. Sometimes, more syringe pumps (like double pumps) are not essential for these systems as some syringe pump has an adaptor for multiple syringe. A continuous flow supply can be applied to manufacturing in industry.

7.2.4.2 New rotating part

The cylindrical vessel used can apply new dimensions such as diameter and orifice size. The guiding groove design inside the vessel can improve solution streams to the orifice if machining allows. An easy-to-clean design is required.

References

1. Liang, D., Hsiao, B. S. & Chu, B. Functional electrospun nanofibrous scaffolds for biomedical applications. *Adv. Drug Deliv. Rev.* **59,** 1392–1412 (2007).
2. Huang, Z.-M., Zhang, Y.-Z., Kotaki, M. & Ramakrishna, S. A review on polymer nanofibers by electrospinning and their applications in nanocomposites. *Compos. Sci. Technol.* **63,** 2223–2253 (2003).
3. Bhardwaj, N. & Kundu, S. C. Electrospinning: A fascinating fiber fabrication technique. *Biotechnol. Adv.* **28,** 325–347 (2010).
4. Zhang, X. & Lu, Y. Centrifugal Spinning: An Alternative Approach to Fabricate Nanofibers at High Speed and Low Cost. *Polym. Rev.* **54,** 677–701 (2014).
5. Mahalingam, S. & Edirisinghe, M. Forming of Polymer Nanofibers by a Pressurised Gyration Process. *Macromol. Rapid Commun.* **34,** 1134–1139 (2013).
6. Mahalingam, S., Raimi-Abraham, B. T., Craig, D. Q. M. & Edirisinghe, M. Formation of Protein and Protein-Gold Nanoparticle Stabilized Microbubbles by Pressurized Gyration. *Langmuir ACS J. Surf. Colloids* (2014). doi:10.1021/la502181g
7. Karuppuswamy, P. *et al.* Functionalized hybrid nanofibers to mimic native ECM for tissue engineering applications. *Appl. Surf. Sci.* **322,** 162–168 (2014).
8. Wong, D. E., Dai, M., Talbert, J. N., Nugen, S. R. & Goddard, J. M. Biocatalytic polymer nanofibers for stabilization and delivery of enzymes. *J. Mol. Catal. B Enzym.* **110,** 16–22 (2014).

9. Kim, T. G., Lee, D. S. & Park, T. G. Controlled protein release from electrospun biodegradable fiber mesh composed of poly(epsilon-caprolactone) and poly(ethylene oxide). *Int. J. Pharm.* **338,** 276–283 (2007).
10. Sanchez-Garcia, E., Doerr, M., Hsiao, Y.-W. & Thiel, W. QM/MM Study of the Monomeric Red Fluorescent Protein DsRed.M1. *J. Phys. Chem. B* **113,** 16622–16631 (2009).
11. Campbell, R. E. *et al.* A monomeric red fluorescent protein. *Proc. Natl. Acad. Sci.* **99,** 7877–7882 (2002).
12. Yuca, E. *et al.* In vitro labeling of hydroxyapatite minerals by an engineered protein. *Biotechnol. Bioeng.* **108,** 1021–1030 (2011).
13. Leung, V. & Ko, F. Biomedical applications of nanofibers. *Polym. Adv. Technol.* **22,** 350–365 (2011).
14. Xu, L., Zhao, X., Xu, C. & Kotov, N. A. Water-Rich Biomimetic Composites with Abiotic Self-Organizing Nanofiber Network. *Adv. Mater.* **30,** 1703343 (2018).
15. Yanagisawa, Y., Nan, Y., Okuro, K. & Aida, T. Mechanically robust, readily repairable polymers via tailored noncovalent cross-linking. *Science* **359,** 72–76 (2018).
16. Ashammakhi, N. *et al.* Biodegradable Nanomats Produced by Electrospinning: Expanding Multifunctionality and Potential for Tissue Engineering. *J. Nanosci. Nanotechnol.* **7,** 862–882 (2007).
17. Teo, W.-E., He, W. & Ramakrishna, S. Electrospun scaffold tailored for tissue-specific extracellular matrix. *Biotechnol. J.* **1,** 918–929 (2006).
18. Hipler, U.-C., Elsner, P. & Fluhr, J. W. Antifungal and antibacterial properties of a silver-loaded cellulosic fiber. *J. Biomed. Mater. Res. B Appl. Biomater.* **77B,** 156–163 (2006).

19. Townsend-Nicholson, A. & Jayasinghe, S. N. Cell electrospinning: a unique biotechnique for encapsulating living organisms for generating active biological microthreads/scaffolds. *Biomacromolecules* **7,** 3364–3369 (2006).
20. Jayasinghe, S. N., Irvine, S. & McEwan, J. R. Cell electrospinning highly concentrated cellular suspensions containing primary living organisms into cell-bearing threads and scaffolds. *Nanomed.* **2,** 555–567 (2007).
21. Yan, S. *et al.* Electrospinning of PVA/sericin nanofiber and the effect on epithelial-mesenchymal transition of A549 cells. *Mater. Sci. Eng. C* **79,** 436–444 (2017).
22. Persano, L., Camposeo, A., Tekmen, C. & Pisignano, D. Industrial Upscaling of Electrospinning and Applications of Polymer Nanofibers: A Review. *Macromol. Mater. Eng.* **298,** 504–520 (2013).
23. Hartgerink, J. D., Beniash, E. & Stupp, S. I. Self-assembly and mineralization of peptide-amphiphile nanofibers. *Science* **294,** 1684–1688 (2001).
24. Ellis-Behnke, R. G. *et al.* Nano neuro knitting: Peptide nanofiber scaffold for brain repair and axon regeneration with functional return of vision. *Proc. Natl. Acad. Sci. U. S. A.* **103,** 5054–5059 (2006).
25. Demir, H. V. *et al.* Spatially Selective Assembly of Quantum Dot Light Emitters in an LED Using Engineered Peptides. *Acs Nano* **5,** 2735–2741 (2011).
26. Nochomovitz, R., Amit, M., Matmor, M. & Ashkenasy, N. Bioassisted multi-nanoparticle patterning using single-layer peptide templates. *Nanotechnology* **21,** (2010).
27. Hattori, T. *et al.* A High-Affinity Gold-Binding Camel Antibody: Antibody Engineering for One-Pot Functionalization of Gold Nanoparticles as Biointerface Molecules. *Bioconjug. Chem.* **23,** 1934–1944 (2012).

28. Kacar, T. *et al.* Directed Self-Immobilization of Alkaline Phosphatase on Micro-Patterned Substrates Via Genetically Fused Metal-Binding Peptide. *Biotechnol. Bioeng.* **103,** 696–705 (2009).
29. Dickerson, M. B., Sandhage, K. H. & Naik, R. R. Protein- and Peptide-Directed Syntheses of Inorganic Materials. *Chem. Rev.* **108,** 4935–4978 (2008).
30. Hnilova, M. *et al.* Single-step fabrication of patterned gold film array by an engineered multi-functional peptide. *J. Colloid Interface Sci.* **365,** 97–102 (2012).
31. Tamerler, C. & Sarikaya, M. Molecular biomimetics: Utilizing naturels molecular ways in practical engineering. *Acta Biomater.* **3,** 289–299 (2007).
32. Park, T. J. *et al.* Protein nanopatterns and biosensors using gold binding polypeptide as a fusion partner. *Anal. Chem.* **78,** 7197–7205 (2006).
33. Yazici, H. *et al.* Biological response on a titanium implant-grade surface functionalized with modular peptides. *Acta Biomater.* **9,** 5341–5352 (2013).
34. Wang, H., Nakata, E. & Hamachi, I. Recent Progress in Strategies for the Creation of Protein-Based Fluorescent Biosensors. *Chembiochem* **10,** 2560–2577 (2009).
35. Uzun, S. D., Kayaci, F., Uyar, T., Timur, S. & Toppare, L. Bioactive Surface Design Based on Functional Composite Electrospun Nanofibers for Biomolecule Immobilization and Biosensor Applications. *Acs Appl. Mater. Interfaces* **6,** 5235–5243 (2014).
36. Evans, J. S., Samudrala, R., Walsh, T. R., Oren, E. E. & Tamerler, C. Molecular design of inorganic-binding polypeptides. *Mrs Bull.* **33,** 514–518 (2008).
37. Whaley, S. R., English, D. S., Hu, E. L., Barbara, P. F. & Belcher, A. M. Selection of peptides with semiconductor binding specificity for directed nanocrystal assembly. *Nature* **405,** 665–668 (2000).

38. Naik, R. R., Brott, L. L., Clarson, S. J. & Stone, M. O. Silica-precipitating peptides isolated from a combinatorial phage display peptide library. *J. Nanosci. Nanotechnol.* **2,** 95–100 (2002).
39. Cetinel, S. *et al.* Addressable self-immobilization of lactate dehydrogenase across multiple length scales. *Biotechnol. J.* **8,** 262–272 (2013).
40. Saquing, C. D., Manasco, J. L. & Khan, S. A. Electrospun Nanoparticle-Nanofiber Composites via a One-Step Synthesis. *Small* **5,** 944–951 (2009).
41. Hnilova, M. *et al.* Effect of Molecular Conformations on the Adsorption Behavior of Gold-Binding Peptides. *Langmuir* **24,** 12440–12445 (2008).
42. Corni, S., Hnilova, M., Tamerler, C. & Sarikaya, M. Conformational Behavior of Genetically-Engineered Dodecapeptides as a Determinant of Binding Affinity for Gold. *J. Phys. Chem. C* **117,** 16990–17003 (2013).
43. Hnilova, M. *et al.* Fabrication of hierarchical hybrid structures using bio-enabled layer-by-layer self-assembly. *Biotechnol. Bioeng.* **109,** 1120–1130 (2012).
44. Nachev, P. *et al.* Magnetic Oculomotor Prosthetics for Acquired Nystagmus. *Ophthalmology* (2017). doi:10.1016/j.ophtha.2017.05.028
45. Singh, R. K. *et al.* Potential of Magnetic Nanofiber Scaffolds with Mechanical and Biological Properties Applicable for Bone Regeneration. *PLoS ONE* **9,** e91584 (2014).
46. Ulbrich, K. *et al.* Targeted Drug Delivery with Polymers and Magnetic Nanoparticles: Covalent and Noncovalent Approaches, Release Control, and Clinical Studies. *Chem. Rev.* **116,** 5338–5431 (2016).
47. Wang, Y. & Kohane, D. S. External triggering and triggered targeting strategies for drug delivery. *Nat. Rev. Mater.* **2,** 17020 (2017).

48. Chandna, A., Batra, D., Kakar, S. & Singh, R. A review on target drug delivery: magnetic microspheres. *J. Acute Dis.* **2,** 189–195 (2013).
49. Arruebo, M., Fernández-Pacheco, R., Ibarra, M. R. & Santamaría, J. Magnetic nanoparticles for drug delivery. *Nano Today* **2,** 22–32 (2007).
50. Jurgons, R. *et al.* Drug loaded magnetic nanoparticles for cancer therapy. *J. Phys. Condens. Matter* **18,** S2893–S2902 (2006).
51. Perera, A. S. CHAPTER 4:Sustainable Magnetic Nanocatalysts in Heterogeneous Catalysis. in *Magnetic Nanomaterials* 99–119 (2017). doi:10.1039/9781788010375-00099
52. Hoare, T. *et al.* Magnetically Triggered Nanocomposite Membranes: A Versatile Platform for Triggered Drug Release. *Nano Lett.* **11,** 1395–1400 (2011).
53. Oliveira, H. *et al.* Magnetic field triggered drug release from polymersomes for cancer therapeutics. *J. Controlled Release* **169,** 165–170 (2013).
54. Lee, J. Magnetically Triggered Drug Release from Liposome Embedded Gel. *J. Nanomedicine Biotherapeutic Discov.* **4,** (2014).
55. Bi, H., Ma, S., Li, Q. & Han, X. Magnetically triggered drug release from biocompatible microcapsules for potential cancer therapeutics. *J. Mater. Chem. B* **4,** 3269–3277 (2016).
56. Veiseh, O., Gunn, J. W. & Zhang, M. Design and fabrication of magnetic nanoparticles for targeted drug delivery and imaging. *Adv. Drug Deliv. Rev.* **62,** 284–304 (2010).
57. Gobbo, O. L., Sjaastad, K., Radomski, M. W., Volkov, Y. & Prina-Mello, A. Magnetic Nanoparticles in Cancer Theranostics. *Theranostics* **5,** 1249–1263 (2015).

58. Sun, C., Lee, J. & Zhang, M. Magnetic nanoparticles in MR imaging and drug delivery☆. *Adv. Drug Deliv. Rev.* **60,** 1252–1265 (2008).

59. Qureshi, A., Gurbuz, Y. & Niazi, J. H. Biosensors for cardiac biomarkers detection: A review. *Sens. Actuators B Chem.* **171–172,** 62–76 (2012).

60. Gao, Y., Lim, J., Teoh, S.-H. & Xu, C. Emerging translational research on magnetic nanoparticles for regenerative medicine. *Chem. Soc. Rev.* **44,** 6306–6329 (2015).

61. Schmauch, M. M., Mishra, S. R., Evans, B. A., Velev, O. D. & Tracy, J. B. Chained Iron Microparticles for Directionally Controlled Actuation of Soft Robots. *ACS Appl. Mater. Interfaces* **9,** 11895–11901 (2017).

62. Hergt, R., Dutz, S., Müller, R. & Zeisberger, M. Magnetic particle hyperthermia: nanoparticle magnetism and materials development for cancer therapy. *J. Phys. Condens. Matter* **18,** S2919–S2934 (2006).

63. Pankhurst, Q. A., Thanh, N. T. K., Jones, S. K. & Dobson, J. Progress in applications of magnetic nanoparticles in biomedicine. *J. Phys. Appl. Phys.* **42,** 224001 (2009).

64. Fusco, S. *et al.* Shape-Switching Microrobots for Medical Applications: The Influence of Shape in Drug Delivery and Locomotion. *ACS Appl. Mater. Interfaces* **7,** 6803–6811 (2015).

65. Temel, F. Z. & Yesilyurt, S. Magnetically actuated micro swimming of bio-inspired robots in mini channels. in *Mechatronics (ICM), 2011 IEEE International Conference on* 342–347 (IEEE, 2011).

66. Xu, T., Yu, J., Yan, X., Choi, H. & Zhang, L. Magnetic Actuation Based Motion Control for Microrobots: An Overview. *Micromachines* **6,** 1346–1364 (2015).

67. Floyd, S., Pawashe, C. & Sitti, M. An Untethered Magnetically Actuated Micro-Robot Capable of Motion on Arbitrary. in *Surfaces," Proceedings of the 2008 IEEE International Conference on Robotics and Automation* (Press).
68. Thomas, C. R. *et al.* Noninvasive remote-controlled release of drug molecules in vitro using magnetic actuation of mechanized nanoparticles. *J. Am. Chem. Soc.* **132,** 10623–10625 (2010).
69. Singh, R. K. *et al.* Multifunctional Hybrid Nanocarrier: Magnetic CNTs Ensheathed with Mesoporous Silica for Drug Delivery and Imaging System. *ACS Appl. Mater. Interfaces* **6,** 2201–2208 (2014).
70. Chen, J.-P., Yang, P.-C., Ma, Y.-H., Tu, S.-J. & Lu, Y.-J. Targeted delivery of tissue plasminogen activator by binding to silica-coated magnetic nanoparticle. *Int. J. Nanomedicine* **7,** 5137–5149 (2012).
71. Mody, V. V. *et al.* Magnetic nanoparticle drug delivery systems for targeting tumor. *Appl. Nanosci.* **4,** 385–392 (2014).
72. Song, T., Zhang, Y. Z. & Zhou, T. J. Fabrication of magnetic composite nanofibers of poly(ε-caprolactone) with FePt nanoparticles by coaxial electrospinning. *J. Magn. Magn. Mater.* **303,** e286–e289 (2006).
73. Sung, Y. K., Ahn, B. W. & Kang, T. J. Magnetic nanofibers with core (Fe3O4 nanoparticle suspension)/sheath (poly ethylene terephthalate) structure fabricated by coaxial electrospinning. *J. Magn. Magn. Mater.* **324,** 916–922 (2012).
74. Wang, S. *et al.* Magnetic composite nanofibers fabricated by electrospinning of Fe3O4/gelatin aqueous solutions. *Mater. Sci. Eng. B* **190,** 126–132 (2014).
75. Agarwal, S., Wendorff, J. H. & Greiner, A. Use of electrospinning technique for biomedical applications. *Polymer* **49,** 5603–5621 (2008).

76. Deitzel, J. M., Kleinmeyer, J., Harris, D. E. A. & Tan, N. B. The effect of processing variables on the morphology of electrospun nanofibers and textiles. *Polymer* **42,** 261–272 (2001).
77. Marquidia Pacheco, Joel Pacheco & Ricardo Valdivia. *Synthesis of Carbon Nanofibers by a Glow-Arc Discharge.* (INTECH Open Access Publisher, 2010).
78. Subbiah, T., Bhat, G. S., Tock, R. W., Parameswaran, S. & Ramkumar, S. S. Electrospinning of nanofibers. *J. Appl. Polym. Sci.* **96,** 557–569 (2005).
79. Li, Y. & Yao, S. High stability under extreme condition of the poly(vinyl alcohol) nanofibers crosslinked by glutaraldehyde in organic medium. *Polym. Degrad. Stab.* **137,** 229–237 (2017).
80. Sill, T. J. & von Recum, H. A. Electrospinning: Applications in drug delivery and tissue engineering. *Biomaterials* **29,** 1989–2006 (2008).
81. Liang, D., Hsiao, B. S. & Chu, B. Functional electrospun nanofibrous scaffolds for biomedical applications. *Adv. Drug Deliv. Rev.* **59,** 1392–1412 (2007).
82. Agarwal, S., Wendorff, J. H. & Greiner, A. Use of electrospinning technique for biomedical applications. *Polymer* **49,** 5603–5621 (2008).
83. Xie, J., Jiang, J., Davoodi, P., Srinivasan, M. P. & Wang, C.-H. Electrohydrodynamic atomization: A two-decade effort to produce and process micro-/nanoparticulate materials. *Chem. Eng. Sci.* **125,** 32–57 (2015).
84. Bolbasov, E. N. *et al.* Ferroelectric polymer scaffolds based on a copolymer of tetrafluoroethylene with vinylidene fluoride: Fabrication and properties. *Mater. Sci. Eng. C* **40,** 32–41 (2014).
85. Teo, W.-E. & Ramakrishna, S. Electrospun nanofibers as a platform for multifunctional, hierarchically organized nanocomposite. *Compos. Sci. Technol.* **69,** 1804–1817 (2009).

86. Varesano, A., Carletto, R. A. & Mazzuchetti, G. Experimental investigations on the multi-jet electrospinning process. *J. Mater. Process. Technol.* **209,** 5178–5185 (2009).
87. Greiner, A. & Wendorff, J. H. Electrospinning: A Fascinating Method for the Preparation of Ultrathin Fibers. *Angew. Chem. Int. Ed.* **46,** 5670–5703 (2007).
88. Baji, A., Mai, Y.-W., Wong, S.-C., Abtahi, M. & Chen, P. Electrospinning of polymer nanofibers: Effects on oriented morphology, structures and tensile properties. *Compos. Sci. Technol.* **70,** 703–718 (2010).
89. Teo, W. E. & Ramakrishna, S. A review on electrospinning design and nanofibre assemblies. *Nanotechnology* **17,** R89–R106 (2006).
90. Mellado, P. *et al.* A simple model for nanofiber formation by rotary jet-spinning. *Appl. Phys. Lett.* **99,** 203107 (2011).
91. Lu, Y. *et al.* Centrifugal spinning: A novel approach to fabricate porous carbon fibers as binder-free electrodes for electric double-layer capacitors. *J. Power Sources* **273,** 502–510 (2015).
92. Badrossamay, M. R., McIlwee, H. A., Goss, J. A. & Parker, K. K. Nanofiber Assembly by Rotary Jet-Spinning. *Nano Lett.* **10,** 2257–2261 (2010).
93. Hammami, M. A., Krifa, M. & Harzallah, O. Centrifugal force spinning of PA6 nanofibers – processability and morphology of solution-spun fibers. *J. Text. Inst.* **105,** 637–647 (2014).
94. Badrossamay, M. R. *et al.* Engineering hybrid polymer-protein super-aligned nanofibers via rotary jet spinning. *Biomaterials* **35,** 3188–3197 (2014).
95. Lu, Y. *et al.* Centrifugal spinning: A novel approach to fabricate porous carbon fibers as binder-free electrodes for electric double-layer capacitors. *J. Power Sources* **273,** 502–510 (2015).

96. Yanilmaz, M., Lu, Y., Li, Y. & Zhang, X. SiO2/polyacrylonitrile membranes via centrifugal spinning as a separator for Li-ion batteries. *J. Power Sources* **273,** 1114–1119 (2015).
97. Dabirian, F., Hosseini Ravandi, S. A., Pishevar, A. R. & Abuzade, R. A. A comparative study of jet formation and nanofiber alignment in electrospinning and electrocentrifugal spinning systems. *J. Electrost.* **69,** 540–546 (2011).
98. Dabirian, F., Hosseini Ravandi, S. A. & Pishevar, A. R. The effects of operating parameters on the fabrication of polyacrylonitrile nanofibers in electro-centrifuge spinning. *Fibers Polym.* **14,** 1497–1504 (2013).
99. Hong, X., Edirisinghe, M. & Mahalingam, S. Beads, beaded-fibres and fibres: Tailoring the morphology of poly(caprolactone) using pressurised gyration. *Mater. Sci. Eng. C* **69,** 1373–1382 (2016).
100. Illangakoon, U., Mahalingam, S., Matharu, R. & Edirisinghe, M. Evolution of Surface Nanopores in Pressurised Gyrospun Polymeric Microfibers. *Polymers* **9,** 508 (2017).
101. Wu, X. *et al.* New Generation of Tunable Bioactive Shape Memory Mats Integrated with Genetically Engineered Proteins. *Macromol. Biosci.* **17,** 1600270 (2017).
102. Jayasinghe, S. N. & Suter, N. Pressure driven spinning: A multifaceted approach for preparing nanoscaled functionalized fibers, scaffolds, and membranes with advanced materials. *Biomicrofluidics* **4,** 014106 (2010).
103. Zhuang, X. *et al.* Solution blowing of submicron-scale cellulose fibers. *Carbohydr. Polym.* **90,** 982–987 (2012).

104. Ellison, C. J., Phatak, A., Giles, D. W., Macosko, C. W. & Bates, F. S. Melt blown nanofibers: Fiber diameter distributions and onset of fiber breakup. *Polymer* **48,** 3306–3316 (2007).

105. Deravi, L. F. *et al.* Design and Fabrication of Fibrous Nanomaterials Using Pull Spinning. *Macromol. Mater. Eng.* **302,** 1600404 (2017).

106. Hong, X., Mahalingam, S. & Edirisinghe, M. Simultaneous Application of Pressure-Infusion-Gyration to Generate Polymeric Nanofibers. *Macromol. Mater. Eng.* **302,** 1600564 (2017).

107. Luo, C. J., Stoyanov, S. D., Stride, E., Pelan, E. & Edirisinghe, M. Electrospinning versus fibre production methods: from specifics to technological convergence. *Chem. Soc. Rev.* **41,** 4708 (2012).

108. Guimarães, A. *et al.* Solving cell infiltration limitations of electrospun nanofiber meshes for tissue engineering applications. *Nanomed.* **5,** 539–554 (2010).

109. Martins, A., Araújo, J. V., Reis, R. L. & Neves, N. M. Electrospun nanostructured scaffolds for tissue engineering applications. *Nanomed.* **2,** 929–942 (2007).

110. Zhang, Y., Lim, C. T., Ramakrishna, S. & Huang, Z.-M. Recent development of polymer nanofibers for biomedical and biotechnological applications. *J. Mater. Sci. Mater. Med.* **16,** 933–946 (2005).

111. Zafar, M. *et al.* Potential of Electrospun Nanofibers for Biomedical and Dental Applications. *Materials* **9,** 73 (2016).

112. Tamimi, E. *et al.* Biomechanical Comparison of Glutaraldehyde-Crosslinked Gelatin Fibrinogen Electrospun Scaffolds to Porcine Coronary Arteries. *J. Biomech. Eng.* **138,** 011001-011001-12 (2015).

113. Tamayol, A. *et al.* Fiber-based tissue engineering: Progress, challenges, and opportunities. *Biotechnol. Adv.* **31,** 669–687 (2013).

114. Ahmed, J., Matharu, R. K., Shams, T., Illangakoon, U. E. & Edirisinghe, M. A Comparison of Electric-Field-Driven and Pressure-Driven Fiber Generation Methods for Drug Delivery. *Macromol. Mater. Eng.* 1700577 (2018). doi:10.1002/mame.201700577

115. Gosline, J. M., Guerette, P. A., Ortlepp, C. S. & Savage, K. N. The mechanical design of spider silks: from fibroin sequence to mechanical function. *J. Exp. Biol.* **202,** 3295–3303 (1999).

116. Gomes, M. E. *et al.* Starch–poly(ε-caprolactone) and starch–poly(lactic acid) fibre-mesh scaffolds for bone tissue engineering applications: structure, mechanical properties and degradation behaviour. *J. Tissue Eng. Regen. Med.* **2,** 243–252 (2008).

117. Sinclair, K. D., Webb, K. & Brown, P. J. The effect of various denier capillary channel polymer fibers on the alignment of NHDF cells and type I collagen. *J. Biomed. Mater. Res. A* **95A,** 1194–1202 (2010).

118. Wan, A. C. A., Liao, I.-C., Yim, E. K. F. & Leong, K. W. Mechanism of Fiber Formation by Interfacial Polyelectrolyte Complexation. *Macromolecules* **37,** 7019–7025 (2004).

119. Fei, X., Li, S., Cao, L., Zhang, B. & Yu, M. Multifunctional polymer drug loading system with pH-sensitive, fluorescent and targeting property. *Mater. Sci. Eng. C* **77,** 1151–1159 (2017).

120. Li, P., Zhang, Z., Su, Z. & Wei, G. Thermosensitive polymeric micelles based on the triblock copolymer poly(D,L -lactide)- *b* -poly(*N* -isopropyl acrylamide)- *b* -

poly(D,L -lactide) for controllable drug delivery. *J. Appl. Polym. Sci.* **134,** 45304 (2017).

121. Baghbani, F., Chegeni, M., Moztarzadeh, F., Mohandesi, J. A. & Mokhtari-Dizaji, M. Ultrasonic nanotherapy of breast cancer using novel ultrasound-responsive alginate-shelled perfluorohexane nanodroplets: In vitro and in vivo evaluation. *Mater. Sci. Eng. C* **77,** 698–707 (2017).

122. Ansari, M., Bigham, A., Hassanzadeh-Tabrizi, S. A. & Abbastabar Ahangar, H. Synthesis and characterization of Cu 0.3 Zn 0.5 Mg 0.2 Fe 2 O 4 nanoparticles as a magnetic drug delivery system. *J. Magn. Magn. Mater.* **439,** 67–75 (2017).

123. Nikjoo, D. & Aroguz, A. Z. Dual responsive polymeric bionanocomposite gel beads for controlled drug release systems. *J. Appl. Polym. Sci.* **134,** 45143 (2017).

124. Liu, T. *et al.* A novel grapheme oxide-modified collagen-chitosan bio-film for controlled growth factor release in wound healing applications. *Mater. Sci. Eng. C* **77,** 202–211 (2017).

125. Farzin, A., Fathi, M. & Emadi, R. Multifunctional magnetic nanostructured hardystonite scaffold for hyperthermia, drug delivery and tissue engineering applications. *Mater. Sci. Eng. C* **70,** 21–31 (2017).

126. Chi, Y., Zhang, G., Xiang, Y., Cai, D. & Wu, Z. Fabrication of a Temperature-Controlled-Release Herbicide Using a Nanocomposite. *ACS Sustain. Chem. Eng.* **5,** 4969–4975 (2017).

127. Eranka Illangakoon, U. *et al.* Gyrospun antimicrobial nanoparticle loaded fibrous polymeric filters. *Mater. Sci. Eng. C* **74,** 315–324 (2017).

128. Aytimur, A., Koçyiğit, S., Uslu, İ. & Gökmeşe, F. Preparation and Characterization of Polyvinyl Alcohol Based Copolymers as Wound Dressing Fibers. *Int. J. Polym. Mater. Polym. Biomater.* **64,** 111–116 (2015).

129. Gelebart, A. H. *et al.* Making waves in a photoactive polymer film. *Nature* **546,** 632–636 (2017).

130. Uhrich, K. E., Cannizzaro, S. M., Langer, R. S. & Shakesheff, K. M. Polymeric Systems for Controlled Drug Release. *Chem. Rev.* **99,** 3181–3198 (1999).

131. Granberg, R. A. & Rasmuson, Å. C. Solubility of Paracetamol in Pure Solvents. *J. Chem. Eng. Data* **44,** 1391–1395 (1999).

132. Glavanović, S., Glavanović, M. & Tomišić, V. Simultaneous quantitative determination of paracetamol and tramadol in tablet formulation using UV spectrophotometry and chemometric methods. *Spectrochim. Acta Part Mol. Spectrosc.* **157,** 258–264 (2016).

133. Zhang, S. *et al.* Coupling Infusion and Gyration for the Nanoscale Assembly of Functional Polymer Nanofibers Integrated with Genetically Engineered Proteins. *Macromol. Rapid Commun.* **36,** 1322–1328 (2015).

134. He, J.-H., Wan, Y.-Q. & Yu, J.-Y. Effect of concentration on electrospun polyacrylonitrile (PAN) nanofibers. *Fibers Polym.* **9,** 140–142 (2008).

135. McKee, M. G., Wilkes, G. L., Colby, R. H. & Long, T. E. Correlations of solution rheology with electrospun fiber formation of linear and branched polyesters. *Macromolecules* **37,** 1760–1767 (2004).

136. Kong, L. & Ziegler, G. R. Role of Molecular Entanglements in Starch Fiber Formation by Electrospinning. *Biomacromolecules* **13,** 2247–2253 (2012).

137. Yuan, X. Y., Zhang, Y. Y., Dong, C. H. & Sheng, J. Morphology of ultrafine polysulfone fibers prepared by electrospinning. *Polym. Int.* **53,** 1704–1710 (2004).

138. Wannatong, L., Sirivat, A. & Supaphol, P. Effects of solvents on electrospun polymeric fibers: preliminary study on polystyrene. *Polym. Int.* **53,** 1851–1859 (2004).

139. Wongsasulak, S., Kit, K. M., McClements, D. J., Yoovidhya, T. & Weiss, J. The effect of solution properties on the morphology of ultrafine electrospun egg albumen-PEO composite fibers. *Polymer* **48,** 448–457 (2007).

140. Zeng, J. *et al.* Poly(vinyl alcohol) nanofibers by electrospinning as a protein delivery system and the retardation of enzyme release by additional polymer coatings. *Biomacromolecules* **6,** 1484–1488 (2005).

141. Zhong, H., Gilmanshin, R. & Callender, R. An FTIR study of the complex melting behavior of alpha-lactalbumin. *J. Phys. Chem. B* **103,** 3947–3953 (1999).

142. Mallapragada, S. K. & Peppas, N. A. Dissolution mechanism of semicrystalline poly(vinyl alcohol) in water. *J. Polym. Sci. Part B Polym. Phys.* **34,** 1339–1346 (1996).

143. Mansur, H. S., Sadahira, C. M., Souza, A. N. & Mansur, A. A. P. FTIR spectroscopy characterization of poly (vinyl alcohol) hydrogel with different hydrolysis degree and chemically crosslinked with glutaraldehyde. *Mater. Sci. Eng. C* **28,** 539–548 (2008).

144. Bichara, L. C., Lanús, H. E., Ferrer, E. G., Gramajo, M. B. & Brandán, S. A. Vibrational Study and Force Field of the Citric Acid Dimer Based on the SQM Methodology. *Adv. Phys. Chem.* **2011,** 1–10 (2011).

145. Cornell, R. M. & Schwertmann, U. *The iron oxides structure, properties, reactions, occurrences, and uses*. (Weinheim Wiley-VCH, 2003).

146. Behera, S. UV-Visible Spectrophotometric Method Development and Validation of Assay of Paracetamol Tablet Formulation. *J. Anal. Bioanal. Tech.* **03,** (2012).

147. Huang, X. & Brazel, C. S. On the importance and mechanisms of burst release in matrix-controlled drug delivery systems. *J. Control. Release Off. J. Control. Release Soc.* **73,** 121–136 (2001).

148. Berger, J. *et al.* Structure and interactions in covalently and ionically crosslinked chitosan hydrogels for biomedical applications. *Eur. J. Pharm. Biopharm.* **57,** 19–34 (2004).